



TECHNISCHE UNIVERSITÄT MÜNCHEN  
FAKULTÄT CHEMIE  
LEHRSTUHL FÜR ORGANISCHE CHEMIE II

Target identification of natural products by activity based protein profiling  
and  
A whole proteome inventory of background photocrosslinker binding

Wolfgang Heydenreuter

Vollständiger Abdruck der von der Fakultät für Chemie der Technischen  
Universität München zur Erlangung des akademischen Grades eines

Doktors der Naturwissenschaften (Dr. rer. nat)

genehmigten Dissertation.

Vorsitzender: Prof. Dr. Lukas Hintermann  
Prüfer der Dissertation: 1. Prof. Dr. Stephan A. Sieber  
2. Prof. Dr. Tobias A.M. Gulder

Die Dissertation wurde am 06.07.2016 bei der bei der Technischen Universität  
München eingereicht und durch die Fakultät für Chemie am 28.07.2016  
angenommen.



TECHNISCHE  
UNIVERSITÄT  
MÜNCHEN

TECHNISCHE UNIVERSITÄT MÜNCHEN  
FAKULTÄT CHEMIE  
LEHRSTUHL FÜR ORGANISCHE CHEMIE II

**Target identification of natural products by activity  
based protein profiling  
and  
A whole proteome inventory of background  
photocrosslinker binding**

Vollständiger Abdruck zur Erlangung des akademischen Grades eines  
Doktors der Naturwissenschaften (Dr. rer. nat)

**Wolfgang Heydenreuter**



Meiner Familie gewidmet



“Success is not final, failure is not fatal: it is the courage to continue that counts.”

— Winston S. Churchill



## Danksagung

Zu allererst möchte ich mich sehr herzlich bei Prof. Dr. Stephan A. Sieber für die Aufnahme in seinen Arbeitskreis bedanken. Für sein stetiges Vertrauen in meine Arbeit, die Aufgeschlossenheit gegenüber neuer Projekte und besonders für seine große Begeisterung für die Forschung und die mir gegebenen Freiheiten bei der Entwicklung eigener Projekte bin ich sehr dankbar.

Bedanken möchte ich mich auch bei den Mitgliedern der Prüfungskommission für ihre Bemühungen bei der Bewertung dieser Arbeit.

Die vielen Ergebnisse wären nie ohne die großartige Zusammenarbeit mit Kooperationspartnern sowohl in als auch außerhalb des Sieber-Labs entstanden. Ganz besonders möchte ich Simone Braig und ihren Mitarbeitern vom Lehrstuhl für Pharmazeutische Biologie der LMU für die ausgesprochen produktive Zusammenarbeit im Rahmen des Neocarzilin-Projektes bedanken. Meinen Laborkollegen Philipp Kleiner, Elena Kunhold, Matthias Stahl, Jan Vomacka, Megan Wright und Vadim Korotkov danke ich für die gemeinsame Arbeit an diversen Projekten im Zuge meiner Doktorarbeit.

Mein großer Dank gilt ebenso Megan Wright und Matthias Stahl für ihre Bemühungen dieser Arbeit die Mängel auszutreiben.

Für ihre jahrelange Unterstützung im Laboralltag danke ich ganz besonders Mona Wolff und Katja Bäuml, die durch ihren unermüdlichen Einsatz stets eine produktive Arbeitsumgebung aufrechterhalten haben. Ferner möchte ich mich bei den unzähligen Praktikanten (Forschungspraktikum oder Bachelorarbeit) bedanken, die durch ihr stetiges Engagement viele, besonders synthetische Projekte, maßgeblich vorangetrieben haben. Es ist schön zu sehen, dass einige nun fester Bestandteil des Sieber-Labs geworden sind.

Bei meinen Laborkollegen möchte ich mich für die großartige Zeit und deren Hilfsbereitschaft bedanken. Besonders erwähnen möchte ich hier Dr. Georg "*Eure Dudeheit*" Rudolf für legendäre Kino- und Bouldersessions sowie philosophische Diskussionen über die emotionale Tiefe von Sharknado-Filmen, Dr. Jürgen "*Fernet Branca*" Eirich für entspannte Golfsessions an der Isar und das Belächeln rheinischer Golfkünste, Dr. Maria "*Marie*" Dahmen für die Präsentation dieser Künste und diverse Kletterhallenbesuche, Dr. Roman Kolb für das Vorleben von Sarkasmus und Zynismus in vollendeter Form, Volker "*Rául von Schalke*" Kirsch und Christian "*Fetzle*" Fetzer für exzellente Zockersessions und rege Diskussion über die Signifikanz bakterieller Proteasen. So isch lässig ! Des Weiteren danke ich Philipp Kleiner, Annabelle "*Anni*" Hoegl, Johannes



“Leeeman“ Lehmann, Mathias “Horst Seeler“ Hackl, Elena “Lenchen“ Kunhold, Dr. Franziska “Franjo“ Mandl, Dr. Max Koch, Dr. Megan Wright, Dr. Pavel Kielkowski, Barbara “Babsarella“ Hofbauer, Thomas “Elfmetergott“ Gronauer, Markus Lakemeyer, Matthias Stahl, Weining Zhao, Jan Vomacka, Dr. Nina Bach, Dóra Balogh, Dr. Joanna Krysiak, Dr. Malte Gersch, Dr. Matthew Nodwell, Dr. Johannes Kreuzer, Dr. Thomas Menzel, Dr. Vadim Korotkov und Dr. Tanja Wirth für die tolle Atmosphäre und die Unterstützung über all die Jahre.

Der aktuellen Generation von Masterstudenten namentlich Johnny Drechsel, Ines Hübner und Anja Fux wünsche ich auf ihrem künftigen Weg alles Gute.

Mein größter Dank gilt meinen Eltern, Gisela und Peter Heydenreuter, sowie meiner Schwester Christine für deren bedingungslose Unterstützung über all die Jahre. Auch möchte ich mich ganz besonders bei Isabel Buchsbaum für ihren liebevollen Rückhalt in den letzten drei Jahren bedanken. Ich kann mich glücklich schätzen, dass es euch gibt.

---

## Table of Contents

<b>Table of Contents</b>	<b>I</b>
<b>Introductory Remarks</b>	<b>IV</b>
<b>Summary</b>	<b>V</b>
<b>Zusammenfassung</b>	<b>VI</b>
<b>1 Introduction</b>	<b>1</b>
1.1 Activity based protein profiling (ABPP)	1
1.2 Electrophilic natural products and covalent inhibitors	5
1.3 Scope of this work	6
<b>2 Target identification of falcarinol in human cancer cells</b>	<b>9</b>
2.1 Polyynes and falcarinol	9
2.2 ALDH2	10
2.3 Results and discussion	12
2.3.1 Synthesis of activity-based probes	12
2.3.2 Total synthesis of falcarinol and stipudiol	13
2.3.3 Bioactivity in eukaryotic cells and bacteria	15
2.3.4 Protein reactivity in human cancer cells	16
2.4 Concluding remarks and outlook	22
<b>3 A whole proteome inventory of background photocrosslinker binding</b>	<b>23</b>
3.1 Photocrosslinkers	23
3.2 Results and discussion	26
3.2.1 Synthesis of minimal photoprobes	26
3.2.2 Protein reactivity in human cancer cells A549 and HeLa	27
3.2.3 Gel-free analysis of photocrosslinker-specific targets via quantitative proteomics	28
3.2.4 Diazirine-specific photome	30
3.2.5 Target analysis of the PKA inhibitor H8 as a proof-of-principle	34
3.3 Conclusion and outlook	38
<b>4 Target identification of neocarzilin A-C in human cancer cells</b>	<b>39</b>
4.1 Cancer as a challenge for mankind	39
4.1.1 Tumor migration	40
4.1.2 Neocarzilin	41
4.2 Results and discussion	41
4.2.1 Synthesis of an activity-based probe	41
4.2.2 Synthesis of neocarzilins A-C	42
4.2.3 Reactivity to proteins in human cancer cells	43
4.2.4 Quantitative proteomics	45
4.2.5 Target validation	47
4.2.5.1 Labeling of VAT-1 knockdown cells	47
4.2.5.2 Labeling of recombinant VAT-1 in E. coli	48
4.2.6 Function of VAT-1	48
4.2.7 Inhibition of migration and chemotaxis by neocarzilin A	49
4.2.8 Effects of neocarzilin A and C on cellular viability and apoptosis	50

---

4.2.9	Effect of neocarzilin A on mitochondria	52
4.2.10	Identification of potential interaction partners of VAT-1 by co-immunoprecipitation	54
4.3	Conclusion and outlook	57
<b>5</b>	<b>Experimental Section</b>	<b>59</b>
5.1	Organic Synthesis	59
5.1.1	General Methods and Materials	59
5.1.2	Synthetic procedures for chapter 2: Target identification of falcarinol in cancer cells.	60
5.1.3	Synthetic procedures for chapter 3: A whole proteome inventory of background photocrosslinker binding	78
5.1.4	Synthetic procedures for Chapter 4: Target identification of neocarzilin A-C in human cancer cells.	88
5.2	Biochemistry	98
5.2.1	General methods and materials	98
5.2.1.1	Cell culture	98
5.2.1.2	MTT- Assay	98
5.2.1.3	Labeling reagents	100
5.2.1.4	In situ labeling	100
5.2.1.5	Analytical gel based analysis	101
5.2.2	Biochemical procedures for Chapter 2: Target identification of falcarinol in cancer cells	101
5.2.2.1	Click reaction and preparative gel-free analysis	101
5.2.2.2	Preparative gel based analysis	102
5.2.2.3	Gel based target identification	104
5.2.2.4	Gel free target identification	105
5.2.2.5	Binding peptide identification	106
5.2.2.6	Binding site identification	106
5.2.2.7	Recombinant expression of target protein	107
5.2.2.8	PCR	107
5.2.2.9	Gateway cloning	108
5.2.2.10	ALDH2 in vitro-labeling	108
5.2.2.11	ALDH2 activity assay	109
5.2.3	Biochemical procedures for Chapter 3: A whole proteome inventory of background photocrosslinker binding	109
5.2.3.1	Analytical in situ AfBPP labelling	109
5.2.3.2	Preparative <i>in situ</i> labelling and quantification <i>via</i> SILAC	110
5.2.3.3	Mass spectrometry	111
5.2.3.4	Bioinformatics	112
5.2.4	Biochemical procedures for Chapter 4: Target identification of neocarzilin A-C in human cancer cells	114
5.2.4.1	Click reaction and preparative gel-free analysis	114
5.2.4.2	Preparative gel free analysis using label free quantification	114
5.2.4.3	Mass spectrometry	115
5.2.4.4	Recombinant expression of target protein	116
5.2.4.5	PCR	117
5.2.4.6	Gateway cloning	117
5.2.4.7	Recombinant expression and analytical labeling in <i>E.coli</i>	118
5.2.4.8	Co-Immunoprecipitation	119
<b>6</b>	<b>Bibliography</b>	<b>121</b>
<b>7</b>	<b>List of abbreviations, acronyms and symbols</b>	<b>141</b>

---

<b>8</b>	<b>Appendices</b>	<b>144</b>
8.1	Selected $^1\text{H}$ and $^{13}\text{C}$ NMR Spectra for Chapter 2	144
8.2	Selected $^1\text{H}$ and $^{13}\text{C}$ NMR Spectra for Chapter 4	149
<b>9</b>	<b>Curriculum Vitae</b>	<b>154</b>

---

## Introductory Remarks

The present doctoral dissertation was accomplished between February 2012 and July 2016 under the supervision of Prof. Dr. Stephan A. Sieber at the Chair of Organic Chemistry II of the Technische Universität München.

Parts of this thesis are based on the following publications and manuscripts in preparation for publication:

**Chapter 2:** Heydenreuter, W., Kunold, E. & Sieber, S. A. Alkynol natural products target ALDH2 in cancer cells by irreversible binding to the active site. *Chem. Commun. (Camb)* **51**, 15784-15787 (2015).

**Chapter 3:** Kleiner, P., Heydenreuter, W., Stahl, M., Korotkov, V. S., Sieber, S. A. A whole proteome inventory of background photocrosslinker binding. *Submitted to Angewandte Chemie*.

**Chapter 4:** *Manuscript in preparation.*

All compounds mentioned in the theoretical part of this thesis are indexed consecutively with Arabic numerals in the format **X.Y** while **X** being the number of the project chapter and **Y** being in the order of appearance. This doctoral thesis was compiled with Microsoft Word 2013 and all structural formulas were assembled with CambridgeSoft ChemBioDraw Ultra (13.0, 2013) under the ACS document 1996 guidelines. NMR spectra were edited with MestReNova (9.00, 2013). Processing of fluorescent SDS-PAGE scan was performed with Fujifilm Multi Gauge 3.0. Processing and plotting of assay data was performed with GraphPad Prism 6.05 and Adobe Illustrator CS5 was employed for creation of figures and graphs.

---

## Summary

Falcarinol is a polyene natural product with potent cytotoxic and antibacterial activities. Although its electrophilic properties have been known for quite some time, its mode of action is unclear and only a few protein targets have been discovered so far. Chapter 2 describes the design and application of a falcarinol-inspired probe carrying a terminal alkyne to elucidate covalent targets in human lung cancer cells via an ABPP (activity based protein profiling) approach. The catabolic enzyme aldehyde dehydrogenase 2 (ALDH2) was identified as a covalent target of falcarinol and validated by binding site identification and activity assays. Furthermore, the related natural product stipudiol was synthesized for the first time and also shown to alkylate and inhibit ALDH2. To further identify noncovalent interactions of falcarinol and related natural products, a probe containing a photo-labile diazirine was designed and applied in affinity based protein profiling (AfBPP). The results of this screening were compared to the photome dataset, which was developed in chapter 3.

The specificity of photo crosslinkers in photo affinity labeling experiments is the subject of chapter 3. For this purpose, a set of minimal probes, containing the most commonly applied photocrosslinkers (benzophenone, aryl azide and diazirine) was synthesized and screened in a SILAC-AfBPP approach in the two human cancer cell lines A549 and HeLa. Diazirine was identified as the photoreactive group with the lowest background binding, although the degree of covalent modification mostly depended on probe size and design. An overlay of protein enrichment of four synthesized diazirine probes in both cell lines identified a set of reappearing protein hits which form the diazirine "photome". When applied to the interpretation of profiling data of two complex photoprobes, several proteins that were significantly enriched could be excluded by comparison to the photome list. One of these complex photoprobes was a diazirine modified version of H8, a potential inhibitor of cAMP-dependent protein kinase (PKA). Among other hits, PKA could be identified, validating this predicted target of H8 in whole proteome studies for the first time. These results not only confirmed the photome as a valuable dataset but also demonstrated the value of employing photo crosslinkers in AfBPP methodologies to identify protein targets of small molecules.

Applying the ABPP methodology to unravel covalent targets of neocarzilins, a cytotoxic secondary metabolite from *Streptomyces carzinostaticus* was the main endeavor of chapter 4. Following the total synthesis of neocarzilins A-C, a modified version of neocarzilin A, bearing a terminal alkyne was applied in *in situ* profiling of the human cancer cell line HepG2. The synaptic vesicle membrane protein VAT-1 homolog (VAT-1) was identified as

---

a high affinity target of neocarzilin A, but not neocarzilin C. Previous reports have linked this protein to tumor migration, a crucial step in metastasis and the primary reason for high mortality rates in advanced cancer. Indeed, a significant decrease in migration was observed when cancer cells were treated with neocarzilin in the range of 500 nM. Exposure to similar concentrations over longer times led to inhibition of proliferation but only minor induction of apoptosis. Furthermore, Neocarzilin was shown to induce clustering and impair main functions of mitochondria. A co-immunoprecipitation with a VAT-1 antibody revealed a connection to PI3 kinase, a protein with an important role in signal transduction and regulation of key cell processes, like growth, proliferation, migration and adhesion. Further studies may expose the cellular function of VAT-1 and its role in cellular pathways. Since metastasis and tumor migration are the two factors responsible for poor treatment response and survival rates of multiple cancers, VAT-1 may also be a promising point of attack for future drugs.

## Zusammenfassung

Falcarinol gehört zur Klasse der Polyacetylene und besitzt stark cytotoxische und antibakterielle Eigenschaften. Obwohl seine elektrophile Natur seit langem bekannt ist, wurden bis heute nur wenige proteinogene Angriffsziele identifiziert. Das zweite Kapitel dieser Arbeit beschäftigt sich mit dem Design einer Sonde mit Alkintag zur Identifizierung von kovalenten Zielstrukturen unter Anwendung der ABPP-Methodologie. Diese führte zur Identifizierung der mitochondrialen Aldehyddehydrogenase (ALDH2) als molekulares Target von Falcarinol in der humanen Lungenkrebslinie A549, welches durch Aktivitätsassays und Bestimmung der Bindestelle bestätigt wurde. Des Weiteren konnte der verwandte Naturstoff Stipudiol in einer ersten Totalsynthese synthetisiert und ebenso als Inhibitor der ALDH2 identifiziert werden. Zur Bestimmung nichtkovalenter Interaktionen wurde eine weitere Sonde synthetisiert, welche neben einem terminalen Alkin eine fotolabile Diazirinegruppe trägt. Diese wurde in affinitätsbasiertem Profiling eingesetzt. Die Interpretation angereicherter Proteine mit Hilfe des "Phantom"-Datensatzes wurde in Kapitel 3 durchgeführt.

Die Spezifität von Fotocrosslinkern in affinitätsbasierten Targetidentifizierungen war das zentrale Thema in Kapitel 3. Zu diesem Zweck wurde eine kleine Bibliothek von Minimalsonden synthetisiert, welche die etabliertesten Fotocrosslinker (Benzophenon, Arylazid, Diazirine) beinhalteten. Diese wurden mit Hilfe von AfBPP (affinity based protein profiling) auf ihre Anreicherungsmuster zellulärer Proteine untersucht. Die Experimente

---

wurden in zwei humanen Krebszelllinien, A549 und HeLa, durchgeführt und die Proteine mit Hilfe von SILAC (stable isotope labeling with amino acids in cell culture) quantifiziert. Diazirine konnten allgemein als die Klasse von Fotocrosslinkern mit dem geringsten unspezifischen Labeling identifiziert werden, obwohl die Anzahl angereicherter Proteine hauptsächlich von Größe und Sondendesign abhing. Die Überlappung der Vulcano-Blots von vier Diazirin-Fotosonden offenbarte eine Sammlung von regelmäßig abundant angereicherten Proteinen, das "Photom". Durch Vergleich mit Anreicherungsdaten zweier komplexer Fotosonden konnten mehrere signifikant angereicherte Proteine als unspezifisch ausgeschlossen werden. Eine Fotosonde des bekannten Kinaseinhibitors H8 konnte das bereits bekannte Target, die cAMP-abhängige Proteinkinase (PKA) zum ersten Mal in einem AfBPP-Experiment identifizieren. Dies ist eine wertvolle Validierung des Photoms und der affinitätsbasierten Targetidentifizierung mit Hilfe von Fotocrosslinkern.

Die Anwendung von ABPP zur Identifizierung kovalenter Targets der Neocarziline, cytotoxischer polyketider Naturstoffe von *Streptomyces carzinostaticus*, ist das Leitthema von Kapitel 4. Neben der Totalsynthese der Neocarziline A-C wurde ebenfalls ein mit einem terminalen Alkintag modifizierter Naturstoff synthetisiert. Dieser konnte in einem gelfreien SILAC-ABPP-Ansatz das synaptic vesicle membrane protein VAT-1 homolog (VAT-1) als hochaffines Zielprotein von Neocarzilin A identifizieren, jedoch nicht von Neocarzilin C. Die Literaturrecherche ergab einen direkten Zusammenhang von hoher Expression dieses Proteins und starker Migrationsaktivität in diversen metastasierenden Glioblastomen, dem Hauptgrund für schlechte Prognosen und Überlebensraten dieser Krebsart. Tatsächlich konnte eine starke Inhibition der Migration besonders in Brustkrebslinien mit Konzentrationen von 500 nM Neocarzilin A erreicht werden. Bei längerer Inkubation zeigte Neocarzilin A starke Inhibition der Proliferation jedoch ohne nennenswerte Induktion der Apoptose. Des Weiteren verursachte Neocarzilin A eine Clusterbildung von Mitochondrien und reduzierte deren Membranpotential. Potentielle Interaktionspartner von VAT-1 wurden mit einer Co-Immunpräzipitation ermittelt, darunter auch PIK3, eine Kinase, welche in diversen regulatorischen Prozessen des Zellwachstums, der Proliferation, Migration und Adhäsion involviert ist. Die Aufklärung der Funktion von VAT-1 in zellulären Signalwegen ist von wesentlicher Bedeutung, da sie womöglich neue Wege zur Bekämpfung schlecht therapierbarer, invasiver Tumore eröffnet.





# 1 Introduction

## 1.1 Activity based protein profiling (ABPP)

The identification of small molecule-protein interactions is one of the main goals of chemical biology. There are numerous methods to identify the molecular targets of bioactive compounds that bind their protein targets covalently or non-covalently. An innovative and powerful method is activity-based protein profiling (ABPP). What makes this technique so powerful is its ability to visualize and evaluate protein interactions with small molecules based on their activity, not their abundance.<sup>1,2</sup> As protein abundance does not directly correlate with activity due to posttranslational modifications, standard proteomic approaches may not be able to capture important changes in protein structure and function that impact on cellular physiology.<sup>3</sup> Normally, only enzymes that are correctly folded and with the appropriate posttranslational modifications are reactive enough to be targeted by an ABPP probe. The ABPP methodology requires a covalent interaction between probe and protein, mostly through reaction of an electrophilic probe and a nucleophilic amino acid moiety of the target protein. Activity directed protein labeling was first reported by Powers *et al.*<sup>4,5</sup> and further advanced by Cravatt *et al.*<sup>6-9</sup> and Boygo *et al.*<sup>10,11</sup> The standard structure of an ABPP probe includes an electrophilic, protein reactive “warhead”, which forms the bond to the target protein and a reporter tag for visualization and/or enrichment (Figure 1.1). A spacer group separates the electrophile from the reporter tag. In many cases this spacer group is also responsible for noncovalent interactions between probe and target protein, which are often required for efficient binding.

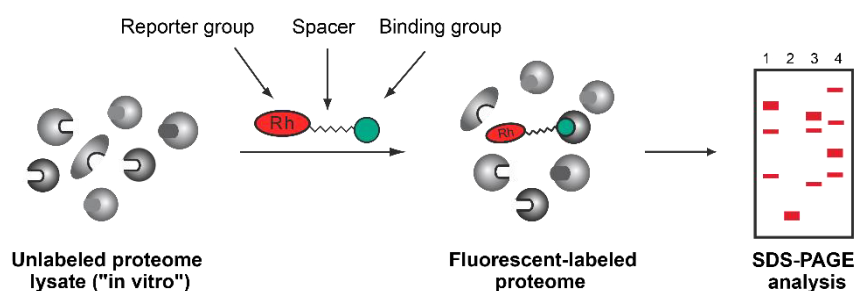


**Figure 1.1:** Basic concept of analytic *in vitro* ABPP with fluorophore as reporter tag.

Applying this concept to intact cells (*in situ*) ensures that all proteins are in their native state and the *status quo* of a cell is profiled, which is the true power of this methodology. As the reporter groups are often bulky and/or charged (dyes, biotin tags, etc.), cell permeability and steric compatibility with the target can be compromised. Therefore, small reporter tags like terminal alkynes or azides are used, which are chemically orthogonal to functional

groups in cells. A small tag also allows more complex small molecules like natural products to be modified without significant alteration of their secondary structure.<sup>12</sup>

After incubation, the cells are lysed and the tags can be “clicked” (ligated by click chemistry) to larger visualization or enrichment tags via copper-mediated [2+3]-cycloadditions (Figure 1.2).<sup>8</sup> The Copper(I)-catalyzed Azide-Alkyne Cycloaddition (CuAAC) is the most frequently used reaction to connect alkynes and azides in various aqueous buffers with high bioorthogonality and solid reaction rates.<sup>13–15</sup>

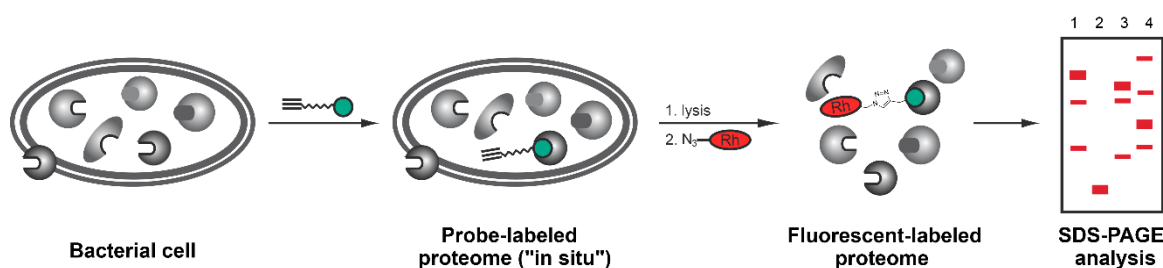


**Figure 1.2:** *In situ* analytical labeling with subsequent fluorescence readout.

A variety of reactive chemical groups have been used for profiling proteins, such as fluorophosphonates,<sup>6</sup> vinylsulfones,<sup>16</sup> epoxides<sup>11</sup> or  $\beta$ -lactones.<sup>17</sup> The active sites of enzymes often possess highly nucleophilic groups. Although these nucleophiles are also present in the peptidic backbone of the protein, the reactivity of amino acid sidechains within the active center towards strong electrophiles is increased since a high nucleophilicity is required for turnover of natural substrates. By tuning the electrophilic properties or concentrations of a probe, it is possible to get a reactivity profile of entire enzyme classes which share a common reactivity motive.<sup>6,18</sup> As nucleophilicity, steric demand and noncovalent interactions are factors that determine binding efficiency, alteration of these parameters can deliver basic structure activity relationships between probe and target.

The identification of labeled proteins via high resolution mass spectrometry (HR-MS) requires enrichment of the desired protein to reduce the enormous complexity of the total proteome. In a gel-based approach, the tags are clicked to a trifunctional linker, which contains an attachment site (e.g. azide), a fluorophore for visualization and an enrichment tag (e.g. biotin). In standard protocols, the tagged proteins are enriched on avidin-coated beads, cleaved off and separated on SDS gels. The desired bands are cut out and the proteins digested and subjected to HR-MS (Figure 1.3).

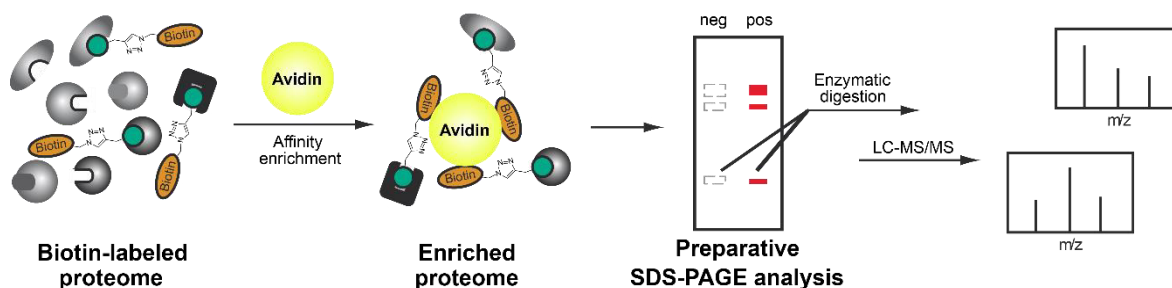


**Figure 1.3:** Basic concept of gel-based *in situ* preparative labeling and subsequent target identification via HR-MS.

With the constant improvements in HR-MS technology, in particular increased sensitivity and data collection, gel-based target identification has become obsolete. The fluorescent scan is used to guide the cutting of bands; however many protein targets may be of low abundance, making them undetectable in this type of gel-based approach. Some proteins do not run well on gels and the risk of introducing external contaminants is also increased. Cutting gel bands is also imprecise and lacks reproducibility. The state of the art technology for quantitative proteomics with HR-MS in human cells is SILAC<sup>19</sup> (Stable isotope labeling by amino acids in cell culture).

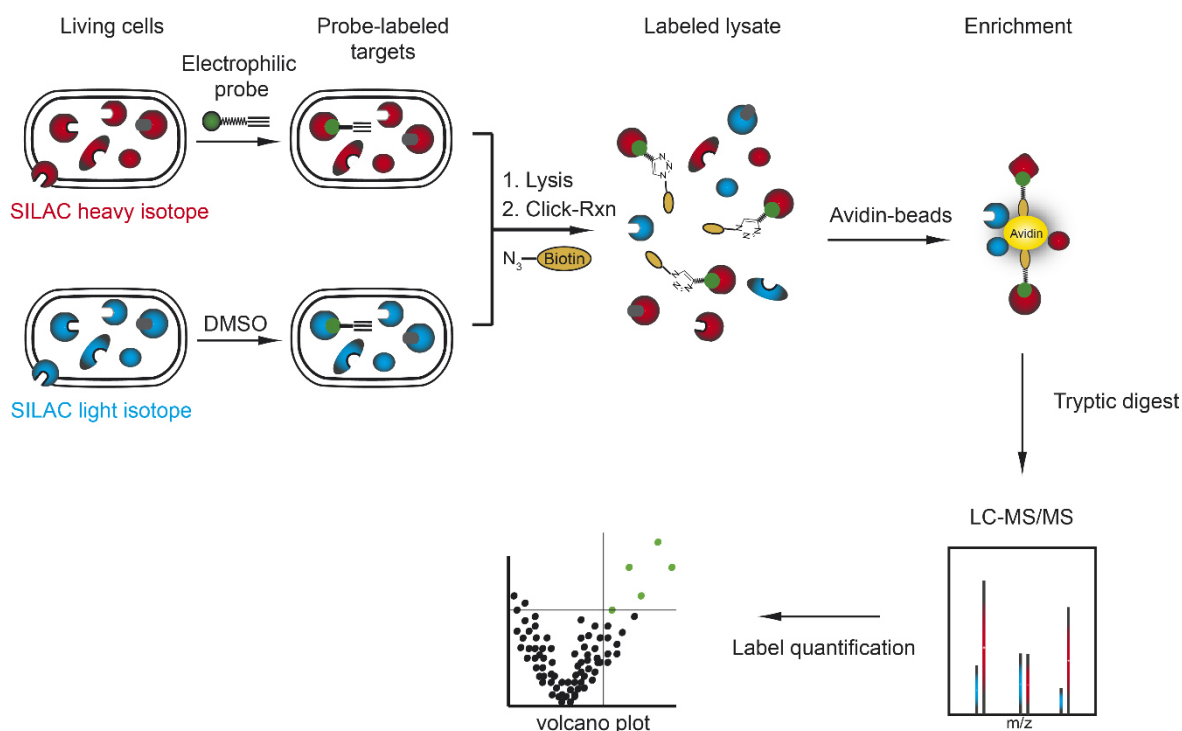


**Figure 1.4:** Workflow of SILAC-ABPP.

By incorporating amino acids with unnatural isotope pattern into the proteomes, different labeling states of cells can be distinguished by mass spectrometry. The quantification of identical peptides with different isotope profiles enables the determination of enrichment factors and therefore the identification of labeled protein targets. By combining the samples

early in the workflow, technical variations between the replicates are reduced, a big advantage over methods applying late stage chemical modifications. The standard SILAC-ABPP workflow is shown in Figure 1.4.

Although SILAC has been applied in bacteria,<sup>20</sup> the method is mostly limited to eukaryotic cells. Cells also undergo metabolic and proteomic changes in response to the incorporation of amino acids with unnatural isotope profiles. An already established method in proteomics is label free quantification<sup>21–24</sup> (Figure 1.5). The big advantage of this method is that it is applicable to “normal” cells and tissue without the need for an isotopic label or chemical modification. Also an arbitrary number of states can be measured and compared with each other. As the samples are processed separately, the changes between the samples require reliable mass spectrometer performance and *in silico* processing to compensate. A higher number of replicates might be necessary to obtain reliable statistics.

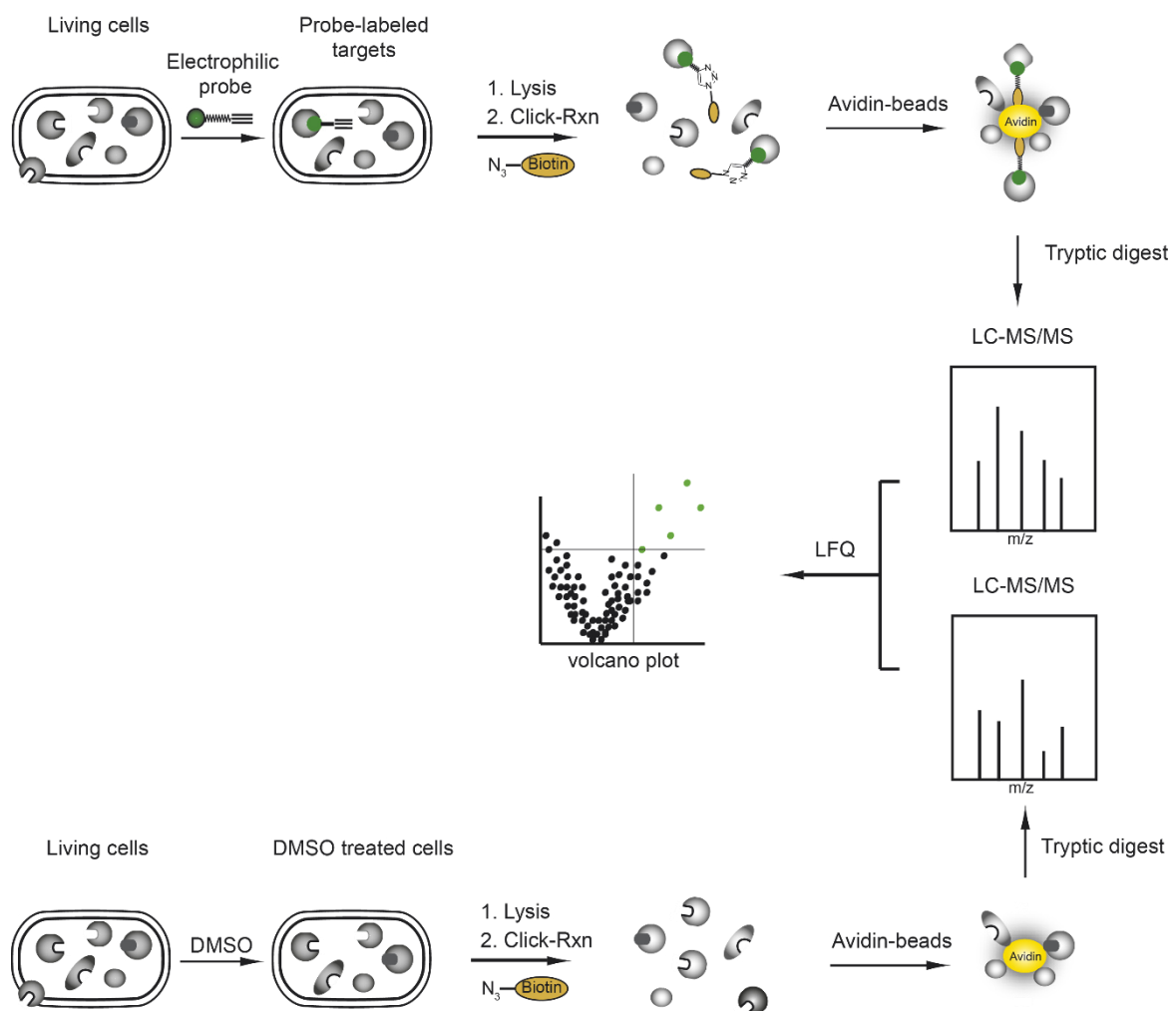
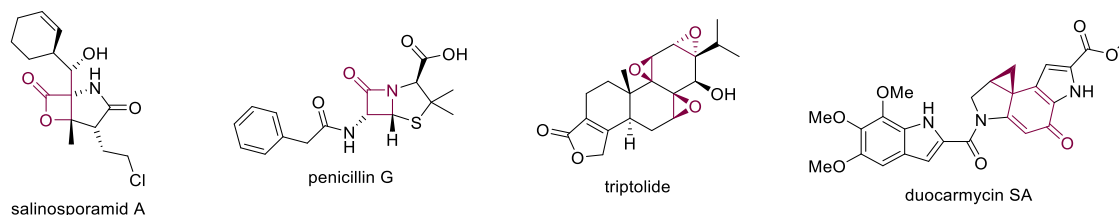


**Figure 1.5:** Workflow of label free ABPP (LFQ = label free quantification).

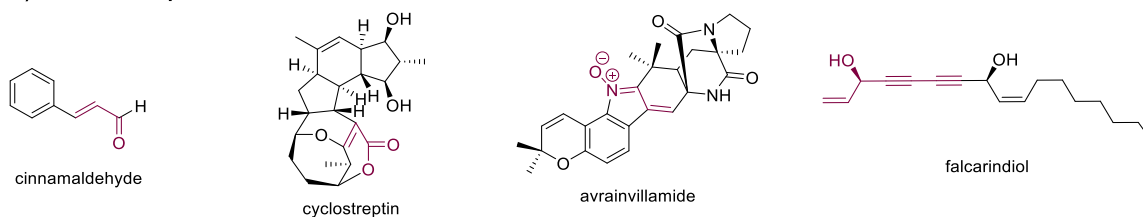
## 1.2 Electrophilic natural products and covalent inhibitors

The assignment of nucleophilicity and electrophilicity in nature is relatively clear. The main classes of the primary metabolites (DNA, proteins, sugars) possess only nucleophilic complexation while secondary metabolites like natural products cover the entire scope of reactivity. This and their structural variance and complexity make natural products the perfect tools to study, influence and understand life itself. As the interactions of natural products with biological systems depend on multiple variables, their activity is often hard to predict in a systematic manner. Distinct structure activity relationships however are found in one class of natural products: electrophilic natural products.<sup>25</sup> They possess electron deficient moieties, which can be attacked by the nucleophilic residues of proteins and nucleic acids. A covalent bond is then formed, which in many cases results in an irreversible inhibition of the biomolecules functionality. Among the most common electrophilic moieties in natural products are  $\beta$ -lactones<sup>26,27</sup> and  $\beta$ -lactams<sup>28–32</sup>, epoxides<sup>33–40</sup> and Michael acceptors.<sup>33,41,42–49</sup> but also disulfides,<sup>50,51</sup> chlorodihydroisoxazoles<sup>52,53</sup> and carbamates<sup>54</sup> are potent electrophiles (Figure 1.6).

### A) Ring strained scaffolds



### B) Michael acceptors



### C) Other electrophiles

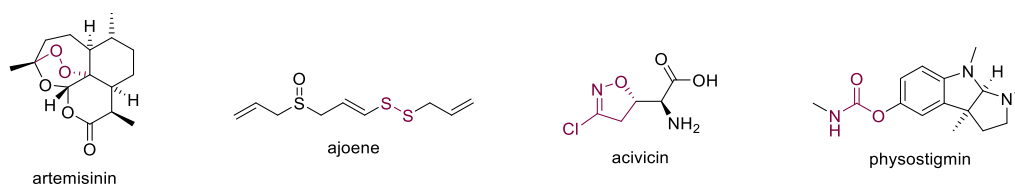


**Figure 1.6:** A selection of electrophilic natural products bearing different electrophilic groups.

An exception are endoperoxides, which require activation via Fe(II)-ions to form reactive oxygen species and biradicals. Technically, they do not belong to the electrophilic natural products, however there are mentioned here due to their ability to covalently modify

enzymes.<sup>55,56</sup> The scope of reactivity in these natural products is wide, addressing all potential nucleophilic sites in proteins, including alcohols (serine, threonine), thiols (cysteine) and amines (lysine, histidine).

Furthermore, covalently binding inhibitors display certain advantages over reversible ones. The chemical properties of an electrophile can be tuned to address a nucleophile with a specific reactivity pattern only present in a certain enzyme class. As the electrophile requires not only a specific reactivity but also a spatial fit to react with a nucleophile, high selectivity for a certain protein can be achieved even within a superfamily of enzymes with high structural homology.<sup>57-62</sup> Due to the strong covalent interaction formed between electrophile and enzyme, ligand efficiencies are extremely high in comparison to potential reversible binding, leading to higher stability and endurance of inhibition.<sup>63,64</sup> There have been concerns about possible side effects of covalent binding drugs due to non-specific covalent modifications, with the result that irreversible drugs have been generally avoided in the pharmaceutical industry in the last 20 years.<sup>65,66</sup> However, due to the safe usage of many covalent drugs for decades and recent developments in targeted covalent inhibitors (TCI)<sup>61</sup> as well as improved understanding of the pharmacologic basis of drug related toxicities (e.g. idiosyncratic drug reaction),<sup>65,67-72</sup> electrophilic drugs have experience a renaissance in recent years.<sup>73</sup> A selection of covalent drugs in use or in development is shown in Figure 1.7.

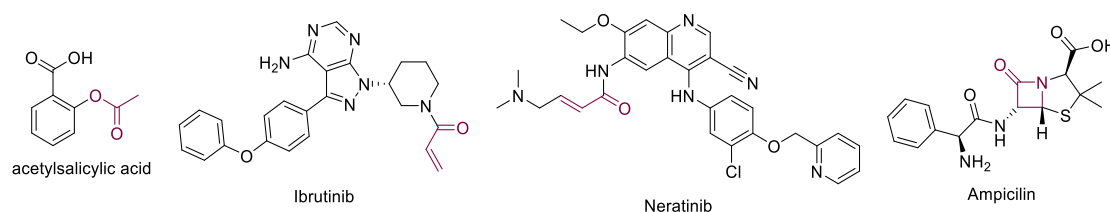


**Figure 1.7:** A selection of covalent drugs currently used (acetyl salicylic acid, Ibrutinib, Ampicillin) or in clinical trials (Neratinib). Electrophilic moiety highlighted in red.

### 1.3 Scope of this work

The essence of this work is target identification of covalently binding natural products in human cancer cells. To achieve this goal, ABPP methodology combined with state of the art quantitative mass spectrometry were applied. Furthermore, potential targets were validated involving overexpression of native proteins, activity assays and knockdown studies applying RNA interference.

**Chapter 2** describes work to understand the bioactivity of polyacetylenes such as falcarinol in human cancer cells. Simplified probes were synthesized and applied in *in situ* profiling of human cancer cell lines. In addition to elucidating covalent targets, a photoprobe was designed to unravel potential non-covalent proteome interactions of this natural product. Potential targets obtained by quantitative mass spectrometry were confirmed using activity based assays and binding site identification.

**Chapter 3** is concerned with the reliability of hits generated by photoaffinity labeling. The high number of non-specific background binders is a feature often encountered in profiling experiments with photocrosslinkers. A collection of background binders for common photocrosslinker systems, called the 'photome', was established to address this major difficulty in interpreting proteomic data.

The effects of the *Streptomyces* derived electrophilic natural product neocarzilin on human cancer cells is the subject of **chapter 4**. Covalent targets were identified by applying an activity-based probe derived from neocarzilin A and B. Furthermore the total synthesis of all known neocarzilins A-C enabled the investigation of their influence on cell migration and mitochondrial integrity in different metastatic cancer cell lines.

A graphical abstract illustrates the basic workflows in chapters 2-4 and how they are inter-related (Figure 1.8).



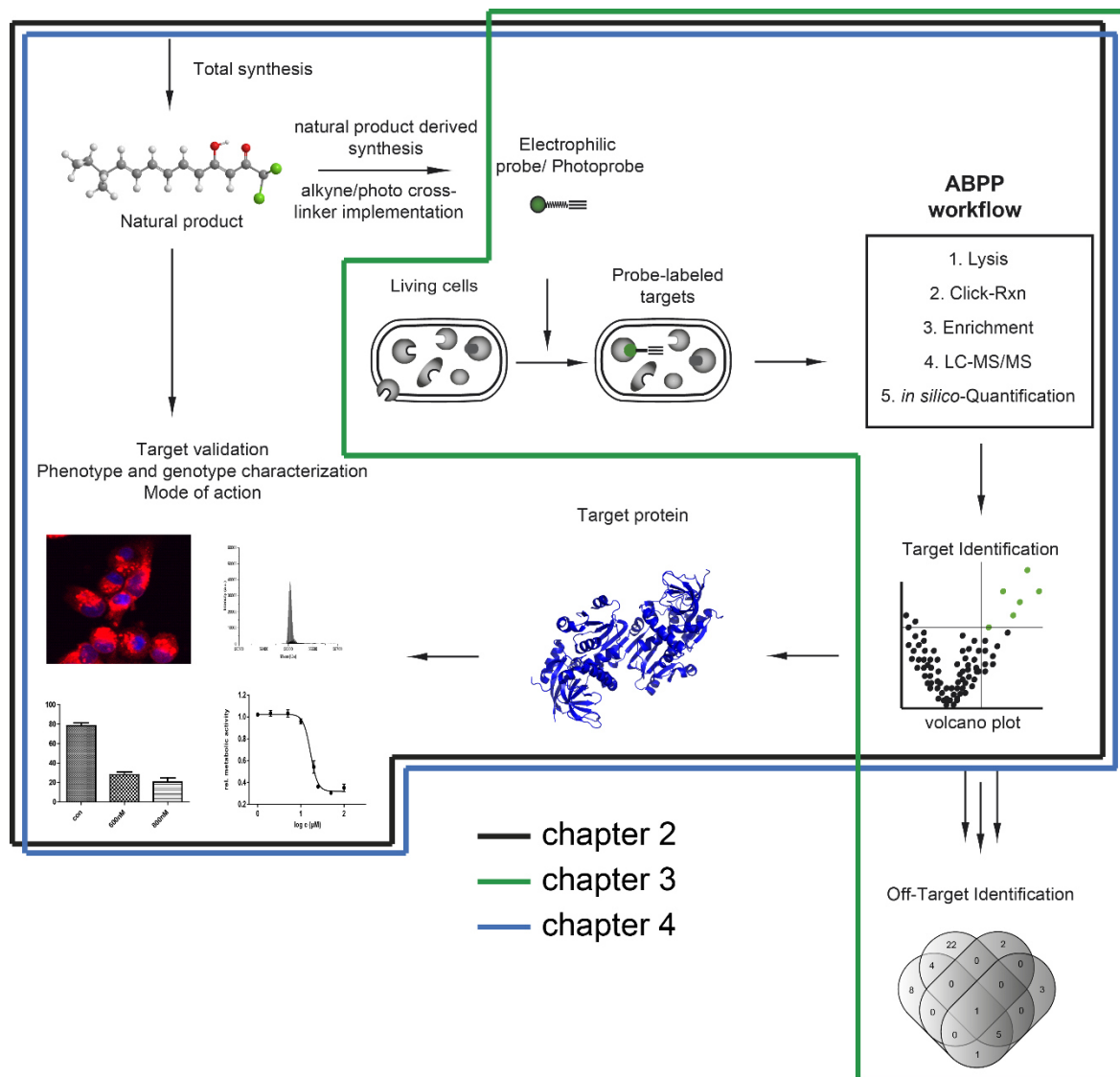


**Figure 1.8:** Scope of this work: Workflows for exploring the mode of action and targets of natural products. Different chapters deal with different parts of this workflow, as indicated.

This chapter is based on already published data:

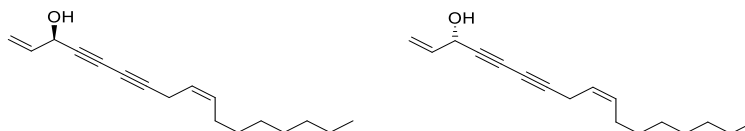
Heydenreuter, W., Kunold, E. & Sieber, S. A. Alkynol natural products target ALDH2 in cancer cells by irreversible binding to the active site. *Chem. Commun. (Camb)* **51**, 15784-15787 (2015).

## 2 Target identification of falcarinol in human cancer cells

### 2.1 Polyynes and falcarinol

Polyynes represent a vast group of highly lipophilic natural products with structurally diverse scaffolds. More than 1600 members have been isolated from various biological sources including plants,<sup>74,75</sup> fungi,<sup>76</sup> bacteria, corals and sponges.<sup>77–80</sup> The vast array of bioactivities of these compounds include antibacterial,<sup>81</sup> cytotoxic,<sup>77,82</sup> antifungal<sup>74</sup> and antiviral<sup>83</sup> properties.

The most prominent member of this class of natural products is falcarinol (**2.1**), also known as panaxynol. Both enantiomers of falcarinol have been isolated from various plants such as sickleweed (*Falcaria vulgaris*), Chinese ginseng (*Panax ginseng*), European ivy (*Hedera heix*) and different vegetables including parsley and carrots. Therefore, falcarinol has been the subject of various investigations, mostly in the field of nutrition and dietary research. Recent studies suggest that the health promoting and cancer protecting qualities of a carrot rich diet might result mainly from the hormesis effect of falcarinol and related polyacetylenes and not from  $\beta$ -carotene.<sup>84,85</sup> These results are also in accordance with a study attributing the anti-inflammatory properties of purple carrot cultivars to polyacetylenes.<sup>86</sup> However no molecular mechanism explaining these phenotypes has been elucidated so far.

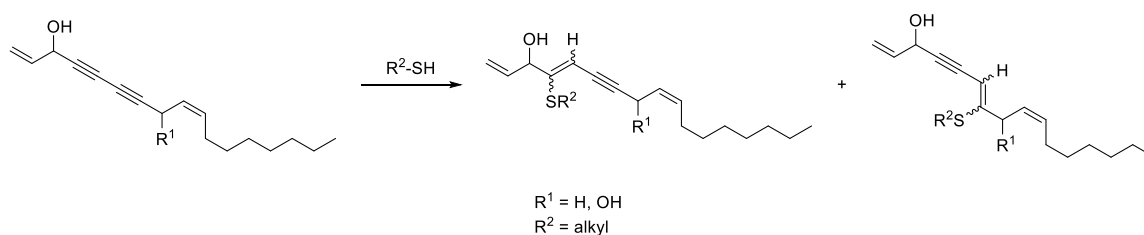


**Scheme 2.1:** (*R*)- and (*S*)- falcarinol.

Alongside these likely beneficial health effects, falcarinol also acts a strong irritant, causing allergic skin reactions when handling ivy.<sup>87</sup> These findings suggest that falcarinol and related compounds have the ability to covalently modify proteins.<sup>88,89</sup> Direct covalent modification *in vitro* was confirmed for the alkylation of the anandamide binding site of the cannabinoid receptor 1 (CB<sub>1</sub>). The associated dermatitis is believed to be a consequence of

falcarinol acting as an antagonist of CB<sub>1</sub> in keratinocytes, which results in increased chemokine expression and aggravation of histamine action.<sup>89</sup>

There have been different propositions concerning the mode of action of falcarinol. Previous studies suggested the formation of a stabilized carbocation at C3 under acidic conditions as the origin of its reactivity towards nucleophiles.<sup>88,90</sup> Although that might be the mode of action in some cases, the main reactivity of falcarinol (and related compounds) is attributed to the electrophilic diyne moiety, which acts as a Michael acceptor for soft nucleophiles like activated thiols (Scheme 2.2).<sup>91</sup>



**Scheme 2.2:** Reactivity of falcarinol and falcarindiol with thiols.

## 2.2 ALDH2

Aldehyde dehydrogenase 2 is the most prominent member of the aldehyde dehydrogenase superfamily, an enzyme class responsible for the degradation of reactive aldehydes to carboxylic acids. It is a homo tetramer in its native environment and the crucial enzyme for detoxification of both acetaldehyde, the primary degradation product of ethanol, and endogenous aldehyde metabolites and environmental toxins like 4-hydroxy-2-nonenal<sup>92,93</sup> and acrolein.<sup>94,95</sup> A point mutation at position 504 (E → K) leads to a completely inactive isoform, which has serious ramifications for aldehyde detoxification. Almost 50 % of the northeast Asian population are heterozygous for the variant gene, resulting in an accumulation of acetaldehyde after alcohol consumption as the resulting ALDH2\* displays only minor activity.<sup>96,97</sup> This so-called flushing syndrome is not only associated with toxification symptoms, but also with an 100-fold higher risk for esophageal cancer,<sup>98,99</sup> increased morbidity following myocardial infarction and increased risk for Alzheimer's disease and other neurodegenerative diseases associated with aging.<sup>100–103</sup>

As the name implies, ALDHs oxidize aldehydes to carboxylic acids. A thiolate anion derived from cysteine acts as the nucleophile in the active center to attack the carbonyl (Figure 2.1B) and the stabilized tetrameric intermediate then transfers a hydride to NAD or NADP (Figure 2.1C). The thioester is hydrolyzed to release the carboxylic acid as well as one

molecule of NADH/NADPH (Figure 2.1D-E). NAD/NADP is bound next to the active site and the cycle begins again.<sup>97</sup> This mode of action is highly conserved in all ALDHs, though each ALDH possesses unique substrate specificity.<sup>104</sup> ALDHs are bifunctional enzymes as they also possess esterase activity.<sup>105</sup>

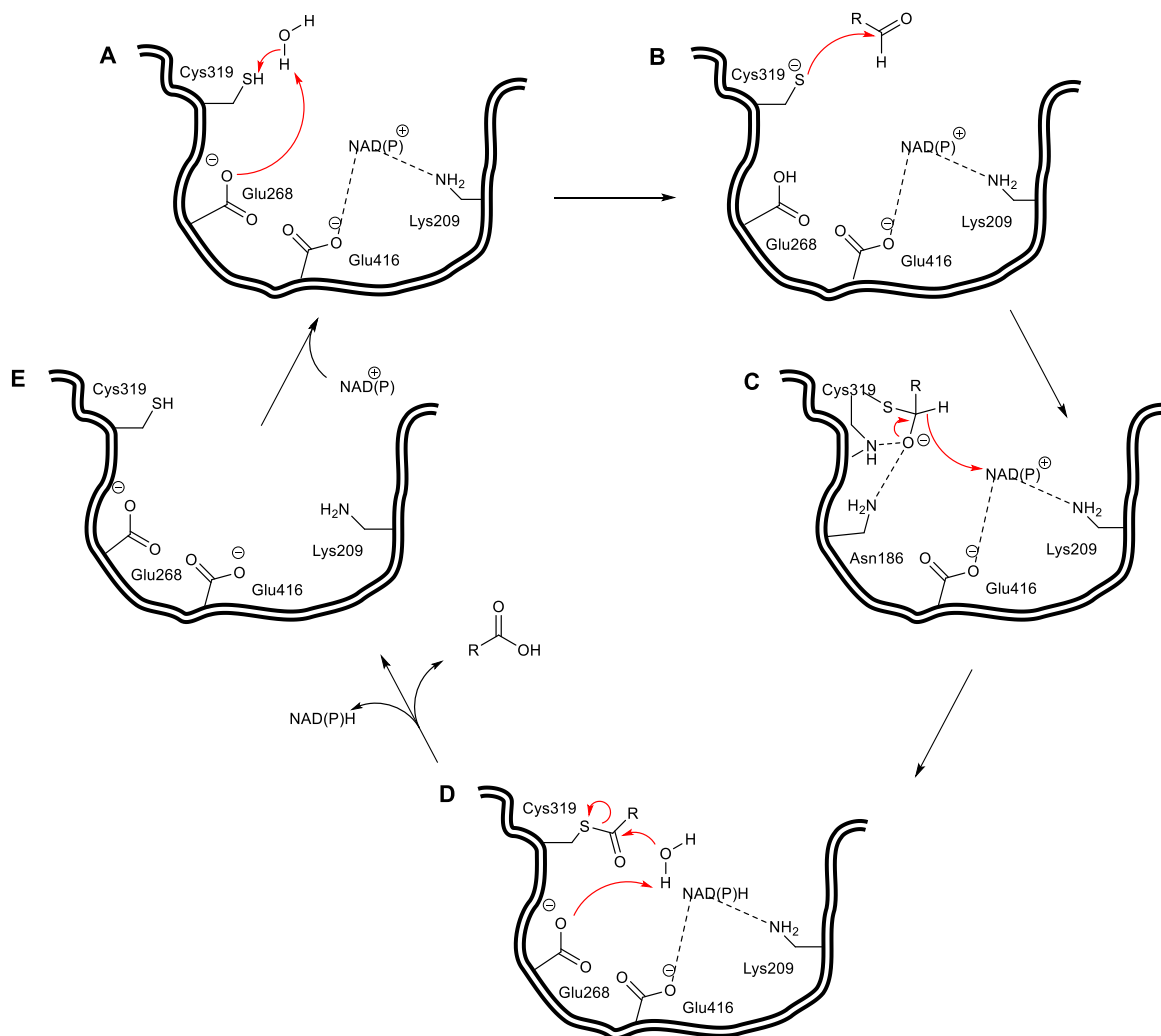


**Figure 2.1:** Mechanism of aldehyde oxidation in ALDH2.

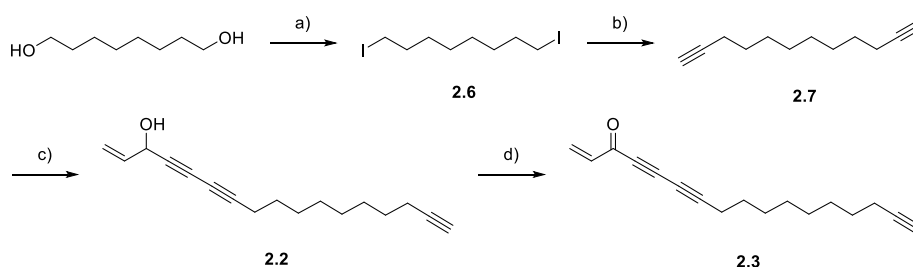
## 2.3 Results and discussion

### 2.3.1 Synthesis of activity-based probes

Although there have been a few reports about the molecular targets of falcarinol and falcarinol-like natural products, mechanistic analysis of the molecular mode of action and target identification in a full proteome scale are lacking. A SILAC-ABPP approach was recently used to unravel the molecular targets of callispongynic acid, a long chain polyene isolated from a marine sponge. A suite of metabolic enzymes was identified that are involved in the metabolism and degradation of lipids and fatty acids. This natural product however not only bears an polyene moiety but also a propargylic acid, which might be the main reason of its electrophilic nature.<sup>106</sup>

To unravel the molecular targets of falcarinol and related natural products, simplified probes for application in ABPP were designed. To capture the important structural features of falcarinol while keeping the structure simple and uncompromised, the reporter tag was attached at the end of the hydrophobic chain. The double bond at C9 was not included in the probes to facilitate synthesis. As both enantiomers of falcarinol are biologically active and have been isolated from natural sources, all probes were used as racemic mixtures.

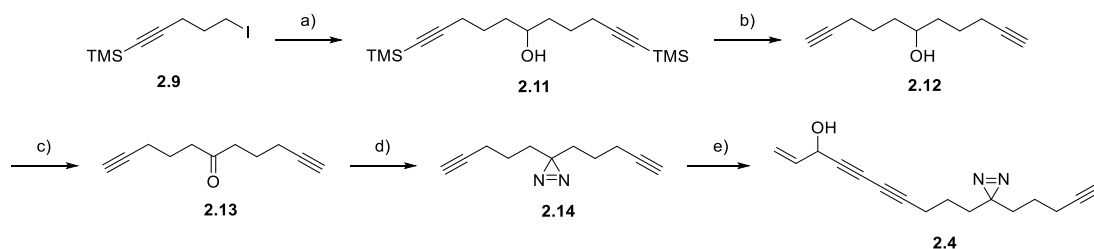
Falcarinol-inspired probe **2.2** was synthesized starting from 1,8-octandiol. Both hydroxyl groups were converted to the corresponding iodides **2.6** by tosylation and subsequent iodination under *Finkelstein* conditions. The iodide was treated with an excess of ((trimethylsilyl)ethynyl)-lithium in a THF/DMPU mixture to afford 1,11-dodecadiin (**2.7**) after removal of the TMS-groups. 5-bromopent-1-en-4-yn-3-ol (**2.8**) was synthesized in two steps from ethynyltrimethylsilane and acroleine followed by silver(I)-catalyzed Si-Br-exchange. Both fragments were coupled in a *Chadiot-Chodkiewicz* reaction to give probe **2.2**. Allylic oxidation with manganese(IV)-dioxide yielded the oxidized probe **2.3** (Scheme 2.3).



**Scheme 2.3:** Synthesis of probes **2** and **3**: a) 1. NEt<sub>3</sub> (4.00 eq), TsCl (2.10 eq), CH<sub>2</sub>Cl<sub>2</sub>; 2. NaI (2.00 eq), acetone, 0 °C → rt, 16 h, 71 %; b) 1. Ethynyltrimethyl-silane (2.30 eq), nBuLi (2.30 eq), THF, -78 °C; 2. 1 (1.00 eq), DMPU; 3. K<sub>2</sub>CO<sub>3</sub> (2.00 eq), MeOH, rt, 76 %; c) NH<sub>2</sub>OH.HCl, EtNH<sub>2</sub> (70-%), CuCl (10 mol-%), 5-bromopent-1-en-4-yn-3-ol (**2.8**) (3, 0.75 eq), MeOH, CH<sub>2</sub>Cl<sub>2</sub>, 0 °C → rt, 4h, 56 %; d) MnO<sub>2</sub> (20.0 eq), Et<sub>2</sub>O, rt, 4 h, 36 %.

To identify possible noncovalent binders of falcarinol, we devised a photoprobe to capture reversible targets by photoinduced alkylation. As there are several photocrosslinkers to choose from (see Chapter 3), the simple and linear structure of falcarinol made a modification of the scaffold unfeasible with large and bulky photoreactive groups like benzophenone and arylazide. The clear choice was a symmetric alkyl diazirine, which could be integrated into the alkyl chain without affecting the reactive hepta-1-en-4,6-diyn-3-ol-unit. Yao *et al.* demonstrated the utility of alkyldiazirines as effective photocrosslinkers by covalently linking known kinase inhibitors to their targets and identifying them via pulldown/MS analysis.<sup>107</sup>

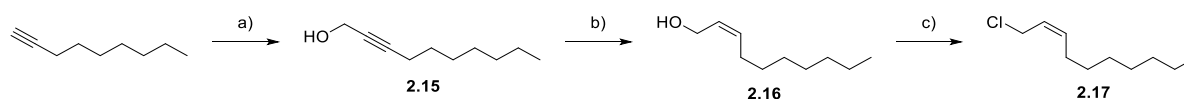
The synthesis of diazirine fragment **2.14** was accomplished in 4 steps starting from (5-iodopent-1-yn-1-yl)trimethylsilane (**2.9**). Lithium-halogen exchange with *tert*-butyl lithium and addition of the Li-organyl to 6-(trimethylsilyl)hex-5-ynal (**2.10**) yielded alcohol **2.11**. The TMS-groups were removed in quantitative yield to give **2.12**. Oxidation with PCC yielded the corresponding ketone **2.13**, which was further converted to diazirine **2.14**. Coupling with 5-bromopent-1-en-4-yn-3-ol (**2.8**) under similar conditions as described before for **2.2** gave photo probe **2.4** (Scheme 2.4).



**Scheme 2.4:** Synthesis of **4**: a) *t*BuLi (2.05 eq), 6-(trimethylsilyl)hex-5-ynal (**2.10**) (1.00 eq), Heptane/THF, -78 °C → rt, 16 h, 66%; b) K<sub>2</sub>CO<sub>3</sub> (2.30 eq), MeOH, rt, 16h, quant.; c) PCC (1.50 eq), CH<sub>2</sub>Cl<sub>2</sub>, rt, 12 h, 83%; d) 1. NH<sub>3</sub> (MeOH) (20.0 eq), H<sub>2</sub>NOSO<sub>3</sub>H (1.30 eq); 2. I<sub>2</sub>, MeOH, -10 °C → rt, 16 h, 30 %; e) NH<sub>2</sub>OH.HCl (0.33 eq), EtNH<sub>2</sub> (70-%), CuCl (10 mol-%), 5-bromo-pent-1-en-4-yn-3-ol (**2.8**) (0.75 eq), MeOH, CH<sub>2</sub>Cl<sub>2</sub>, 0 °C → rt, 4h, 31 %.

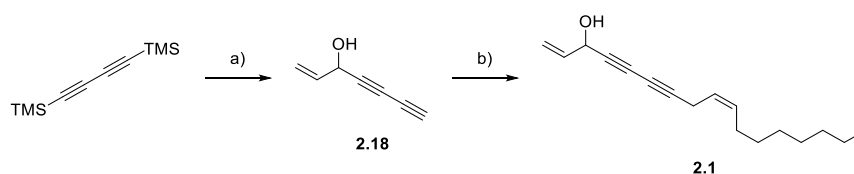
### 2.3.2 Total synthesis of falcarinol and stipudiol

For cell studies and validation of possible targets racemic falcarinol was synthesized according to the known procedure of McLaughlin *et al.*<sup>108</sup> The eastern part of falcarinol was synthesized in three steps beginning from commercially available 1-nonyne. The deprotonated alkyne was treated with paraformaldehyde to give the propargylic alcohol **2.15**. The hydrogenation of the alkyne under heterogenic catalysis using nickel boride (P-2) yielded the *Z*-olefin **2.16** in nearly quantitative yield. The conversion of the alcohol to the allyl chloride **2.17** was achieved by *Appel* reaction (Scheme 2.5).



**Scheme 2.5:** Synthesis of western part of falcarinol: a) nBuLi (1.10 eq), acroleine (1.20 eq), THF,  $-78\text{ }^{\circ}\text{C} \rightarrow \text{rt}$ , 93 %; b)  $\text{Ni}(\text{OAc})_2 \cdot 4\text{H}_2\text{O}$  (0.25 eq),  $\text{NaBH}_4$  (0.25 eq), 1,2-Diaminoethane (0.70 eq),  $\text{H}_2$  (1 atm), MeOH,  $0\text{ }^{\circ}\text{C} \rightarrow \text{rt}$ , 16 h, 99 %; c)  $\text{PPh}_3$  (1.20 eq),  $\text{CCl}_4$ ,  $80\text{ }^{\circ}\text{C}$ , 16 h, 94 %.

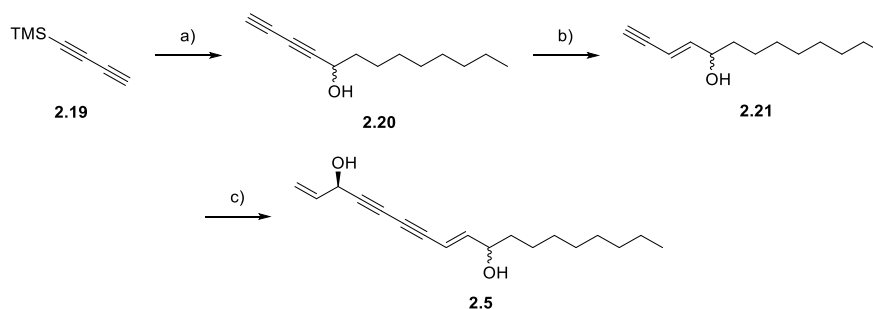
The western part of falcarinol, hepta-1-en-4,6-diyne-3-ol (**2.18**) was synthesized from commercially available 1,4-bis(trimethylsilyl)buta-1,3-diyne and acroleine in one step. Coupling of **2.17** and **2.18** under *Jeffrey-type*<sup>109</sup> conditions yielded racemic falcarinol (Scheme 2.6). It should be noted that large amounts of the undesired 1,3-coupling product were formed. Although a separation of both isomers were challenging, sufficient amounts of falcarinol could be isolated for biological evaluation.



**Scheme 2.6:** Completion of total synthesis of **1**: a) MeLi (1.00 eq), THF,  $0\text{ }^{\circ}\text{C}$ , 4 h; acroleine (1.10 eq),  $-78\text{ }^{\circ}\text{C} \rightarrow \text{rt}$ , 2 h; NaOH, THF/ $\text{H}_2\text{O}$ , rt, 1 h, 80 %; b)  $\text{Bu}_4\text{NCl}$  (1.12 eq),  $\text{K}_2\text{CO}_3$  (1.20 eq), CuCl (0.10 eq), **18** (1.05 eq), DMF, rt, 7 h, 71 % (+ 25 % 1,3-isomer).

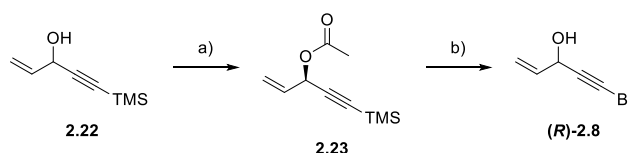
Since probes **2.2**, **2.3** and **2.4** were basically designed as simplified scaffolds of 1,4-bis(trimethylsilyl)buta-1,3-diyne- containing natural products, it was of interest to synthesize a natural product with a slightly different eastern fragment to determine if the results of the minimal approach were applicable to other polyynes. For this reason stipudiol, a C18 polyacetylene compound recently isolated from the rhizomes of *Panax stipuleanatus* was chosen. Stipudiol displayed strong cytotoxic effects in leukemia and colon cancer cell lines.<sup>110</sup>

First, the right fragment of stipudiol was generated, starting with the enantioselective addition of TMS-diyne **2.19** (TMS-diyne was generated by lithiation of 1,4-bis(trimethylsilyl)buta-1,3-diyne with MeLi at  $0\text{ }^{\circ}\text{C}$  and subsequent quenching with water)<sup>111</sup> to nonanal to generate alkynol **2.20**,<sup>112</sup> which was subsequently reduced to enyne **2.21** using  $\text{LiAlH}_4$ . Unfortunately, the enantioselectivity of the alkyne addition to the aldehyde was low (53 % ee). As there were no procedures available which demonstrated better selectivity, this reaction was not further optimized (Scheme 2.7).



**Scheme 2.7:** Total synthesis of stipudiol: a) 1. MeLi (1.10 eq), H<sub>2</sub>O; 2. (S)-binol (40 mol-%), Cy<sub>2</sub>NH (5 mol-%), ZnEt<sub>2</sub> (3.00 eq); 3. Ti(OiPr)<sub>4</sub> (1.00 eq) nonanal (1.00 eq); 4. 1 M NaOH, Et<sub>2</sub>O, THF, rt, 20 h, 58 %; b) LiAlH<sub>4</sub> (1.20 eq), THF, 0 °C → rt, 3 h (69 %); c) NH<sub>2</sub>OH.HCl (1.70 eq) ethylamine, (R)-5-bromopent-1-en-4-yn-3-ol ((R)-**9**, 1.20 eq), CuCl (9 mol-%), MeOH, 1.5 h, 66 %.

Optically pure (R)-5-bromopent-1-en-4-yn-3-ol ((R)-**2.8**) was obtained from 5-(trimethylsilyl)-pent-1-en-4-yn-3-ol (**2.22**) according to a literature procedure involving chiral resolution with *PS* Lipase (Scheme 2.8).<sup>113</sup>



**Scheme 2.8:** Synthesis of (R)-**2.8** employing chiral resolution of **2.23**.

To complete the total synthesis, **2.21** and (R)-**2.8** were converged employing *Chadiot-Chodkiewicz* coupling conditions as described before for probes **2.2** - **2.4**.

### 2.3.3 Bioactivity in eukaryotic cells and bacteria

To determine the effect on mammalian cells, evaluation of falcarinol related probes and stipudiol was initiated by screening these compounds against the human cancer cell lines A549 (lung adenocarcinoma) and HepG2 (hepatocellular carcinoma) in a MTT cytotoxicity assay. The cells were incubated for 24 h with different concentrations of probes and natural product. All compounds exhibited a moderate toxicity in the low micromolar range which was in accordance with previous reported data for falcarinol and suggested that the minor modifications did not alter biological activity significantly (Table 2.1).<sup>114,115,116</sup>



**Table 2.1:** IC<sub>50</sub> values (μM) of compounds **2.2** – **2.5** in A549 and HepG2. n.d. = not determined.

Compound	A549	HepG2
<b>2.2</b>	2.49 ± 0.06	n.d.
<b>2.3</b>	1.36 ± 0.30	3.05 ± 0.26
<b>2.4</b>	2.09 ± 0.42	1.93 ± 0.33
<b>2.5</b>	1.86 ± 0.28	n.d.

As it is known that falcarinol and related polyaceetylenes also possess antibacterial properties,<sup>74,117,118</sup> probes **2.2** – **2.4** were tested against *Staphylococcus aureus* NCTC and *Listeria monocytogenes*. All probes inhibited growth of *Staphylococcus aureus* NCTC at concentrations of 100 μM. Higher activities were observed in *Listeria monocytogenes*: 75-100 μM for **2.4**, 25-50 μM for **2.2** and less than 10 μM for **2.3**.

#### 2.3.4 Protein reactivity in human cancer cells

To gain an overview of possible protein targets, *in situ* ABPP experiments were conducted in A549 with probes **2.2** and **2.3**: the cells were incubated for 1 h in the IC<sub>50</sub> range (5 μM), lysed and treated with Rhodamine azide under click chemistry conditions.<sup>15,119,120</sup> Subsequent SDS-PAGE and fluorescent scanning revealed a prominent band between 50 and 60 kDa.

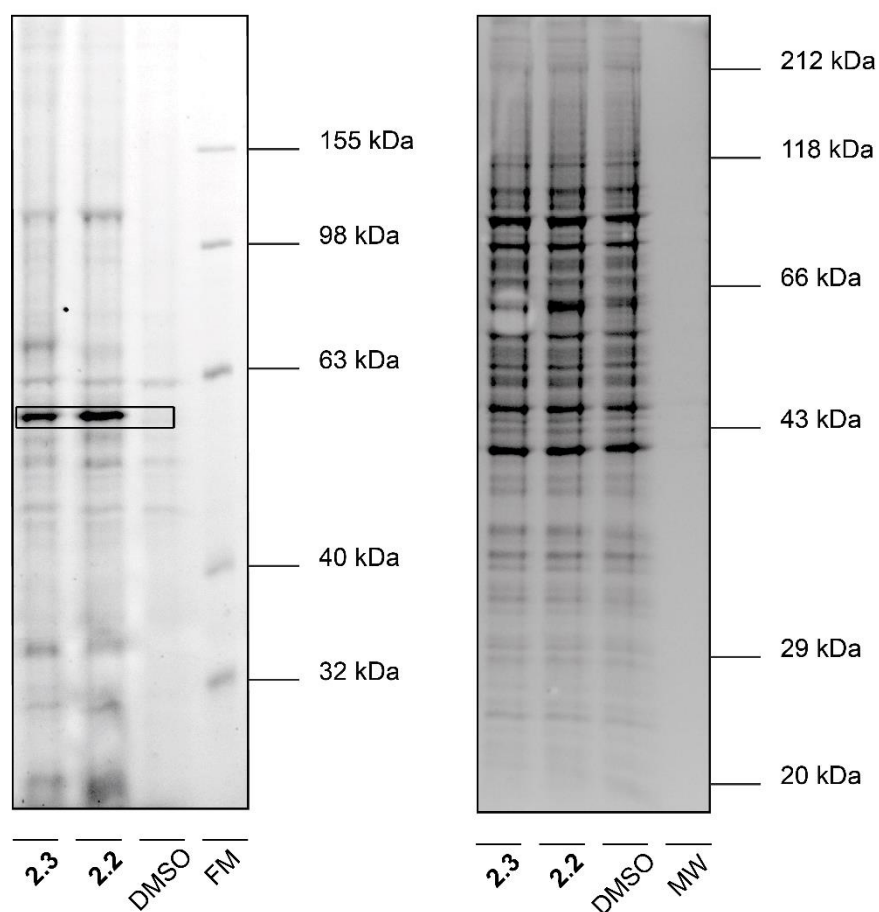


**Figure 2.2:** In situ labeling of A549 cells with alkyne-tagged probes. Fluorescent gel (left) and corresponding coomassie stain (right) after labeling with **2.2** and **2.3** (5  $\mu$ M, 1 h incubation). FM = fluorescent marker.

Since **2.3** showed a highly similar labeling pattern to **2.2** but cannot be activated by protonation and subsequent loss of water, a carbocation is unlikely to be the reactive intermediate.

First gel-based preparative ABPP employing a trifunctional rhodamine-biotin-azide for enrichment and visualization was applied.<sup>121</sup> The tagged proteins were enriched and upon preparative SDS-PAGE, the 60-kDa band was isolated, digested and analyzed via LC-MS/MS. MS analysis revealed aldehyde dehydrogenase 2 (ALDH2) as a possible irreversible target. To validate this result and to identify possible covalent and noncovalent targets in a gel-free approach, we utilized photoprobe **2.4** and A549 cells with either heavy or light isotope-labeled amino acids (SILAC).<sup>19</sup> After incubation with **2.4** for 1 h, the cells were irradiated with long wave UV light (360 nm) for 30 min and lysed. Subsequent click reaction with biotin-azide was followed by enrichment over avidin beads. The enriched proteins were digested with trypsin and analyzed by LC-MS/MS. Again, ALDH2 was one of the most prominent hits; other hits included heme oxygenase 2 (HMOX2), homo sapiens

translocase of outer mitochondrial membrane 22 homolog (TOMM22), cytochrome b5 Type B (CYB5B), serum paraoxonase/lactonase 3 (PON3) and cathepsin D (CTSD).

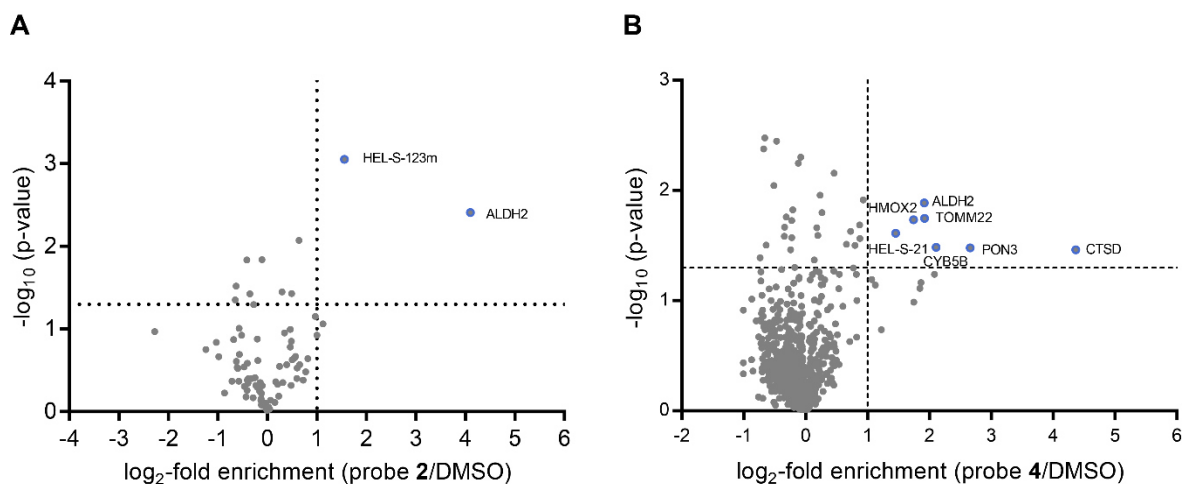


**Figure 2.3:** A) Gel-based LC-MS/MS identification of ALDH2 as a target protein of **2**. The volcano plot shows the statistical significance of proteins (student's t-test p-value, FDR corrected), that were identified from the gel band (55 – 60 kDa, Figure 2.2). Ratios were calculated from MS1 intensities of proteins cut from the band (probe **2**-treated proteome) or cut from the corresponding gel area from the DMSO-treated proteome. B) Quantitative proteome enrichment analysis of **4** treated A549 cells compared to DMSO treated control after irradiation, click reaction with biotin azide and pull-down with avidin beads. The volcano plot shows the statistical significance of enrichment levels (student's t-test p-value) as a function of average protein ratios from three biological replicates in probe-treated vs. control cells.

Due to the strong enrichment of ALDH2 in both gel-based and gel-free approaches, this protein was chosen for further evaluation regarding binding mode and inhibition properties. To confirm that ALDH2 was a covalent target, recombinant ALDH2 (Abnova) was spiked into A549 cell lysate and incubated with different concentrations of **2.2**. To ensure that correct folding of protein was required for binding, a control portion of ALDH2 was heat-denatured at 96 °C prior to incubation. Dose dependent labeling of ALDH2 was observed, as apparent from the appearance of two strong bands in the A549 proteome. This was expected as the recombinant ALDH2 has a lower molecular mass than the native one (Figure 2.4).

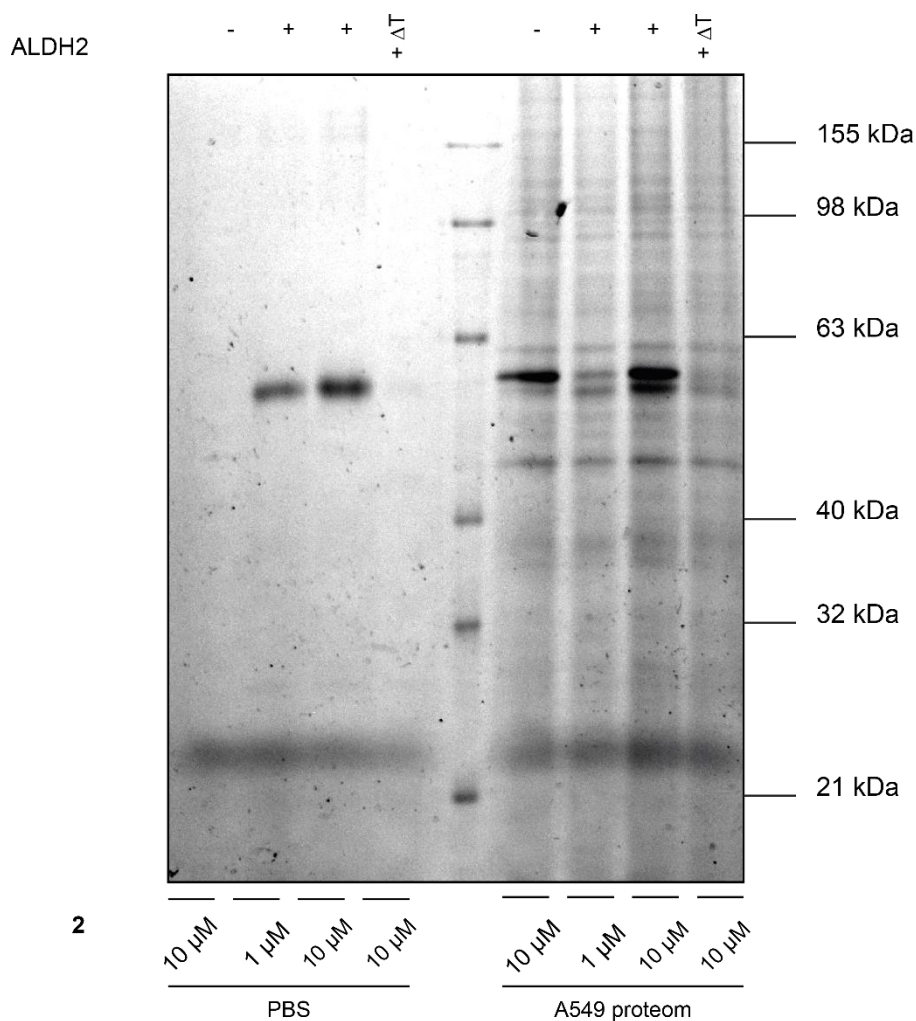


**Figure 2.4:** Labelling of recombinant ALDH2 (in PBS) and spiking of ALDH2 in A549 proteome; M(ALDH2 recomb.) = 54.6 kDa, M(ALDH2 nat.) = 56.4 kDa.

Since it was now clear that ALDH2 was covalently modified by falcarinol-type natural products, the truncated protein (protein without mitochondrial transit peptide) bearing a His-tag was overexpressed in *E. coli* to determine the binding site and inhibition kinetics. The purified protein was incubated with natural products **2.1** and **2.5** in Tris buffer at rt for 3 h and the residual activity measured in a NAD<sup>+</sup>-coupled assay.<sup>122,123</sup> A 25-fold excess of falcarinol almost completely inhibited ALDH2 while stipudiol reduced the activity only to approximately 50 % after that particular timeframe (Figure 5D). The residual activity was in good agreement with the level of alkylation in ALDH2 (Figure 5A-C).

ALDH2 contains a triade of reactive cysteines in its catalytic center (Cys318-320). Cys319 is the nucleophile of the active site and needs to be deprotonated for a nucleophilic attack on aldehydes. The confidence for alkylation of non-catalytic cys320 was higher than 90 % and although the experiment was repeated several times under different conditions, the fragmentation spectra did not allow for an unequivocal assignment of any one of the three

cysteine residues in the active site as the definitive binding site of the compound (Figure 2.5).

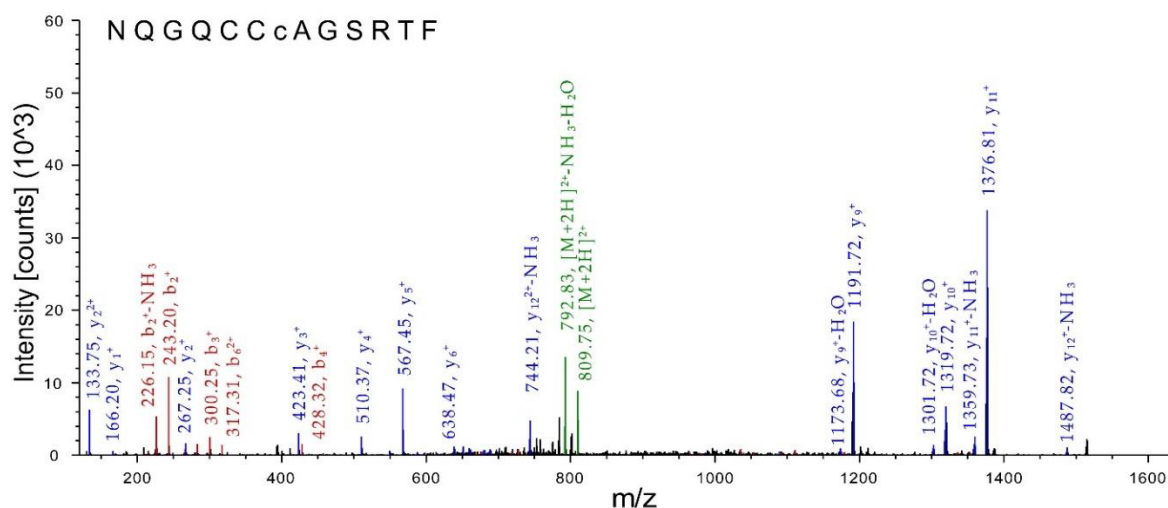


**Figure 2.5:** Fragment spectrum of the peptide NQGQCCAGSRTF (2+, m/z = 809.862 Da), which has been confidently identified (1 % FDR) carrying one falcarinol-modification (SEQUEST, -0.45 ppm, XCorr: 3.50). Localization probability of 0.94, determined using ptmRS, points to C7 (C320 in ALDH2) as the binding site.

It would be, however, not unusual if the catalytic cys319 were not the site of falcarinol binding. *Koch et al.* revealed that duorcamin, a strong alkylating natural product, inhibits ALDH1A1 by binding to cys302, a cysteine adjacent to the active site cys301.<sup>124</sup> ALDH1A1 shows high sequence homology to ALDH2 and is also capable of oxidizing aliphatic aldehydes with various chain lengths. As ALDH2 features a narrow hydrophobic channel leading to the active site, binding to one of the cysteines in the active center leads to complete blockage of the channel and the active site. This assumption is supported by the fact that the chemical chaperon Alda-1<sup>125,103</sup> was unable to restore catalytic function of ALDH2 once the protein was completely alkylated by falcarinol. Furthermore only monoalkylation of the protein was observed, suggesting that the remaining cysteines in proximity to the active site are blocked (Data not shown here).

To quantify the potency and binding kinetics of falcarinol and stipudiol towards ALDH2, the kinetic parameters  $K_i$  and  $k_{inact}$  were determined according to Kitz and Wilson via time-dependent inhibition measurements, due to the covalent and irreversible nature of the inhibition. With a  $K_i$  of 2.95  $\mu\text{M}$  and  $k_{inact}$  of 0.32  $\text{h}^{-1}$ , falcarinol displays similar inhibitory activity towards ALDH2 to known inhibitors.<sup>97</sup> Although the  $K_i$  value of stipudiol is reduced to ca. 20  $\mu\text{M}$ , ALDH2 represents a mutual target for both natural products (Figure 2.5E,F).

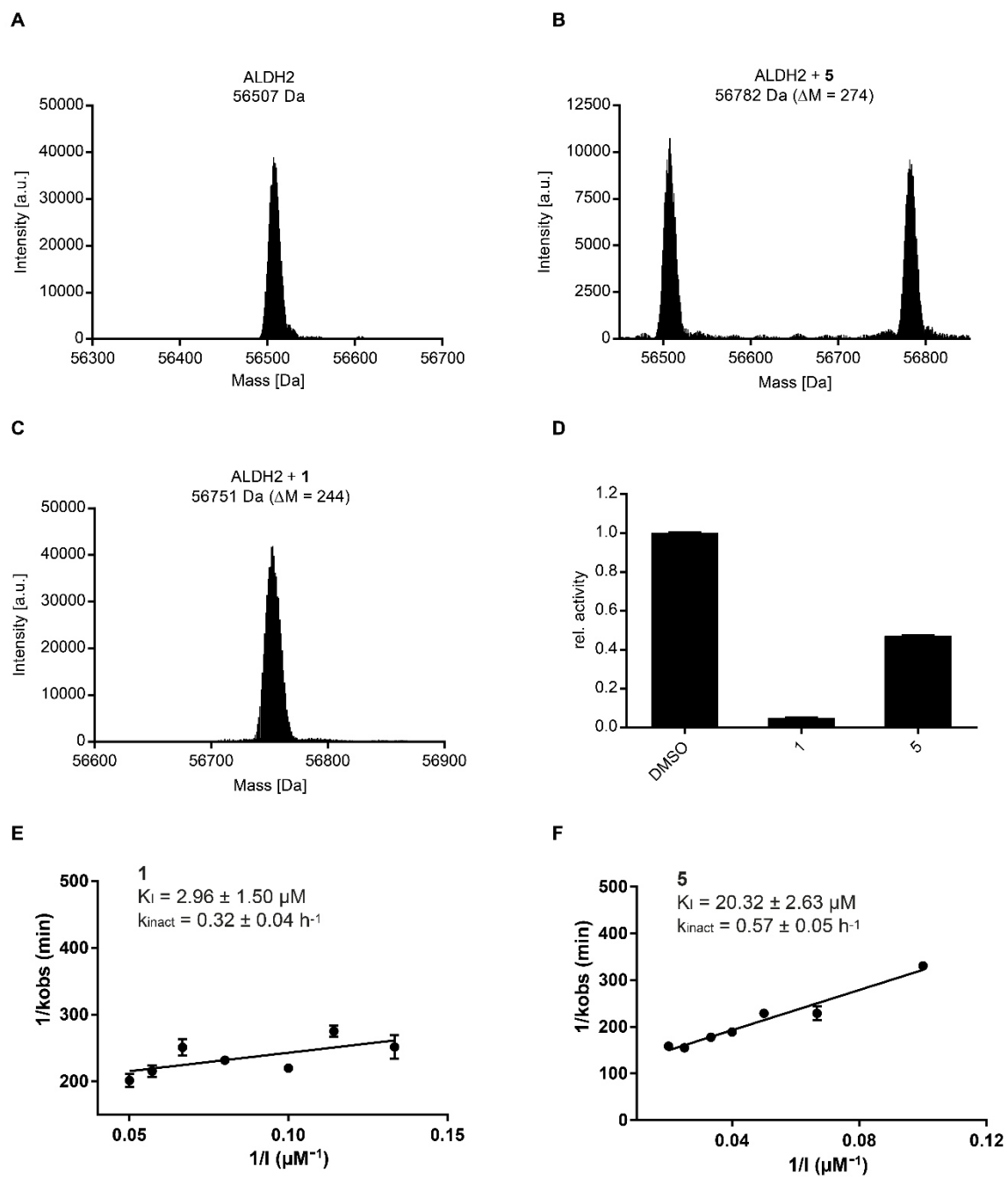


**Figure 2.6:** Full-length protein masses of ALDH2 (A), ALDH2 + 2.5 (B) and ALDH2 + 2.1 (C) and residual activity of ALDH2 after incubation (25x, 3h, rt) with 2.1 and 2.5 (D). Determination of  $K_i$  and  $k_{inact}$  according to the method of Kitz and Wilson for falcarinol (2.1, E) and stipudiol (2.5, F) with ALDH2 ( $n = 3$ ).

## 2.4 Concluding remarks and outlook

In summary, ALDH2 was identified here as a mutual target of falcarinol-like natural products, a new inhibitor class for this important metabolic enzyme. The aim was to design minimal activity based probes to identify covalent binding partners of falcarinol and related natural products in a full proteome approach. Extending this principle to affinity based protein profiling by introduction of a photolabile diazirine to unravel noncovalent protein interactions of falcarinol, revealed half a dozen significantly enriched proteins. The assessment of these hits was conducted in conjunction with a whole proteome inventory of diazirine dependent non-specific binding in human cells (see chapter 3).

Since ALDH2 is a major enzyme for aldehyde detoxification, the synthesized probes might serve as valuable tools to further study the inhibition of ALDH2 and its impact on cellular function. Although inhibition of ALDH2 leads to an increase reactive aldehydes and therefore elevated cellular stress and increased DNA damage and apoptosis rates,<sup>99,126–128</sup> even the complete knockout of this enzyme does not account for the relative high cytotoxicity of falcarinol-like compounds.<sup>129</sup> While inhibition of ALDH2 by falcarinol might contribute to its toxicity, the phenotype is likely also linked to a different cellular target not identified or validated in this study. As the potential hormesis effects of falcarinol and related compounds have not been elucidated so far either, further study of these natural products applying proteomics might be a rewarding endeavor. Furthermore, these probes could be readily applied to unravel the origin of their antimicrobial properties in *Staphylococcus aureus* and *Listeria monocytogenes*.

The following chapter is based on data submitted for publication:

Kleiner, P., Heydenreuter, W., Stahl, M., Korotkov, V. S., Sieber, S. A. A whole proteome inventory of background photocrosslinker binding. *Submitted*.

P. Kleiner, W. Heydenreuter and V.S. Korotkov synthesized probes. P. Kleiner and W. Heydenreuter performed labelling experiments, executed proteome enrichments and ran mass spectrometry measurements. P. Kleiner and M. Stahl analyzed data. M. Stahl developed and created overlays and conducted bioinformatics analyses. S.A. Sieber designed the research and wrote the manuscript with input from all authors.

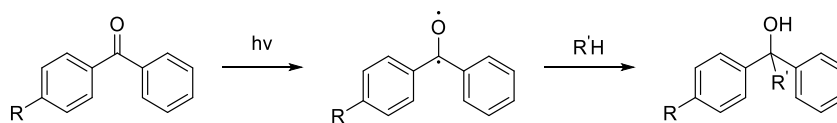
## **3 A whole proteome inventory of background photocrosslinker binding**

### **3.1 Photocrosslinkers**

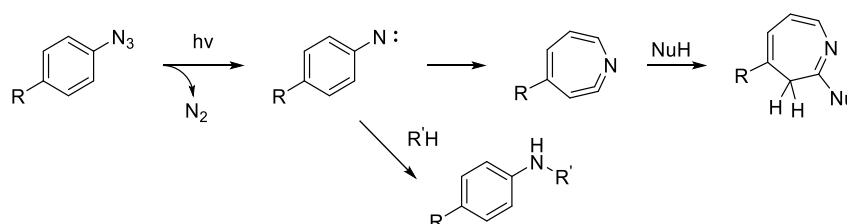
Photocrosslinkers are chemically inert groups that form extremely reactive intermediates upon irradiation with UV light. These reactive species are capable of forming covalent bonds with molecular structures in the vicinity. There are three types of photo crosslinkers currently commonly used in chemical and biological applications: Benzophenones, aryl azides and diazirines (scheme 3.1). While benzophenones form a reversible biradical intermediate upon radiation with UV light, the excitations of aryl azides and diazirines is followed by the loss of N<sub>2</sub> which leads to reactive 6-electron species, nitrene and carbene, respectively. The reversibility of the benzophenone excitation was thought to be advantageous as a biradical which is not in close proximity to a molecule for binding relaxes back to its ground state. It can then undergo further excitation until it forms a covalent bond to a molecule in its vicinity.<sup>130</sup> However this reversibility and the large size of the benzophenone pharmacophore is responsible for high background binding.<sup>131,132</sup> Arylazides irreversible form reactive singlet nitrenes upon radiation with UV and subsequent loss of nitrogen. Two main disadvantages can limit their application in biochemical experiments: 1. The absorption wavelength is quite short (250-280 nm) which could cause photolytic damage to biomolecules. 2. The predominant reaction path of the singlet nitrene is the rearrangement to 1,2-didehydroazepine, an intermediate susceptible to nucleophilic attack, but not reactive enough to insert into R-H (R = C;N,S;O) bonds.<sup>133,134</sup>



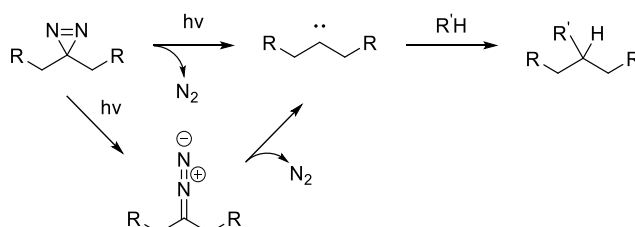
A) Benzophenone



B) Arylazide



C) Diazirine



**Scheme 3.1:** Different photo crosslinkers and their fragmentation patterns after irradiation with UV. (R = H, alkyl, aryl etc.; R' stands for any group containing bonds with hydrogen).

Diverse modifications to compensate for these drawbacks have been made. The shift of the absorption maxima to higher wavelength can be achieved by attaching electron-withdrawing moieties like nitro groups to the aromatic ring. However, this also increases steric bulk and reduces solubility. Platz *et al.* were able to suppress ring expansion by introducing fluorine substituents at both *ortho*-positions, leading to increased half-lives of the resulting nitrenes.<sup>135</sup>

Currently the most popular group of photocrosslinkers are the diazirines (alkyl- and arylsubstituted). They combine high reactivity with minimal steric bulk and high chemical stability.<sup>136,137</sup> The resulting carbene inserts rapidly into R-H (R = C;N,S;O) bonds. If there is no binding partner in close proximity, the carbene is quenched by the surrounding solvent or forms a stable olefin product by rearrangement in the excited state (RIES).<sup>130,138,139</sup> The excited state can rearrange to the diazoisomer, which slowly decomposes to the carbene.<sup>140-142</sup> This undesirable side product forms in different amounts depending on the substitution pattern of the diazirine,<sup>137</sup> contributing to non-specific protein labeling.<sup>140-142</sup>

The behavior of these three photo crosslinkers in a cellular context as well as their crosslinking efficiency has been the subject of several studies. While dialkyldiazirines were favored due to their small size and reactivity, the investigations demonstrated that optimal crosslinking results are not only dependent on the intrinsic photochemical properties and the nature of the protein-ligand interaction but also the balance between crosslink and quenching of the reactive intermediate (Figure 3.1).<sup>143,144</sup> To assess behavior and non-specific binding in particular of the three standard crosslinker systems currently in use in chemical proteomics, a set of these photocrosslinkers embedded in minimal aromatic and aliphatic structures was synthesized and their binding patterns analyzed using SILAC-AfBPP (Affinity based protein profiling).

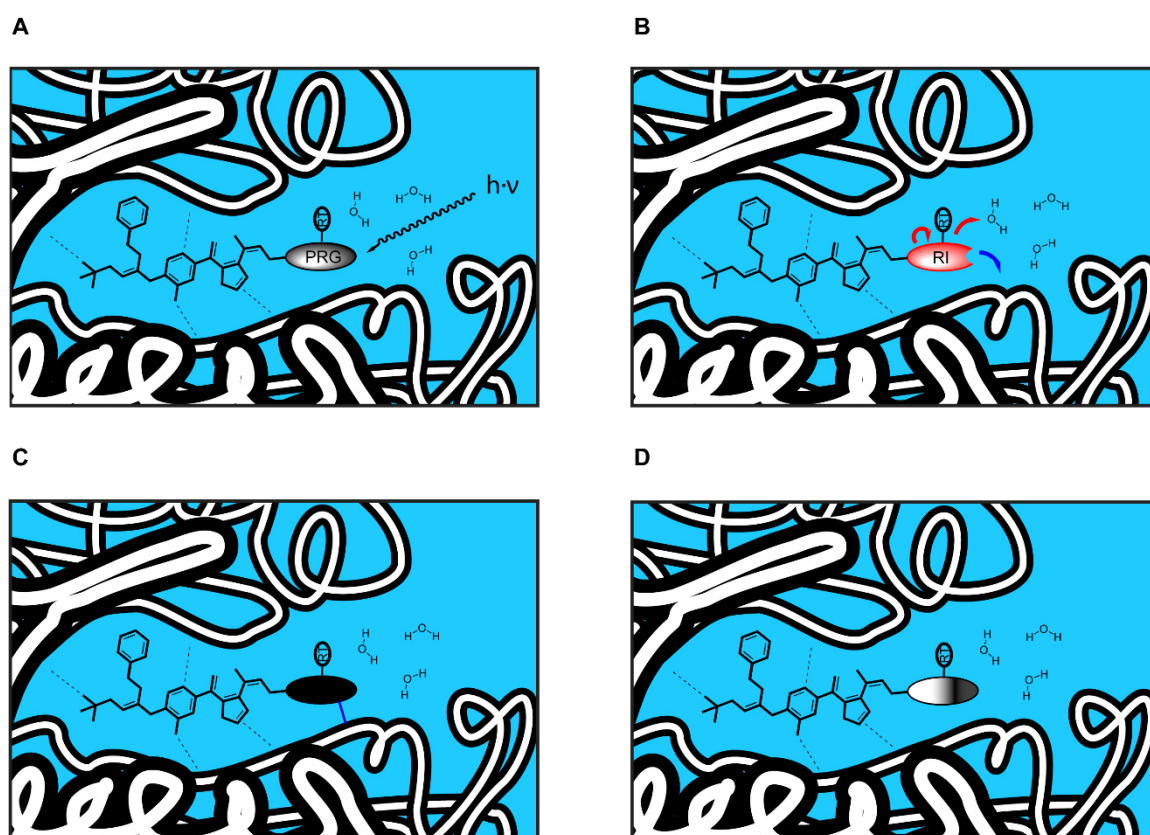


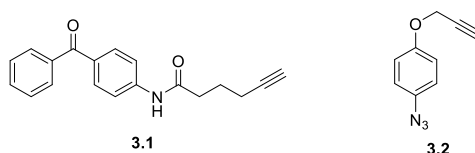
**Figure 3.1:** Interaction of ligand bearing a photoprobe with target protein. A) A noncovalent interaction between small molecule and protein structure. The photoreactive group (PRG) carrying a reporter tag (RT) is activated through UV irradiation. B) PRG decomposes to form reactive intermediates (RI) like 6-electron intermediates (carbenes, nitrenes) or biradicals. The three main paths are: (i) intramolecular reaction to form stable product or return to the ground state, respectively. (ii) Quenching of RI with surrounding water (red arrows). (iii) Insertion into R-H (R = C, O, N, S) bonds (blue arrow). C) Insertion leads to small molecule covalently attached to the protein. D) Irreversible photo crosslinkers: reactive moiety decomposed, no further activation via UV light possible. Reversible photo crosslinkers: excitation to form reactive intermediate possible  $\rightarrow$  B.

## 3.2 Results and discussion

ABPP is powerful method for the identification of molecular targets of covalent binding probes. However, most interactions between a ligand and a protein are of a noncovalent nature, mediated by H-bond bridges, ionic interactions and *Van der Waals* forces. Techniques that employ harsh denaturing conditions like proteomic enrichment and mass-spectrometry (MS) identification would normally not be suitable to study these rather fragile interactions. To circumvent this problem, small molecules can be modified with a photo crosslinker that enables them to form a covalent bond to a structure in the vicinity upon radiation with UV light. This AfBPP (Affinity based protein profiling) is an established method for target identification of small molecules in cells. Although the crosslinking properties of photocrosslinkers and their suitability for biochemical studies have been intensively studied, there have been only a few reports about non-specific photocrosslinker-associated off-target binding.<sup>145</sup> The knowledge of this “photome”, however, is crucial for identifying true targets and distinguishing them from common, photocrosslinker-specific off-targets.

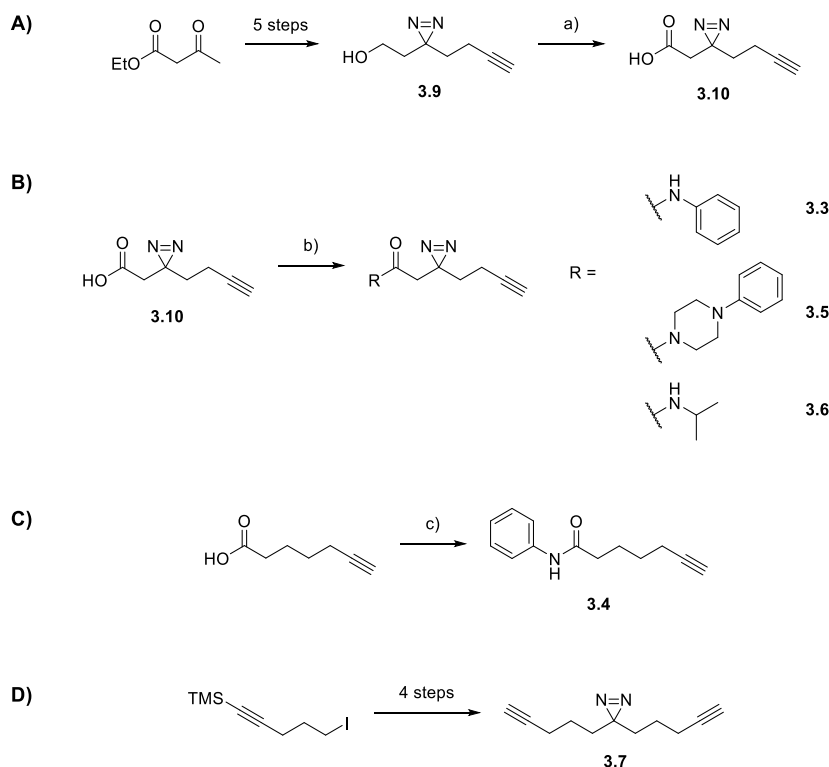
### 3.2.1 Synthesis of minimal photoprobes

To obtain a global overview of specific photocrosslinker-related targets, a library of probes containing benzophenones, arylazides and diazirines was synthesized. To reduce the ligand interactions to a minimum, the photo reactive groups were integrated into small molecular scaffolds which were equipped with a terminal alkyne for subsequent modification and analysis via click chemistry. As this approach was mainly focused on diazirines, only two minimal photocrosslinkers bearing a benzophenone and an aryl azide were synthesized. Benzophenone probe **3.1** was obtained by coupling of commercially available 4-aminobenzophenone and 5-hexynoic acid using standard peptide coupling conditions. The direct propargylation of 4-azidophenol resulted in aryl azide probe **3.2** (scheme 2).<sup>146</sup>



**Scheme 3.2:** Structure of minimal benzophenone probe **3.1** and arylazide probe **3.2**.

3 of 4 diazirine probes were based on the minimal diazirine photocrosslinker developed by Yao *et al.*<sup>107</sup> Oxidation of alcohol **3.8** yielded carboxylic acid **3.9** which was amidated with different primary and secondary amines to give probes **3.3**, **3.5** and **3.6**. Click control **3.4** was synthesized by the coupling of aniline with 5-hexynoic acid. Finally, minimal diazirine **3.7** was synthesized according to an already established procedure (see chapter 2).



**Scheme 3.3:** Synthesis of minimal diazirine probes. A) Synthesis of minimal diazirine containing carboxylic acid: a) Jones reagent (4.00 eq), acetone, 0 °C, 2 h, 88 %. B) Synthesis of minimal photoprobes **3.3**, **3.5** and **3.6**. b) HOBt (1.50 eq), EDCI (1.50 eq), DIPEA (2.00 eq), DMF, rt, 16 h, 77 % for **3.3**, 92 % for **3.4**, 89 % for **3.5**. C) Synthesis of click control **3.4**. c) b) HOBt (1.50 eq), EDCI (1.50 eq), DIPEA (2.00 eq), DMF, rt, 16 h, 99 %. D) Synthesis of symmetric diazirin probe **3.7**.

### 3.2.2 Protein reactivity in human cancer cells A549 and HeLa

To determine the light induced proteome binding of the minimal photoprobes, the two commonly used human cancer cell lines A549 and HeLa were chosen as test systems. The cells were incubated for 1 h at a concentration of 10  $\mu$ M and irradiated at appropriate wavelengths (320-360 nm for benzophenone and diazirine, 280-300 nm for arylazide). The cells were lysed, clicked to Rhodamine azide and analyzed on SDS-PAGE via fluorescent scanning. As expected, probes showed strong labelling in the soluble fraction, indicating good cell permeability, although cell lysis was performed using SDS-detergent, which also solubilizes some membrane proteins. Benzophenone **3.1** showed the strongest labelling, probably a result of the large pharmacophore and the reversibility of its biradical intermediate. The labelling pattern of all diazirine probes was nearly identical while the intensity was similar to that of arylazide **3.2** (figure 3.2). Although negative control **3.4** possessed neither electrophilic nor photo-inducible reactivity, a similar labelling pattern as for the diazirine probes was observed. As this is highly unusual, it might be the result of metabolic degradation of the probe or the result of photolytic generation of reactive intermediates during irradiation.

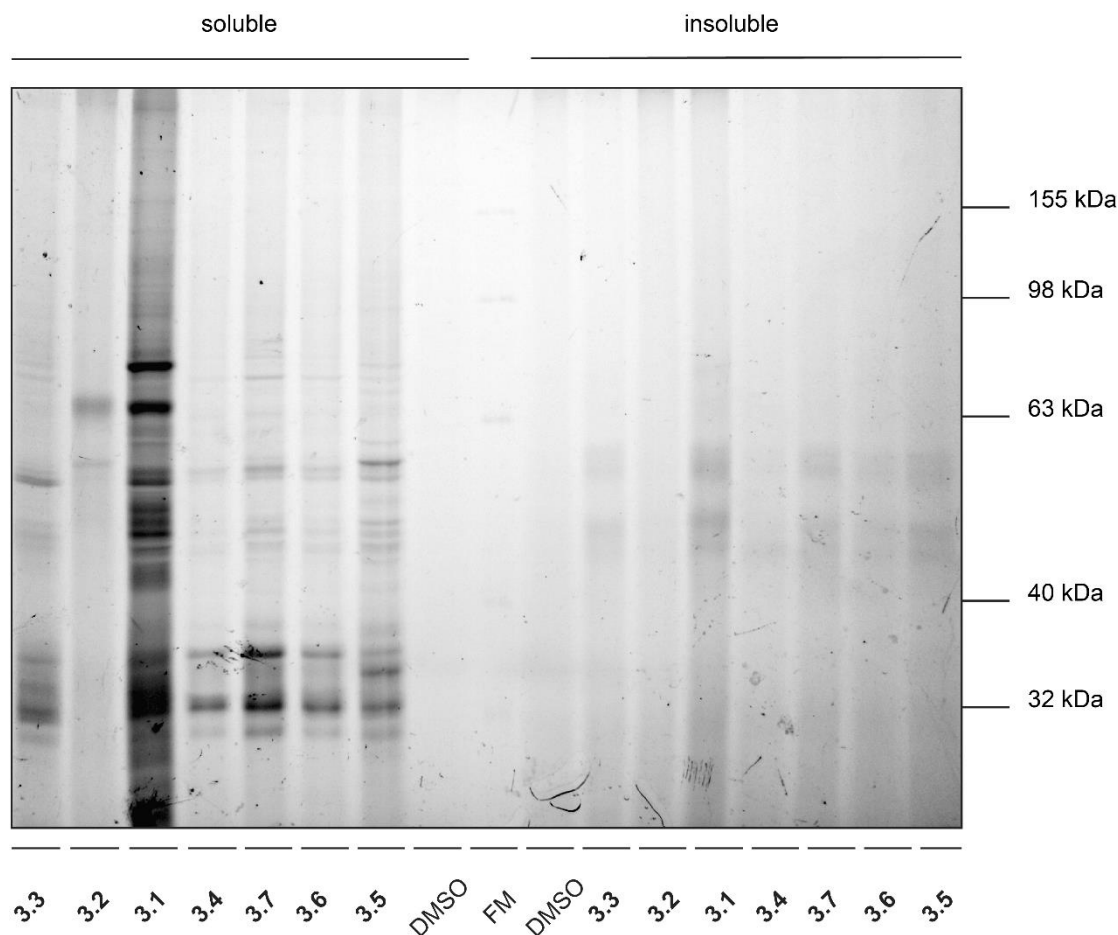


**Figure 3.2:** *In situ* analytical labeling with minimal photoprobes (**3.1** benzophenone, **3.2** aryl azide, **3.3**, **3.5-3.7** diazirine, **3.4** click control) in A549 (10  $\mu$ M, 30 min irradiation time).

### 3.2.3 Gel-free analysis of photocrosslinker-specific targets via quantitative proteomics

To quantify labelling of all probes in live cells gel-free proteomics with SILAC was applied.<sup>19</sup> As discussed in chapter 1, this method is currently the best method for target identification using AfBPP. Heavy and light cells were incubated with probe (3  $\mu$ M) or DMSO, irradiated, lysed and the states mixed. After enrichment and subsequent digestion with trypsin, the peptides were analyzed by high resolution liquid chromatography tandem MS (LC-MS/MS). The comparison and quantification of probe labelled states with those incubated with DMSO gave enrichment factors which were plotted against the negative decadic logarithm of the corresponding p-values.  $\log_2$  ratios of  $> 1$  (enrichment factor  $> 2$ ) with a  $p$ -value of  $< 0.05$  were regarded as significant hits. The comparison of benzophenone probe **3.1** with aryl azide **3.2**, phenyl-substituted diazirine **3.3** and negative control **3.4** reflected the analytical labelling, as the benzophenone probe resulted in strong enrichment of multiple proteins, while only a few hits were obtained with diazirine and arylazide probes (figure 3.3).

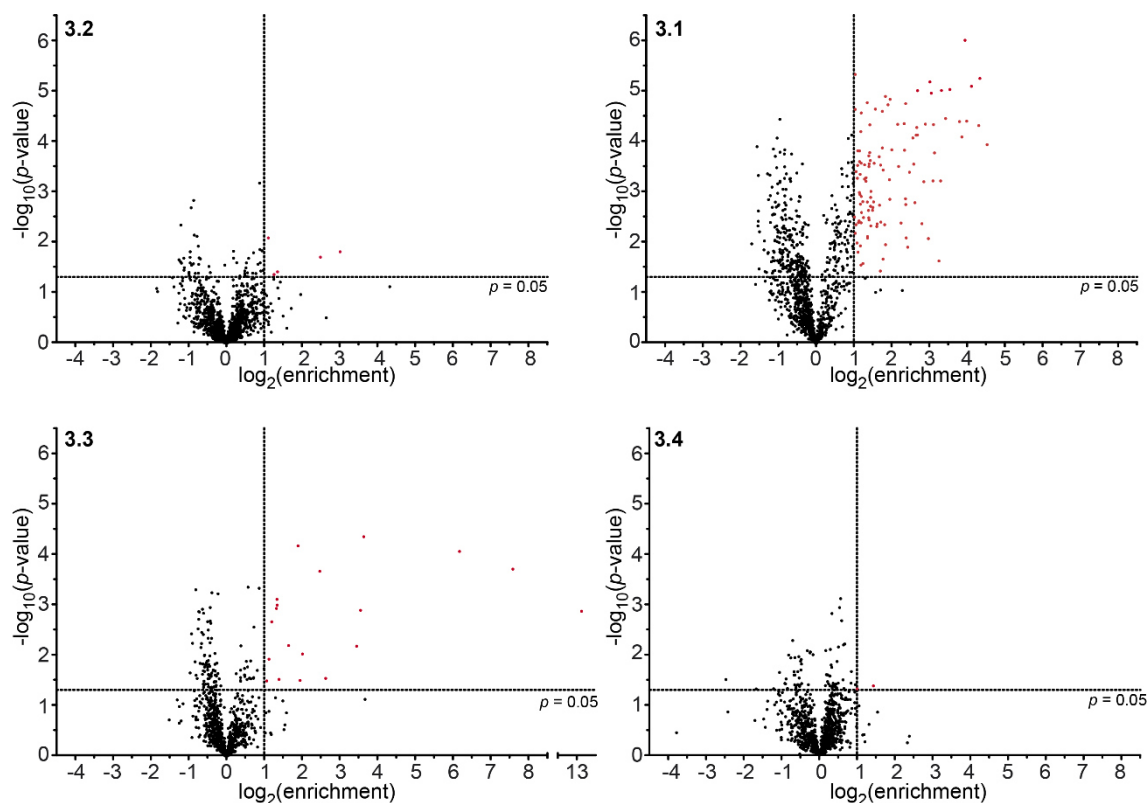


**Figure 3.3:** Volcano plots of enriched proteins in SILAC experiments with the three basic photocrosslinkers **3.1** (benzophenone), **3.2** (aryl azide), **3.3** (diazirine) and negative control **3.4** in A549. A  $\log_2(\text{enrichment})$  of 1 equates to an enrichment of 2 of probe labeled state over DMSO control. All protein hits in compliance with specified parameters for a significant hit ( $\log_2(\text{enrichment}) > 1$ ,  $p\text{-value} < 0.05$ ) are highlighted in red.

Interestingly, many more significantly enriched proteins were obtained when conducting this experiment in HeLa cells. Furthermore, the hits obtained were specific for each type of photocrosslinker with only marginal overlap between the different probes and no single protein found in all samples. The results of all four probes are summarized in Venn diagrams for A549 and HeLa (Figure 3.4).

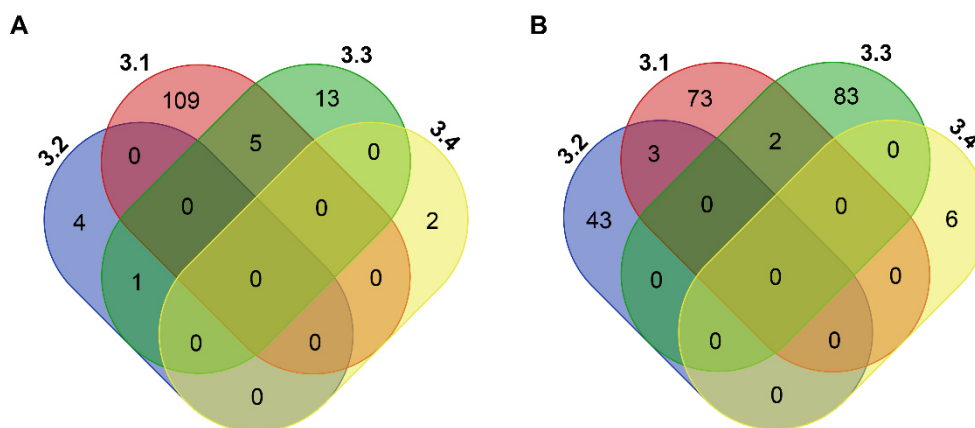


**Figure 3.4:** Venn diagram of significantly enriched proteins for probes **3.1** – **3.4** in A549 (A) and HeLa (B).

While the missing overlap of hits of different photocrosslinkers is not surprising due to their distinct structural differences, their variable behaviour in different cell lines is unexpected. Erratic performance levels on MS instruments as well as different protein concentrations during enrichment and storage of peptides might also contribute to divergent levels of identified peptides.

### 3.2.4 Diazirine-specific photome

Since diazirines are privileged photocrosslinker systems due to their size and reactivity and frequently used systems in chemical biology,<sup>107,147</sup> the protein binding properties of probes **3.5**, **3.6** and **3.7** were also investigated in a gel free approach in A549 and HeLa. Probe **3.5** displayed the most intense labelling, followed by probe **3.7**. In A549, these results correlate well with the different potential interaction sites on the probes. Probe **3.5** possesses a secondary amine which has ambivalent character since it can function as a H-bond acceptor or a H-bond donor. The tertiary amine could also function as a H-bond acceptor, while the benzene ring can interact with other aromatic residues via  $\pi$ -stacking. These chemical properties increase the probability of probe-protein interaction and covalent linkage in case of photo activation. The long aliphatic chain of **3.7** might preferentially bind to larger hydrophobic parts resulting in higher binding affinities than **3.6** which is structurally limited due to its small size. Structural differences might be also responsible for the minor overlap of only one protein significantly enriched in all diazirines in A549, although analytical gel analysis suggested higher similarity. The overlap between different probes was even lower in HeLa, although the total number of enriched proteins was higher. This fact also illustrates the importance of considering cell line-specific differences in photo affinity labelling.

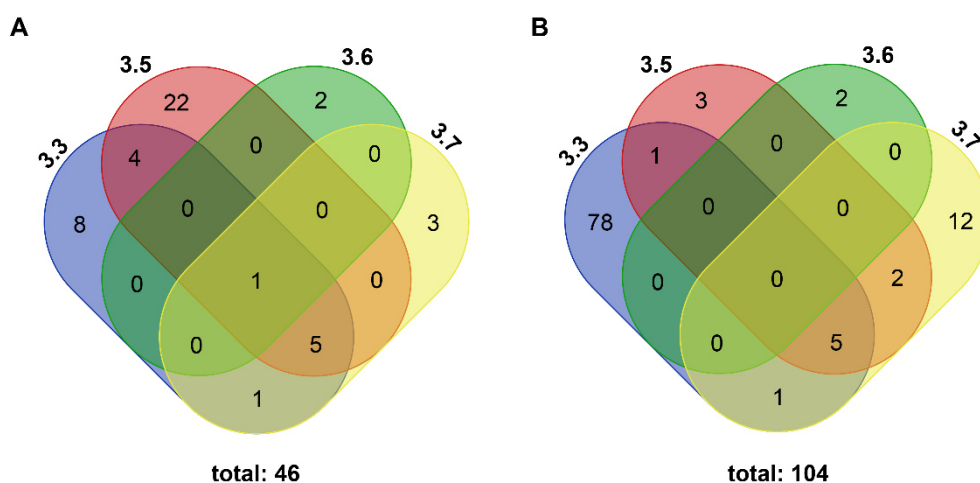


**Figure 3.5:** Venn diagram of significantly enriched proteins for diazirine probes **3.3**, **3.5-3.7** in A549 (A) and HeLa (B).

To obtain a global overview of diazirine photo background, the logarithmised enrichment ratios of all diazirine probes were merged by common majority protein IDs, summed up and normalized by the number of valid values (only proteins with at least 3 quantified enrichment ratios out of 6 replicates were included). Since the average ratios of unenriched proteins becomes zero after application of the logarithm, the photocrosslinker-specific targets are summed up over all samples, whereas scaffold-specific protein groups reside in the noise.

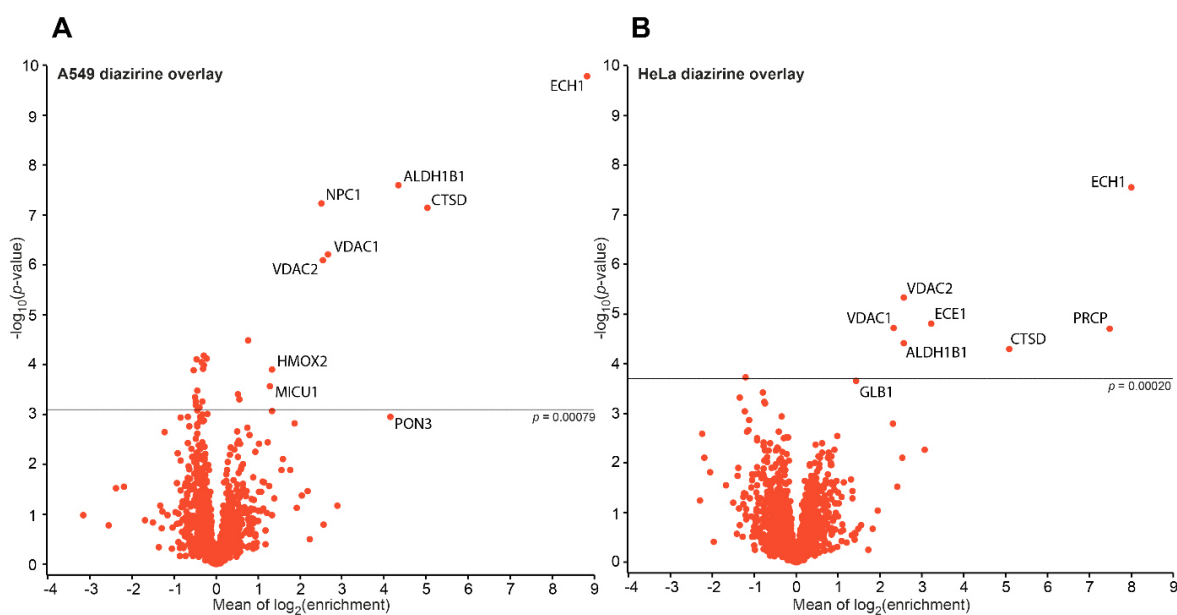


**Figure 3.6:** A) Volcano plot of the combined and overlaid AfBPP results in A549 cells. In order to compile a main list of highly significant photome members, the significance level was adjusted to  $p = 0.00079$  by the method of Benjamini and Hochberg ( $FDR = 0.05$ ). B) Volcano plot for the experiments with HeLa cells. The significance level was corrected to  $p = 0.00020$ .

The sum volcano blots revealed overall nine significantly enriched proteins in A549 and eight in HeLa (Figure 3.6). The detected proteins VDAC1 (Voltage-dependent anion-selective channel protein 1), VDAC2 (Voltage-dependent anion-selective channel protein 2), CTSD (Cathepsin D) and ECH1 (Delta(3,5)-Delta(2,4)-dienoyl-CoA isomerase, mitochondrial) were found in both cell lines. The proteins could be classified into three superfamilies:<sup>148,149</sup> (i) channels or channel-associated proteins (e.g. VDAC1&2), (ii) catabolic enzymes (e.g. CTSD) and (iii) small molecule binders (e.g. ALDH1B1). The VDACS, for example, are highly abundant channels that allow the diffusion of small molecules through the mitochondrial outer membrane.<sup>150</sup> Light-dependent activation and covalent binding to the channel during passage through might explain why these proteins are labelled with different diazirines. A similar mode of action can be assumed for metabolic enzymes such as ALDH1B1 and ECH1, which are responsible for degrading not only cell-derived metabolites but also substances of foreign origin like drugs or toxins. Considering the particularly high expression levels of metabolic enzymes in cancer cells, the small



number of proteins hit by diazirine minimal probes demonstrate the utility of this photocrosslinking group for affinity-based target identification. Since these protein are overall enriched among all diazirine probes regardless of their structural differences, it is reasonable to mark them as nonspecific background binders and exclude them in future diazirine based target identifications. A compilation of all protein hits in A549 and HeLa together with their abundance (iBAQ), function and localisation is given in Table 3.1. (iBAQ, intensity-based absolute quantification: In iBAQ, the sum of intensities of all tryptic peptides for each protein is divided by the number of theoretically observable peptides. The resulting iBAQ intensities provide an accurate determination of the relative abundance of all proteins identified in a sample.)<sup>151–153</sup>

**Table 3.1:** Diazirine photome exclusion list (Hits with a minimum  $\log_2(\text{enrichment})$  of 1 and a minimum Benjamini-Hochberg significance level of  $p = 0.00079$  (A549) or  $p = 0.00020$  (HeLa, FDR = 0.05) were selected from Figures 3.6A and 3.6B. Where a significant hit in one cell line was not enriched in the other, the non-significant enrichment value is given and indicated in the table with \*. iBAQ abundances were taken from ProteomicsDB.<sup>154</sup>

Protein name	Gene name	Cell line	Mean of $\log_2$ enrichment	Detected x times out of 6 with probe				Abundance $\log_{10}$ (iBAQ)	Function	Localisation
				DA-1	DA-2	DA-3	DA-4			
Delta(3,5)-Delta(2,4)-dienoyl-CoA isomerase	ECH1	A549	8.83	6	6	6	6	6.56	beta-oxidation	mitochondrion, peroxisome
		HeLa	8.01	6	4	2	6	5.90		
Cathepsin D	CTSD	A549	5.04	6	6	6	6	6.51	protease	lysosome
		HeLa	5.10	4	4	2	6	5.94		
Aldehyde dehydrogenase X	ALDH1B1	A549	4.34	6	6	4	6	5.69	acetaldehyde detoxification	mitochondrion
		HeLa	2.57	6	6	6	6	5.99		
Niemann-Pick C1 protein	NPC1	A549	2.51	6	6	6	6	5.00	cholesterol transporter	lysosome
		HeLa	1.95*	0	3	0	0	4.84		
Voltage-dependent anion-selective channel protein 1	VDAC1	A549	2.67	6	6	6	6	7.14	hydrophilic porin	mitochondrion
		HeLa	2.32	6	6	6	6	6.81		
Voltage-dependent anion-selective channel protein 2	VDAC2	A549	2.54	6	6	6	6	6.91	hydrophilic porin	mitochondrion
		HeLa	2.57	6	6	6	6	6.57		
Heme oxygenase 2	HMOX2	A549	1.33	6	6	3	4	5.44	heme degradation	ER
		HeLa	0.55*	5	3	4	3	5.44		
Lysosomal Pro-X carboxypeptidase	PRCP	A549	-	-	-	-	-	4.58	protease	lysosome
		HeLa	7.48	0	5	0	4	5.31		
Endothelin-converting enzyme 1	ECE1	A549	-	-	-	-	-	4.18	endothelin cleavage	lysosome
		HeLa	3.22	4	5	1	6	5.32		
Calcium uptake protein 1	MICU1	A549	1.27	2	4	0	3	4.63	associated with $\text{Ca}^{2+}$ transporter	mitochondrion
		HeLa	0.37*	1	2	1	3	4.59		

To evaluate the general utility of the photome exclusion list, an analysis of the proteomic data obtained by applying a falcarinol derived photoprobe in A549 was conducted (see chapter 2). ALDH2 was previously identified and validated as a covalent target of this probe. However, several additional non-covalent targets also met the criteria for significant enrichment. Most of these could be excluded by comparison to the photome list, an indication for the applicability of this concept to future target identifications involving diazirine photo crosslinkers (Figure 3.7).

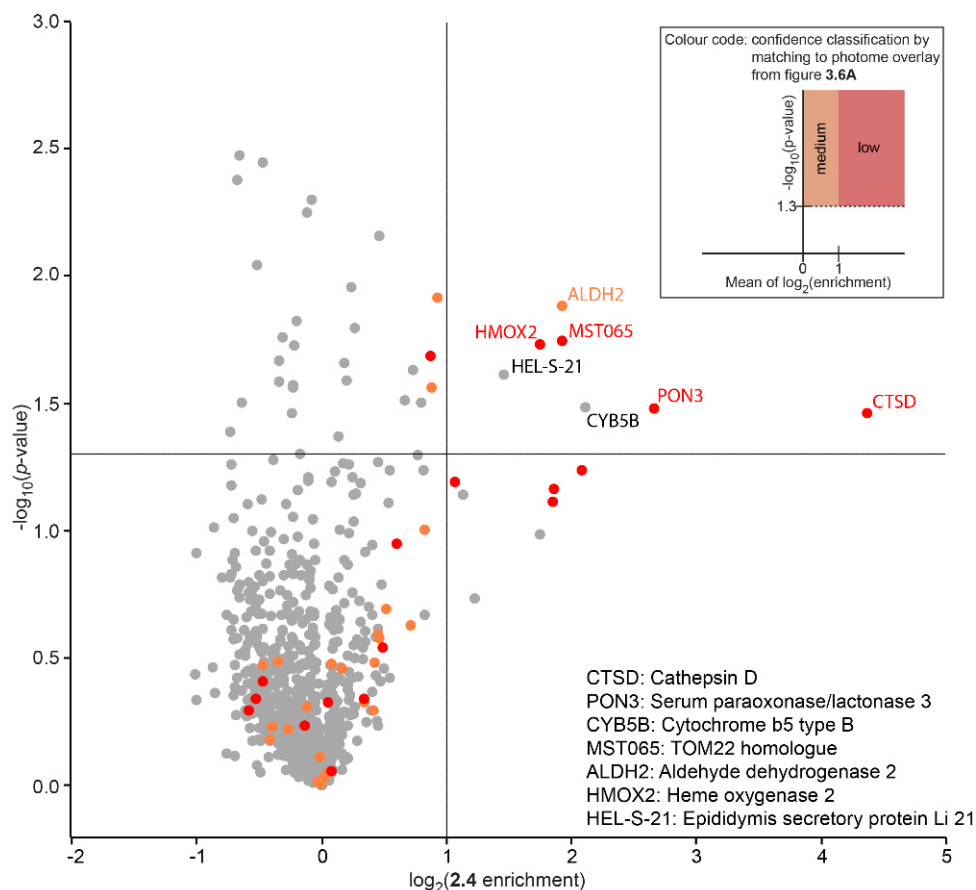
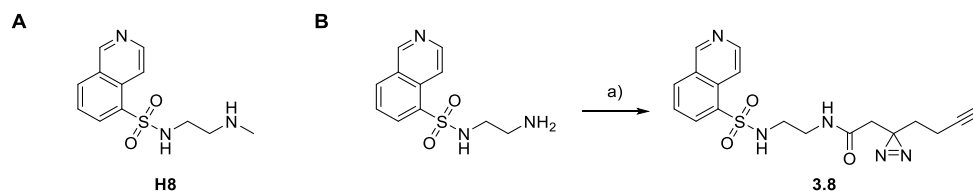


**Figure 3.7:** Alignment of the A549 photome with falcarinol photoprobe 2.4 enrichment. The match between the datasets was performed based on gene or protein names. Hits with low confidence for being a specific falcarinol target are depicted in red ( $\log_2(\text{photome enrichment}) > 1$  and  $p > 0.05$ ), medium confident proteins are shown in orange ( $0 < \log_2(\text{photome enrichment}) \leq 1$  and  $p > 0.05$ ). Remaining proteins not detected in the photome are depicted in grey. See also the color code representation of the legend in the upper right corner.

### 3.2.5 Target analysis of the PKA inhibitor H8 as a proof-of-principle

Although the photome list proved valuable in the interpretation of potential hits of a falcarinol derived photoprobe, further validation of this concept was required. The isoquinoline H8, a widely applied inhibitor of cAMP-dependent protein kinase (PKA)<sup>155–159</sup> was chosen as an appropriate test system for the following reasons: i) Isoquinolinsulfonamide H8 and its structurally related analogue H89 are gold standards in PKA research and binding to this target is confirmed by numerous studies.<sup>159</sup> AfBPP with this molecule should reveal PKA as a validated positive control. ii) A crystal structure in complex with H-inhibitors is available facilitating the chemical design of a functionalized probe retaining PKA affinity. iii) There are concerns about H8 and H89 selectivity in cells suggesting engagement in other pathways. iv) A full proteome analysis of this important inhibitor class is lacking and insights into its specificity for PKA and other targets would be valuable for future applications in cellular studies.

Since short aliphatic diazirine alkyne linkers displayed the lowest background labelling (Number of enriched proteins of **3.6** + **3.7** significantly lower than for probes **3.3** + **3.5**, see Figure 3.5), the demethylated derivative of H8 was coupled to carboxylic acid **3.10** under the same coupling conditions as for probes **3.3-3.6** to furnish photoprobe **3.8** (Scheme 3.4).



**Scheme 3.4:** A) Structure of kinase inhibitor H8, B) Synthesis of photoprobe **3.8**, conditions: a) **3.10** (1.00 eq), HOBt (1.50 eq), EDC (1.50 eq), DIEA (2.00 eq), DMF, rt, 16 h, 93%.

Crystallography data of PKA in complex with H-inhibitors indicated that this position was easily amenable for a chain extension, since the isoquinoline is buried in the ATP-pocket and the photolinker would presumably protrude outside the catalytic pocket towards the regulatory subunits.<sup>160</sup> Using the standard SILAC-ABPP procedure as for all other probes in A549, 30 hits were identified as matching the cut-off criteria. These hits were classified into three categories according to their enrichment in the photome overlay: (i) high probability for diazirine dependent binding (five hits depicted in red:  $\log_2(\text{enrichment})$  in photome  $> 1$  and  $p < 0.05$ ), (ii) medium probability for diazirine dependent binding (six hits depicted in orange:  $0 < \log_2(\text{enrichment}) \leq 1$  and  $p < 0.05$ ), (iii) low probability for diazirine dependent binding (19 remaining hits depicted in grey which are not significantly enriched in the photome).

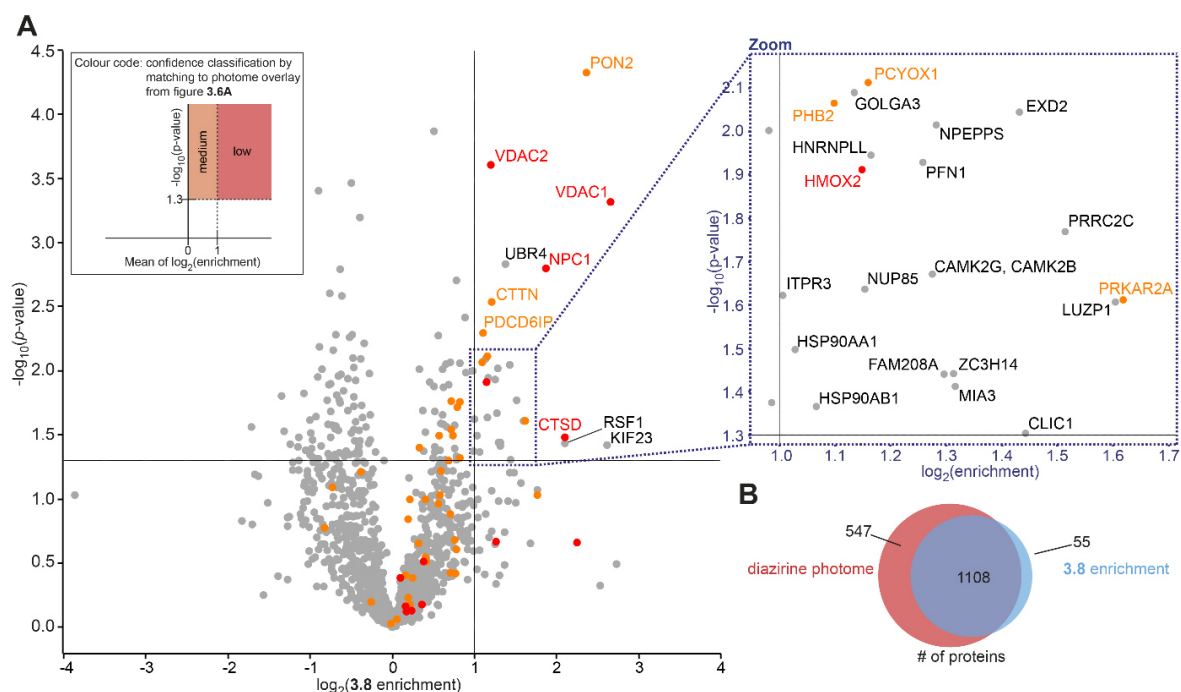


**Figure 3.9:** AfBPP of kinase inhibitor H8 and photome-based confidence validation. A) Volcano plot representation of H8p AfBPP with 3  $\mu\text{M}$  probe (enlargement of the blue box shown on the right). Identified proteins were aligned with the diazirine photome (Figure 2d) and classified as high probability for diazirine dependent binding (depicted in red,  $\log_2(\text{photome enrichment}) > 1, p < 0.05$ ), medium probability for diazirine dependent binding (orange,  $0 < \log_2(\text{photome enrichment}) \leq 1, p < 0.05$ ) or low probability for diazirine dependent binding (grey, remaining proteins). Colour code legend for a graphical representation of the hit positions in the photome in the upper left corner. B) Overlap of all proteins present in photome (red) and proteins identified in the H8p enrichment (blue).

Conducting a cytoscape search,<sup>161</sup> many high confidence proteins were linked to nucleotide binding, including ATP/cAMP, DNA and poly adenine RNA. These findings were not surprising, considering that the isochinoline of H-inhibitors mimics the bicyclic aromatic ring system of adenine and thereby blocks the ATB-binding site in kinases. The proposed target of H8, PKA, was identified - the first time this has been observed in a whole proteome approach. Furthermore, many highly enriched proteins could be excluded as non-specific background targets, which further confirms the photome as a valuable tool in AfBPP. A complete list of all significantly enriched proteins is given in Table 3.2.

**Table 3.2:** Target identification and photome alignment of H8-derived probe **3.8**. Protein targets involved in adenine binding and hydrolytic reactions are indicated. The probability for a probe specific target identification according to the diazirine photome is depicted by colour: low: red, medium: orange, high: black. Refer to Figure 3.17 for a graphical representation of the data. (\* = not significant).

Protein name	Gene name	log2 enrichment		molecular function			
		H8p	photome	polyA RNA binding	ATP/cAMP binding	DNA binding	hydrolytic activity
Voltage-dependent anion-selective channel protein 1	VDAC1	2.66	2.67				
Kinesin-like protein KIF23	KIF23	2.61	0.32*		■		
Serum paraoxonase/arylesterase 2	PON2	2.36	0.62				■
Remodeling and spacing factor 1	RSF1	2.10	0.68*				
Cathepsin D	CTSD	2.10	5.04				■
Niemann-Pick C1 protein	NPC1	1.87	2.51				
cAMP-dependent protein kinase type II- alpha regulatory subunit	PRKAR2A	1.62	0.70		■		
Leucine zipper protein 1	LUZP1	1.60	0.48*			■	
Protein PRRC2C	PRRC2C	1.51	0.20*	■			
Chloride intracellular channel protein 1	CLIC1	1.44	0.44*				
Exonuclease 3-5 domain containing protein 2	EXD2	1.43	0.14*				■
E3 ubiquitin-protein ligase UBR4	UBR4	1.38	0.23*				
Melanoma inhibitory activity protein 3	MIA3	1.32	-0.02*				
Zinc finger CCCH domain-containing protein 14	ZC3H14	1.31	-0.38	■			
Protein FAM208A	FAM208A	1.30	-	■			
Puromycin-sensitive aminopeptidase	NPEPPS	1.28	0.51*				■
Calcium/calmodulin-dependent protein kinase Type II gamma/beta	CAMK2G, CAMK2B	1.27	0.51*		■		■
Profilin-1	PFN1	1.26	0.75*	■			
Src substrate cortactin	CTTN, EMS1	1.21	0.86				
Voltage-dependent anion-selective channel protein 2	VDAC2	1.20	2.54				
Heterogenous nuclear ribonucleoprotein L-like	HNRNPLL, HNRPLL	1.16	-1.27*	■			
Preylcysteine oxidase 1	PCYOX1	1.16	0.59				
Nuclear pore complex protein Nup85	NUP85	1.15	-0.10*				
Heme oxygenase 2	HMOX2	1.15	1.33				
Golgin subfamily A member 3	GOLGA3	1.13	0.20*				
Programmed cell death 6-interacting protein	PDCD6IP	1.11	0.64				
Prohibitin-2	PHB2	1.10	0.55				
Heatshock protein HSP 90-beta	HSP90AB1	1.07	0.46*	■			
Heatshock protein HSP 90-alpha	HSP90AA1, EL52	1.03	0.34*	■			

### 3.3 Conclusion and outlook

AfBPP is a powerful methodology to identify protein targets of small molecules in live cells. To apply this method to natural products and other bioactive compounds, it is crucial to integrate a reporter tag and, usually, a photocrosslinker moiety into the core structure of the molecule without compromising structural integrity and therefore bioactivity. While it is, in many cases, quite simple to maintain the pharmacophore of a natural product while integrating small, biorthogonal reporter tags like alkynes or azides, the modification with a photocrosslinker moiety is somewhat more challenging. Photocrosslinkers like arylazides and benzophenone are sterically demanding, rendering them unsuitable for small and complex structures, unless an aromatic moiety already present can be modified to an aryl azide or benzophenone. As demonstrated here and in previous studies, diazirines possess superior properties, making them the number one choice for photoaffinity experiments. However, the properties of a photoprobe are not only determined by its photochemical reactivity and size but also by its overall structure, hydrophobicity and most importantly its potential interactions with the proteome. It is therefore essential to consider these factors in designing the photoprobe. As it is impossible to take all these factors into account and structures of bioactive compounds are often limited in possible modification sites, it is probably advisable to synthesize a set of different photoaffinity probes to improve reliability and statistical evaluation, especially in an untargeted approach. Furthermore, although the analytical labelling patterns of different diazirine photocrosslinkers were very similar, quantitative mass analysis yielded significantly different results. This suggests that gel-based analysis lacks sensitivity and specificity.

The “photome” provided here is a reference list for conducting photoaffinity experiments in live cells. Further data, especially from more complex photoprobes, may further enhance this collection of off-targets, providing an encyclopedia for modern target identification involving diazirine photo labels. The superior properties of alkyl diazirines (concerning nonspecific background labelling) in comparison to benzophenones and aryl azides is probably due to a combination of relative size and their reduced potential to interact with other molecules through noncovalent interactions. While benzophenone and aryl azides can form  $\pi$ -stacking interactions and hydrogen bonds, both nitrogens in the tricyclic ring of a diazirine are electron-poor, which not only explains their susceptibility towards strong nucleophiles, but also their rather limited capability to function as a H-bond acceptor. These noncovalent interactions are however crucial for close proximity and increase the probability for covalent bond formation of reactive species with biomolecules.

This chapter is based on data prepared for publication:

W. Heydenreuter designed the project and conducted probe and natural product synthesis, target-ID, validation and co-ip, S. Braig executed biochemical assays and imaging, M. Stahl ran Cytoscape analysis, J. Vomacka performed statistical evaluation of proteomic data, S. A. Sieber designed the research and supervised the project.

## **4 Target identification of neocarzilin A-C in human cancer cells**

### **4.1 Cancer as a challenge for mankind**

Cancer is one of the big scourges of modern society. It causes almost one third of all fatalities in the Western world with the percentage still going up as life expectancy increases. Although treatment and survival rates have dramatically improved over the last 30 years,<sup>162,163</sup> some cancer diagnoses like glioblastoma, lung-, liver- or pancreas carcinoma often still equal a death sentence.<sup>164–166</sup>

There are two major problems in cancer treatment, which will probably make this disease a challenge far into the second half of the 21<sup>st</sup> century. First of all, cancer cells are rogue cells, which have lost several cellular mechanisms that control normal growth and replication. The fact that they derive from normal healthy tissue means that treatment strategies always involve interfering with cellular processes and pathways. Since these processes are well regulated and balanced in normal tissue, side effects will arise from influencing them. The second major problem is the diversity of cancers (or neoplasms). There are more than 100 different cancers which have to be addressed differently as they are caused by hundreds of diverse cellular defects. In particular, the identification of genetic factors responsible for the susceptibility to tumorigenesis have been intensively studied since the 1970s.<sup>167</sup> Since every cancer is derived from a genetically unique individual, therapies accounting for that factor are becoming more and more important in order to maximize therapeutic effectiveness, reduce side effects and improve quality of life.<sup>168–172</sup>

The first approach in standard cancer treatment includes the surgical resection of the tumor mass and compromised lymph nodes.<sup>173,174</sup> To reduce the size of tumors that are inoperable or to destroy residual tumor cells, high dose radiation therapy ( $\gamma$ -rays) is applied.<sup>175</sup> The third pillar of this triade is chemotherapy. This chemical approach to compromise and destroy cancer cells has spawned dozens of small molecules and antibodies since the



1940s.<sup>176–178</sup> Although strongly cytotoxic but relatively non specific compounds are still the backbone of current therapies, the development of targeted therapy and immunotherapy are new approaches to improve clinical outcome. While targeted therapy aims at disrupting pathways that are critical for tumor survival and proliferation, immunotherapy tries to sensitize the immune system to actively combat cancer cells. As tumor cells can also achieve resistance to chemotherapeutics, the most promising approach may be a combinatorial therapy addressing different molecular targets within a neoplasm.<sup>179,180</sup>

The molecular context and factors involved in cancer origin, survival and expansion are very complex and not yet fully understood. Hanahan and Weinberg proposed the concept of the hallmarks of cancer, characteristics a malignant tumor mass acquires during its multistep development from healthy tissue. These hallmarks include sustaining proliferative signalling, resisting cell death, enabling replicative immortality, evading growth suppressors, inducing angiogenesis, activating invasion and metastasis, evading immune destruction and reprogramming of energy metabolism.<sup>181,182</sup> This concept illustrates not only the complexity of tumorigenesis, but also the challenges therapies are faced with.<sup>163</sup>

#### 4.1.1 Tumor migration

Malign tumors grow invasively into surrounding tissue and destroy it, a result of tapping into close-by blood vessels to improve nutrition and oxygen supply. Furthermore tumor migration and metastasis lead to expansion in other parts of the body, resulting in secondary neoplasms in vital organs like lung, liver or brain. The detachment and migration of single cells from the central tumor mass results in a quick relapse of the cancer once the primary tumor has been erased, e.g. by surgical removal. This contributes to high fatality rates in the case of glioblastomas,<sup>183</sup> hepatocellular carcinoma<sup>184,185</sup> and lung cancer.<sup>186</sup>

Although inhibition of cancer cell proliferation is a primary goal of drug development and natural product screening campaigns, inhibition of migration, an important step in metastasis, represents an intriguing alternative pathway for medicinal intervention. Migration is a complex multi-step process initiated by actin polymerization to protrude the cell membrane and facilitate interaction with the surrounding tissue.<sup>187,188</sup> Several key regulators including small GTPases (e.g. CDC42 and Rho)<sup>189–193</sup> as well as chemokines and phosphatidylinositol kinases (PIKs) are crucial propagators of this initial step in motility.<sup>194–198</sup> Furthermore, focal contacts between membrane localized integrin receptors<sup>199–203</sup> and the extracellular matrix induces a signaling cascade resulting in the recruitment of surface proteases to dissipate surrounding tissue and promote migration.<sup>204–207</sup> Currently, clinical development of anti-migration drugs is largely focused on a limited

number of targets such as integrins<sup>208,209</sup> and selectins.<sup>210</sup> Although the complex modes of tumor migration and metastasis are not completely unveiled, the targeting of essential pathways with small molecules like natural products could be a huge step towards the development of drugs combating metastatic cancer.

#### 4.1.2 Neocarzilins

Neocarzilins A and B were first isolated in 1992 by Nozoe *et al.* from a culture broth of *Streptomyces carzinostaticus* var. F14.<sup>211</sup> Neocarzilins are trichlorinated polyenones with slightly acidic character due to their enolic hydroxyl group which is stabilized through an intramolecular hydrogen bond. Their biosynthesis, involving a novel type I PKS system, was elucidated in 2004 by Otsuka *et al.*<sup>212</sup> Neocarzilins A and B were isolated during that investigation and are probably the precursors of Neocarzilins C and D in their biosynthesis. Neocarzilins A and B showed only weak antimicrobial activity against gram positive strains *Micrococcus luteus* and *Bacillus megaterium*. It displayed however strong cytotoxicity in the human chronic myelogenous leukemia cell line K562, with an IC<sub>50</sub> of 185 nM. Studies towards any comprehensive SAR (structure-activity relationship) in human cancer cells have not been published so far. Nevertheless, the acidic hydroxyl group seems to be essential for good activity as the corresponding methylether displayed only moderate toxicity in the range of 6 μM.<sup>213</sup>

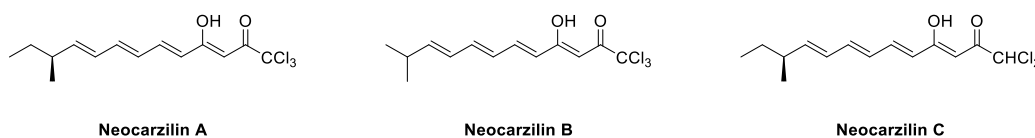


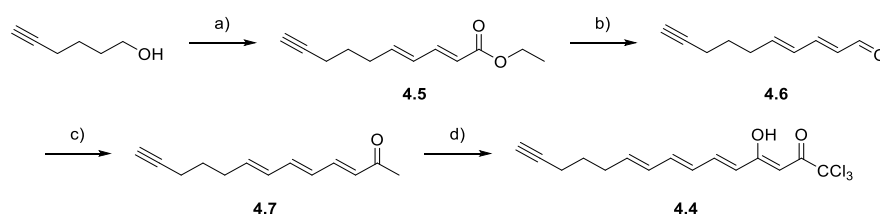
Figure 4.1: Structures of Neocarzilins A-C.

## 4.2 Results and discussion

### 4.2.1 Synthesis of an activity-based probe

The linear scaffold of Neocarzilins makes it an ideal target for integrating a reporter tag without compromising molecular structure and reactivity. Furthermore, neocarzilins possess two distinct electrophilic moieties, trichloroketone and an electron deficient polyene system, capable of forming covalent bonds to nucleophilic protein sites. To elucidate covalent binding properties of neocarzilins, a slightly modified natural product bearing an alkyne tag at its aliphatic region was designed. The synthesis was accomplished in six linear steps starting from commercially available 5-hexynol. The alcohol was

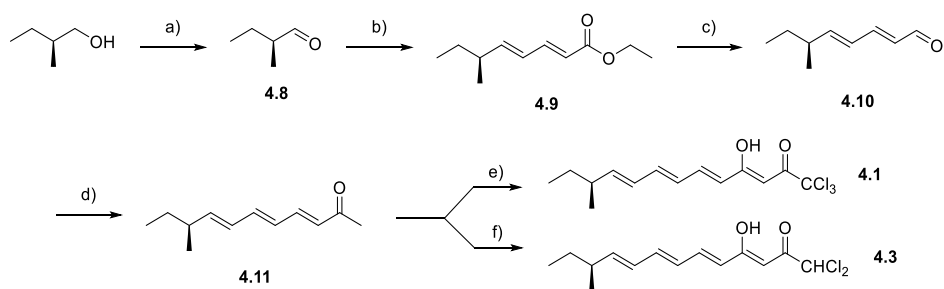
converted to the corresponding aldehyde under *Swern* conditions and converted to diene **4.5** through olefination employing a *Horner Wadsworth Emmons* (HWE) reaction. The ester was reduced to the allylic alcohol and reoxidized to aldehyde **4.6**. Heating of aldehyde **4.6** with an excess of (Triphenylphosphoranylidene)-2-propanone in toluene gave unstable trienone **4.7**. Deprotonation of both alkyne and ketone with 2 equivalents of lithium bis(trimethylsilyl)amide and subsequent quenching of the reaction mixture with 1 equivalent of trichloroacetic anhydride resulted in probe **4.4** as the sole product (Scheme 4.1). The good selectivity can be explained by the higher nucleophilicity of the enolate in comparison to the acetylide.



**Scheme 4.1:** Synthesis of probe **4.4**: a) 1. DMSO (2.22 eq),  $(\text{COCl})_2$  (1.11 eq),  $\text{NEt}_3$  (4.50 eq); 2. LiHMDS (1.00 eq), ethyl (*E*)-4-(diethoxyphosphoryl)-but-2-enoate (**4.15**) (1.00 eq),  $\text{CH}_2\text{Cl}_2$ , THF,  $-78^\circ\text{C} \rightarrow \text{rt}$ , 4 h, 38 % over 2 steps; b) DIBAL-H (2.10 eq),  $\text{MnO}_2$  (20.0 eq), THF, hexane,  $-78^\circ\text{C} \rightarrow \text{rt}$ , 5 h, 54 % over 2 steps; c) 1-(Triphenylphosphoranylidene)-2-propanone (2.00 eq), toluene,  $100^\circ\text{C}$ , 16 h, 54 %; d) 1. LiHMDS (2.00 eq); 2. trichloroacetic anhydride (1.00 eq), THF,  $-78^\circ\text{C}$ , 3 h, 45 %.

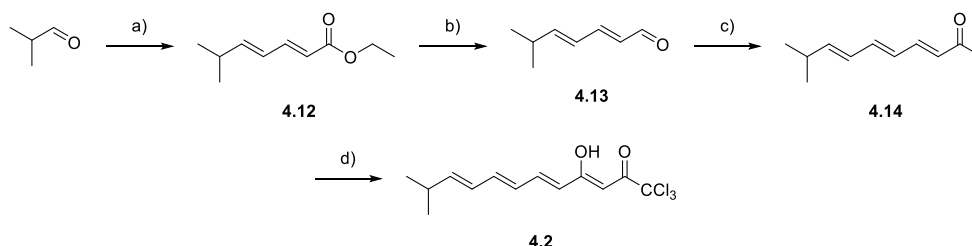
## 4.2.2 Synthesis of neocarzilins A-C

The first and only synthesis of neocarzilin A was published by *Nozoe et al.* in 1992.<sup>213</sup> The synthesis was accomplished in 8 steps starting from (*L*)-isoleucine. Modifying this procedure, Neocarzilin A was synthesized in a linear sequence with six steps and an overall yield of 19 %. The route followed a similar sequence developed for the synthesis of probe **4.4**. Commercially available enantiopure (*S*)-2-methylbutan-1-ol was converted to the chiral aldehyde **4.8** which gave dien **4.9** when treated with (*E*)-(1-(diethoxyphosphoryl)-4-ethoxy-4-oxobut-2-en-1-yl)lithium in THF (generated from LiHMDS and Ethyl (*E*)-4-(diethoxyphosphoryl)but-2-enoate). The ester was reduced to the corresponding alcohol with DIBAL-H and reoxidized to give aldehyde **4.10**. Ketone **4.11** was obtained by *Wittig* reaction of aldehyde **4.10** with (Triphenylphosphoranylidene)-2-propanone. Aldol reaction with trichloroacetic anhydride yielded neocarzilin A (**4.1**); the corresponding dechloro-product neocarzilin C (**4.3**) was obtained using 2 equivalents of dichloroacetic anhydride (scheme 4.2).



**Scheme 4.2:** Synthesis of Neocarzilins A (**4.1**) and C (**4.3**): a) TEMPO (1 mol-%), KBr (0.10 eq), NaOCl (2.00 eq),  $\text{CH}_2\text{Cl}_2$ /carbonate-buffer pH = 8.6, 0 °C, 45 min, 85 %; b) 1. LiHMDS (1.00 eq), 2. ethyl (*E*)-4-(diethoxyphosphoryl)-but-2-enoate (**4.15**) (1.00 eq), THF, -78 °C  $\rightarrow$  -40 °C, 3 h, 76 %; c) DIBAL-H (2.10 eq)  $\text{MnO}_2$  (20.0 eq), THF, hexane, -78 °C  $\rightarrow$  rt, 5 h, 72 % over 2 steps; d) 1-(Triphenylphosphoranylidene)-2-propanone (2.00 eq), toluene, 100 °C, 16 h, 59 %; e) 1. LiHMDS (1.05 eq); 2. Trichloroacetic anhydride (2.00 eq), THF, -78 °C, 3 h, 71 %; f) 1. LiHMDS (1.05 eq), 2. Dichloroacetic anhydride (2.00 eq), THF, -78 °C, 3 h, 44 %.

Neocarzilin B was synthesized in the same manner starting from isobutyraldehyde. Olefin **4.12** was obtained through *HWE* reaction with ethyl (*E*)-4-(diethoxyphosphoryl)-but-2-enoate (**4.15**). Following a reduction-oxidation sequence to yield **4.13**, ketone **4.14** was synthesized through *Wittig* reaction and was finally converted to neocarzilin B through aldol reaction as described before (Scheme 4.3).



**Scheme 4.3:** Synthesis of Neocarzilin B: a) LiHMDS (1.00 eq) ethyl (*E*)-4-(diethoxyphosphoryl)-but-2-enoate (**4.15**) (1.00 eq), THF, -78 °C  $\rightarrow$  rt, 4 h, 51 %; b) DIBAL-H (2.10 eq),  $\text{MnO}_2$  (20.0 eq), THF, hexane, -78 °C  $\rightarrow$  rt, 5 h, 83 % over 2 steps; c) 1-(Triphenylphosphoranylidene)-2-propanone (2.00 eq), toluene, 100 °C, 16 h, 60 %; d) 1. LiHMDS (1.00 eq), 2. trichloroacetic anhydride (2.00 eq), THF, -78 °C, 3 h, 83 %.

### 4.2.3 Reactivity to proteins in human cancer cells

Neocarzilin A has been evaluated for potential biological activities after its first isolation from *Streptomyces carzinostaticus*. It displayed high cytotoxicity in human chronic myelogenous leukemia cell line K562 with an  $\text{IC}_{50}$  of 185 nM.<sup>211</sup> Although this cancer cell line was available for testing in the current study, initial labeling experiments gave unsatisfying results as the labeling was blurry and distinct labeling with high background was only observed at concentrations of 10  $\mu\text{M}$  and higher (data not shown). Therefore labeling was carried out in various adherent cell lines to determine the best cell line for analytical fluorescent analysis. A dominant band was observed at 45-50 kDa in all tested cell lines; however the clearest results were obtained in HepG2 (hepatocellular carcinoma) and MCF-7 (breast adenocarcinoma). Labeling could be observed down to 1 nM, with an unusual increase in

labeling intensity with lower concentrations. The strongest labeling was achieved with 100-500 nM with decreasing intensity at higher and lower concentrations (Figure 4.2). A decrease in band intensity at higher concentrations could be the result of increasing toxicity of the probe leading to stress-induced degradation of macromolecules throughout the cell.<sup>214</sup> If the probe labels a receptor, the decrease of signal intensity might be the result of specific degradation of the receptor-ligand complex after endocytosis and signal transduction.<sup>215</sup>

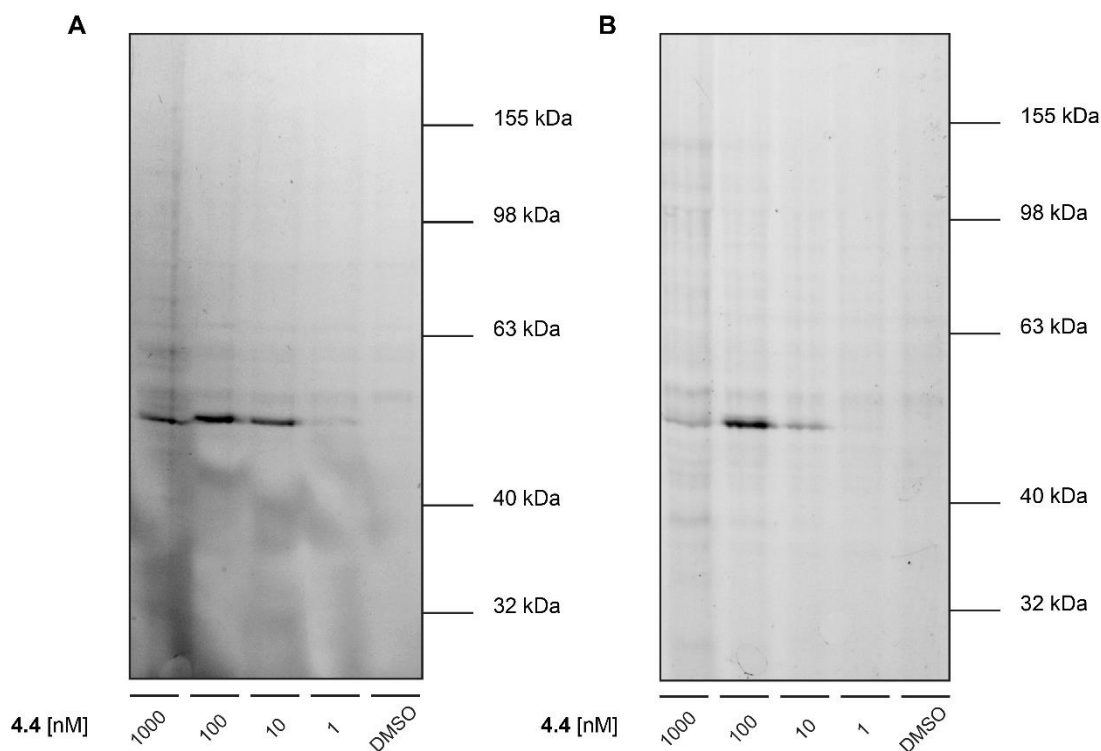


**Figure 4.2:** Fluorescent SDS-gel of *in situ* labeled HepG2 (A) and MCF-7 cells (B).

For further labeling experiments and target identification, HepG2 was chosen, since it displayed the most distinct labeling pattern. To verify binding of the natural products to the unknown protein, competitive labeling with neocarzilin A (**4.1**) and neocarzilin C (**4.3**) was conducted (Figure 4.3). HepG2 cells were incubated with different concentrations of **4.1** and **4.3** for 1 h before treatment with 100 nM of probe **4.4**.

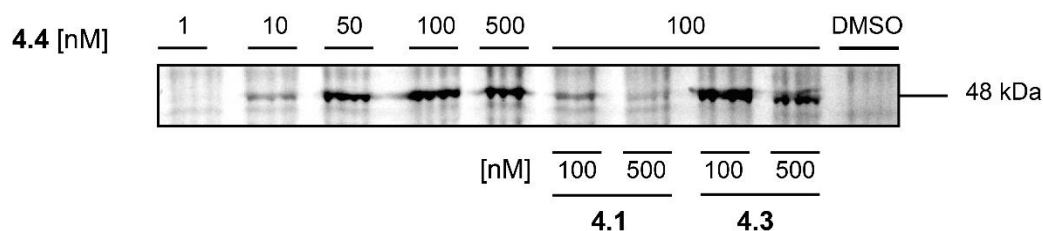


**Figure 4.3:** Competitive *in situ* labeling in HepG2. Fluorescent signal of prominent band is outcompeted by neocarzilin A (**4.1**) but not neocarzilin C (**4.3**).

Figure 4.2 clearly shows the strong affinity of neocarzilin A (**4.1**) to the labeled protein since 500 nM are sufficient to almost completely erase the fluorescent signal. Interestingly, neocarzilin C (**4.3**) does not seem to be able to block the binding site of probe **4.4**, an indication of the lower reactivity of the dichloroketone. This finding also suggests, that in this particular case neocarzilin binds to the protein via chloride-substitution at C1, not by conjugate addition to the polyenone system.

#### 4.2.4 Quantitative proteomics

In an attempt to determine the identity of this protein, a gel-based approach was the first choice. Cells were incubated with 500 nM of probe **4.4** for 1 h, scraped off, lysed and clicked to a trifunctional linker containing a fluorophore and biotin.<sup>121</sup> After enrichment on avidin beads, the proteins were detached from the beads by heat denaturation at 96 °C. However no fluorescent signal could be detected after SDS-PAGE. If the chloroketone binds to a cysteine moiety, the chloromethylation of the nucleophilic site might reduce the electron density on the heteroatom sufficiently to favor an elimination reaction to the corresponding dehydroalanine at higher temperatures. This would result in removal of the fluorescent tag and loss of the signal. Since a gel based approach was unsuccessful in unraveling the protein targets of **4.4**, a gel-free SILAC approach was chosen since this does not involve aggressive heating of the sample. Either heavy or light isotope labelled cells were treated with probe **4.4** for 1 h, the cells lysed, corresponding states pooled. Subsequent click reaction with biotin-azide was followed by enrichment via avidin beads. The enriched proteins were digested with trypsin and analyzed by LC-MS/MS.

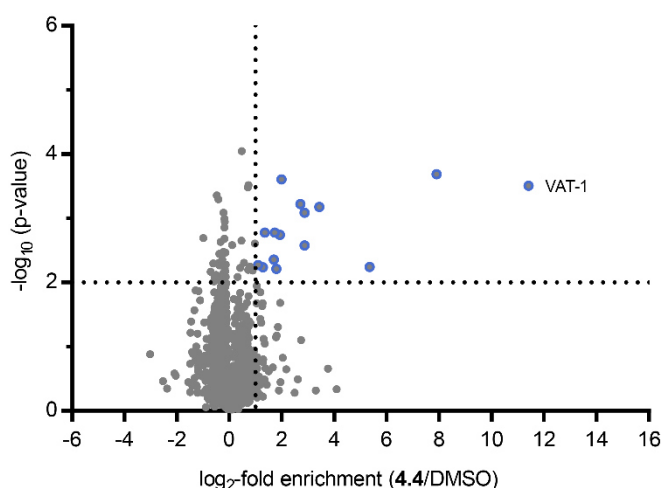


**Figure 4.4:** Volcano plot of *in situ* gel-free SILAC-ABPP experiment in human hepatocellular carcinoma cell line HepG2 with 500 nM **4.4**. The volcano plot shows the statistical significance of enrichment levels (Student's *t*-test *p*-value) as a function of average protein ratios from 6 biological replicates in probe-treated vs. control cells. Hits matching the criteria ( $\log_2(\text{enrichment}) > 1$ ,  $p\text{-value} < 0.01$ ) are highlighted (A more strict  $p\text{-value} < 0.01$  was set due to a higher number of replicates) .

The enrichment values and statistical analysis are illustrated in the volcano plot in figure 4.4. A list of 15 proteins matching the cut-off criteria ( $\log_2(\text{enrichment}) > 1$ ,  $p\text{-value} < 0.01$  (a more strict cut-off than  $p\text{-value} < 0.05$  was chosen due to an increased number of replicates)) were identified. The protein with the strongest enrichment was the synaptic vesicle membrane protein VAT-1 homolog (VAT-1).

**Table 4.1:** List of significantly enriched proteins according to the specified cut-off criteria ( $\log_2(\text{enrichment}) > 1$ ,  $p\text{-value} < 0.01$ ).

Protein name	Gene-ID	$\log_2\text{-fold enrichment}$	$-\log_{10}(p\text{-value})$
Synaptic vesicle membrane protein VAT-1 homolog	VAT1	11,41	3,51
Heme oxygenase 2	HMOX2	7,90	3,69
Cytochrome b5 type B	CYB5B	5,35	2,24
Retinal dehydrogenase 1	ALDH1A1	3,43	3,18
Cytoskeleton-associated protein 4	CKAP4	2,87	2,58
Glutathione S-transferase omega-1	GSTO1	2,89	3,09
Aldehyde dehydrogenase, mitochondrial	ALDH2	2,71	3,22
Sarcoplasmic/endoplasmic reticulum calcium ATPase 2	ATP2A2	1,99	3,61
Inactive tyrosine-protein kinase 7	PTK7	1,92	2,74
Neutral cholesterol ester hydrolase 1	NCEH1	1,80	2,21
Perilipin-2	PLIN2	1,73	2,78
Antigen peptide transporter 1	TAP1	1,69	2,36
Glutaredoxin-3	GLRX3	1,36	2,78
Voltage-dependent anion-selective channel protein 3	VDAC3	1,27	2,24
AP-3 complex subunit beta-1	AP3B1	1,10	2,28

The fact that some of these proteins (ALDH2, ALDH1A1, GSTO1) possess highly nucleophilic cysteines in their active site might indicate thiols as a preferred alkylation target of neocarzilins.

To further confirm VAT-1 as a molecular target of probe **4.4**, HepG2 cells were incubated with 100 nM of **4.4** while a second batch of cells were treated with 500 nM of neocarzilin A (**4.1**) prior to incubation with probe. After lysis, click and enrichment, the absolute protein quantities and ratios were determined by label-free quantification.<sup>216</sup> Again VAT-1 was identified as the clearest hit, with an average  $\log_2(\text{enrichment})$  of 4 (Figure 4.5A). From

the 15 hits obtained by SILAC-ABPP, only VAT-1 and HMOX2 were also found in the label-free approach. This deviation might be attributed to the lower probe concentration (100 nM vs. 500 nM), but also to the different workflow, since label-free quantification requires high background for optimal performance. (The washing of the beads after enrichment to remove nonspecifically bound proteins was executed with low concentrated urea solution to maintain high protein background).<sup>217</sup> The main goal of this experiment was to determine if Neocarzilin A (**4.1**) was able to outcompete the probe. Competition could be clearly demonstrated by comparison of the absolute log<sub>2</sub> intensities obtained for unique VAT-1 peptides (Figure 4.5B).

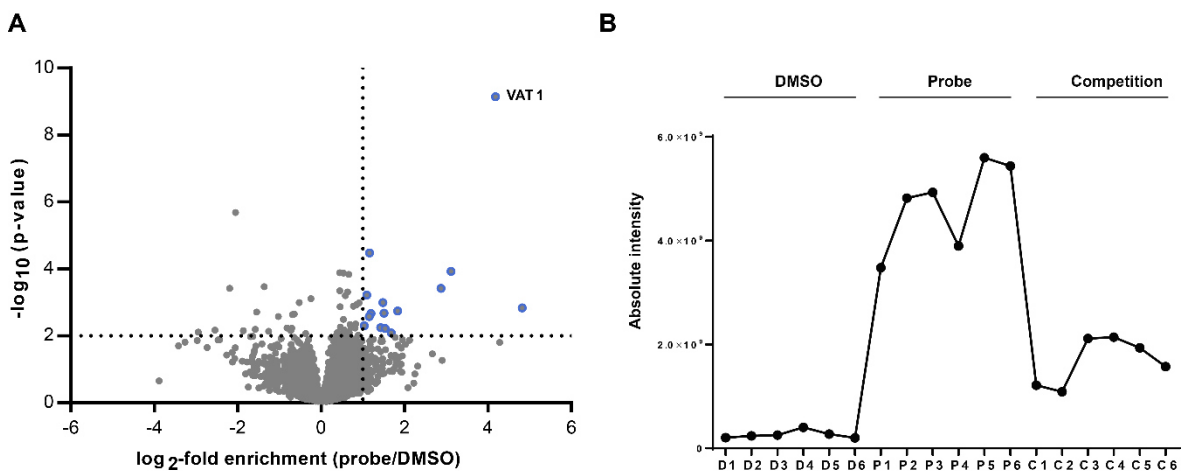


**Figure 4.5:** A) Volcano plot of an *in situ* label-free ABPP experiment with 100 nM **4.4**. The volcano plot shows the statistical significance of enrichment levels (Student's *t*-test *p*-value) as a function of average protein ratios from 6 biological replicates in probe-treated vs. DMSO-treated cells. Hits matching the criteria ((log<sub>2</sub>(enrichment) > 1, *p*-value < 0.01) are highlighted. B) Absolute intensities of unique VAT1-peptides in six replicates each treated with DMSO (D1-D6), probe **4.4** (P1-P6) and neocarzilin A (**4.1**) + probe **4.4** (C1-C6).

## 4.2.5 Target validation

### 4.2.5.1 Labeling of VAT-1 knockdown cells

In order to correlate analytical labeling and quantitative proteomics, cells were transfected with siRNA of VAT-1 and labeled with different concentrations of probe **4.4**. Since only one band was visible in analytical labeling experiments at concentrations of 10-100 nM and this protein band appeared in the range of 40-50 kDa, VAT-1 was assumed to be the labeled protein. This presumption turned out to be accurate, as the intensity of the labeling was strongly reduced in cells with reduced VAT-1 content (Figure 4.6).



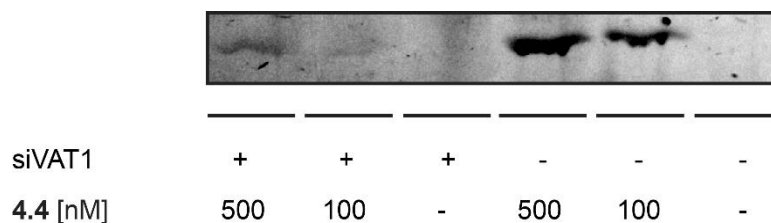


**Figure 4.6:** Analytical labeling of VAT-1- knockdown cells in comparison to control-treated cells.

#### 4.2.5.2 Labeling of recombinant VAT-1 in *E. coli*

As a more direct approach for validating neocarzilin binding to VAT-1, the recombinant protein was overexpressed in *E. coli* Lemo21 (DE3), a strain optimized for membrane protein overexpression.<sup>218</sup> For this purpose, the gene sequence of VAT-1 was cloned into expression vector pET300 containing an N-terminal His-tag and a TEV cleavage site. Despite extensive optimization of expression, isolation and purification conditions, sufficient amounts of correctly folded protein could not be obtained. However, labeling of overexpressed VAT-1 in *E. coli* could be observed (Figure 4.7).

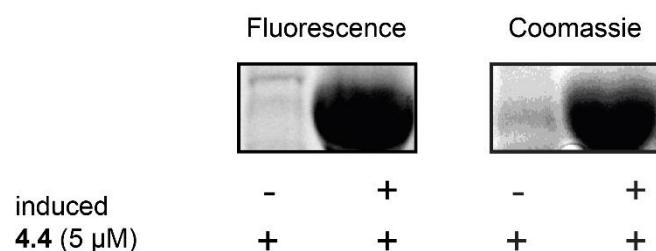


**Figure 4.7:** Labeling of overexpressed recombinant VAT-1 in membrane fraction of *E. coli* Lemo21 (DE3).

Although no active protein could be obtained for final validation through activity assays or binding site identification, the evidence was strong enough to assess VAT-1 as a covalent target of neocarzilins and further continue investigating this protein.

#### 4.2.6 Function of VAT-1

VAT-1 (Synaptic vesicle membrane protein VAT-1 homolog) is a 41.9 kDa integral membrane protein which was first isolated from the synaptic vesicles of the electric organ of the Pacific electric ray *Torpedo californica*.<sup>219</sup> The mammalian homologue shows ATPase activity<sup>220</sup> and is involved in  $Ca^{2+}$  dependent processes in keratinocyte physiology.<sup>221</sup> A study by Eura *et al.* suggests that MIB, the rat homologue of VAT-1 is essential for cellular function by regulating mitochondrial membrane dynamics in cooperation with Mitofusin proteins.<sup>222</sup> Furthermore Mertsch *et al.* demonstrated that VAT-1 is overexpressed in certain glioblastomas and high levels of this protein were directly related to increased tumor migration.<sup>183</sup> The involvement of VAT-1 in the migration of cancer cells made this protein an

interesting subject for study and to determine if neocarzilin would be able to influence or inhibit cellular migration.

#### 4.2.7 Inhibition of migration and chemotaxis by neocarzilin A

Since VAT-1 downregulation has been shown to result in a strong inhibition in certain glioblastomas, several metastatic cell lines were chosen to determine if the chemical modification of VAT-1 was capable of inducing similar changes of migratory behavior. As only one glioblastoma cell line (U87) was available for testing, the invasive breast cancer cell lines MDA-MB-231 (human metastatic breast adenocarcinoma) and 4T1 (murine breast cancer), were selected as alternative test systems.

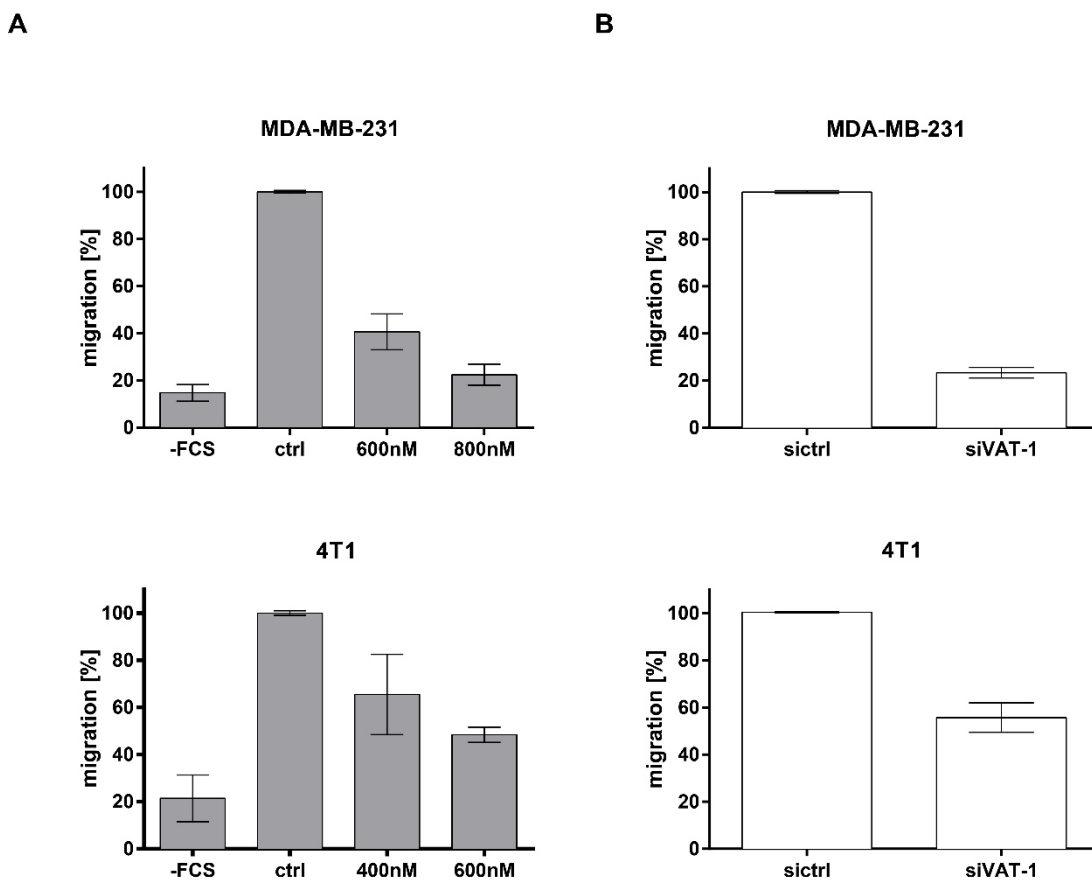


**Figure 4.8:** A) Migration pattern measured in a Boyden chamber assay of breast cancer cell lines at different concentrations of **4.1** after 24 h. B) Level of migration after 24 h treatment with siVAT-1 (-FCS = without Fetal Calf Serum, ctrl = control, untreated cells).

The Boyden chamber assay<sup>223</sup> was chosen for this experiment since it is the most widely accepted assay to investigate migration behavior. In this assay, cells move through a polycarbonate membrane along a gradient of a chemoattractant, in most cases FCS (Fetal Calf Serum). As a control to link VAT-1 downregulation with the decrease of migration, MDA-MB-231 cells and 4T1 were transfected with siRNA of VAT-1 in parallel. A strong

inhibitory effect on cell migration was observed after 24 h in cell lines MDA-MB-231 and 4T1 (Figure 4.8). The directed migration of MDA-MB-231 cells could be terminated almost completely at concentrations of 800 nM. However, U87 only showed minimal inhibition of migration not only in knockdown studies but also at neocarzilin concentrations of up to 1  $\mu$ M (data not shown here). This indicated that the involvement of VAT-1 in migration regulation might be cell line specific. A closer look at different chemotaxis parameters revealed not only an overall reduction of migration, but also a significant influence on velocity, directness and covered distance (Figure 4.9).

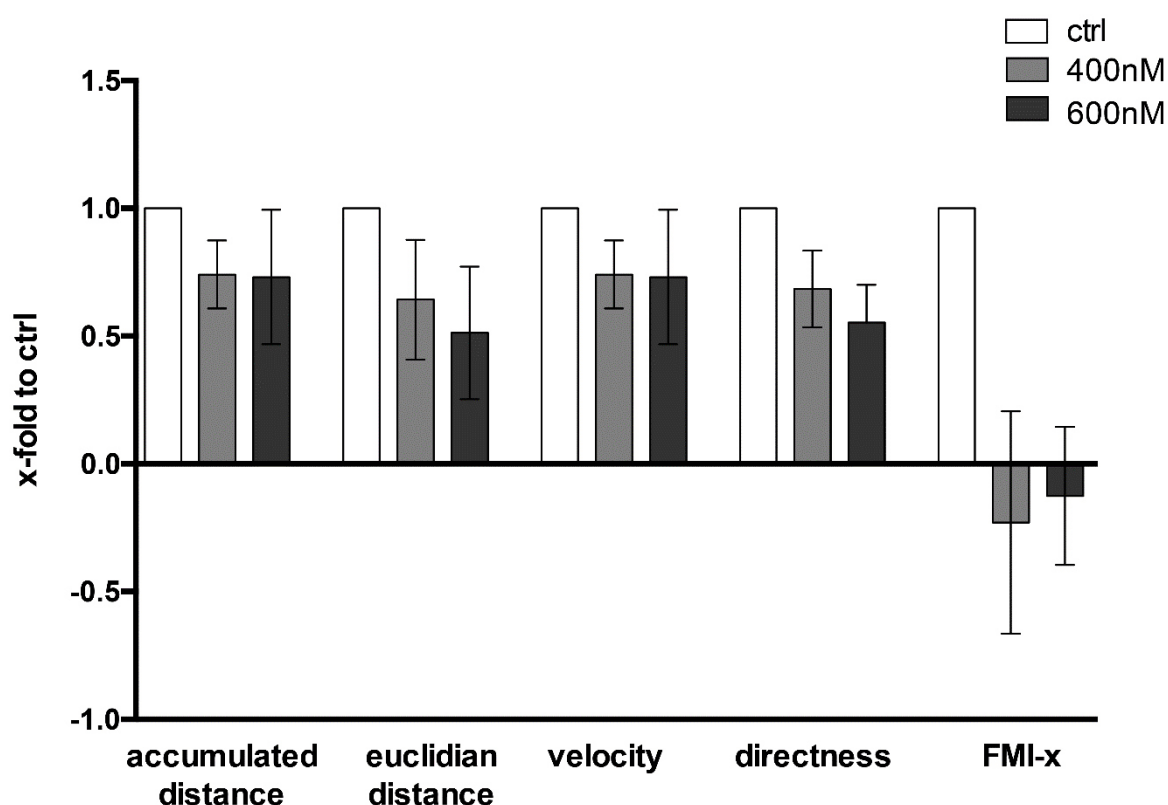


**Figure 4.9:** Influence of different neocarzilin A concentrations on chemotaxis parameters of MDA-MB-231 (FMI-x: Efficiency of the forward migration along x-axis (gradient axis)).

#### 4.2.8 Effects of neocarzilin A and C on cellular viability and apoptosis

As impairment of cellular motility could have been arisen from high cellular toxicity of neocarzilin, the influences of neocarzilin A (4.1) and neocarzilin C (4.3) on proliferation and apoptosis induction were investigated. To measure antiproliferative properties, cells were incubated with different concentrations of neocarzilin A (4.1) for 24 h and 48 h and subsequently stained with crystal violet. Inhibition of proliferation was observed only after 48 h while neocarzilin A did not show any effect after 24 h in all cell lines (Figure 4.10).

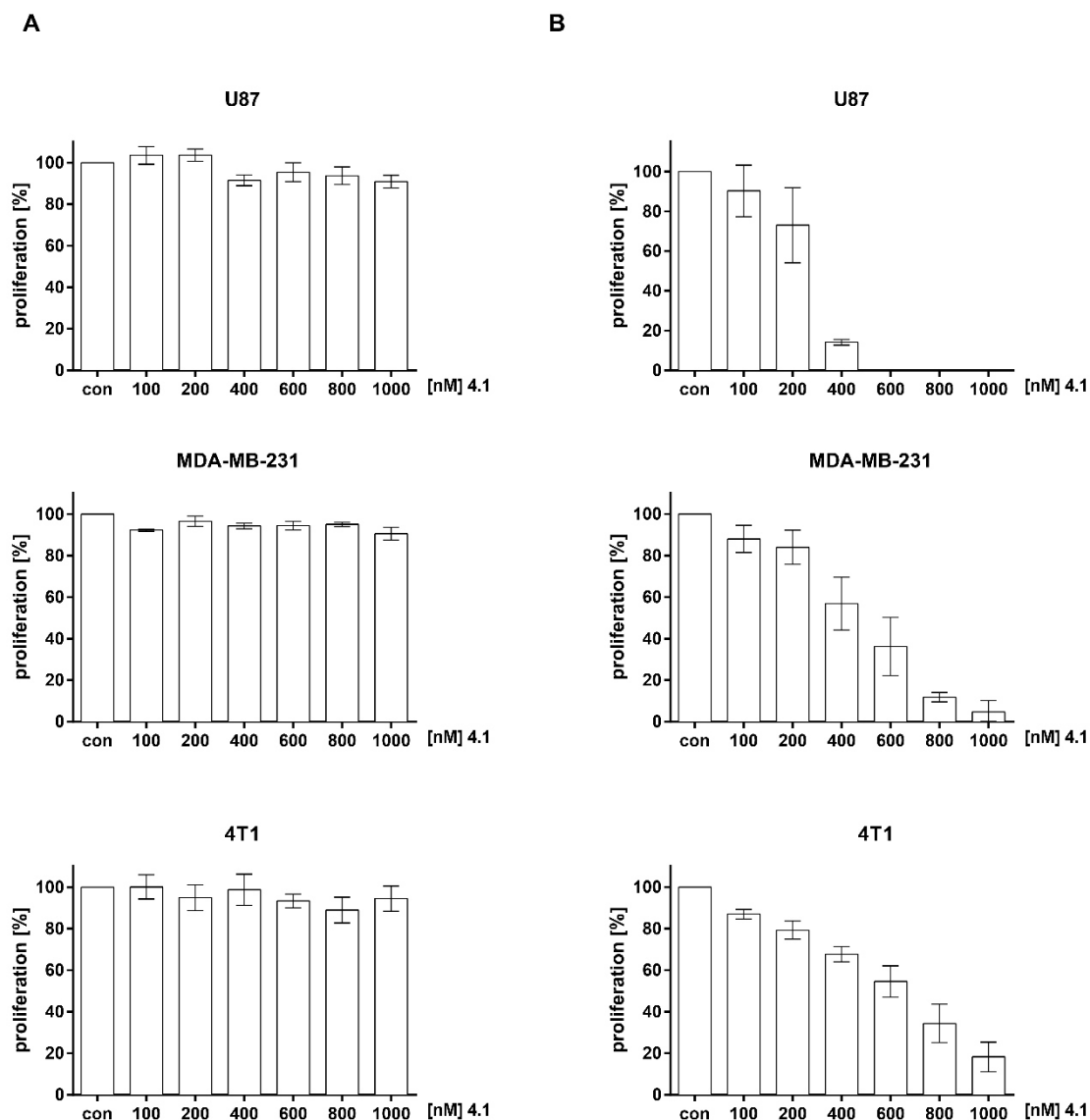


**Figure 4.10:** Crystal violet assay of neocarzilin A (**4.1**) in different cell lines after 24 h (A) and 48 h (B) ( $n = 3$ ).

These results confirmed that neocarzilin-induced abrogation of migration was not due to inhibition of proliferation, but was a clear anti-migratory effect. The inhibition of proliferation by neocarzilin C (**4.3**) for all cell lines was significantly lower ( $>1 \mu\text{M}$ ), probably due to the reduced reactivity of the dichloroketone moiety. Significant inhibition of migration was not observed, a result which is in good agreement with the lack of binding of neocarzilin C to VAT-1 in competitive labeling experiments (see Figure 4.3). To quantify the potential capability of neocarzilin A (**4.1**) to trigger apoptosis, Nicoletti assays<sup>224</sup> with MDA-MB-231 and 4T1 were performed. This assay quantifies the amount of DNA in cells so that the population of cells at different stages in the cell cycle can be quantified. Since apoptotic cells degrade their DNA by endonucleases, cells entering programmed cell death display a sub-G0/G1 peak in the fluorescence histogram. This can be used to quantify the relative

amount of cells entering this stage. After 48 h, the induction of apoptosis was below 10 % in both cell lines, even at concentrations capable of mostly abrogating proliferation (Figure 4.11).

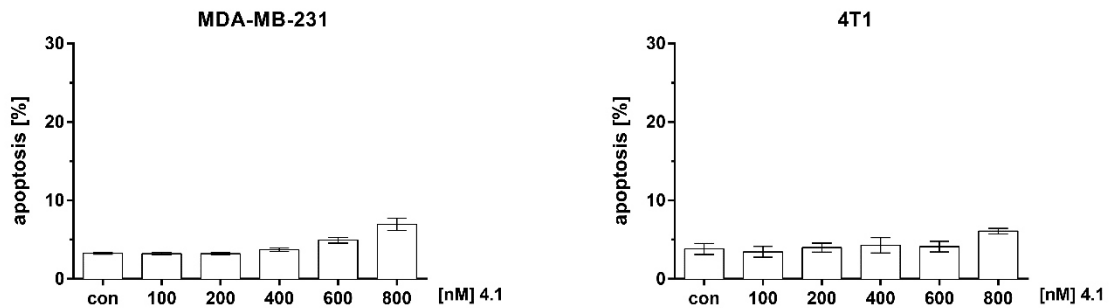


**Figure 4.11:** Apoptosis induction of neocarzilin A in MDA-MB-231 and 4T1 after 48 h.

#### 4.2.9 Effect of neocarzilin A on mitochondria

Neocarzilin A not only effected cell migration and proliferation but also had significant influence on the condition and motility pattern of mitochondria. MDA-MB-231 cells were incubated with different concentrations of the natural product for 24 h and stained with MitoTracker Red,<sup>225</sup> a covalent dye to label mitochondria. It displayed concentration-dependent clustering of the organelles.

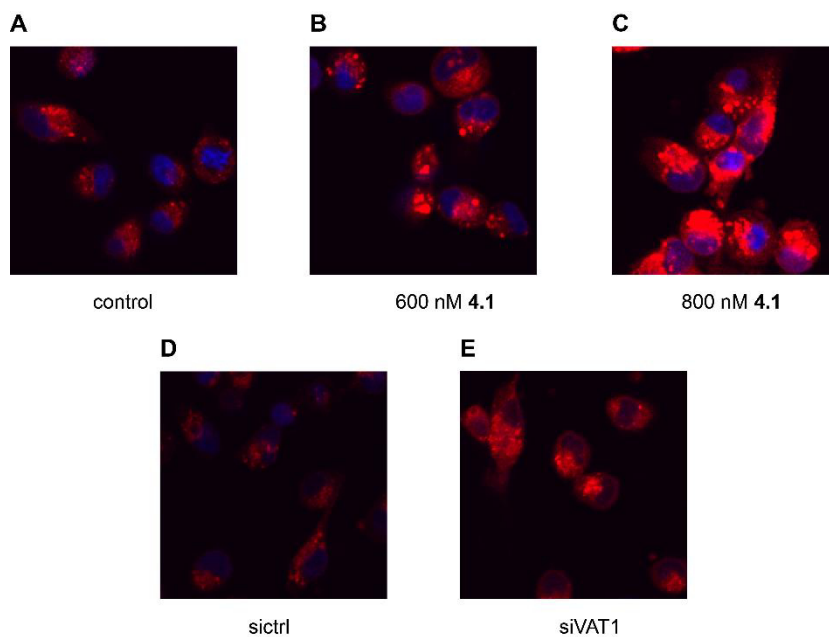


**Figure 4.12:** Mitotracker staining (red) of MDA-MB-231 cells after 24 h with DMSO (A), different concentrations of neocarzilin A (4.1) (B, C), control siRNA (D) and siVAT1 (E). Nuclei were stained with DAPI and are shown in blue.

This agglomeration effect was also observed when VAT-1 knockdown cells were stained, indicating the influence of VAT-1 on mitochondrial organization and movement (Figure 4.12). Although apoptosis induction was only fractional even at concentrations up to 1  $\mu$ M (see Figure 4.11), mitochondria displayed strongly impaired function when treated with neocarzilin for 24 h. When stained with JC-1, a dye which exhibits potential-dependent accumulation in mitochondria, the number of red fluorescent cells decreased and shifted to green (Figure 4.13A). This depolarisation of the mitochondrial membrane often indicates the first steps of apoptosis, a process accompanied by the alteration of the oxidation/reduction potential, leading to reduced ATP synthesis (Figure 4.13B).<sup>226</sup> Furthermore an increase in the production of ROS (reactive oxygen species) could be observed in step with rising neocarzilin concentrations (Figure 4.13C).

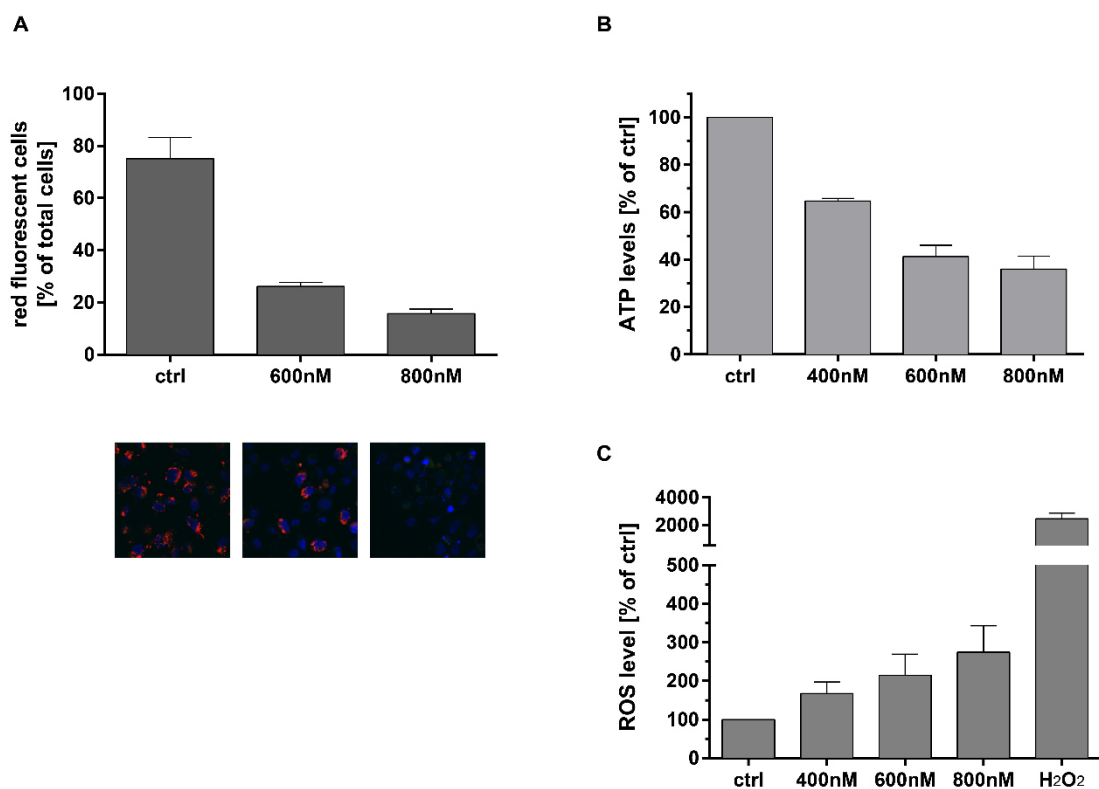


**Figure 4.13:** A) Neocarzilin A mediated membrane depolarisation using JC-1 fluorescence as readout. Concentration-dependent reduction of ATP-levels (B) and increase of ROS-production (C) due to neocarzilin exposure in MDA-MB-231.

The depolarisation of the membrane might be the result and/or the cause for increased levels of ROS. ROS trigger the “reactive oxygen species (ROS)-induced ROS-release” (RIRR), which leads to the collapse of the mitochondrial membrane potential and further contributes to the formation of ROS. ROS can be released into cytosol and trigger RIRR in neighboring mitochondria. This mitochondrion-to-mitochondrion ROS-signaling constitutes

a positive feedback mechanism for enhanced ROS production leading to potentially significant mitochondrial and cellular injury.<sup>226–228</sup>

#### **4.2.10 Identification of potential interaction partners of VAT-1 by co-immunoprecipitation**

To gain further insight into VAT-1 cellular function, experiments to identify potential interaction partners were performed. Co-immunoprecipitation uses the specific interaction of an antibody to its epitope to extract the desired protein from cell lysates. Since proteins form defined protein-protein interactions, not only the target protein, but also its interaction partners are enriched by pulldown. The antibodies can be immobilized on beads bearing protein-A/G. After digestion of the captured proteins on the beads, the resulting peptides can be analyzed by MS.<sup>217</sup> The big advantage of this method is the capture of proteins in their native state (provided lysis conditions are gentle) including posttranslational and cell-line specific modifications, a requirement for meaningful and unbiased information about specific protein-protein interactions.

To this end, HepG2 cells were lysed and subsequently mixed with protein-A/G coupled agarose beads and antiVAT-1 antibody or an isotype control. After incubation, washing, alkylation and digestion steps, the resulting peptides were subjected to MS-analysis. As expected, VAT-1 was the protein with the highest enrichment (15 x higher enrichment than for the 2<sup>nd</sup> highest enriched protein), a good indication for high antibody affinity (Figure 4.14).

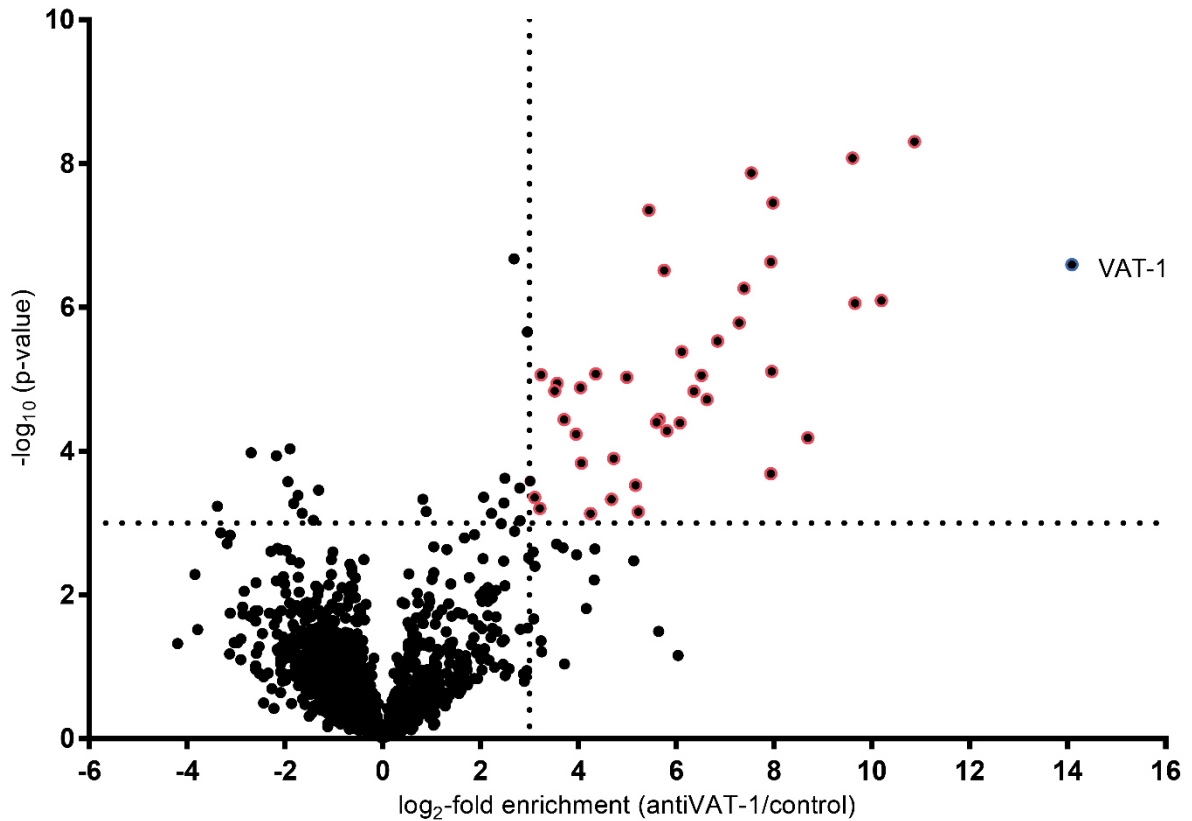


**Figure 4.14:** Volcano plot of a co-immunoprecipitation with antiVAT-1 in HepG2 cells. The volcano plot shows the statistical significance of enrichment levels (student's t-test p-value) as a function of average protein ratios from five biological replicates in siVAT-1-treated vs. isotype-control treated cells. VAT-1 is highlighted in blue, proteins with selected significance criteria ( $\log_2(\text{enrichment}) > 3$ ,  $p\text{-value} < 0.001$ ) are highlighted in red.

Among the proteins with the highest enrichment and statistical significance, phosphatidylinositol 3-kinase (PI3K) was the most obvious one regarding the observed phenotypes. Since this protein is involved in key cellular functions like cell growth, proliferation and migration,<sup>229,230</sup> the interactions of VAT-1 with this protein might contribute to the cellular effects triggered by neocarzilin A. Onishi *et al.* demonstrated that the PI3K-Akt pathway promotes microtubule stabilization, a key step in establishing cell polarity and subsequent cell migration.<sup>231</sup>

A list of the 15 highest enriched proteins is given in Table 4.2.



**Table 4.2:** Potential VAT-1 interaction partners identified by co-immunoprecipitation with a VAT-1 specific antibody.

<b>Protein name</b>	<b>Gene name</b>	<b>log<sub>2</sub>-fold enrichment</b>	<b>-log<sub>10</sub> (p-value)</b>
Synaptic vesicle membrane protein VAT-1 homolog	VAT1	14,08	6,59
Aspartate--tRNA ligase, mitochondrial	DARS2	10,87	8,30
(3R)-hydroxyacyl-CoA dehydrogenase	HSD17B4	10,19	6,10
Late secretory pathway protein AVL9 homolog	KIAA0241;AVL9	9,65	6,06
Copper-transporting ATPase 2	ATP7B	9,60	8,08
Very large A-kinase anchor protein	CRYBG3	8,69	4,19
Phosphatidylinositol 3-kinase catalytic subunit type 3	PIK3C3	7,98	7,45
Polyribonucleotide nucleotidyltransferase 1, mitochondrial	PNPT1	7,95	5,11
Coiled-coil domain-containing protein 9	CCDC9	7,93	6,63
SUN domain-containing protein 2	UNC84B;SUN2	7,93	3,69
Phosphoinositide 3-kinase regulatory subunit 4	PIK3R4	7,53	7,87
Microtubule cross-linking factor 1	MTCL1	7,38	6,26
Minor histocompatibility protein HA-1	HMHA1	7,28	5,79
Succinate dehydrogenase flavoprotein subunit, mitochondrial	SDHA	6,84	5,53
Rho GTPase-activating protein 17	ARHGAP17	6,63	4,72

Although influencing PI3K and subsequent signaling pathways might be a rational for the observed migration inhibition, there are no reports about a direct VAT-1/PI3K interaction in the literature. A database search for known VAT1 interaction partners using Cytoscape<sup>161</sup> could not identify a common hit. Seven known interaction partners of PI3K (Beclin-1, Nuclear receptor-binding factor 2, Endoplasmic reticulum chaperone, Beclin 1-associated autophagy-related key regulator, monofunctional C1-tetrahydrofolate synthase, mitochondrial, glutathione S-transferase P) were also identified with the co-immunoprecipitation using antiVAT-1. Since many of the identified proteins are involved in multiple cellular pathways, it was impossible to extract a coherent mode of action. However, a majority were linked to various isoforms

of tubulins (e.g. Microtubule cross-linking factor 1, Rho GTPase-activating protein 17). Tubulins are the building blocks of the microtubule, major components of the cytoskeleton. They are involved in intracellular transport and mitosis.<sup>232,233</sup> Most importantly, as mentioned before, they play a crucial role in cell migration,<sup>231,234</sup> a potential link to VAT-1 dependent migration behavior. Rho GTPases for example capture and stabilize microtubules through their effectors (e.g. IQGAP1, mDia and Par6) near the cell cortex, leading to polarised cell morphology and directional cell migration.<sup>190</sup> The Rho GTPase-activating protein 17, which was also identified as a potential interaction partner of VAT-1 or PI3K, plays a crucial role in the apical polarity of epithelial cells, an important step in cell motility and migration.<sup>235</sup>

### 4.3 Conclusion and outlook

The total synthesis of all known neocarzilins and a corresponding ABPP probe enabled the proteome wide identification of covalent targets of this class of polyene natural products in human cells. SILAC and label-free quantification was used in an ABPP approach employing an alkyne modified natural product to unravel covalent protein targets. Although two dozen potential targets were identified, this study focused on the synaptic vesicle membrane protein VAT-1 homolog (VAT-1), an integral membrane protein which could be observed down to 1 nM in analytical labeling experiments. The intriguing role of this protein in the cell migration of metastatic cancer led to the further characterization of the effects of neocarzilins on tumor tissue. Neocarzilin inhibited migration of diverse cancer cell lines in the nanomolar range, which was in good accordance with VAT-1 knockdown studies. Neocarzilin-treated cells also showed impaired velocity and directness of migration. Furthermore neocarzilin A displayed strong antiproliferative properties after two days but induced no apoptosis. Imaging studies also revealed clustering of mitochondria and a reduction of mitochondrial membrane potential. Since there was not much known about the role of VAT-1 in human cells, co-immunoprecipitation was performed to elucidate potential interaction partners of VAT-1. The regulatory and the catalytic subunit of the PI3K complex (phosphatidylinositol 3-kinase) were among the most confident hits. Since PI3K enzymes are responsible for signal transduction and multiple regulatory functions in cells, the interaction with VAT-1 might account for the observed phenotypes. Nevertheless further extensive studies need to be carried out to clarify the complex effects of VAT-1 inhibition and/or the influence of other proteins targeted by the neocarzilins. These studies would not only include investigation of changes in the proteome and metabolome of neocarzilin treated cells, but also the phenotypic effects and stability of neocarzilins *in vivo*.

Small molecules still represent the most important tool for combating various diseases, from bacterial infections to tumor formation. The inhibition of migration and metastasis with small molecules is a major endeavor in the fight against cancer. However, there is no drug currently available on the market which is capable of intervening these processes. Addressing this problem is even more pressing since over 90 % of all cancer deaths are due to the formation of metastases.<sup>236</sup> VAT-1 might represent an attractive new target for future research on anti-metastatic drugs not only through its inhibition but also for understanding the complex network of signaling and regulation that underlies cell migration and metastasis.

## 5 Experimental Section

### 5.1 Organic Synthesis

#### 5.1.1 General Methods and Materials

All chemicals and reagents were purchased reagent grade or higher from commercial sources (Sigma-Aldrich Co. LLC, Thermo Fisher Scientific Inc., Merck KGaA, ABCR GmbH & Co. KG, TCI Europe GmbH, Alfa Aesar, Roth). All technical solvents were distilled prior to use. Anhydrous solvents were purchased from commercial sources (Sigma-Aldrich Co. LLC, Thermo Fisher Scientific Inc., VWR International, LLC).

Cooling baths [ice/water (0 °C), ice/acetone (-10 °C), ice/NaCl (-20 °C) and dry ice/acetone (-78 °C)] were used to maintain low temperatures as indicated in the experimental procedures. All temperatures were measured externally. All reactions were performed in oven-dried glassware under an argon atmosphere. Analytical thin-layer chromatography (TLC) was carried out on Merck silica-gel plates, using short wave UV light (254 nm) or common TLC stains (KMnO<sub>4</sub>, Hessian) to visualize components, as indicated for each compound. Silica gel (Kieselgel 60, 40–63 µm, Merck KGaA) was used for flash column chromatography.

Preparative TLC was carried out on TLC Silica gel 60 F<sub>254</sub> (20 x 20 cm) plates from Merck KGaA or pre-coated TLC plates DIL G-200 from MACHEREY-NAGEL GmbH & Co. KG. The compounds were detected with short wave UV light (254 nm) and scraped off with a scalpel.

Reversed phase HPLC (RP-HPLC) analysis was performed on a Waters 2695 separation module, equipped with a Waters PDA 2996 and a Waters XBridge C18 column (3.5 µm, 4.6 x 100 mm, flow = 1.2 mL/min). For preparative scale RP-HPLC separation a Waters 2545 quaternary gradient module combined with a Waters PDA 2998 and Waters XBridge™Prep C18 (5.0 µm, 30 x 150 mm, flow = 50 mL/min or 10 µm, 50 x 250 mm, flow = 130 mL/min) column or a YMC Triart C18 (3.5 µm, 10 x 250 mm, flow = 10 mL/min) column was used. The mobile phase for elution consisted of a gradient mixture of 0.1 % (v/v) TFA in water (buffer A, HPLC grade), 0.1 % (v/v) TFA in acetonitrile (buffer B, HPLC grade), water (buffer C, HPLC grade) and acetonitrile (buffer D, HPLC grade).

Following setup was used for analytical HPLC separation of enantiomers: Daicel ChiralPak AD-RH (250 x 4.6 mm). Further components: P580 Pump, ASI-100 Automated Sample Injector, UVD 340 U Photodiode Array Detector (Dionex).

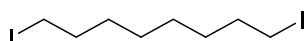
For analytical gas chromatography (GC), a HP 6890 Series GC-System of Agilent was used (flame ionisation detector and hydrogen as a carrier gas at 160 kPa). For measurements on an achiral stationary phase, a HP-5-column (Poly-dimethyl/diphenyl-siloxane, 95/5) was used. For measurements on a chiral stationary phase, 2,3-Dimethyl-6-TBDMS- $\beta$ -cyclodextrine-modified columns were used.

$^1\text{H}$ - and  $^{13}\text{C}$ -NMR spectra were recorded on a Bruker Avance I 300 (300 MHz), a Bruker Avance I (500 MHz) or a Bruker Avance III 500 (500 MHz) NMR-System and referenced to the residual proton/carbon signal of the deuterated solvent ( $\text{CDCl}_3$ : 7.26, 77.16;  $\text{D}_2\text{O}$ : 4.79; acetone- $\text{D}_6$ : 2.05, 29.84, 206.26;  $\text{DMSO-}D_6$ : 2.50, 39.52). Chemical shifts are reported in parts per million (ppm). Coupling constants (J) are in hertz and multiplicity is reported as follows: s = singlet, br s = broad singlet, d = doublet, t = triplet, q = quartet, m = multiplet or unresolved.

HR-ESI-MS, HR-LC-ESI-MS, HR-APCI-MS and HR-LC-APCI-MS mass spectra were recorded with a LTQ FT Ultra coupled with an UltiMate 3000 HPLC system (Thermo Fisher Scientific Inc.).

### 5.1.2 Synthetic procedures for chapter 2: Target identification of falcarinol in cancer cells.

#### 1,8-Diiodooctane (2.6)



Chemical Formula:  $\text{C}_8\text{H}_{16}\text{I}_2$   
Molecular Weight: 366,02

To a solution of 8.00 g (54.7 mmol, 1.00 eq) octane-1,8-diol and 30.3 mL (22.1 g, 219 mmol, 4.00 eq)  $\text{NEt}_3$  in  $\text{CH}_2\text{Cl}_2$  (60 mL) 21.9 g (115 mmol, 2.10 eq) tosyl chloride were added at 0 °C. The solution was warmed up to rt over 30 min and water (60 mL) was added. The phases were separated, the aqueous phase was extracted two times with  $\text{CH}_2\text{Cl}_2$  (2 x 50 mL) and the combined organic fractions washed with brine (50 mL). After filtration over  $\text{Na}_2\text{SO}_4$ , the solvent was removed under reduced pressure. The crude product octane-1,8-diyl bis(4-methylbenzenesulfonate) was directly used without further purification. 22.6 g (49.7 mmol, 1.00 eq) tosylate were dissolved in acetone (100 mL) and 14.9 g (99.4 mmol, 2.00 eq)  $\text{NaI}$  were added. After 16 h at rt, the reaction was stopped by addition of water. The mixture was extracted with hexane (3 x 50 mL), the combined organic fraction dried

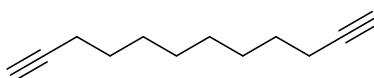
and the solvent was removed under reduced pressure. Filtration over a plug of silica yielded 14.3 g (38.9 mmol, 77 %) iodide.

$R_f = 0.35$  (hexanes) [KMnO<sub>4</sub>]

<sup>1</sup>H NMR (360 MHz, CDCl<sub>3</sub>, 300 K):  $\delta$  (ppm) = 3.19 (t,  $J = 7.0$  Hz, 4H), 1.89 – 1.74 (m, 4H), 1.47 – 1.25 (m, 8H).

<sup>13</sup>C NMR (91 MHz, CDCl<sub>3</sub>, 300 K):  $\delta$  (ppm) = 33.6, 30.5, 28.5, 7.3.

### Dodeca-1,11-diyne (2.7)



Chemical Formula: C<sub>12</sub>H<sub>18</sub>

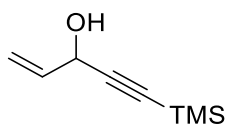
Molecular Weight: 162,28

To 4.03 g (41.0 mmol, 3.00 eq) ethynyltrimethylsilane in anhydrous THF (50 mL) *n*BuLi (12.6 mL, 2.5 M in hexane, 31.5 mmol, 2.30 eq) was added at 0 °C. The reaction mixture was stirred for 30 min at this temperature and 5.00 g (13.7 mmol, 1.00 eq) iodide **2.6** in dry DMPU (40 mL) was added. The solution was stirred for another hour and then quenched by addition of cold water. The mixture was extracted three times with hexane (3 x 50 mL). The organic fractions were combined, dried and filtered. After removal of the solvent, the crude product was dissolved in 150 mL MeOH and 4.72 g (34.1 mmol, 2.50 eq) K<sub>2</sub>CO<sub>3</sub> were added at rt. The mixture was stirred for 3 h. Water (100 mL) and hexane (150 mL) were added, the phases separated and the aqueous phase reextracted with hexane (2 x 50 mL). The combined organic fractions were dried over Na<sub>2</sub>SO<sub>4</sub> and the solvent evaporated. Purification via flash chromatography (hexanes) yielded 1.70 g (10.5 mmol, 76 %) of diyne as a colorless oil.

$R_f = 0.40$  (hexanes) [KMnO<sub>4</sub>]

<sup>1</sup>H NMR (360 MHz, CDCl<sub>3</sub>, 300 K):  $\delta$  (ppm) = 2.18 (td,  $J = 7.0, 2.6$  Hz, 4H), 1.93 (t,  $J = 2.6$  Hz, 2H), 1.58 – 1.47 (m, 4H), 1.44 – 1.24 (m, 8H).

<sup>13</sup>C NMR (91 MHz, CDCl<sub>3</sub>, 300 K):  $\delta$  (ppm) = 84.9, 68.2, 29.1, 28.8, 28.6, 18.5.

**5-(Trimethylsilyl)pent-1-en-4-yn-3-ol (2.22)**

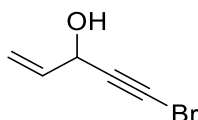
Chemical Formula: C<sub>8</sub>H<sub>14</sub>OSi  
Molecular Weight: 154,28

4.00 g (5.80 mL, 40.7 mmol, 1.00 eq) ethynyltrimethylsilane in dry THF (120 mL) was cooled to -78 °C and 16.3 mL (40.7 mmol, 2.5 M in hexane, 1.00 eq) nBuLi were added. After 30 min at -78 °C, 2.73 g (3.26 mL, 48.9 mmol, 1.20 eq) acroleine were added. The reaction solution was warmed up to rt. The reaction was quenched with sat. NH<sub>4</sub>Cl-solution (150 mL), extracted with Et<sub>2</sub>O (3x100 mL), dried over Na<sub>2</sub>SO<sub>4</sub> and filtrated. The solvent was removed under reduced pressure and the crude product filtered through a plug of silica. 4.50 g (29.2 mmol, 72 %) alcohol as a slightly yellow oil were obtained.

*R<sub>f</sub>* = 0.55 (CH<sub>2</sub>Cl<sub>2</sub>) [KMnO<sub>4</sub>]

<sup>1</sup>H NMR (300 MHz, CDCl<sub>3</sub>, 300 K): δ (ppm) = 5.96 (ddd, *J* = 17.1, 10.1, 5.3 Hz, 1H), 5.46 (dt, *J* = 17.0, 1.4 Hz, 1H), 5.22 (dt, *J* = 10.1, 1.3 Hz, 1H), 4.93 – 4.77 (m, 1H), 2.09 (d, *J* = 6.4 Hz, 1H), 0.18 (s, 9H)

<sup>13</sup>C NMR (91 MHz, CDCl<sub>3</sub>, 300 K): δ (ppm) = 136.8, 116.7, 104.1, 91.3, 63.7, -0.1.

**5-Bromopent-1-en-4-yn-3-ol (2.8)<sup>237</sup>**

Chemical Formula: C<sub>5</sub>H<sub>5</sub>BrO  
Molecular Weight: 161,00

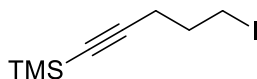
2.50 g (16.2 mmol, 1.00 eq) 5-(trimethylsilyl)pent-1-en-4-yn-3-ol were dissolved in acetone (65 mL) and 550 mg (3.24 mmol, 1.00 eq) silver(I) nitrate and 4.33 g (24.3 mmol, 1.50 eq) NBS were added. The mixture was stirred for 4 h at rt and quenched with water (35 mL). The reaction mixture was extracted with Et<sub>2</sub>O (3 x 30 mL), the combined organic fractions dried and the solvent evaporated under reduced pressure. Purification via flash chromatography (CH<sub>2</sub>Cl<sub>2</sub>) yielded 2.33 g (14.5 mmol, 89 %) bromo alkyne **3** as a yellow oil.

*R<sub>f</sub>* = 0.51 (CH<sub>2</sub>Cl<sub>2</sub>) [UV, CAM, KMnO<sub>4</sub>]

**<sup>1</sup>H NMR** (300 MHz, CDCl<sub>3</sub>, 300 K): δ (ppm) = 5.95 (ddd, *J* = 17.0, 10.1, 5.3 Hz, 1H), 5.47 (*virt. dt*, *J* = 17.0, 1.3 Hz, 1H), 5.25 (*virt. dt*, *J* = 10.2, 1.2 Hz, 1H), 4.90 (*virt. dt*, *J* = 5.4, 1.5 Hz, 1H).

**<sup>13</sup>C NMR** (75 MHz, CDCl<sub>3</sub>, 300 K): δ (ppm) = 136.8, 117.5, 79.3, 64.5, 47.4.

**(5-Iodopent-1-yn-1-yl)trimethylsilane (2.9)**



Chemical Formula: C<sub>8</sub>H<sub>15</sub>ISi

Molecular Weight: 266,20

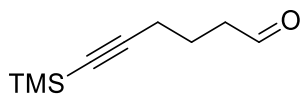
8.00 g (45.8 mmol, 1.00 eq) chloride was added to a solution of 13.7 g (91.6 mmol, 2.00 eq) NaI in acetone (100 mL). The solution was heated to reflux for 16 h. After the reaction mixture was cooled to rt, the precipitated salt was removed by filtration and water was added. The mixture was extracted with Et<sub>2</sub>O (2 x 100 mL), the organic fractions combined, dried and the solvent removed under reduced pressure. 9.50 g (35.7 mmol, 78 %) iodide were obtained as a yellow oil.

*R<sub>f</sub>* = 0.54 (hexanes) [KMnO<sub>4</sub>]

**<sup>1</sup>H NMR** (360 MHz, CDCl<sub>3</sub>, 300 K): δ (ppm) = 3.29 (t, *J* = 6.8 Hz, 1H), 2.36 (t, *J* = 6.8 Hz, 1H), 2.00 (p, *J* = 6.8 Hz, 1H), 0.15 (s, 4H).

**<sup>13</sup>C NMR** (91 MHz, CDCl<sub>3</sub>, 300 K): δ (ppm) = 0.1, 5.0, 20.8, 32.1, 85.7, 104.7.

**6-(Trimethylsilyl)hex-5-ynal (2.10)**



Chemical Formula: C<sub>9</sub>H<sub>16</sub>OSi

Molecular Weight: 168,31

To 5.00 g (29.3 mmol, 1.00 eq) 6-(trimethylsilyl)hex-5-yn-1-ol in dry CH<sub>2</sub>Cl<sub>2</sub> (20 mL) 20.0 mL (117 mmol, 4.00 eq) Hünigs base were added. The solution was cooled to -20 °C and 18.6 g (117 mmol, 4.00 eq) Pyr·SO<sub>3</sub> in DMSO (30 mL) were added dropwise over 20 min. The reaction solution was stirred for another 20 min and then quenched with 1 N HCl at -20 °C. The reaction was extracted with CH<sub>2</sub>Cl<sub>2</sub> (3 x 30 mL), dried over Na<sub>2</sub>SO<sub>4</sub> and filtrated.



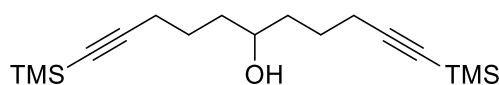
Purification via flash chromatography (hexanes/EtOAc 15:1 → 10:1) yielded 3.10 g (18.4 mmol, 63 %) aldehyde as a yellow liquid.

$R_f$  = 0.51 (hexanes/EtOAc 10:1) [KMnO<sub>4</sub>]

<sup>1</sup>H NMR (360 MHz, CDCl<sub>3</sub>, 300 K): δ (ppm) = 9.81 (t,  $J$  = 1.4 Hz, 1H), 2.58 (td,  $J$  = 7.2, 1.4 Hz, 2H), 2.30 (t,  $J$  = 6.9 Hz, 2H), 1.84 (p,  $J$  = 7.0 Hz, 2H), 0.14 (s, 9H).

<sup>13</sup>C NMR (91 MHz, CDCl<sub>3</sub>, 300 K): δ (ppm) = 202.0, 106.0, 86.0, 42.8, 21.2, 19.4, 0.2.

**1,11-Bis(trimethylsilyl)undeca-1,10-diyn-6-ol (2.11)**



Chemical Formula: C<sub>17</sub>H<sub>32</sub>OSi<sub>2</sub>

Molecular Weight: 308,61

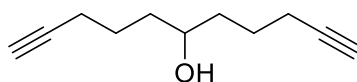
To a solution of 4.28 g (16.1 mmol, 1.00 eq) (5-iodopent-1-yn-1-yl)trimethylsilane in 75 mL Heptane/Et<sub>2</sub>O (3:2) at -78 °C were added 19.4 mL (33.0 mmol, 1.70 M in pentane, 2.05 eq) <sup>t</sup>BuLi. The reaction mixture was stirred for 30 min before addition of 3.25 g (19.3 mmol, 1.20 eq) aldehyde in Et<sub>2</sub>O (10 mL). The reaction mixture was warmed up to rt and quenched with water. The layers were separated and the aqueous phase was extracted with Et<sub>2</sub>O (2x50 mL). The combined organic fractions were dried, filtered and the solvent was removed under reduced pressure. Purification via flash chromatography (hexanes/Et<sub>2</sub>O 4:1 → 1:2) yielded 3.30 g (10.7 mmol, 66 %) as a colorless oil.

$R_f$  = 0.35 (hexanes/Et<sub>2</sub>O 1:1) [UV, CAM, KMnO<sub>4</sub>]

<sup>1</sup>H NMR (360 MHz, CDCl<sub>3</sub>, 300 K): δ (ppm) = 3.77 – 3.58 (m, 1H), 2.30 – 2.20 (m, 4H), 1.67 – 1.45 (m, 9H), 0.14 (s, 18H).

<sup>13</sup>C NMR (91 MHz, CDCl<sub>3</sub>, 300 K): δ (ppm) = 107.4, 85.0, 71.0, 36.6, 24.8, 19.9, 0.3.

HRMS ESI calcd. for C<sub>18</sub>H<sub>33</sub>O<sub>3</sub>Si<sub>2</sub> [M+HCOOH-H]<sup>+</sup>: 353.1974, found: 353.1977.

**Undeca-1,10-diyn-6-ol (2.12)**Chemical Formula: C<sub>11</sub>H<sub>16</sub>O

Molecular Weight: 164,25

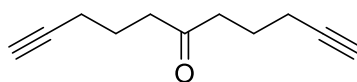
3.30 g (10.7 mmol, 1.00 eq) alcohol **4** were dissolved in MeOH (30 mL) and 3.40 g (24.6 mmol, 2.30 eq) K<sub>2</sub>CO<sub>3</sub> were added at rt. The mixture was stirred overnight. Standard workup with NH<sub>4</sub>Cl solution (20 mL) and subsequent extraction with Et<sub>2</sub>O (2 x 30 mL) was applied. Purification via flash chromatography (hexanes/EtOAc 6:1) yielded 1.76 g (10.7 mmol, quant.) as a colorless oil.

*R<sub>f</sub>* = 0.32 (hexanes /Et<sub>2</sub>O = 3:1) [CAM, KMnO<sub>4</sub>]

**<sup>1</sup>H NMR** (360 MHz, CDCl<sub>3</sub>, 300 K): δ (ppm) = 3.75 – 3.59 (m, 1H), 2.23 (dt, *J* = 6.5, 3.3 Hz, 4H), 1.96 (t, *J* = 2.7 Hz, 2H), 1.72 – 1.49 (m, 8H).

**<sup>13</sup>C NMR** (91 MHz, CDCl<sub>3</sub>, 300 K): δ (ppm) = 84.4, 71.1, 68.7, 36.6, 24.6, 18.5.

**HRMS ESI** calcd. for C<sub>12</sub>H<sub>17</sub>O<sub>3</sub> [M+FA-H]<sup>-</sup>: 209.1183, found: 209.1189.

**Undeca-1,10-diyn-6-one (2.13)**Chemical Formula: C<sub>11</sub>H<sub>14</sub>O

Molecular Weight: 162,23

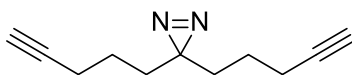
1.85 g (11.3 mmol, 1.00 eq) alcohol **5** were dissolved in CH<sub>2</sub>Cl<sub>2</sub> (150 mL) and 3.64 g (16.9 mmol, 1.50 eq) PCC and 1.11 g (13.6 mmol, 1.20 eq) NaOAc were added. The reaction mixture was stirred at rt for 20 h. The reaction mixture was filtered through a short plug of silica and the solvent evaporated. Purification via flash chromatography (hexanes/EtOAc 20:1) yielded 1.50 g (9.25 mmol, 82 %) ketone as a clear oil.

*R<sub>f</sub>* = 0.44 (hexanes/Et<sub>2</sub>O = 9:1) [CAM, KMnO<sub>4</sub>]

**<sup>1</sup>H NMR** (360 MHz, CDCl<sub>3</sub>, 300 K): δ (ppm) = 2.57 (td, *J* = 7.3, 1.4 Hz, 4H), 2.32 – 2.17 (m, 4H), 1.96 (d, *J* = 2.6 Hz, 2H), 1.79 (t, *J* = 7.2 Hz, 4H).

**<sup>13</sup>C NMR** (91 MHz, CDCl<sub>3</sub>, 300 K): δ (ppm) = 209.7, 83.6, 69.1, 41.3, 22.3, 17.9.

**HRMS ESI** calcd. for C<sub>11</sub>H<sub>15</sub>O [M+H]<sup>+</sup>: 163.1117, found: 163.1118.

**3,3-Di(pent-4-yn-1-yl)-3H-diazirine (2.14)**Chemical Formula: C<sub>11</sub>H<sub>14</sub>N<sub>2</sub>

Molecular Weight: 174,25

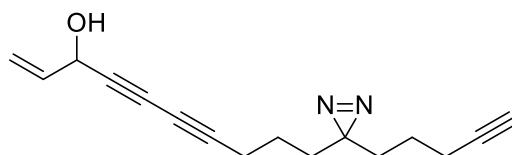
To a 25 mL flask containing 500 mg (3.08 mmol, 1.00 eq) ketone **6** in an ice bath, 6.60 mL (46.2 mmol, 15.0 eq) 7 N ammonia in MeOH were added. After sealing of the flask, the reaction mixture was stirred at -10 °C for 5 h. 450 mg (3.98 mmol, 1.32 eq) hydroxylamine O-sulfonic acid were dissolved in methanol and added dropwise into the reaction mixture. After stirring overnight, most ammonia was removed by gently blowing argon through the suspension using a glass pipette and the white precipitate was filtered off. After removal of the solvents under reduced pressure, the residue was redissolved in methanol followed by the addition of 640 μL (4.62 mmol, 1.5 equiv.) triethylamine. Subsequently, the solution was cooled to 0 °C, and iodine was slowly added until the color of iodine persisted for 1 min. After 2 h, water and Et<sub>2</sub>O were added. The organic phase was separated and the aqueous phase extracted with hexane (2 x 20 mL). The combined organic fractions were dried and filtered. Purification via flash chromatography (hexanes/Et<sub>2</sub>O 25:1 → 10:1) yielded 208 mg (1.12 mmol, 36 %) diazirine as a colorless oil.

*R*<sub>f</sub> = 0.87 (hexanes/EtOAc = 10:1) [CAM, KMnO<sub>4</sub>]

<sup>1</sup>H-NMR (360 MHz, 300 K, CDCl<sub>3</sub>): δ 2.16 (td, *J* = 6.9, 2.6 Hz, 4H), 1.94 (t, *J* = 2.7 Hz, 2H), 1.55 – 1.47 (m, 4H), 1.39 – 1.27 (m, 4H).

<sup>13</sup>C-NMR (90 MHz, 300 K, CDCl<sub>3</sub>): δ 83.5, 69.1, 31.9, 28.1, 22.9, 18.1.

HRMS ESI calcd. for C<sub>11</sub>H<sub>15</sub>N<sub>2</sub> [M+H]<sup>+</sup>: 175.1229, found: 175.1231.

**10-(3-(Pent-4-yn-1-yl)-3H-diazirin-3-yl)deca-1-en-4,6-diyn-3-ol (2.4)**Chemical Formula: C<sub>16</sub>H<sub>18</sub>N<sub>2</sub>O

Molecular Weight: 254,33

To a solution of 13 mg (0.19 mmol, 0.33 eq.) hydroxylaminehydrochloride in MeOH (1 mL) at 0 °C was added a solution of 0.20 mL ethylamine (70-%) and 5.70 mg (0.06 mmol, 0.10 eq.) CuCl in MeOH (1 mL). 100 mg (0.57 mmol, 1.00 eq.) diyne **7** in CH<sub>2</sub>Cl<sub>2</sub> (1 mL) were

added at 0 °C. 69 mg (0.43 mmol, 0.75 eq.) bromo alkyne **3** in CH<sub>2</sub>Cl<sub>2</sub> (0.5 mL) were added over 30 min. The mixture was stirred for 4 h. The reaction was ceased by addition of water and the emulsion was extracted with Et<sub>2</sub>O (2 x 30 mL). After evaporation of the solvent, the resulting brown-orange oil was submitted to flash chromatography (hexanes/EtOAc 10:1 → 3:1). 34.0 mg (0.13 mmol, 31 %) of the desired diazirine were isolated as a brown oil.

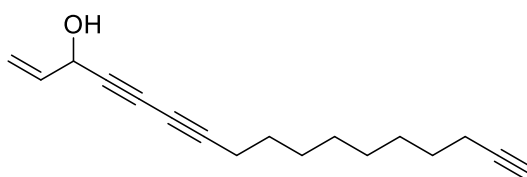
$R_f$  = 0.35 (hexanes/EtOAc 6:1) [KMnO<sub>4</sub>]

**<sup>1</sup>H NMR** (360 MHz, CDCl<sub>3</sub>, 300 K): δ (ppm) = 5.94 (ddd,  $J$  = 17.0, 10.1, 5.3 Hz, 1H), 5.46 (*virt. dt*,  $J$  = 17.0, 1.2 Hz, 1H), 5.25 (*virt. dt*,  $J$  = 10.1, 1.2 Hz, 1H), 4.92 (s, 1H), 2.27 (td,  $J$  = 6.8, 0.9 Hz, 2H), 2.16 (td,  $J$  = 6.9, 2.6 Hz, 2H), 1.95 (t,  $J$  = 2.6 Hz, 1H), 1.92 (s, 1H), 1.59 – 1.46 (m, 4H), 1.34 (dt,  $J$  = 9.6, 6.9 Hz, 4H).

**<sup>13</sup>C NMR** (91 MHz, CDCl<sub>3</sub>, 300 K): δ (ppm) = 136.2, 117.3, 83.5, 81.0, 74.4, 71.3, 69.2, 65.2, 63.7, 32.0, 31.9, 28.1, 22.8, 22.6, 19.0, 18.1.

**HRMS ESI** calcd. for C<sub>16</sub>H<sub>19</sub>N<sub>2</sub>O [M+H]<sup>+</sup>: 255.1497, found: 255.1493.

### Heptadeca-1-en-4,6,16-triyn-3-ol (**2.2**)



Chemical Formula: C<sub>17</sub>H<sub>22</sub>O

Molecular Weight: 242,36

To a solution of 42.0 mg (0.66 mmol, 0.33 eq.) hydroxylaminehydrochloride in MeOH (2 mL) was added a solution of 0.60 mL ethylamine (70-%) and 20.0 mg (0.20 mmol, 0.10 eq.) CuCl in MeOH (0.5 mL). 212 mg (1.30 mmol, 1.00 eq.) diyne **2** in CH<sub>2</sub>Cl<sub>2</sub> (3 mL) were added at 0 °C. 158 mg (0.98 mmol, 0.75 eq.) bromo alkyne **3** in CH<sub>2</sub>Cl<sub>2</sub> (1.5 mL) were added over 30 min. The mixture was stirred for 4 h. The reaction was terminated by addition of water and the mixture was extracted with Et<sub>2</sub>O (3 x 20 mL). The combined organic fractions were dried and the solvent evaporated under reduced pressure. Purification via flash chromatography (hexanes/EtOAc 10:1 → 3:1) yielded 90.0 mg (0.37 mmol, 38 %) diyne as a slightly yellow oil.

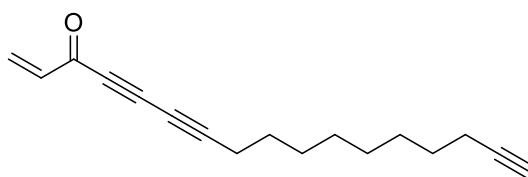
$R_f$  = 0.31 (hexanes/EtOAc 6:1) [CAM, KMnO<sub>4</sub>]

**<sup>1</sup>H NMR** (360 MHz, CDCl<sub>3</sub>, 300 K): δ (ppm) = 5.95 (ddd, *J* = 17.0, 10.1, 5.3 Hz, 1H), 5.46 (*virt. dt*, *J* = 17.0, 1.3 Hz, 1H), 5.24 (*virt. dt*, *J* = 10.1, 1.2 Hz, 1H), 4.92 (*virt. dt*, *J* = 5.4, 1.3 Hz, 1H), 2.37 – 2.09 (m, 4H), 1.94 (t, *J* = 2.6 Hz, 1H), 1.85 (s, 1H), 1.57 – 1.22 (m, 12H).

**<sup>13</sup>C NMR** (91 MHz, CDCl<sub>3</sub>, 300 K): δ (ppm) = 136.4, 117.2, 84.9, 82.6, 74.0, 71.6, 68.3, 64.5, 63.7, 29.0, 28.9, 28.8, 28.6, 28.2, 19.4, 18.5.

**HRMS APCI** calcd. for C<sub>17</sub>H<sub>21</sub>O [M-H]<sup>-</sup>: 241.1595, found: 241.1598.

**Heptadeca-1-en-4,6,16-triyn-3-one (2.3)**



Chemical Formula: C<sub>17</sub>H<sub>20</sub>O

Molecular Weight: 240,35

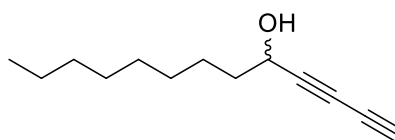
80.0 mg (0.33 mmol, 1.00 eq) **2.2** were dissolved in Et<sub>2</sub>O (20 mL) and 574 mg (6.60 mmol, 20.0 eq) activated MnO<sub>2</sub> were added. The mixture was stirred at rt for 2 h. The mixture was filtered through a short plug of silica and the solvent removed under reduced pressure. Purification via flash chromatography (hexanes → hexanes/EtOAc 20:1) yielded 53 mg (0.22 mmol, 67 %) ketone as a yellow oil.

*R<sub>f</sub>* = 0.57 (hexanes/Et<sub>2</sub>O 20:1) [UV, KMnO<sub>4</sub>]

**<sup>1</sup>H NMR** (360 MHz, CDCl<sub>3</sub>, 300 K): δ (ppm) = 6.65 – 6.47 (m, 1H), 6.48 – 6.33 (m, 1H), 6.19 (d, *J* = 10.1 Hz, 1H), 2.37 (t, *J* = 7.0 Hz, 2H), 2.18 (td, *J* = 7.0, 2.6 Hz, 2H), 1.94 (d, *J* = 2.7 Hz, 1H), 1.64 – 1.23 (m, 12H).

**<sup>13</sup>C NMR** (91 MHz, CDCl<sub>3</sub>, 300 K): δ (ppm) = 178.0, 138, 134.2, 90.5, 84.8, 70.6, 68.3, 64.1, 29.2, 29.0, 28.9, 28.8, 28.6, 27.9, 19.8, 18.5.

**HRMS APCI** calcd. for C<sub>17</sub>H<sub>21</sub>O [M+H]<sup>+</sup>: 241.1586, found: 241.1587.

**Trideca-1,3-diyn-5-ol (2.20)**Chemical Formula: C<sub>13</sub>H<sub>20</sub>O

Molecular Weight: 192,30

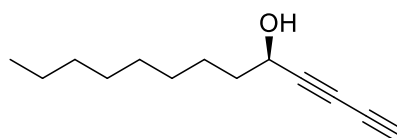
1.00 g (5.14 mmol, 1.00 eq) 1,4-bis(trimethylsilyl)buta-1,3-diyne was dissolved in anhydrous Et<sub>2</sub>O (10 mL) under argon and 3.53 mL (5.64 mmol, 1.6 M in Et<sub>2</sub>O, 1.10 eq) MeLi were added at 0 °C. The reaction mixture was stirred at that temperature for 3 h and then cooled to -20 °C. 800 mg (5.64 mmol, 1.10 eq) nonanal were added and the reaction warmed up to rt. After 1 h, the reaction was quenched by addition of sat. NH<sub>4</sub>Cl solution (20 mL). The mixture was extracted with Et<sub>2</sub>O (2 x 30 mL). After filtration of the combined organic fractions over Na<sub>2</sub>SO<sub>4</sub>, the solvent was removed under reduced pressure. The crude product was dissolved in THF (20 mL) and 1 M NaOH (20 mL) was added. The mixture was stirred at rt for 15 min and acidified by addition of 2 M HCl (20 mL). After extraction with Et<sub>2</sub>O (2 x 20 mL), the combined organic fractions were dried over Na<sub>2</sub>SO<sub>4</sub>. The solvent was evaporated and the resulting crude product purified via flash chromatography (hexanes/Et<sub>2</sub>O 10:1). 516 mg (2.68 mmol, 52 %) alcohol as a red-brown oil were obtained.

**R<sub>f</sub>** = 0.47 (hexanes/Et<sub>2</sub>O 3:1) [UV, CAM, KMnO<sub>4</sub>]

**<sup>1</sup>H NMR** (360 MHz, CDCl<sub>3</sub>, 300 K): δ (ppm) = 4.41 (m, 1H), 2.19 (d, *J* = 0.9 Hz, 1H), 1.95 (d, *J* = 4.3 Hz, 1H), 1.77 – 1.67 (m, 2H), 1.50 – 1.38 (m, 2H), 1.35 – 1.21 (m, 10H), 0.88 (td, *J* = 6.9, 6.0, 3.4 Hz, 3H).

**<sup>13</sup>C NMR** (91 MHz, CDCl<sub>3</sub>, 300 K): δ (ppm) = 77.5, 69.2, 68.6, 67.6, 62.9, 37.5, 32.0, 29.6, 29.4, 29.3, 25.1, 22.8, 14.3.

**HRMS APCI** calcd. for C<sub>13</sub>H<sub>21</sub>O [M+H]<sup>+</sup>: 193.1586, found: 193.1587.

**(R)-Trideca-1,3-diyne-5-ol (2.20)**<sup>112</sup>Chemical Formula: C<sub>13</sub>H<sub>20</sub>O

Molecular Weight: 192,30

4.00 g (20.6 mmol, 1.00 eq) 1,4-bis(trimethylsilyl)buta-1,3-diyne was dissolved in anhydrous Et<sub>2</sub>O (40 mL) under argon and 14.2 mL (22.7 mmol, 1.6 M in Et<sub>2</sub>O, 1.10 eq) MeLi was added at 0 °C. The reaction mixture was stirred at that temperature for 3 h and then quenched with sat. NH<sub>4</sub>Cl solution. The phases were separated and the organic phase washed with brine and dried over Na<sub>2</sub>SO<sub>4</sub>. The solvent was removed under reduced pressure and the crude product was directly used for the next step.

To 733 mg (6.00 mmol, 3.00 eq) diyne in Et<sub>2</sub>O (20 mL) were subsequently added 229 mg (0.80 mmol, 0.40 eq) (*S*)-binol, 18.1 mg Cy<sub>2</sub>NH (0.10 mmol, 0.05 eq) and 4.00 mL (6.00 mmol, 1.5 M in toluene, 3.00 eq) ZnEt<sub>2</sub>. The mixture was stirred for 16 h at rt. 568 mg (2.00 mmol, 1.00 eq) Ti(O<sup>*i*</sup>Pr)<sub>4</sub> and 285 mg (2.00 eq, 1.00 eq) nonanal were added and the solution stirred for additional 3 h. The reaction was stopped by addition of sat. NH<sub>4</sub>Cl solution, the phases separated and the aqueous phase extracted with Et<sub>2</sub>O (3 x 20 mL). After filtration of the combined organic fractions over Na<sub>2</sub>SO<sub>4</sub>, the solvent was removed under reduced pressure. The crude product was dissolved in THF (10 mL) and 1 M NaOH (10 mL) was added. After 30 min, 2 M HCl (10 mL) was added and the mixture extracted with Et<sub>2</sub>O (2 x 20 mL). The combined organic fractions were washed with brine, dried and the solvent removed under reduced pressure. Purification via flash chromatography (hexanes/Et<sub>2</sub>O 10:1) yielded 222 mg (1.15 mmol, 58 %) as a red-brown oil.

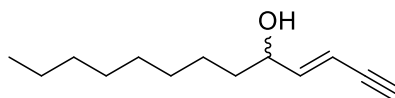
$R_f = 0.47$  (hexanes/Et<sub>2</sub>O 3:1) [UV, CAM, KMnO<sub>4</sub>]

<sup>1</sup>H NMR (360 MHz, CDCl<sub>3</sub>, 300 K): δ (ppm) = 4.41 (m, 1H), 2.19 (d, *J* = 0.9 Hz, 1H), 1.95 (d, *J* = 4.3 Hz, 1H), 1.77 – 1.67 (m, 2H), 1.50 – 1.38 (m, 2H), 1.35 – 1.21 (m, 10H), 0.88 (t, *J* = 6.9 Hz, 3H).

<sup>13</sup>C NMR (91 MHz, CDCl<sub>3</sub>, 300 K): δ (ppm) = 77.5, 69.2, 68.6, 67.6, 62.9, 37.5, 32.0, 29.6, 29.4, 29.3, 25.1, 22.8, 14.3.

HRMS APCI calcd. for C<sub>13</sub>H<sub>21</sub>O [M+H]<sup>+</sup>: 193.1586, found: 193.1587.

[α]<sup>22</sup><sub>D</sub> = - 5.7 (c = 2.5, CH<sub>2</sub>Cl<sub>2</sub>)

**(E)-Tridec-3-en-1-yn-5-ol (2.21)**Chemical Formula: C<sub>13</sub>H<sub>22</sub>O

Molecular Weight: 194,32

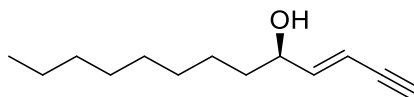
50.0 mg (0.26 mmol, 1.00 eq) (*E*)-Trideca-1,3-diyne-5-ol were dissolved in THF (2.50 mL) and cooled to 0 °C. 310 μL (0.31 mmol, 1 M in THF, 1.20 eq) LiAlH<sub>4</sub> were added and the yellow solution was stirred for 3 h at rt. The reaction was stopped by addition of sat. NH<sub>4</sub>Cl solution, the phases separated and the aqueous phase extracted with Et<sub>2</sub>O (3 x 20 mL). After filtration of the combined organic fractions over Na<sub>2</sub>SO<sub>4</sub>, the solvent was removed under reduced pressure. Purification via flash chromatography (hexanes/Et<sub>2</sub>O 10:1) yielded 36.7 mg (0.19 mmol, 73 %) allyl alcohol as a yellow oil.

*R<sub>f</sub>* = 0.47 (hexanes/Et<sub>2</sub>O 3:1) [UV, CAM, KMnO<sub>4</sub>]

<sup>1</sup>H NMR (360 MHz, CDCl<sub>3</sub>, 300 K): δ (ppm) = 6.25 (dd, *J* = 16.0, 5.9 Hz, 1H), 5.69 (ddd, *J* = 16.0, 2.3, 1.5 Hz, 1H), 4.16 (qd, *J* = 6.2, 1.5 Hz, 1H), 2.88 (d, *J* = 2.2 Hz, 1H), 1.61 (s, 1H), 1.58 – 1.47 (m, 2H), 1.20 – 1.40 (m, 12H), 0.94 – 0.79 (m, 3H).

<sup>13</sup>C NMR (91 MHz, CDCl<sub>3</sub>, 300 K): δ (ppm) = 147.8, 108.7, 81.8, 77.9, 72.2, 37.0, 32.0, 29.6, 29.4, 25.4, 22.8, 14.3.

HRMS APCI calcd. for C<sub>13</sub>H<sub>23</sub>O [M+H]<sup>+</sup>: 195.1743, found: 195.1743.

**(R,E)-Tridec-3-en-1-yn-5-ol (2.21)**Chemical Formula: C<sub>13</sub>H<sub>22</sub>O

Molecular Weight: 194,32

50.0 mg (0.26 mmol, 1.00 eq) (*R,E*)-Trideca-1,3-diyne-5-ol were dissolved in THF (2.50 mL) and cooled to 0 °C. 310 μL (0.31 mmol, 1 M in THF, 1.20 eq) LiAlH<sub>4</sub> were added and the yellow solution stirred for 3 h at rt. The reaction is stopped by addition of sat. NH<sub>4</sub>Cl solution, the phases separated and the aqueous phase extracted with Et<sub>2</sub>O (3 x 20 mL). After filtration of the combined organic fractions over Na<sub>2</sub>SO<sub>4</sub>, the solvent is removed under reduced



pressure. Purification via flash chromatography (hexanes/Et<sub>2</sub>O 10:1) yielded 35.2 mg (0.18 mmol, 69 %) allyl alcohol as a yellow oil.

$R_f$  = 0.47 (hexanes/Et<sub>2</sub>O 3:1) [UV, CAM, KMnO<sub>4</sub>]

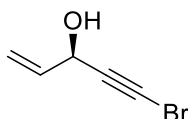
<sup>1</sup>H NMR (360 MHz, CDCl<sub>3</sub>, 300 K): δ (ppm) = 6.25 (dd,  $J$  = 16.0, 5.9 Hz, 1H), 5.69 (ddd,  $J$  = 16.0, 2.3, 1.5 Hz, 1H), 4.16 (qd,  $J$  = 6.2, 1.5 Hz, 1H), 2.88 (d,  $J$  = 2.2 Hz, 1H), 1.61 (s, 1H), 1.58 – 1.47 (m, 2H), 1.20 – 1.40 (m, 12H), 0.94 – 0.79 (m, 3H).

<sup>13</sup>C NMR (91 MHz, CDCl<sub>3</sub>, 300 K): δ (ppm) = 147.8, 108.7, 81.8, 77.9, 72.2, 37.0, 32.0, 29.6, 29.4, 25.4, 22.8, 14.3.

HRMS APCI calcd. for C<sub>13</sub>H<sub>23</sub>O [M+H]<sup>+</sup>: 195.1743, found: 195.1743.

[α]<sup>22</sup><sub>D</sub> = - 12.6 (c = 2.0, CH<sub>2</sub>Cl<sub>2</sub>)

**(*R*)-5-Bromopent-1-en-4-yn-3-ol ((*R*)-2.8)**<sup>113</sup>



Chemical Formula: C<sub>5</sub>H<sub>5</sub>BrO  
Molecular Weight: 161,00

A mixture of 761 mg (4.73 mmol, 1.00 eq) 5-(trimethylsilyl)pent-1-en-4-yn-3-ol, 200 mg (≥ 20000 U/g) Amano Lipase from *Pseudomonas fluorescens*, 800 mg molecular sieve 4Å and 2.13 g (24.7 mmol, 5.20 eq) vinyl acetate in 40 ml dry hexane was stirred under argon at rt for 48 h. The reaction mixture was filtered over a plug of celite and the solvent removed. Purification via flash chromatography (hexanes/Et<sub>2</sub>O 50:1 → 5:1) yielded 0.39 g (1.99 mmol, 42 %) (*R*)-5-(trimethylsilyl)pent-1-en-4-yn-3-yl acetate and 0.30 g (1.94 mmol, 41 %, > 99 % ee) (*S*)-5-(trimethylsilyl)pent-1-en-4-yn-3-ol.

250 mg (1.27 mmol, 1.00 eq) acetylated product was dissolved in MeOH (1.25 mL) and 375 mg (2.55 mmol, 2.00 eq) K<sub>2</sub>CO<sub>3</sub> was added. The mixture was stirred at rt for 2.5 h and then quenched with water (2 mL). The mixture was extracted with Et<sub>2</sub>O (2 x 20 mL) and the combined organic fraction dried and the solvent evaporated. The crude alcohol was dissolved in acetone (1 mL) and 325 mg (1.91 mmol, 1.50 eq) NBS and 64.8 mg (0.38 mmol, 0.30 eq) AgNO<sub>3</sub> were added. The suspension was stirred for 1h in the dark. Water was added and the mixture extracted with Et<sub>2</sub>O (2 x 20 mL). The combined organic fractions were washed with brine, dried and the solvent evaporated. Purification via flash

chromatography (CH<sub>2</sub>Cl<sub>2</sub>) yielded 136 mg (0.84 mmol, 67 %) bromo alkyne **10** as a yellow liquid.

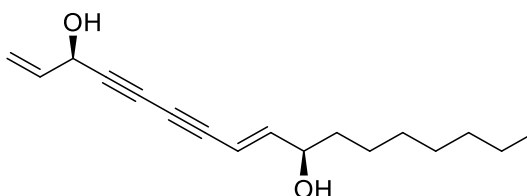
$R_f$  = 0.47 (hexanes/Et<sub>2</sub>O 3:1) [UV, CAM, KMnO<sub>4</sub>]

<sup>1</sup>H NMR (300 MHz, CDCl<sub>3</sub>, 300 K): δ (ppm) = 5.97 – 5.84 (m, 1H), 5.64 – 5.49 (m, 1H), 5.39 – 5.26 (m, 1H).

<sup>13</sup>C NMR (75 MHz, CDCl<sub>3</sub>) δ 169.7, 133.0, 119.1, 100.2, 92.5, 64.8, 21.2, -0.1.

[α]<sup>22</sup><sub>D</sub> = - 33.5 (c = 2.0, CH<sub>2</sub>Cl<sub>2</sub>)

**(3*R*,10*R*,*E*)-Heptadeca-1,8-dien-4,6-diyne-3,10-diol (2.5)**



Chemical Formula: C<sub>17</sub>H<sub>24</sub>O<sub>2</sub>

Molecular Weight: 260,38

To a solution of 36 mg (0.52 mmol, 1.68 eq) hydroxylaminehydrochloride in MeOH (1 mL) at 0 °C was added a solution of 0.20 mL ethylamine (70-%) and 2.97 mg (0.03 mmol, 0.10 eq) CuCl in MeOH (1 mL). 50 mg (0.26 mmol, 0.84 eq.) (*R,E*)-Tridec-3-en-1-yn-5-ol in MeOH (0.5 mL) were added at 0 °C. 50 mg (0.31 mmol, 1.00 eq.) bromo alkyne in MeOH (0.5 mL) were added over 30 min. The mixture was stirred for 1.5 h. The reaction was ceased by addition of water and the emulsion was extracted with Et<sub>2</sub>O (2 x 30 mL). After evaporation of the solvent, the resulting brown-orange oil was submitted to flash chromatography (hexanes/EtOAc 6:1 → 2:1). 47.0 mg (0.18 mmol, 69 %) of stipudiol was isolated as a brown oil.

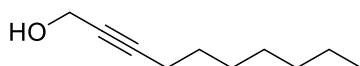
$R_f$  = 0.47 (hexanes/Et<sub>2</sub>O 3:1) [UV, CAM, KMnO<sub>4</sub>]

<sup>1</sup>H NMR (360 MHz, CDCl<sub>3</sub>, 300 K): δ (ppm) = 6.33 (dd,  $J$  = 15.9, 5.6 Hz, 1H), 5.96 (ddd,  $J$  = 17.1, 10.1, 5.3 Hz, 1H), 5.77 (*virt.* dq,  $J$  = 16.0, 1.2 Hz, 1H), 5.48 (*virt.* dq,  $J$  = 17.0, 1.2 Hz, 1H), 5.26 (*virt.* dt,  $J$  = 10.1, 1.2 Hz, 1H), 4.97 (dd,  $J$  = 5.4, 1.2 Hz, 1H), 4.19 (qd,  $J$  = 6.3, 1.6 Hz, 1H), 1.57 – 1.46 (m, 2H), 1.27 (m, 12H), 0.95 – 0.79 (m, 2H).

<sup>13</sup>C NMR (91 MHz, CDCl<sub>3</sub>, 300 K): δ (ppm) = 150.1, 136.1, 117.4, 108.2, 80.5, 77.7, 73.7, 72.2, 71.1, 63.8, 37.0, 32.0, 29.6, 29.6, 29.4, 25.3, 22.8, 14.3.

HRMS ESI calcd. for C<sub>19</sub>H<sub>27</sub>O<sub>4</sub> [M+HCOOH-H]<sup>+</sup>: 319.1915, found: 319.1918.

$[\alpha]_D^{22} = -23.2$  ( $c = 2.0$ ,  $\text{CH}_2\text{Cl}_2$ ).

**Dec-2-yn-1-ol (2.15)**

Chemical Formula:  $\text{C}_{10}\text{H}_{18}\text{O}$

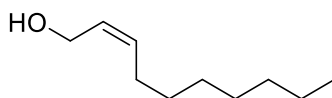
Molecular Weight: 154,25

4.80 g (38.7 mmol, 1.00 eq) 1-nonyne were dissolved in anhydrous THF (50 mL) under argon atmosphere. The stirred solution was cooled to  $-78\text{ }^\circ\text{C}$ , and 16.2 mL (2.5 M in hexane, 40.5 mmol, 1.05 eq) *n*BuLi were added dropwise by syringe. After 40 min at  $-78\text{ }^\circ\text{C}$ , 1.21 g (40.6 mmol, 1.05 eq) paraformaldehyde were added portionwise. The mixture was allowed to warm to rt and stirred overnight. The reaction was quenched with  $\text{H}_2\text{O}$  followed by addition of  $\text{Et}_2\text{O}$  (20 mL). The organic phase was separated, and the aqueous layer was extracted with  $\text{Et}_2\text{O}$  (2 x 30 mL). The combined extracts were dried over anhydrous  $\text{MgSO}_4$  and concentrated under reduced pressure. Flash chromatography (hexanes/ $\text{EtOAc}$  5:1) yielded 5.39 g (35.0 mmol, 91 %) of dec-2-yn-1-ol as a clear, colorless oil.

$R_f = 0.26$  (hexanes/ $\text{EtOAc}$  5:1) [ $\text{KMnO}_4$ ]

$^1\text{H NMR}$  (360 MHz,  $\text{CDCl}_3$ , 300 K):  $\delta$  (ppm) = 4.35 – 4.14 (m, 1H), 2.34 – 2.08 (m, 1H), 1.50 (p,  $J = 6.8$  Hz, 1H), 1.43 – 1.23 (m, 4H), 0.88 (t,  $J = 7.0$  Hz, 1H).

$^{13}\text{C NMR}$  (91 MHz,  $\text{CDCl}_3$ , 300 K):  $\delta$  (ppm) = 14.2, 19.1, 23.0, 29.0, 29.2, 29.3, 32.1, 51.8, 78.7, 87.1.

**(Z)-Dec-2-en-1-ol (2.16)<sup>238</sup>**

Chemical Formula:  $\text{C}_{10}\text{H}_{20}\text{O}$

Molecular Weight: 156,27

To an 250-mL flask were added 889 mg (3.56 mmol, 1.00 eq)  $\text{Ni}(\text{OAc})_2 \cdot 4\text{H}_2\text{O}$  and MeOH (39 mL) under argon atmosphere. The blue-green solution was cooled to  $0\text{ }^\circ\text{C}$ , and 134 mg (3.56 mmol, 1.00 eq)  $\text{NaBH}_4$  were added in one portion under argon. With the vigorous evolution of gas, the mixture turned black immediately. The ice bath was removed, and the suspension was stirred for 5 min at room temperature. 581 mg (645  $\mu\text{L}$ , 9.68 mmol, 2.70 eq) 1,2-diaminoethane were added under argon, and the resulting mixture was further

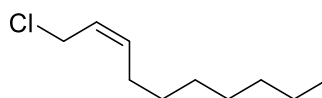
stirred for 5 min. A solution of 2.20 g (14.3 mmol, 1.00 eq) dec-2-yn-1-ol in MeOH (13 mL) were added to the above reaction mixture. A hydrogen-filled balloon was attached and hydrogen flushed through the solution for 10 min. The reaction mixture was stirred under a H<sub>2</sub> atmosphere overnight. Afterwards, the catalyst was filtered off through a plug of silica and the solvent removed under reduced pressure. The desired allylic alcohol was obtained in quantitative yield (2.23 g, 14.3 mmol) and directly used for the next step.

$R_f$  = 0.23 (hexanes/EtOAc 5:1) [KMnO<sub>4</sub>]

<sup>1</sup>H NMR (360 MHz, CDCl<sub>3</sub>, 300 K):  $\delta$  (ppm) = 5.66 – 5.47 (m, 2H), 4.19 (d,  $J$  = 6.0 Hz, 2H), 2.07 (q,  $J$  = 6.9 Hz, 2H), 1.47 – 1.18 (m, 10H), 0.88 (t,  $J$  = 6.5 Hz, 3H).

<sup>13</sup>C NMR (91 MHz, CDCl<sub>3</sub>, 300 K):  $\delta$  (ppm) = 14.5, 23.1, 27.6, 29.5, 29.6, 30.0, 32.2, 58.9, 128.7, 133.6.

**(Z)-1-Chlorodec-2-ene (2.17)**



Chemical Formula: C<sub>10</sub>H<sub>19</sub>Cl

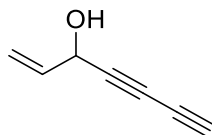
Molecular Weight: 174,71

2.20 g (14.1 mmol, 1.00 eq) alcohol **2.16** and 4.13 g (15.8 mmol, 1.12 eq) PPh<sub>3</sub> in CCl<sub>4</sub> (14 mL) was stirred at 80 °C for 16 h. The solvent was removed and hexane (30 mL) was added. The precipitated triphenylphosphineoxide was filtered off and the solvent removed under reduced pressure. Purification via flash chromatography (hexanes) yielded 2.31 g (13.2 mmol, 94 %).

$R_f$  = 0.56 (hexanes) [KMnO<sub>4</sub>]

<sup>1</sup>H NMR (360 MHz, CDCl<sub>3</sub>, 300 K):  $\delta$  (ppm) = 5.60 – 5.66 (m, 2H), 4.10 (d,  $J$  = 6.7 Hz, 2H), 2.17 – 2.05 (m, 2H), 1.40 – 1.23 (m, 10H), 0.90 (t,  $J$  = 6.5 Hz, 3H).

<sup>13</sup>C NMR (91 MHz, CDCl<sub>3</sub>, 300 K):  $\delta$  (ppm) = 14.5, 23.1, 27.5, 29.5, 29.6, 29.7, 32.2, 39.9, 125.5, 135.9.

**Hepta-1-en-4,6-diyn-3-ol (2.18)**<sup>108</sup>Chemical Formula: C<sub>7</sub>H<sub>6</sub>O

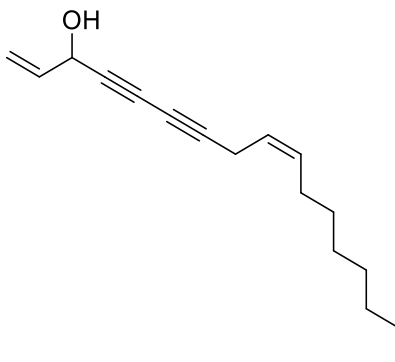
Molecular Weight: 106,12

To a solution of 6.00 g (30.9 mmol, 1.00 eq) 1,4-bis(trimethylsilyl)buta-1,3-diyne in anhydrous THF (60 mL) at 0 °C under argon were added 20.6 mL (30.9 mmol, 1.5 M in Et<sub>2</sub>O, 1.00 eq) MeLi-LiBr and the reaction mixture was stirred for 3 h. The solution was cooled to -78 °C and 1.73 g (2.06 mL, 30.9 mmol, 1.00 eq) acrolein were added. The reaction mixture was warmed to rt for 3 h and acidified with 1 M HCl<sub>(aq.)</sub> (pH = 3). After extraction with Et<sub>2</sub>O (2 x 50 mL), the combined organic fractions were dried, filtered and the solvent removed under reduced pressure. The crude product 7-(trimethylsilyl)hepta-1-en-4,6-diyn-3-ol was dissolved in THF (40 mL) and 1 M NaOH (40 mL) was added. The mixture was stirred for 30 min at rt and acidified with 1 M HCl. The mixture was extracted with Et<sub>2</sub>O (2 x 50 mL), the combined organic fractions dried, filtered, and the solvent removed under reduced pressure. Purification via flash chromatography (hexanes/EtOAc 8:1 → 4:1) yielded 2.61 g (24.6 mmol, 80 %) hepta-1-en-4,6-diyn-3-ol as an orange oil.

$R_f$  = 0.35 (hexanes/EtOAc 6:1) [UV, KMnO<sub>4</sub>]

<sup>1</sup>H NMR (360 MHz, CDCl<sub>3</sub>, 300 K): δ (ppm) = 5.95 (ddd,  $J$  = 17.1, 10.2, 5.3 Hz, 1H), 5.49 (ddd,  $J$  = 17.1, 1.5, 0.9 Hz, 1H), 5.28 (dt,  $J$  = 10.2, 1.1 Hz, 1H), 4.92 (ddd,  $J$  = 6.6, 5.2, 1.3 Hz, 1H), 2.23 (d,  $J$  = 1.0 Hz, 1H), 1.99 (br d,  $J$  = 6.4 Hz, 1H).

<sup>13</sup>C NMR (91 MHz, CDCl<sub>3</sub>, 300 K) δ (ppm) = 63.7, 67.7, 69.5, 70.8, 75.2, 117.9, 136.1.

**(Z)-Heptadeca-1,9-dien-4,6-diyn-3-ol, (+/-)-falcarinol (2.1)**<sup>108</sup>

Chemical Formula: C<sub>17</sub>H<sub>24</sub>O  
Molecular Weight: 244,38

To a stirred solution of 0.16 g (1.51 mmol, 1.00 eq) alcohol **2.18** in anhydrous DMF (10 mL) were added 0.05 g (0.18 mmol, 0.12 eq) Bu<sub>4</sub>N<sup>+</sup>Cl<sup>-</sup>, 0.26 g (1.88 mmol, 1.25 eq) K<sub>2</sub>CO<sub>3</sub> and 0.02 g (0.11 mmol, 0.07 eq.) CuI. After the mixture was stirred for 15 min at room temperature, chloroalkene **2.17** (0.28 g, 1.60 mmol), dissolved in DMF (2 mL), was added dropwise within 15 min. The resulting solution was stirred at room temperature for further 12 h. After the reaction was complete, it was quenched with water (15 mL) and Et<sub>2</sub>O (50 mL). After phase separation, the organic phase was dried and concentrated. The residue was purified by flash chromatography (hexanes/EtOAc 6:1). 1,1- and 1,3-product separation was problematic due to similar *R<sub>f</sub>* - values. 261 mg (1.07 mmol, 71 %) racemic falcarinol and 91.9 mg (0.38 mmol, 25 %) 1,3-isomer were obtained as yellow oils.

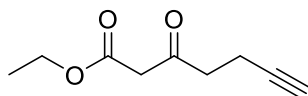
*R<sub>f</sub>* = 0.35 (hexanes/EtOAc 5:1) [UV, KMnO<sub>4</sub>]

<sup>1</sup>H NMR (360 MHz, CDCl<sub>3</sub>, 300 K): δ (ppm) = 5.94 (ddd, *J* = 17.1, 10.2, 5.3 Hz, 1H), 5.56 – 5.43 (m, 2H), 5.42 – 5.33 (m, 1H), 5.24 (dt, *J* = 10.1, 1.2 Hz, 1H), 4.92 (br s, 1H), 3.03 (d, *J* = 6.9 Hz, 2H), 2.02 (q, *J* = 7.2 Hz, 2H), 1.86 (s, 1H), 1.42 – 1.16 (m, 10H), 0.94 – 0.80 (m, 3H).

<sup>13</sup>C NMR (91 MHz, CDCl<sub>3</sub>, 300 K) δ (ppm) = 14.3, 17.9, 22.9, 27.4, 29.37, 29.4, 29.5, 32.0, 63.8, 64.2, 71.5, 74.3, 80.5, 117.3, 122.1, 133.3, 136.4.

### 5.1.3 Synthetic procedures for chapter 3: A whole proteome inventory of background photocrosslinker binding

#### Ethyl 3-oxohept-6-ynoate (3.9)<sup>107</sup>



Chemical Formula: C<sub>9</sub>H<sub>12</sub>O<sub>3</sub>  
Molecular Weight: 168,19

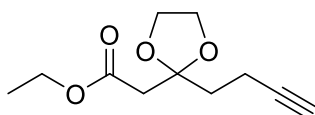
To a solution of 3.37 g (84.7 mmol, 60 wt-% in paraffin oil, 1.10 eq) NaH in anhydrous THF (200 mL) were added 9.71 mL (10.0 g, 76.8 mmol, 1.00 eq) ethylacetoacetate in THF (10 mL) dropwise at 0 °C. After 10 min, 32.4 mL (80.9 mmol, 2.5 M in hexanes, 1.05 eq) *n*BuLi were added dropwise and the mixture was stirred for 10 min. 5.83 mL (9.14 g, 76.8 mmol, 1.00 eq) propargyl bromide were added quickly and the mixture stirred for 2 h at 0 °C. The reaction was terminated by addition of 4.40 mL (76.8 mmol, 1.00 eq) AcOH and water (20 mL) and the mixture extracted with Et<sub>2</sub>O (2 x 50 mL). The combined organic fractions were washed with brine, dried and the solvent evaporated under reduced pressure. The crude product was purified via fractionated distillation to give 4.80 g (28.6 mmol, 37 %) ethyl 3-oxohept-6-ynoate as a yellowish oil.

$R_f$  = 0.21 (hexanes/EtOAc 8:1) [KMnO<sub>4</sub>].

<sup>1</sup>H NMR (360 MHz, CDCl<sub>3</sub>, 300 K): δ (ppm) = 4.19 (q, *J* = 7.1 Hz, 2H), 3.45 (s, 2H), 2.80 (t, *J* = 7.1 Hz, 2H), 2.46 (td, *J* = 7.1 Hz, 4*J* = 2.7 Hz, 2H), 1.95 (t, *J* = 2.7 Hz, 1H), 1.27 (t, *J* = 7.1 Hz, 3H).

<sup>13</sup>C NMR (91 MHz, CDCl<sub>3</sub>, 300 K) δ (ppm) = 200.7, 167.0, 82.7, 69.1, 61.6, 49.4, 41.7, 14.2, 13.0

#### Ethyl 2-(2-(but-3-yn-1-yl)-1,3-dioxolan-2-yl)acetate (3.10)<sup>107</sup>



Chemical Formula: C<sub>11</sub>H<sub>16</sub>O<sub>4</sub>  
Molecular Weight: 212,25

A solution of 10.0 g (59.5 mmol, 1.00 eq) ketone, 29.3 mL (24.6 g, 119 mmol, 2.00 eq) 1,2-bis-(trimethylsiloxy)-ethane and 570 μL (670 mL, 3.01 mmol, 0.05 eq) TMSOTf in CH<sub>2</sub>Cl<sub>2</sub> (50 mL) was stirred at rt for 3.5 h. The reaction was quenched by addition of sat. NaHCO<sub>3</sub>

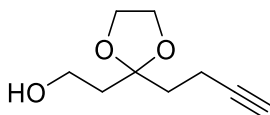
solution, the phases were separated and the aqueous phase reextracted with  $\text{CH}_2\text{Cl}_2$  (2 x 50 mL). The combined organic fractions were dried, filtered and the solvent removed under reduced pressure. Purification via flash chromatography (hexanes/EtOAc 8:1) yielded 9.53 g (44.9 mmol, 75 %) acetal as a yellow oil.

$R_f = 0.20$  (hexanes/EtOAc 9:1) [ $\text{KMnO}_4$ ]

$^1\text{H NMR}$  (360 MHz,  $\text{CDCl}_3$ , 300 K):  $\delta$  (ppm) = 4.12 (q,  $J = 7.1$  Hz, 2H), 4.02 – 3.89 (m, 4H), 2.61 (s, 2H), 2.33 – 2.22 (m, 2H), 2.14 – 2.04 (m, 2H), 1.90 (t,  $J = 2.7$  Hz, 1H), 1.23 (t,  $J = 7.1$  Hz, 3H).

$^{13}\text{C NMR}$  (91 MHz,  $\text{CDCl}_3$ , 300 K):  $\delta$  (ppm) = 169.2, 108.4, 84.0, 68.2, 65.3, 60.7, 42.8, 36.5, 14.2, 12.9.

**2-(2-(But-3-yn-1-yl)-1,3-dioxolan-2-yl)ethan-1-ol (3.11)<sup>107</sup>**



Chemical Formula:  $\text{C}_9\text{H}_{14}\text{O}_3$

Molecular Weight: 170.21

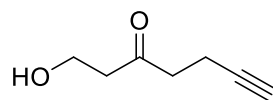
To a suspension of 1.87 g (49.4 mmol, 1.10 eq)  $\text{LiAlH}_4$  in anhydrous  $\text{Et}_2\text{O}$  (116 mL) were added dropwise 9.53 g (44.9 mmol, 1.00 eq) acetal in  $\text{Et}_2\text{O}$  (20 mL). The reaction was stirred for 30 min at 0 °C and for 2.5 h at rt. The reaction was terminated by the addition of ice water at 0 °C. After separation of the phases and extraction of the aqueous phase with  $\text{Et}_2\text{O}$  (2 x 30 mL), the combined organic fractions were dried over  $\text{Na}_2\text{SO}_4$ , filtered, and the solvent removed under reduced pressure. The crude product was purified by flash chromatography (hexanes/EtOAc 3:1) to yield 5.14 g (30.2 mmol, 67 %) of the alcohol as a slightly yellow oil.

$R_f = 0.11$  (hexanes/EtOAc 4:1) [ $\text{KMnO}_4$ ]

$^1\text{H NMR}$  (250 MHz,  $\text{CDCl}_3$ , 300 K):  $\delta$  (ppm) = 4.02 – 3.92 (m, 4H), 3.80 – 3.67 (m, 2H), 2.60 (s, 1H), 2.34 – 2.18 (m, 2H), 2.00 – 1.82 (m, 5H).

$^{13}\text{C NMR}$  (63 MHz,  $\text{CDCl}_3$ , 300 K):  $\delta$  (ppm) = 111.1, 84.0, 68.3, 65.0, 58.7, 38.4, 36.0, 13.2.



**1-Hydroxyhept-6-yn-3-one (3.12)<sup>107</sup>**Chemical Formula: C<sub>7</sub>H<sub>10</sub>O<sub>2</sub>

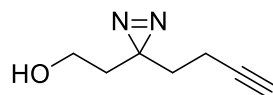
Molecular Weight: 126,16

5.14 g (30.2 mmol, 1.00 eq) acetal were dissolved in acetone (275 mL) and 1.30 g (7.55 mmol, 0.25 eq) *p*-TsOH were added and the solution stirred for 24 h at rt. Water (100 mL) was added and the mixture was extracted with Et<sub>2</sub>O (3 x 50 mL). The combined organic fractions were washed with sat. NaHCO<sub>3</sub> solution and dried. After evaporation of the solvent, the crude product was purified via flash chromatography (hexanes/EtOAc 1:1) to yield 1.55 g (12.8 mmol, 41 %) ketone as a yellow oil.

*R<sub>f</sub>* = 0.34 (hexanes/EtOAc 1:1) [KMnO<sub>4</sub>]

<sup>1</sup>H NMR (250 MHz, CDCl<sub>3</sub>, 300 K): δ (ppm) = 3.85 (t, *J* = 5.4 Hz, 2H), 2.76 – 2.62 (m, 4H), 2.52 – 2.37 (m, 3H), 1.95 (t, *J* = 2.7 Hz, 1H).

<sup>13</sup>C NMR (63 MHz, CDCl<sub>3</sub>, 300 K): δ (ppm) = 209.1, 82.9, 69.0, 57.8, 44.7, 41.9, 12.9.

**2-(3-(But-3-yn-1-yl)-3*H*-diazirin-3-yl) ethanol (3.13)**Chemical Formula: C<sub>7</sub>H<sub>10</sub>N<sub>2</sub>O

Molecular Weight: 138,17

To a flask containing 851 mg (6.80 mmol, 1.00 eq) *1-Hydroxyhept-6-yn-3-one* was added 14.6 mL (7 M in MeOH; 102 mmol, 15.0 eq) NH<sub>3</sub> at -10 °C. The flask was sealed and the mixture was stirred at -10 °C for 4.5 h. Then a solution of 1.00 g (8.84 mmol, 1.30 eq) hydroxylamine-*O*-sulfonic acid in anhydrous MeOH (5 mL) was added dropwise at -10 °C and the reaction mixture was stirred at -10 °C for 1 h in a sealed flask. Subsequently, the reaction mixture was allowed to warm to rt and stirred for 16 h. NH<sub>3</sub> was removed by gently blowing N<sub>2</sub> through the suspension. The precipitate was removed by filtration through a syringe filter (0.45 μm GHP acrodisc) and the precipitate was washed with several portions of anhydrous MeOH. The reaction mixture was treated with 6.97 mL (5.09 g, 50.3 mmol, 7.40 eq) anhydrous NEt<sub>3</sub> and cooled to 0 °C. A solution of 2.24 g (8.84 mmol, 1.30 eq) I<sub>2</sub> in anhydrous MeOH (5 mL) was added dropwise at 0 °C and the mixture was stirred at 0 °C for 1 h. Et<sub>2</sub>O (25 mL) was added and the mixture was washed with brine (25 mL). The

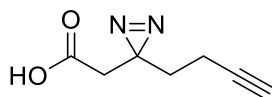
aqueous phase was extracted with Et<sub>2</sub>O (3 x 25 mL), the combined organic layer was dried over Na<sub>2</sub>SO<sub>4</sub>, filtered and the solvent was removed under reduced pressure. The residue was purified by flash column chromatography on silica (hexanes/EtOAc 9:1 → 4:1) to afford 286 mg (2.07 mmol, 30 %) as pale yellow oil.

$R_f$  = 0.20 (hexanes/EtOAc 4:1) [UV, KMnO<sub>4</sub>].

<sup>1</sup>H NMR (500 MHz, CDCl<sub>3</sub>, 300 K): δ [ppm] = 3.49 (q,  $J$  = 6.0 Hz, 2H), 2.05 (td,  $J$  = 7.4, 2.6 Hz, 2H), 2.00 (t,  $J$  = 2.6 Hz, 1H), 1.75 – 1.65 (m, 4H), 1.44 (t,  $J$  = 5.2 Hz, 1H).

<sup>13</sup>C NMR (91 MHz, CDCl<sub>3</sub>, 300 K): δ [ppm] = 83.0, 69.4, 57.6, 35.7, 32.8, 26.7, 13.4.

### 2-(3-(But-3-yn-1-yl)-3H-diazirin-3-yl)acetic acid (3.14)



Chemical Formula: C<sub>7</sub>H<sub>8</sub>N<sub>2</sub>O<sub>2</sub>  
Molecular Weight: 152,15

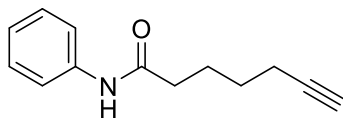
1.30 mL (2 M CrO<sub>3</sub> in H<sub>2</sub>SO<sub>4</sub> aq., 2.60 mmol, 4.00 eq) Jones reagent was added dropwise to a stirred solution of 90.0 mg (0.65 mmol, 1.00 eq) in acetone (5 mL) at 0 °C. The reaction mixture was stirred at RT for 2 h and subsequently quenched with isopropanol (5 mL) and filtered over celite. The filter cake was washed with acetone (3 x 5 mL). Next, the filtrate was dried over Na<sub>2</sub>SO<sub>4</sub>, filtered, concentrated and purified by flash chromatography on silica gel (hexanes/EtOAc 4:1 + 2 % acetic acid) to give 87.0 mg (0.57 mmol, 88 %) as pale yellow oil.

$R_f$  = 0.29 (hexanes/EtOAc 4:1 + 2 % AcOH) [UV, KMnO<sub>4</sub>].

<sup>1</sup>H NMR (300 MHz, CDCl<sub>3</sub>, 300 K): δ [ppm] = 11.44 (br s, 1H), 2.41 (s, 2H), 2.10 – 2.04 (m, 2H), 2.01 (t,  $J$  = 2.6 Hz, 1H), 1.80 (t,  $J$  = 7.3 Hz, 2H).

<sup>13</sup>C NMR (75 MHz, CDCl<sub>3</sub>, 300 K): δ [ppm] = 175.8, 82.5, 69.7, 39.6, 32.0, 25.3, 13.3.

HRMS ESI calc. for C<sub>7</sub>H<sub>7</sub>N<sub>2</sub>O<sub>2</sub> [M-H]: 151.0513; found, 151.0513.

***N*-Phenylhept-6-ynamide (3.4)**<sup>239</sup>

Chemical Formula: C<sub>13</sub>H<sub>15</sub>NO  
Molecular Weight: 201,27

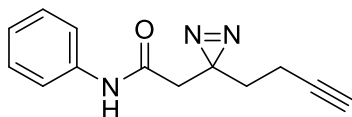
To a mixture of 50.1  $\mu$ L (50.0 mg, 0.40 mmol, 1.00 eq) 6-heptynoic acid and 43.3  $\mu$ L (44.2 mg, 0.48 mmol, 1.20 eq) aniline in DMF (5 mL) were added 80.3 mg (0.59 mmol, 1.50 eq) HOBt·H<sub>2</sub>O, 114 mg (0.59 mmol, 1.50 eq) EDC·HCl and 134  $\mu$ L (102 mg, 0.79 mmol, 2.00 eq) DIEA. The mixture was stirred at rt for 16 h. Subsequently, the reaction was quenched with water (5 mL) and the mixture was extracted with CH<sub>2</sub>Cl<sub>2</sub> (2 x 20 mL). The combined organic phase was washed with sat. NH<sub>4</sub>Cl solution (20 mL), dried over Na<sub>2</sub>SO<sub>4</sub> and filtered. After solvent evaporation, the residue was purified by flash chromatography (hexanes/EtOAc 4:1) to yield 73.3 mg (0.36 mmol, 92 %) as a yellow solid.

$R_f$  = 0.23 (hexanes/EtOAc 4:1) [UV, PMA].

<sup>1</sup>H NMR (300 MHz, CDCl<sub>3</sub>, 300 K):  $\delta$  [ppm] = 7.62 (br s, 1H), 7.51 (d,  $J$  = 7.8 Hz, 2H), 7.30 (t,  $J$  = 7.8 Hz, 2H), 7.09 (t,  $J$  = 7.4 Hz, 1H), 2.37 (t,  $J$  = 7.5 Hz, 2H), 2.22 (td,  $J$  = 7.0, 2.6 Hz, 2H), 1.96 (t,  $J$  = 2.6 Hz, 1H), 1.92 – 1.75 (m, 2H), 1.67 – 1.51 (m, 2H).

<sup>13</sup>C NMR (75 MHz, CDCl<sub>3</sub>, 300 K):  $\delta$  [ppm] = 171.3, 138.0, 129.0, 124.3, 120.0, 84.1, 68.9, 37.1, 27.9, 24.7, 18.3.

HRMS ESI calc. for C<sub>13</sub>H<sub>16</sub>NO [M+H]<sup>+</sup>: 202.1226; found, 202.1224.

**2-(3-(But-3-yn-1-yl)-3*H*-diazirin-3-yl)-*N*-phenylacetamide (3.3)**

Chemical Formula: C<sub>13</sub>H<sub>13</sub>N<sub>3</sub>O  
Molecular Weight: 227,27

To a mixture of 20.0 mg (0.13 mmol, 1.00 eq) carboxylic acid **3.14** and 14.4  $\mu$ L (14.7 mg, 0.16 mmol, 1.20 eq) aniline in DMF (2 mL) were added 26.6 mg (0.20 mmol, 1.50 eq) HOBt·H<sub>2</sub>O, 37.8 mg (0.20 mmol, 1.50 eq) EDC·HCl and 44.6  $\mu$ L (33.9 mg, 0.26 mmol, 2.00 eq) DIEA. The mixture was stirred at rt for 16 h. Subsequently, the reaction was quenched by the addition of water (5 mL) and the mixture was extracted with EtOAc (3 x 10 mL). The combined organic phase was washed with sat. NH<sub>4</sub>Cl solution (20 mL),

dried over Na<sub>2</sub>SO<sub>4</sub> and filtered. After solvent evaporation, the residue was purified by flash chromatography (hexanes/EtOAc 4:1) to yield 23.0 mg (0.10 mmol, 77 %) as a yellow solid.

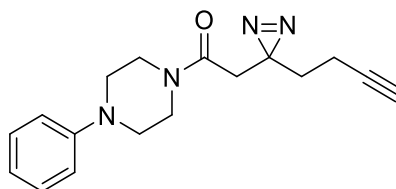
$R_f$  = 0.19 (hexanes/EtOAc 4:1) [UV, KMnO<sub>4</sub>].

<sup>1</sup>H NMR (360 MHz, CDCl<sub>3</sub>, 300 K): δ [ppm] = 7.59 (br s, 1H), 7.51 (d,  $J$  = 7.8 Hz, 2H), 7.33 (t,  $J$  = 7.9 Hz, 2H), 7.18 – 7.09 (m, 1H), 2.42 (s, 2H), 2.10 (td,  $J$  = 7.2, 2.6 Hz, 2H), 2.03 (t,  $J$  = 2.6 Hz, 1H), 1.82 (t,  $J$  = 7.2 Hz, 2H).

<sup>13</sup>C NMR (91 MHz, CDCl<sub>3</sub>, 300 K): δ [ppm] = 166.2, 137.5, 129.2, 125.0, 120.4, 82.8, 69.8, 42.8, 32.1, 26.2, 13.4.

HRMS ESI calc. for C<sub>13</sub>H<sub>14</sub>N<sub>3</sub>O [M+H]<sup>+</sup>: 228.1131; found, 228.1129.

### 2-(3-(But-3-yn-1-yl)-3H-diazirin-3-yl)-1-(4-phenylpiperazin-1-yl)ethan-1-one (3.5)



Chemical Formula: C<sub>17</sub>H<sub>20</sub>N<sub>4</sub>O

Molecular Weight: 296,37

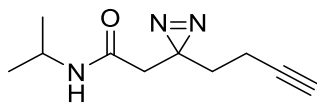
To a mixture of 20.0 mg (0.13 mmol, 1.00 eq) carboxylic acid **3.14** and 24.0 μL (25.5 mg, 0.16 mmol, 1.20 eq) 1-phenylpiperazine in DMF (1 mL) were added 26.6 mg (0.20 mmol, 1.50 eq) HOBt·H<sub>2</sub>O, 37.8 mg (0.20 mmol, 1.50 eq) EDC·HCl and 44.6 μL (33.9 mg, 0.26 mmol, 2.00 eq) DIEA. The mixture was stirred at rt for 16 h. Subsequently, the reaction was quenched by water (5 mL) and the mixture was extracted with EtOAc (3 x 10 mL). The combined organic phase was washed with sat. NH<sub>4</sub>Cl solution (20 mL), dried over Na<sub>2</sub>SO<sub>4</sub> and filtered. After solvent evaporation, the residue was purified by flash chromatography (hexanes/EtOAc 4:1 → 3:2) to yield 34.6 mg (0.12 mmol, 89 %) as a pale yellow solid.

$R_f$  = 0.45 (hexanes/EtOAc 3:2) [UV, PMA].

<sup>1</sup>H NMR (360 MHz, CDCl<sub>3</sub>, 300 K): δ [ppm] = 7.31 – 7.21 (m, 2H), 6.95 – 6.84 (m, 3H), 3.79 – 3.70 (m, 2H), 3.52 – 3.42 (m, 2H), 3.23 – 3.09 (m, 4H), 2.46 (s, 2H), 2.05 (td,  $J$  = 7.3, 2.6 Hz, 2H), 1.97 (t,  $J$  = 2.6 Hz, 1H), 1.77 (t,  $J$  = 7.3 Hz, 2H).

<sup>13</sup>C NMR (91 MHz, CDCl<sub>3</sub>, 300 K): δ [ppm] = 166.6, 150.9, 129.4, 120.8, 116.8, 82.9, 69.5, 49.9, 49.5, 46.1, 41.8, 38.8, 32.1, 26.3, 13.3.

HRMS ESI calc. for C<sub>17</sub>H<sub>21</sub>N<sub>4</sub>O [M+H]<sup>+</sup>: 297.1710; found, 297.1709.

**2-(3-(But-3-yn-1-yl)-3H-diazirin-3-yl)-N-isopropylacetamide (3.6)**Chemical Formula: C<sub>10</sub>H<sub>15</sub>N<sub>3</sub>O

Molecular Weight: 193,25

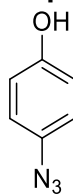
To a mixture of 20.0 mg (0.13 mmol, 1.00 eq) and 13.4  $\mu$ L (9.28 mg, 0.16 mmol, 1.20 eq) isopropylamine in DMF (1 mL) were added 26.6 mg (0.20 mmol, 1.50 eq) HOBT-H<sub>2</sub>O, 37.8 mg (0.20 mmol, 1.50 eq) EDC-HCl and 44.6  $\mu$ L (33.9 mg, 0.26 mmol, 2.00 eq) DIEA. The mixture was stirred at rt for 16 h. Upon solvent evaporation, the residue was purified by flash chromatography (hexanes/EtOAc 9:1  $\rightarrow$  4:1) to yield 25.2 mg (0.13 mmol, 99 %) as a pale oil.

$R_f$  = 0.19 (hexanes/EtOAc 4:1) [PMA].

<sup>1</sup>H NMR (360 MHz, CDCl<sub>3</sub>, 300 K):  $\delta$  [ppm] = 5.57 (br s, 1H), 4.08 (dq,  $J$  = 13.2, 6.6 Hz, 1H), 2.21 (s, 2H), 2.07 (td,  $J$  = 7.2, 2.6 Hz, 2H), 2.01 (t,  $J$  = 2.6 Hz, 1H), 1.76 (t,  $J$  = 7.2 Hz, 2H), 1.17 (d,  $J$  = 6.6 Hz, 6H).

<sup>13</sup>C NMR (91 MHz, CDCl<sub>3</sub>, 300 K):  $\delta$  [ppm] = 166.7, 82.8, 69.6, 42.0, 41.9, 32.2, 26.1, 22.9, 13.4.

**ESI- HRMS ESI** calc. for C<sub>10</sub>H<sub>16</sub>N<sub>3</sub>O [M+H]<sup>+</sup>: 194.1288; found, 194.1286.

**4-Azidophenol**Chemical Formula: C<sub>6</sub>H<sub>5</sub>N<sub>3</sub>O

Molecular Weight: 135,13

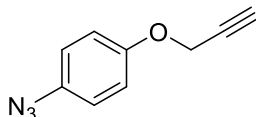
5.00 g (45.0 mmol, 1.00 eq) 4-aminophenol were resuspended in 2 M HCl (100 mL) and 3.72 g (54.0 mmol, 1.22 eq) NaNO<sub>2</sub> in H<sub>2</sub>O (20 mL) were added dropwise at 0 °C. The mixture was stirred for 30 min and a solution of 4.50 g (69.0 mmol, 1.50 eq) NaN<sub>3</sub> in 10 mL H<sub>2</sub>O were added over a period of 5 min. After 15 min, the mixture was extracted with EtOAc (3 x 100 mL) and the organic fractions combined, dried and filtered. After evaporation of the solvent, the crude product was purified using flash chromatography (hexanes/EtOAc 1:5) to give 5.90 g (43.7 mmol, 97 %) 4-azidophenol as a dark purple oil.

$R_f$  = 0.22 (hexanes/EtOAc 1:5)

**<sup>1</sup>H NMR** (300 MHz, CDCl<sub>3</sub>, 300 K): δ [ppm] = 6.94 – 6.88 (m, 2H), 6.86 – 6.78 (m, 2H), 5.01 (br s, 1H).

**<sup>13</sup>C NMR** (91 MHz, CDCl<sub>3</sub>, 300 K): δ [ppm] = 153.1, 132.4, 120.2, 116.7.

### 1-Azido-4-(prop-2-yn-1-yloxy)benzene (3.2)



Chemical Formula: C<sub>9</sub>H<sub>7</sub>N<sub>3</sub>O  
Molecular Weight: 173,18

To a solution of 1.00 g (7.40 mmol, 1.00 eq) 4-azidophenol in anhydrous THF (30 mL) were added 195 mg (8.14 mmol, 1.10 eq) NaH at 0 °C. The mixture was stirred for 30 min and 673 μL (1.06 g, 88.8 mmol, 1.20 eq) propargyl bromide was added. After stirring at rt for 24 h, the reaction was terminated by addition of sat. NH<sub>4</sub>Cl solution and the organic phase separated. The aqueous phase was extracted with EtOAc (2 x 20 mL), the organic fractions combined, dried over Na<sub>2</sub>SO<sub>4</sub>, filtered and the solvent evaporated under reduced pressure. Purification via preparative TLC (hexanes/EtOAc 7:1) yielded 0.89 g (5.14 mmol, 69 %) propargylic ether as a yellow oil which solidified in the freezer.

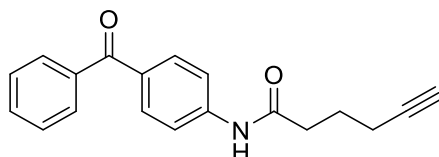
*R<sub>f</sub>* = 0.11 (hexanes/EtOAc 9:1) [UV, KMnO<sub>4</sub>].

**<sup>1</sup>H NMR** (300 MHz, CDCl<sub>3</sub>, 300 K): δ [ppm] = 6.97 (s, 4H), 4.67 (d, *J* = 2.4 Hz, 2H), 2.53 (t, *J* = 2.4 Hz, 1H).

**<sup>13</sup>C NMR** (75 MHz, CDCl<sub>3</sub>, 300 K): δ [ppm] = 155.0, 133.5, 120.1, 116.5, 78.5, 75.9, 56.3.

**HRMS APCI** calcd. for C<sub>18</sub>H<sub>15</sub>N<sub>6</sub>O<sub>2</sub> [2M+H]<sup>+</sup>: 347.1250; found, 347.1250.

### *N*-(4-Benzoylphenyl)hex-5-ynamide (3.1)



Chemical Formula: C<sub>19</sub>H<sub>17</sub>NO<sub>2</sub>  
Molecular Weight: 291,35

To a solution of 0.50 mL (500 mg, 4.46 mmol, 1.00 eq) 5-hexynoic acid in CH<sub>2</sub>Cl<sub>2</sub> (30 mL) was added DMF (0.1 mL). The mixture was cooled to 0 °C and 0.52 mL (762 mg,

6.00 mmol, 1.35 eq) oxalyl chloride was added. The mixture was stirred at this temperature for 1 h. 880 mg (4.46 mmol, 1.00 eq) 4-Aminobenzophenone and Et<sub>3</sub>N (1 mL) were added. The reaction was stirred at rt for 5 h and quenched by the addition of water. The obtained mixture was washed with brine and the phases were separated. The organic phase was dried over Na<sub>2</sub>SO<sub>4</sub>, filtered and concentrated under reduced pressure. The residue was separated by column chromatography (hexanes/EtOAc 2:1) to yield 900 mg (3.09 mmol, 69 %) of the desired product.

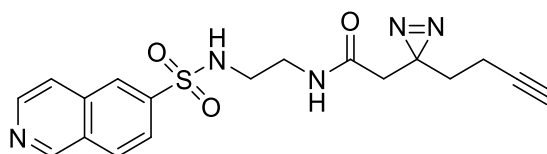
*R<sub>f</sub>* = 0.53 (hexanes/EtOAc 2:1) [KMnO<sub>4</sub>].

<sup>1</sup>H NMR (360 MHz, CDCl<sub>3</sub>, 300 K): δ [ppm] = 8.20 – 7.92 (m, 1H), 7.82 – 7.72 (m, 4H), 7.66 (d, *J* = 8.6 Hz, 2H), 7.61 – 7.54 (m, 1H), 7.50 – 7.43 (m, 2H), 2.54 (t, *J* = 7.3 Hz, 2H), 2.34 – 2.25 (m, 2H), 2.00 – 1.90 (m, 3H).

<sup>13</sup>C NMR (91 MHz, CDCl<sub>3</sub>, 300 K): δ [ppm] = 196.0, 171.3, 142.2, 137.9, 132.9, 132.4, 131.7, 130.0, 128.4, 119.0, 83.4, 69.6, 36.1, 23.9, 17.9.

HRMS ESI calc. for C<sub>19</sub>H<sub>18</sub>NO<sub>2</sub> [M+H]<sup>+</sup>: 292.1338; found, 292.1335.

**2-(3-(But-3-yn-1-yl)-3*H*-diazirin-3-yl)-*N*-(2-(isoquinoline-5-sulfonamido)ethyl)acetamide (3.8)**



Chemical Formula: C<sub>18</sub>H<sub>19</sub>N<sub>5</sub>O<sub>3</sub>S  
Molecular Weight: 385.44

To a mixture of 20.0 mg (0.131 mmol, 1.00 eq) and 39.5 mg (0.157 mmol, 1.20 eq) *N*-(2-aminoethyl)isoquinoline-5-sulfonamide in DMF (1 mL) were added 26.6 mg (0.197 mmol, 1.50 eq) HOBt·H<sub>2</sub>O, 37.8 mg (0.197 mmol, 1.50 eq) EDC·HCl and 44.6 μL (33.9 mg, 0.262 mmol, 2.00 eq) DIEA. The mixture was stirred at rt for 16 h. Upon solvent evaporation, the residue was purified by flash chromatography (CH<sub>2</sub>Cl<sub>2</sub>/MeOH 50:1 → 20:1) to yield 46.6 mg (0.12 mmol, 93 %) as a white solid.

*R<sub>f</sub>* = 0.44 (hexanes/EtOAc 19:1) [UV, PMA].

<sup>1</sup>H NMR (360 MHz, CDCl<sub>3</sub>, 300 K): δ [ppm] = 9.37 (br s, 1H), 8.64 (br s, 1H), 8.51 – 8.39 (m, 2H), 8.27 – 8.19 (m, 1H), 7.71 (t, *J* = 7.8 Hz, 1H), 6.75 (t, *J* = 5.7 Hz, 1H), 6.63 (t,

$J = 5.9$  Hz, 1H), 3.36 (q,  $J = 5.6$  Hz, 2H), 3.07 (q,  $J = 5.8$  Hz, 2H), 2.23 (s, 2H), 2.04 – 1.93 (m, 3H), 1.69 (t,  $J = 7.2$  Hz, 2H).

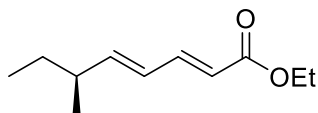
**$^{13}\text{C}$  NMR** (91 MHz,  $\text{CDCl}_3$ , 300 K):  $\delta$  [ppm] = 169.1, 153.0, 144.5, 134.4, 134.0, 133.6, 131.5, 129.2, 126.4, 117.7, 82.8, 69.8, 43.1, 41.2, 39.8, 32.2, 26.1, 13.4.

**HRMS ESI** calc. for  $\text{C}_{18}\text{H}_{20}\text{N}_5\text{O}_3\text{S}$   $[\text{M}+\text{H}]^+$ : 386.1281; found, 386.1279.



### 5.1.4 Synthetic procedures for Chapter 4: Target identification of neocarzin A-C in human cancer cells.

#### Ethyl (*S,2E,4E*)-6-methylocta-2,4-dienoate (4.9)



Chemical Formula: C<sub>11</sub>H<sub>18</sub>O<sub>2</sub>

Molecular Weight: 182,26

To a solution of 6.55 g (26.1 mmol, 1.50 eq) Ethyl (*E*)-4-(diethoxyphosphoryl)but-2-enoate in 20 mL THF was added 26.1 mL (26.1 mmol, 1 M in THF, 1.50 eq) LiHMDS at -78 °C. The solution was stirred at that temperature for 1 h and then 1.50 g (17.4 mmol, 1.00 eq) aldehyde in 10 mL THF were added. The mixture was stirred for 1h at -78 °C and then at 40 °C for 3h. The reaction was quenched by addition of saturated NH<sub>4</sub>Cl solution (30 mL) and the mixture was extracted with Et<sub>2</sub>O (2x50 mL). The combined organic fractions were dried, filtered and the solvent evaporated under reduced pressure. Purification via flash chromatography (hexanes/Et<sub>2</sub>O 15:1 → 5:1) yielded 1.56 g (8.56 mmol, 49 %) ester as a yellow oil.

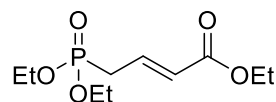
$R_f = 0.79$  (hexanes/Et<sub>2</sub>O 6:1) [UV, KMnO<sub>4</sub>]

<sup>1</sup>H NMR (300 MHz, CDCl<sub>3</sub>, 300 K): δ (ppm) = 7.26 (dd, *J* = 15.4, 10.6 Hz, 1H), 6.23 – 5.94 (m, 2H), 5.86 – 5.72 (m, 1H), 4.19 (q, *J* = 7.1 Hz, 2H), 2.16 (*virt. p.*, *J* = 6.9 Hz, 1H), 1.44 – 1.32 (m, 2H), 1.29 (t, *J* = 7.1 Hz, 3H), 1.02 (d, *J* = 6.7 Hz, 3H), 0.86 (t, *J* = 7.4 Hz, 3H).

<sup>13</sup>C NMR (75 MHz, CDCl<sub>3</sub>, 300 K): δ (ppm) = 167.44, 150.26, 145.39, 126.87, 119.43, 60.29, 38.93, 29.47, 19.65, 14.47, 11.82.

[α]<sup>22</sup><sub>D</sub> = 44.8 (c = 2.0, CH<sub>2</sub>Cl<sub>2</sub>).

#### Ethyl (*E*)-4-(diethoxyphosphoryl)but-2-enoate (4.15)



Chemical Formula: C<sub>10</sub>H<sub>19</sub>O<sub>5</sub>P

Molecular Weight: 250,23

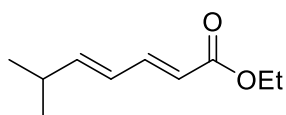
12.2 g (73.7 mmol, 1.13 eq) triethylphosphite and 16.7 g (65.0 mmol, 1.00 eq) ethyl 4-bromocrotonate (75% purity) were heated to 125 °C for 4 h. The crude product was purified

via vacuum distillation (113-116 °C, 0.04 mbar). 16.2 g (64.8 mmol, 88%) desired product were obtained as a slightly yellow oil.

**<sup>1</sup>H NMR** (500 MHz, CDCl<sub>3</sub>, 300 K): δ (ppm) = 6.92-6.83 (dq, *J* = 7.7, 15.4 Hz, 1H), 5.99-5.92 (dd, *J* = 4.9, 15.6 Hz, 1H), 4.23-4.17 (q, *J* = 7.1 Hz, 2H), 4.17-4.06 (*virt.* dddt, *J* = 3.2, 7.1, 10.3, 14.6 Hz, 4H), 2.78-2.69 (dd, *J* = 7.8, 22.9 Hz, 2H), 1.35-1.31 (t, *J* = 7.1 Hz, 6H), 1.35-1.31 (t, *J* = 7.1 Hz, 3H).

**<sup>13</sup>C NMR** (91 MHz, CDCl<sub>3</sub>, 300 K): δ (ppm) = 165.79, 165.76, 137.62, 137.50, 126.07, 125.91, 62.45, 62.38, 60.61, 31.56, 30.03, 16.59, 16.52, 14.36.

### Ethyl (2E,4E)-6-methylhepta-2,4-dienoate (4.12)



Chemical Formula: C<sub>10</sub>H<sub>16</sub>O<sub>2</sub>

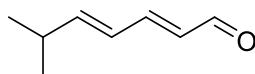
Molecular Weight: 168,24

To a solution of 7.51 g (30.0 mmol, 1.50 eq) ethyl (E)-4-(diethoxyphosphoryl)but-2-enoate in 25 mL THF was added 30.0 mL (30.0 mmol, 1 M in THF, 1.50 eq) LiHMDS at -78 °C. The solution was stirred at that temperature for 1 h and then 1.44 g (20.0 mmol, 1.00 eq) isobutanal in 10 mL THF were added. The mixture was stirred for 1h at -78 °C and then at -40 °C for 3h. The reaction was quenched by addition of saturated NH<sub>4</sub>Cl solution (30 mL) and the mixture extracted with Et<sub>2</sub>O (2 x 50 mL). The combined organic fractions were dried, filtered and the solvent evaporated under reduced pressure. Purification via flash chromatography (hexanes/Et<sub>2</sub>O 15:1 → 5:1) yielded 1.71 g (10.2 mmol, 51 %) ester as a yellow oil.

*R<sub>f</sub>* = 0.76 (hexanes/Et<sub>2</sub>O 6:1) [UV, KMnO<sub>4</sub>]

**<sup>1</sup>H NMR** (360 MHz, CDCl<sub>3</sub>, 300 K): δ (ppm) = 7.32 – 7.20 (m, 2H), 6.24 – 6.02 (m, 2H), 5.80 (d, *J* = 15.4 Hz, 1H), 4.19 (q, *J* = 7.1 Hz, 2H), 2.52 – 2.29 (m, 1H), 1.29 (t, *J* = 7.1 Hz, 3H), 1.04 (d, *J* = 6.8 Hz, 6H).

**<sup>13</sup>C NMR** (91 MHz, CDCl<sub>3</sub>, 300 K): δ (ppm) = 167.42, 151.30, 145.45, 125.62, 119.54, 60.30, 31.66, 21.95, 14.48.

**(2E,4E)-6-Methylhepta-2,4-dienal (4.13)**<sup>240</sup>Chemical Formula: C<sub>8</sub>H<sub>12</sub>O

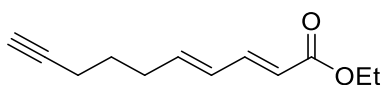
Molecular Weight: 124,18

3.60 g (21.4 mmol, 1.00 eq) ester were dissolved in THF (25 mL) and 37.4 mL (44.9 mmol, 1.2 M in toluene, 2.10 eq) DIBAL-H were added at -78 °C. The reaction was stirred at -78 °C for 4 h and was quenched with sat. K/Na tartrate solution at -78 °C. The mixture was stirred overnight and the phases separated. The aqueous phase was reextracted with Et<sub>2</sub>O (2 x 30 mL), the combined organic fractions dried, filtered and the solvent evaporated. The crude alcohol was dissolved in Et<sub>2</sub>O (50 mL) and 27.9 g (321 mmol, 15.0 eq) MnO<sub>2</sub> were added. The mixture was stirred for 3 h after which the TLC indicated complete consumption of starting material. The reaction mixture was filtered and the solvent evaporated. The crude product was purified by flash chromatography (hexanes/Et<sub>2</sub>O 10:1 → 5:1) to yield 2.20 g (17.7 mmol, 83 % over two steps) aldehyde as a yellow oil.

$R_f$  = 0.63 (hexanes/Et<sub>2</sub>O 6:1) [UV, KMnO<sub>4</sub>]

<sup>1</sup>H NMR (360 MHz, CDCl<sub>3</sub>, 300 K): δ (ppm) = 9.54 (d,  $J$  = 8.0 Hz, 1H), 7.20 – 7.02 (m, 1H), 6.38 – 6.16 (m, 2H), 6.09 (dd,  $J$  = 15.4, 8.1 Hz, 1H), 2.61 – 2.38 (m, 1H), 1.08 (d,  $J$  = 6.8 Hz, 6H).

<sup>13</sup>C NMR (91 MHz, CDCl<sub>3</sub>, 300 K): δ (ppm) = 194.1, 153.9, 153.3, 130.4, 126.0, 31.9, 21.8.

**Ethyl (2E,4E)-deca-2,4-dien-9-ynoate (4.5)**Chemical Formula: C<sub>12</sub>H<sub>16</sub>O<sub>2</sub>

Molecular Weight: 192,26

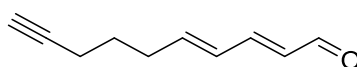
To a solution of 4.55 g (18.2 mmol, 1.00 eq) ethyl (E)-4-(diethoxyphosphoryl)but-2-enoate in THF (36 mL) at -78 °C were added 8.00 mL (20.0 mmol, 2.5 M in hexane, 1.10 eq) nBuLi. The solution was stirred at this temperature for 15 min and 1.75 g (18.2 mmol, purity ca. 90 %, 1.00 eq) 5-hexynal were added. After 15 min, the mixture was warmed up to rt and stirred for 1h. The reaction mixture was quenched by addition of sat. NH<sub>4</sub>Cl solution and extracted with Et<sub>2</sub>O (3 x 40 mL). After filtration over Na<sub>2</sub>SO<sub>4</sub>, the solvent was removed under reduced pressure and the crude product subjected to flash chromatography (hexanes/EtOAc 15:1). 1.88 g (9.87 mmol, 54 %, E/Z = 5:1) ester were isolated as a yellow oil.

$R_f$  = 0.63 (hexanes/ Et<sub>2</sub>O 6:1) [UV, KMnO<sub>4</sub>]

<sup>1</sup>H NMR (250 MHz, CDCl<sub>3</sub>, 300 K): δ (ppm) = 7.34 – 7.16 (m, 1H), 6.27 – 6.02 (m, 2H), 5.80 (dt,  $J$  = 15.4, 0.6 Hz, 1H), 4.20 (q,  $J$  = 7.1 Hz, 2H), 2.39 – 2.12 (m, 4H), 1.97 (t,  $J$  = 2.6 Hz, 1H), 1.74 – 1.58 (m, 2H), 1.29 (t,  $J$  = 7.1 Hz, 3H).

<sup>13</sup>C NMR (63 MHz, CDCl<sub>3</sub>, 300 K): δ (ppm) = 167.3, 144.8, 143.0, 129.3, 119.9, 83.9, 69.0, 60.4, 31.9, 27.6, 18.0, 14.5.

**(2E,4E)-Deca-2,4-dien-9-ynal (4.6)**



Chemical Formula: C<sub>10</sub>H<sub>12</sub>O

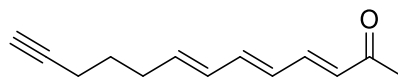
Molecular Weight: 148,21

To a solution of 3.02 g (15.8 mmol, 1.00 eq) ester in THF (60 mL), 27.2 mL (31.5 mmol, 25 wt-% in hexane, 2.00 eq) DIBAL-H were added under argon atmosphere at -78 °C. After stirring for 1.5 h at -78 °C, the mixture was allowed to warm up to room temperature. Then dry methanol (30 mL) and saturated sodium potassium tartrate solution (60 mL) were added slowly. Stirring was continued for another hour, water (60 mL) was added and the resulting mixture was extracted with ether (3 × 60 mL). The organic layer was washed with brine (1 × 60 mL), dried with sodium sulfate and concentrated under reduced pressure. After a suspension of 11.6 g MnO<sub>2</sub> (133 mmol, 20 eq) in Hexane (25 mL) was cooled to 0 °C, 1.00 g (6.67 mmol, 1.00 eq) of the crude product was added. The mixture was stirred for 4 h at rt after which TLC indicated full conversion. The MnO<sub>2</sub> was filtered off and the filtrate was concentrated on the rotary evaporator. Column chromatography (hexanes/Et<sub>2</sub>O 5:1 → 3:1) provided 664 mg (4.48 mmol, 67%) of the product.

$R_f$  = 0.67 (hexanes/Et<sub>2</sub>O 6:1) [UV, KMnO<sub>4</sub>]

<sup>1</sup>H NMR (360 MHz, CDCl<sub>3</sub>, 300 K): δ (ppm) = 9.56 (d,  $J$  = 8.0 Hz, 1H), 7.10 (dd,  $J$  = 15.3, 10.4 Hz, 1H), 6.43 – 6.22 (m, 2H), 6.11 (dd,  $J$  = 15.3, 8.0 Hz, 1H), 2.37 (q,  $J$  = 7.3 Hz, 2H), 2.25 (td,  $J$  = 7.0, 2.7 Hz, 2H), 2.00 (t,  $J$  = 2.6 Hz, 1H), 1.72 (p,  $J$  = 7.2 Hz, 2H).

<sup>13</sup>C NMR (91 MHz, CDCl<sub>3</sub>, 300 K): δ (ppm) = 194.0, 152.4, 145.6, 130.6, 129.6, 83.7, 69.1, 32.1, 27.4, 18.0.

**(3E,5E,7E)-Trideca-3,5,7-trien-12-yn-2-one (4.7)**Chemical Formula: C<sub>13</sub>H<sub>16</sub>O

Molecular Weight: 188,27

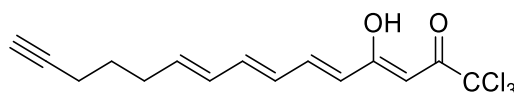
To a solution of 664 mg (4.48 mmol, 1.00 eq) aldehyde in toluene (17 mL), 2.83 g (8.96 mmol, 2.00 eq) 1-(triphenylphosphoranylidene)-2-propanone were added at 0 °C and the solution was allowed to warm up to room temperature. The reaction mixture was heated up to 100 °C and was stirred for 16 h. After the solution had cooled down, brine was added and the mixture extracted with ethyl acetate (3 x 25 mL). The organic layer was washed with brine (1 x 25 mL), dried over Na<sub>2</sub>SO<sub>4</sub> and concentrated on the rotary evaporator. Column chromatography (hexanes/EtOAc 9:1) provided 452 mg (2.40 mmol, 54%) ketone as a yellow oil.

$R_f$  = 0.58 (hexanes/EtOAc 9:1) [UV, KMnO<sub>4</sub>]

<sup>1</sup>H NMR (250 MHz, CDCl<sub>3</sub>, 300 K): δ (ppm) = 7.22 – 7.06 (m, 1H), 6.66 – 6.49 (m, 1H), 6.32 – 6.07 (m, 3H), 5.93 (dt, *J* = 14.7, 7.0 Hz, 1H), 2.34 – 2.16 (m, 4H), 2.27 (s, 3H), 1.97 (t, *J* = 2.7 Hz, 1H), 1.73 – 1.59 (m, 2H).

<sup>13</sup>C NMR (63 MHz, CDCl<sub>3</sub>, 300 K): δ (ppm) = 198.5, 143.7, 141.8, 139.4, 130.9, 129.8, 128.8, 84.0, 68.9, 31.9, 27.8, 27.5, 18.0.

HRMS APCI calcd. for C<sub>13</sub>H<sub>17</sub>O [M+H]<sup>+</sup>:189.1273, found: 189.1273

**(3Z,5E,7E,9E)-1,1,1-trichloro-4-hydroxypentadeca-3,5,7,9-tetraen-14-yn-2-one (4.4)**Chemical Formula: C<sub>15</sub>H<sub>15</sub>Cl<sub>3</sub>O<sub>2</sub>

Molecular Weight: 333,63

To a solution of 120.0 mg (0.64 mmol, 1.00 eq) ketone in 10 mL THF was added 1.31 mL (1.31 mmol, 1 M in THF, 2.05 eq) LiHMDS at -78 °C. The mixture was stirred for 1 h and then 196 mg (116 μL, 0.64 mmol, 1.00 eq) trichloroacetic anhydride were added. The reaction mixture was stirred for 2 h and then quenched with water. The phases were separated, aqueous phase extracted with Et<sub>2</sub>O (20 mL) and the combined organic fractions dried, filtered and the solvent evaporated. Purification via HPLC (gradient 80% → 95 % CH<sub>3</sub>CN) yielded 54 mg (0.16 mmol, 25 %) trichloride as a yellow oil.

$R_f = 0.71$  (hexanes/Et<sub>2</sub>O 10:1) [UV, KMnO<sub>4</sub>]

**RP-HPLC** (analytical setup, method: gradient 2 % B → 100 % B over 20 min):  $t_R = 18.59$  min

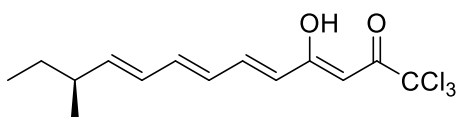
**<sup>1</sup>H NMR** (360 MHz, CDCl<sub>3</sub>, 300 K):  $\delta$  (ppm) = 13.38 (s, 1H), 7.36 (dd,  $J = 15.0, 11.3$  Hz, 1H), 6.61 (dd,  $J = 14.9, 10.7$  Hz, 1H), 6.35 – 6.13 (m, 2H) 6.15 (s, 1H), 6.11 – 5.91 (m, 2H), 2.30 (q,  $J = 7.3$  Hz, 2H), 2.22 (td,  $J = 7.0, 2.7$  Hz, 3H), 1.97 (t,  $J = 2.7$  Hz, 1H), 1.69 – 1.63 (m, 2H).

**<sup>13</sup>C NMR** (91 MHz, CDCl<sub>3</sub>, 300 K):  $\delta$  (ppm) = 186.3, 178.0, 142.7, 142.4, 140.3, 131.0, 128.9, 123.8, 95.3, 93.4, 84.0, 68.9, 32.0, 27.8, 18.0.

**HRMS ESI** calcd. for C<sub>15</sub>H<sub>16</sub>Cl<sub>3</sub>O<sub>2</sub> [M-H]<sup>-</sup>: 331.0065, found: 331.0066

**(S,3Z,5E,7E,9E)-1,1,1-Trichloro-4-hydroxy-11-methyltrideca-3,5,7,9-tetraen-2-one  
(4.1)**

**Neocarzililn A<sup>213</sup>**



Chemical Formula: C<sub>14</sub>H<sub>17</sub>Cl<sub>3</sub>O<sub>2</sub>  
Molecular Weight: 323,64

To a solution of 100 mg (0.56 mmol, 1.00 eq) ketone in 5 mL THF was added 617  $\mu$ L (0.62 mmol, 1 M in THF, 1.10 eq) LiHMDS at -78 °C. The mixture was stirred for 1 h and then 346 mg (205  $\mu$ L, 1.12 mmol, 2.00 eq) trichloroacetic anhydride were added. The mixture was stirred at -78 °C for 3 h and then quenched by addition of 50 mL PBS. After extraction with Et<sub>2</sub>O (2 x 50 mL), the organic phase was dried, filtered and the solvent removed under reduced pressure. Purification via flash chromatography (hexanes/Et<sub>2</sub>O 50:1 → 10:1) yielded 91.3 mg (28.2 mmol, 50 %) neocarzililn A as an orange oil.

$R_f = 0.66$  (hexanes/Et<sub>2</sub>O 10:1) [UV, KMnO<sub>4</sub>]

**RP-HPLC** (analytical setup, method: gradient 2 % D → 100 % D over 20 min):  $t_R = 20.27$  min

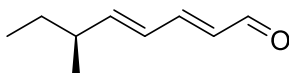
**<sup>1</sup>H NMR** (360 MHz, CDCl<sub>3</sub>, 300 K):  $\delta$  (ppm) = 13.43 (s, 1H), 7.39 (ddd,  $J = 15.1, 11.4, 0.8$  Hz, 1H), 6.70 – 6.58 (m, 1H), 6.33 – 6.26 (m, 1H), 6.23 – 6.13 (m, 2H), 6.02 (d,  $J = 15.0$  Hz, 1H), 5.91 (dd,  $J = 15.2, 7.9$  Hz, 1H), 2.29 – 2.07 (m, 1H), 1.44 – 1.35 (m, 2H), 1.05 (d,  $J = 6.7$  Hz, 3H), 0.89 (t,  $J = 7.4$  Hz, 4H).

**<sup>13</sup>C NMR** (126 MHz, CDCl<sub>3</sub>, 300 K): δ (ppm) = 186.1, 178.0, 147.7, 143.0, 142.8, 128.4, 128.4, 123.3, 95.2, 93.2, 38.9, 29.5, 19.7, 11.8.

**HRMS ESI** calcd. for C<sub>14</sub>H<sub>16</sub>Cl<sub>3</sub>O<sub>2</sub> [M-H]: 321.0221, found: 321.0219.

[α]<sup>22</sup><sub>D</sub> = 45.4 (c = 0.24, CHCl<sub>3</sub>).

**(S,2E,4E)-6-Methylocta-2,4-dienal (4.10)**



Chemical Formula: C<sub>9</sub>H<sub>14</sub>O

Molecular Weight: 138,21

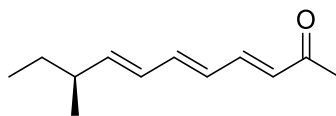
1.40 g (7.68 mmol, 1.00 eq) ester were dissolved in THF (18 mL) and cooled to -78 °C. 16.1 mL (16.1 mmol, 1 M in THF, 2.10 eq) DIBAL-H were added dropwise and the solution stirred at -78 °C for 2 h. The reaction was quenched with MeOH (10 mL) and saturated K/Na tartrate solution (50 mL) and Et<sub>2</sub>O (50 mL) were added. The biphasic mixture was stirred at rt o/n and the phase separated. The aqueous phase was reextracted with Et<sub>2</sub>O (50 mL) and the combined organic fractions dried, filtered and the solvent evaporated. The crude product alcohol was directly used for the next step. The crude product was dissolved in hexane (20 mL) and 13.4 g (154 mmol, 20.0 eq) MnO<sub>2</sub> were added at 0 °C. After 3 h, TLC indicated full conversion. The mixture was filtered and the solvent removed. Purification via flash chromatography (hexanes/EtOAc 12:1) yielded 550 mg (4.00 mmol, 52 % over two steps) aldehyde as a yellow oil.

**R<sub>f</sub>** = 0.58 (hexanes/EtOAc 9:1)

**<sup>1</sup>H NMR** (250 MHz, CDCl<sub>3</sub>, 300 K): δ (ppm) = 9.54 (d, *J* = 8.0 Hz, 1H), 7.09 (dd, *J* = 15.3, 10.2 Hz, 1H), 6.39 – 6.00 (m, 3H), 2.23 (*virt.* hept, *J* = 6.8 Hz, 1H), 1.48 – 1.34 (m, 2H), 1.06 (d, *J* = 6.7 Hz, 3H), 0.89 (t, *J* = 7.4 Hz, 3H).

**<sup>13</sup>C NMR** (63 MHz, CDCl<sub>3</sub>, 300 K): δ (ppm) = 194.1, 153.2, 152.9, 130.3, 127.2, 39.2, 29.4, 19.5, 11.8.

[α]<sup>22</sup><sub>D</sub> = 63.7 (c = 2.0, CH<sub>2</sub>Cl<sub>2</sub>).

**(S,3E,5E,7E)-9-Methylundeca-3,5,7-trien-2-one (4.11)**

Chemical Formula: C<sub>12</sub>H<sub>18</sub>O  
Molecular Weight: 178,28

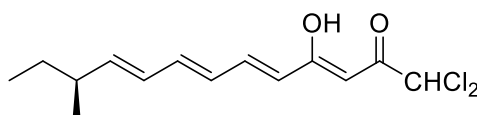
To a solution of 460 mg (3.33 mmol, 1.00 eq) aldehyde **4.10** in toluene (15 mL) were added 2.12 g (6.66 mmol, 2.00 eq) ylide and the mixture was heated up to 100 °C and stirred for 16 h. The brown red solution was allowed to cool to rt and hexane (30 mL) was added. The mixture was filtered and the solvent removed under reduced pressure. The residue was resuspended in hexane and filtered. After removal of the solvent, the crude product was purified via flash chromatography (hexanes/EtOAc 10:1 → 8:1) to yield 351 mg (1.97 mmol, 59 %) ketone as a yellow oil.

$R_f = 0.42$  (hexanes/EtOAc 8:1)

**<sup>1</sup>H NMR** (250 MHz, CDCl<sub>3</sub>, 300 K):  $\delta$  (ppm) = 7.15 (dd,  $J = 15.5, 11.0$  Hz, 1H), 6.58 (dd,  $J = 14.9, 10.6$  Hz, 1H), 6.32 – 6.05 (m, 3H), 5.84 (dd,  $J = 15.2, 7.8$  Hz, 1H), 2.27 (s, 3H), 2.15 (*virt. p*,  $J = 6.9$  Hz, 1H), 1.45 – 1.28 (m, 2H), 1.02 (d,  $J = 6.7$  Hz, 3H), 0.87 (t,  $J = 7.4$  Hz, 3H).

**<sup>13</sup>C NMR** (63 MHz, CDCl<sub>3</sub>, 300 K):  $\delta$  (ppm) = 198.6, 146.8, 143.9, 142.5, 129.5, 128.4, 38.9, 29.6, 27.4, 19.8, 11.9.

$[\alpha]^{22}_D = 58.2$  (c = 0.17, CHCl<sub>3</sub>)

**(S,3Z,5E,7E,9E)-1,1-Dichloro-4-hydroxy-11-methyltrideca-3,5,7,9-tetraen-2-one (4.3)****Neocarzilic C**

Chemical Formula: C<sub>14</sub>H<sub>18</sub>Cl<sub>2</sub>O<sub>2</sub>  
Molecular Weight: 289,20

To a solution of 100 mg (0.56 mmol, 1.00 eq) ketone in 5 mL THF was added 617  $\mu$ L (0.62 mmol, 1 M in THF, 1.10 eq) LiHMDS at -78 °C. The mixture was stirred for 1 h and then 266 mg (169  $\mu$ L, 1.12 mmol, 2.00 eq) dichloroacetic anhydride were added. The mixture was stirred at -78 °C for 3 h and then quenched by addition of 50 mL PBS. After extraction with Et<sub>2</sub>O (2 x 50 mL), the organic phase was dried, filtered and the solvent removed under



reduced pressure. Purification via flash chromatography (hexanes/Et<sub>2</sub>O 20:1 → 10:1) yielded 71.0 mg (0.25 mmol, 44 %) neocarzilin C as an orange oil.

$R_f$  = 0.51 (hexanes/Et<sub>2</sub>O 10:1)

**RP-HPLC** (analytical setup, method: gradient 2 % D → 100 % D over 20 min):  $t_R$  = 18.80 min

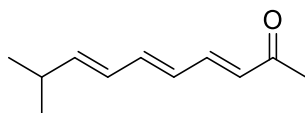
**<sup>1</sup>H NMR** (300 MHz, CDCl<sub>3</sub>, 300 K):  $\delta$  (ppm) = 13.96 (s, 1H), 7.34 (ddd,  $J$  = 15.1, 11.3, 0.8 Hz, 1H), 6.67 – 6.51 (m, 1H), 6.33 – 6.06 (m, 2H), 6.00 – 5.83 (m, 2H), 5.95 (s, 1H), 5.89 (s, 1H), 2.16 (*virt. p*,  $J$  = 6.9 Hz, 1H), 1.41 – 1.33 (m, 1H), 1.03 (d,  $J$  = 6.7 Hz, 3H), 0.87 (t,  $J$  = 7.4 Hz, 3H).

**<sup>13</sup>C NMR** (75 MHz, CDCl<sub>3</sub>, 300 K):  $\delta$  (ppm) = 189.9, 178.5, 147.6, 142.7, 142.6, 128.6, 128.5, 123.6, 95.5, 69.0, 39.1, 29.6, 19.9, 11.9.

**HRMS ESI** calcd. for C<sub>14</sub>H<sub>17</sub>Cl<sub>2</sub>O<sub>2</sub> [M-H]<sup>-</sup>: 287.0611, found: 287.0614

$[\alpha]_D^{22}$  = 43.0 (c = 0.14, CHCl<sub>3</sub>)

**(3E,5E,7E)-9-Methyldeca-3,5,7-trien-2-one (4.14)**



Chemical Formula: C<sub>11</sub>H<sub>16</sub>O

Molecular Weight: 164,25

To a solution of 1.00 g (8.05 mmol, 1.00 eq) aldehyde **4.13** in toluene (30 mL) were added 5.13 g (16.1 mmol, 2.00 eq) ylide and the mixture was heated up to 100 °C and stirred for 16 h. The brown red solution was allowed to cool to rt and hexane (30 mL) was added. The triphenylphosphine oxide was removed by filtration and the solvent removed *in vacuo*. The residue was resuspended in hexane and filtered. After removal of the solvent, the crude product was purified via flash chromatography (hexanes/Et<sub>2</sub>O 5:1) to yield 866 mg (5.27 mmol, 65 %) ketone as a yellow oil.

$R_f$  = 0.40 (hexanes/EtOAc 10:1)

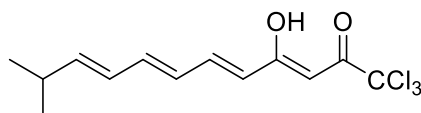
**<sup>1</sup>H NMR** (360 MHz, CDCl<sub>3</sub>, 300 K):  $\delta$  (ppm) = 7.14 (ddd,  $J$  = 15.5, 11.1, 0.7 Hz, 1H), 6.57 (dd,  $J$  = 14.9, 10.6 Hz, 1H), 6.24 (*virt. ddt*,  $J$  = 14.9, 11.1, 0.7 Hz, 1H), 6.18 – 6.05 (m, 2H), 5.93 (dd,  $J$  = 15.2, 6.7 Hz, 1H), 2.47 – 2.35 (m, 1H), 2.26 (s, 3H), 1.03 (d,  $J$  = 6.8 Hz, 6H).

**$^{13}\text{C}$  NMR** (91 MHz,  $\text{CDCl}_3$ , 300 K):  $\delta$  (ppm) = 198.6, 147.9, 143.9, 142.5, 129.5, 128.5, 127.1, 31.6, 27.4, 22.1.

**HRMS APCI** calcd. for  $\text{C}_{11}\text{H}_{17}\text{O}$   $[\text{M}+\text{H}]^+$ : 165.1273, found: 165.1273.

**(3Z,5E,7E,9E)-1,1,1-Trichloro-4-hydroxy-11-methyldodeca-3,5,7,9-tetraen-2-one (4.2)**

**Neocarzilin B**



Chemical Formula:  $\text{C}_{13}\text{H}_{15}\text{Cl}_3\text{O}_2$

Molecular Weight: 309,61

To a solution of 500 mg (3.04 mmol, 1.00 eq) ketone in anhydrous THF (25 mL) were added 3.34 mL (3.34 mmol, 1 M in THF, 1.10 eq) LiHMDS at  $-78\text{ }^\circ\text{C}$ . The mixture was stirred for 1 h and then 1.88 g (1.11 mL, 6.09 mmol, 2.00 eq) trichloroacetic anhydride were added. The mixture was stirred at  $-78\text{ }^\circ\text{C}$  for 3 h and then quenched by addition of 50 mL PBS. After extraction with  $\text{Et}_2\text{O}$  (2 x 50 mL), the organic phase was dried, filtered and the solvent removed under reduced pressure. Purification via flash chromatography (hexanes/ $\text{Et}_2\text{O}$  50:1  $\rightarrow$  10:1) yielded 745 mg (2.41 mmol, 79 %) neocarzilin B as an orange solid.

$R_f$  = 0.46 (hexanes/ $\text{Et}_2\text{O}$  10:1)

**RP-HPLC** (analytical setup, method: gradient 2 % B  $\rightarrow$  100 % B over 20 min):  $t_R$  = 19.55 min

**$^1\text{H}$  NMR** (250 MHz,  $\text{CDCl}_3$ , 300 K):  $\delta$  (ppm) = 13.41 (s, 1H), 7.36 (dd,  $J$  = 15.0, 11.4 Hz, 1H), 6.61 (dd,  $J$  = 14.8, 10.5 Hz, 1H), 6.28 (dd,  $J$  = 14.8, 11.3 Hz, 1H), 6.15 (s, 1H), 6.21 – 6.09 (m, 2H), 6.04 – 5.90 (m, 2H), 2.51 – 2.34 (m, 1H), 1.05 (d,  $J$  = 6.7 Hz, 6H).

**$^{13}\text{C}$  NMR** (63 MHz,  $\text{CDCl}_3$ , 300 K):  $\delta$  (ppm) = 186.2, 178.1, 148.8, 143.1, 142.9, 128.6, 127.3, 123.4, 95.3, 93.3, 31.7, 22.1.

**HRMS ESI** calcd. for  $\text{C}_{13}\text{H}_{14}\text{Cl}_3\text{O}_2$   $[\text{M}-\text{H}]^-$ : 307.0065, found 307.0065.

## 5.2 Biochemistry

### 5.2.1 General methods and materials

#### 5.2.1.1 Cell culture

Human cells (HepG2, A549, MCF-7, HeLa) were grown in DMEM medium (Sigma Life Sciences) or RPMI (Sigma Life Sciences) with 2 mM glutamine (PAA) and 10 % fetal bovine serum (FBS, Sigma Life Sciences) for analytical (6 well) and for preparative (TC dish 150 standard) studies, respectively. For SILAC experiments, A549, HepG2 and HeLa cells were passaged six times in SILAC-DMEM (gibco, Life Technologies) or SILAC-RPMI (gibco, Life Technologies) supplemented with 10 % dialyzed FBS and 2 mM L-glutamine as well as 214  $\mu\text{M}$  [ $^{13}\text{C}_6,^{15}\text{N}_4$ ] L-arginine  $\cdot$  HCl and 419  $\mu\text{M}$  [ $^{13}\text{C}_6,^{15}\text{N}_2$ ] L-lysine  $\cdot$  2 HCl (Cambridge Isotope Laboratories) resulting in “heavy” cells or [ $^{13}\text{C}_6$ ] L-arginine  $\cdot$  HCl and [4,4,5,5- $\text{D}_4$ ]L-lysine  $\cdot$  2 HCl (Cambridge Isotope Laboratories) in corresponding molarities resulting in “light” cells.

For splitting of the cells, the medium was removed by careful suction and the cells washed with 10 mL of PBS. 1 mL (2 mL for T175 TC Flask) Accutase® (Sigma Life Sciences) was added and the cells incubated for 10 min. The desired amount of medium was added and the cells resuspended. According to the ratio of division (1:5-1:10), the desired amount of cell suspension was removed and fresh medium was added to the flask to a final volume of 10-12 mL (T75 flask) or 20-25 mL (T175 flask). For labeling purposes, cells were grown to 70-90 % confluence at the start of the experiment.

Cell counting was conducted in a *Neubauer improved* chamber. Cell suspension was mixed with Trypan Blue (1:1), added to the chamber and the cells were counted. For cryostocks, the cell suspension was concentrated to 1-2 million cells/mL. 100  $\mu\text{L}$  sterile glycerol was added to 900  $\mu\text{L}$  of cell suspension in a cryotube and the mixture was cooled down in a *Cryo 1 °C Cooler* (VWR). After 2 h, the frozen cells were transferred to a liquid nitrogen tank (-196 °C) for long term storage.

#### 5.2.1.2 MTT- Assay

This assay was performed in flat bottom 96 well plates (*Nunclon™ Delta 96-Well MicroWell™ Plates*, Thermo Scientific). A549/HepG2 cells were grown to 30-40 % confluence. The medium was removed and 100  $\mu\text{L}$  medium/well containing 1  $\mu\text{L}$  DMSO compound stock were added to the cells and incubated for 24 h. All concentrations as well as a DMSO control were done in triplicates. 20  $\mu\text{L}$  Thiazolyl Blue Tetrazolium bromide (5

mg/mL in PBS, Sigma Aldrich) were added to the cells and incubated for 2-4 h until complete consumption was observed. After removal of the medium, the resulting formazan was dissolved in 200  $\mu$ L DMSO. Optical density was measured at 570 nm (562 nm) and background subtracted at 630 nm (620 nm) by a TECAN Infinite® M200 Pro.

For calculation of  $IC_{50}$  values, residual viabilities for the respective compound concentrations were fitted to

$$V = \frac{100}{1 + 10^{(\log(IC_{50}) - \log(c)) \cdot N}}$$

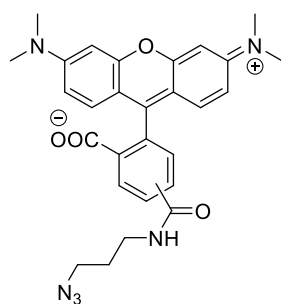
$V$ : viability [%]

$c$ : Inhibitor concentration [M]

$N$ : Hill slope

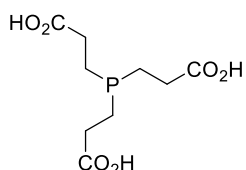
using Graphpad Prism 6.0.

### 5.2.1.3 Labeling reagents



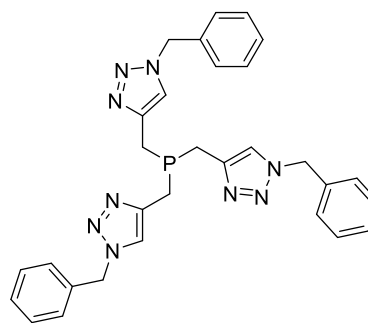
**RhN<sub>3</sub>**

Chemical Formula: C<sub>28</sub>H<sub>29</sub>N<sub>6</sub>O<sub>4</sub>  
Molecular Weight: 513,57



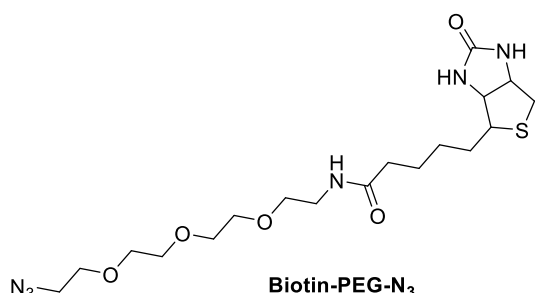
**TCEP**

Chemical Formula: C<sub>9</sub>H<sub>15</sub>O<sub>6</sub>P  
Molecular Weight: 250,19



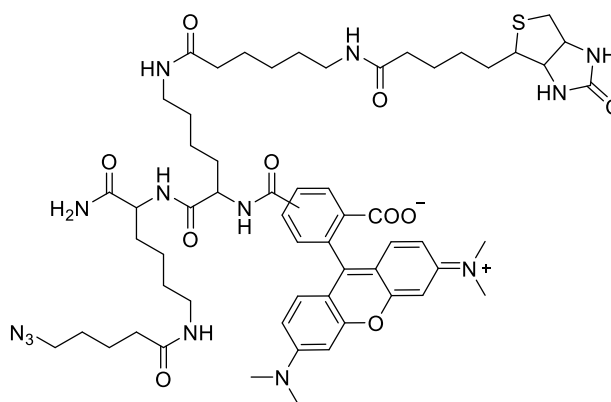
**TBTA**

Chemical Formula: C<sub>30</sub>H<sub>30</sub>N<sub>9</sub>P  
Molecular Weight: 547,61



**Biotin-PEG-N<sub>3</sub>**

Chemical Formula: C<sub>18</sub>H<sub>32</sub>N<sub>6</sub>O<sub>5</sub>S  
Molecular Weight: 444,55



**Trifunctional linker**

Chemical Formula: C<sub>59</sub>H<sub>83</sub>N<sub>13</sub>O<sub>10</sub>S  
Molecular Weight: 1166,45

### 5.2.1.4 In situ labeling

Cells were incubated for 1 h with varying concentrations of probe (stock solution in DMSO, 0.1 % end concentration of DMSO) in a cell incubator at 37 °C. Subsequently, the cells were scraped off and pelletized for 3 min at 600 x g. The pellets were washed with PBS once and then resuspended in lysis buffer (1 % (v/v) NP40 and 1 % (w/v) sodium deoxycholate, analytical scale: 100 µL, preparative scale: 1000 µL) and incubated at 0 °C for 15 min. Soluble and insoluble fractions were separated by centrifugation (30 min, 4 °C, 21·10<sup>3</sup> x g). The insoluble fraction was washed once with PBS (1 x 10 sec, 10 % maximum intensity sonication) and resuspended in 100 µL PBS for analytical, 1000 µL for preparative analysis.

### 5.2.1.5 Analytical gel based analysis

In case of analytical labeling, the click reaction was carried out with 100  $\mu\text{L}$  of proteome. Both cytosol fraction and membrane fraction were analysed separately. 10  $\mu\text{L}$  ABPP Mix (2  $\mu\text{L}$  5-TAMRA- $\text{N}_3$  (baseclick, BCFA-008-10; 5 mM in DMSO), 2  $\mu\text{L}$  fresh TCEP (50 mM in ddH<sub>2</sub>O), 6  $\mu\text{L}$  TBTA ligand (1.667 mM in 80 % tBuOH and 20 % DMSO)) were added. Samples were gently vortexed and the cycloaddition was initiated by the addition of 2  $\mu\text{L}$  CuSO<sub>4</sub> (50 mM in ddH<sub>2</sub>O). The reaction was incubated for 1 h at rt. For analytical gel electrophoresis, 100  $\mu\text{L}$  2 x SDS loading buffer were added and 50  $\mu\text{L}$  were applied on the gel (10 % (w/v) acrylamide, preparation according to instructions recommended by Carl Roth Company). Roti®-Mark STANDARD (Carl Roth GmbH & Co. KG, for Coomassie staining) and BenchMark™ Fluorescent Protein Standard (Life Technologies Corp.) were applied as markers to determine the protein mass. After application of the protein samples, the gels were developed for 4-5 h with 300 V. Fluorescence scans of SDS gels were performed with a Fujifilm Las-4000 luminescent image analyser with a Fujinon VRF43LMD3 lens and a 575DF20 filter. For determination of relative protein amount, gels were stained with Coomassie stain solution (0.25 % (w/v) Coomassie Brilliant Blue R250, 9.20 % (v/v) AcOH, 45.4 % (v/v) EtOH in ddH<sub>2</sub>O).

## 5.2.2 Biochemical procedures for Chapter 2: Target identification of falcarinol in cancer cells

### 5.2.2.1 Click reaction and preparative gel-free analysis

The cytosol and membrane fractions were used for preparative analysis. To determine the protein concentration in lysed samples, a BCA assay (Roti®-Quant Universal Reagent 1+2 (15:1)) was conducted. The corresponding SILAC states were mixed and 120  $\mu\text{L}$  gel-free ABPP Mix (40  $\mu\text{L}$  Biotin-PEG<sub>3</sub>- $\text{N}_3$  (Jena Bioscience, CLK-AZ104P4-100; 10 mM in DMSO), 20  $\mu\text{L}$  fresh TCEP (50 mM in ddH<sub>2</sub>O), 60  $\mu\text{L}$  TBTA Ligand (1.667 mM in 80 % tBuOH and 20 % DMSO)) were added. The final concentrations were 233  $\mu\text{M}$  Biotin-PEG<sub>3</sub>- $\text{N}_3$ , 581  $\mu\text{M}$  TCEP and 58.2  $\mu\text{M}$  TBTA Ligand. The lysates were mixed by vortexing and 20  $\mu\text{L}$  CuSO<sub>4</sub> solution (50 mM in ddH<sub>2</sub>O) were added to initiate the click reaction. The lysates were mixed by vortexing again and incubated for 1h at rt in the dark. After the click-reaction, the lysates were transferred to 15 mL falcon tubes and 8 mL of cold acetone (-80°C, MS grade) were added. Proteins were precipitated ON at -21°C. Then the proteins were pelletized (15 min, 4 °C, 21·10<sup>3</sup> x g) and the supernatant was discarded. The proteins were washed with pre-chilled methanol (2 x 400 mL, -80 °C, resuspension by sonication: 5-10 sec, 10 % max. intensity; 15 min, 4 °C, 21·10<sup>3</sup> x g). Subsequently, the pellet was dissolved in 1 mL 0.2 %

SDS in PBS by sonication and incubated under gentle mixing with 50  $\mu\text{L}$  of pre-washed (3 x 1 mL 0.4 % SDS) avidin-agarose beads (avidin-agarose from egg white, 1.1 mg/mL in aqueous glycerol suspension, Sigma-Aldrich Co. LLC) for 1 h at rt. The beads were washed with 0.2 % SDS in PBS (4 x 1 mL), 6 M urea (4 x 1 mL) and PBS (3 x 1 mL). The beads were suspended in 20 mM HEPES buffer (pH = 7.5) containing 7 M urea and 2 M thiourea. The proteins were reduced by addition of 1 mM DTT (45 min, rt) and then alkylated by 5.5 mM iodoacetamide (30 min, rt, in the dark). The reaction was quenched by addition of 4 mM DTT (30 min, rt). The proteins were first digested with Lys-C (0.5  $\mu\text{g}/\mu\text{L}$  in 50 mM HEPES in ddH<sub>2</sub>O, pH = 8, 1  $\mu\text{L}$ , 4 h in the dark, rt). The digest was then diluted with TEAB (50 mM in ddH<sub>2</sub>O, 600  $\mu\text{L}$ ) and trypsin (0.5  $\mu\text{g}/\mu\text{L}$  in 50 mM acetic acid in ddH<sub>2</sub>O, 1.5  $\mu\text{L}$ ) was added. After incubation for 16 h at 37 °C, the reaction was stopped by addition of formic acid (4  $\mu\text{L}$ ). The beads were pelletized (1 min, 0.1·10<sup>3</sup> x g) and the supernatant was transferred into LoBind tube (Eppendorf AG). The beads were once washed with 0.1 % FA (100  $\mu\text{L}$ , 1 min, 21·10<sup>3</sup> x g) and the supernatant was transferred into the LoBind tube. The samples were desalted using Sep-Pak C18 1 cc Vac Cartridges (Waters Corp.). The cartridges were first equilibrated with MeCN (1 x 1 mL), elution buffer (MeCN/H<sub>2</sub>O/FA = 80:19.5:0.5 v/v/v, 1 x 1 mL) and 0.1 % TFA (in ddH<sub>2</sub>O, 1 x 1 mL). Then the sample was applied and the proteins were washed with 0.1 % TFA (in ddH<sub>2</sub>O, 1 x 1 mL) and 0.5 % FA (in ddH<sub>2</sub>O, 1 x 0.5 mL). The proteins were eluted into a LoBind tube (MeCN/H<sub>2</sub>O/FA = 80:19.5:0.5 v/v/v, 2 x 250  $\mu\text{L}$ ) and concentrated *in vacuo* in a vacuum centrifuge (4 h, 1 mbar, RT). The remaining peptides were stored at -21°C.

### 5.2.2.2 Preparative gel based analysis

Cells were incubated for 1 h with varying concentrations of probe (stock solution in DMSO, 0.1 % end concentration of DMSO) and DMSO in a cell incubator at 37 °C. Subsequently, the cells were scraped off and pelletized for 3 min at 600 g. The pellets were washed with PBS once and then resuspended in 1 mL lysis buffer (1 % (v/v) NP40 and 1 % (w/v) sodium deoxycholate) and incubated at 0 °C for 15 min. Soluble and insoluble fractions were separated by centrifugation (30 min, 4 °C, 21·10<sup>3</sup> x g). As the target protein was mainly in the soluble fraction, the insoluble fraction was discarded. 3  $\mu\text{L}$  trifunctional linker (10 mM in DMSO) were added to 500  $\mu\text{L}$  labeled proteome, followed by 10  $\mu\text{L}$  TCEP solution (53 mM in ddH<sub>2</sub>O) and 30  $\mu\text{L}$  TBTA (83 mM in DMSO). The samples were gently vortexed and the cycloaddition was initiated by the addition of 10  $\mu\text{L}$  CuSO<sub>4</sub> solution (50 mM in ddH<sub>2</sub>O). The reaction was allowed to proceed for 1 h at RT. Procedures for enrichment were carried out together with a control lacking the probe to compare the results of the biotin-avidin enriched samples with the background of unspecific protein binding on avidin-agarose beads. The

proteins were precipitated by addition of cold acetone (6 mL, -80 °C) and incubation for 1 h at -21 °C. Then the proteins were pelletized (15 min, 4 °C,  $21 \cdot 10^3 \times g$ ) and the supernatant was discarded. The proteins were washed with pre-chilled methanol (2 x 400 mL, -80 °C, resuspension by sonication: 5-10 sec, 10 % max. intensity; 15 min, 4 °C,  $21 \cdot 10^3 \times g$ ). Subsequently, the pellet was dissolved in 1 mL 0.4 % SDS in PBS by sonication and incubated under gentle mixing with 50  $\mu$ L of prewashed (3 x 1 mL 0.4 % SDS in PBS) avidin-agarose beads (avidin-agarose from egg white, 1.1 mg/mL in aqueous glycerol suspension, Sigma-Aldrich Co. LLC) for 1 h at RT. The beads were washed with 0.4 % SDS in PBS (3 x 1 mL), aqueous urea (6 M, 2 x 1 mL) and PBS (3 x 1 mL). 50  $\mu$ L of 2x SDS loading buffer were added and the proteins were released for preparative SDS-PAGE by incubation for 6 min at 96 °C. The beads were pelletized (3 min,  $21 \cdot 10^3 \times g$ ), the supernatant was isolated and stored at -80 °C. The supernatant was applied on a preparative gel, and developed for 4-5 h (300 V). After gel electrophoresis, the bands were visualized using a Fujifilm Las-4000 luminescent image analyser. The observed bands were cut out with a scalpel, isolated and reduced to small pieces, prior to further processing.

The gel pieces corresponding to fluorescent bands were directly cut on the gel and washed with ddH<sub>2</sub>O (100  $\mu$ L, 15 min, 550 rpm, rt), MeCN/50 mM ammonium bicarbonate (200  $\mu$ L, 15 min, 550 rpm, RT) and MeCN (100  $\mu$ L, 10 min, 550 rpm, rt). The shrunken gel pieces were swollen in 50 mM ammonium bicarbonate (100  $\mu$ L, 5 min, 550 rpm, rt), before additional MeCN (100  $\mu$ L, 15 min, 550 rpm, rt) was added. The supernatant was removed and the gel pieces were again washed with MeCN (100  $\mu$ L, 10 min, 550 rpm, rt) and then dried under vacuum in a centrifugal evaporator (15 min, 1 mbar, rt). The proteins were reduced by addition of DTT solution (10 mM in 50 mM ammonium bicarbonate, 100  $\mu$ L, 45 min, 550 rpm, 56 °C) to the gel pieces. The pieces were then washed with MeCN (100  $\mu$ L, 10 min, 550 rpm, rt), prior to alkylation with iodacetamide solution (55 mM in 50 mM ammonium bicarbonate, 100  $\mu$ L, 30 min in the dark, 550 rpm, rt). The gel pieces were afterwards washed with MeCN/50 mM ammonium bicarbonate (100  $\mu$ L, 15 min, 550 rpm, rt) and MeCN (100  $\mu$ L, 10 min, 550 rpm, rt) and then dried *in vacuo* in a centrifugal evaporator (15 min, 1 mbar, RT). Digest solution (1% (v/v) trypsin stock solution in 25 mM ABC buffer) was added (100  $\mu$ L, 10 min, 4 °C then 37 °C, 300 rpm overnight). The next day, the supernatant was transferred into a LoBind tube (Eppendorf AG) and 25 mM ammonium bicarbonate (100  $\mu$ L, 15 min sonication, rt) was added to the gel pieces. Then MeCN (100  $\mu$ L) was added and the samples were sonicated for 15 min. The supernatant was then transferred into the same LoBind tube. 5 % FA (100  $\mu$ L, 15 min sonication, rt) was added to the gel pieces, followed by additional MeCN (100  $\mu$ L, 15 min sonication, RT). The supernatant was then transferred into the same LoBind tube and replaced by MeCN (100



$\mu\text{L}$ , 15 min sonication, RT). The supernatant was transferred into the LoBind tube and the solvent was removed *in vacuo* in a vacuum centrifuge (4 h, 1 mbar, RT). The remaining peptides were stored at  $-21^{\circ}\text{C}$ .

Prior to LC-MS/MS measurements, all peptide samples were dissolved in 1 % FA and filtered using centrifugal filters (modified Nylon,  $0.45\ \mu\text{m}$ , low protein binding, VWR International, LLC).

### 5.2.2.3 Gel based target identification

Nanoflow LC-MS/MS analysis was performed with an UltiMate 3000 Nano HPLC system (Thermo Scientific, Sunnyvale, USA) coupled to a LTQ Orbitrap XL (Thermo Scientific, Bremen, Germany). Peptides were loaded on a trap column (Acclaim C18 PepMap100  $75\ \mu\text{m}$  ID x 2 cm) and washed for 10 min with 0.1 % FA ( $5\ \mu\text{L}/\text{min}$  flow rate), then transferred to an analytical column (Acclaim C18 PepMap RSLC,  $75\ \mu\text{m}$  ID x 15 cm) and separated using a 60 min gradient from 4 % to 65 % (46 min from 4 % to 30 %, 11 min to 50 % and 3 min to 65 %) MeCN in 0.1 % FA at a flow rate of  $200\ \text{nL}/\text{min}$ . Peptides were ionized using a nanospray source at 2.1 kV and a capillary temperature of  $200^{\circ}\text{C}$ . Orbitrap XL was operated in data dependent top 5 mode. Full scan acquisition (scan range of 400 – 1400 m/z) was performed in the orbitrap at a resolution of 60000 (at m/z 200) and with an automatic gain control ion target value of  $1\text{e}6$ . Monoisotopic precursor selection as well as dynamic exclusion of 30 s were enabled. Internal calibration was performed using the ion signal of polycyclodimethylsiloxane as lock mass. The five most intense precursors with charge states of greater than 2+ and intensities greater than  $5\text{e}2$  were selected for fragmentation using collision-induced dissociation (CID). Isolation width was 2 m/z. Ions were collected to a target of  $1\text{e}5$  for a maximum injection time of 100 ms and detected in the ion trap at a normal scan rate.

Raw files were analyzed using MaxQuant<sup>241</sup> software (version 1.5.1.2) with Andromeda as search engine. The search included carbamidomethylation of cysteines as a fixed modification and oxidation of methionines and acetylation of protein N-termini as variable modifications. Trypsin was specified as the proteolytic enzyme with N-terminal cleavage to proline and two missed cleavages allowed. Precursor mass tolerance was set to 4.5 ppm (main search) and fragment mass tolerance to 0.5 Da. Searches were performed against the Uniprot database for Homo sapiens (taxon identifier: 9606, 24.11.2014). The second peptide identification option was enabled. False discovery rate determination was carried out using a decoy database and thresholds were set to 1 % both at peptide-spectrum match

and at protein levels. “I = L”, “requantification” and “match between runs” (0.7 min match and 20 min alignment time windows) options were enabled.

Analysis of the resulting *proteingroups.txt*-table was performed with Perseus 1.5.1.6.<sup>242</sup> A total of three biological replicates (groups), each consisting of four technical replicates, were used for protein identification. Putative contaminants, reverse hits and proteins, that were identified by site only, were removed. Ratios were calculated by dividing the intensity signal of the excised band by the intensity of corresponding gel area for the untreated sample. Rows were filtered to contain three valid values per group. Ratios were transformed using  $\log_2(x)$  and normalized using *z-score*. The average values of technical replicates were calculated and *p*-values were obtained using a two sided one sample *t*-test over three biological replicates.

#### 5.2.2.4 Gel free target identification

Nanoflow LC-MS/MS analysis was performed with an UltiMate 3000 Nano HPLC system (Thermo Scientific, Sunnyvale, USA) coupled to an Orbitrap Fusion (Thermo Scientific, San Jose, USA). Peptides were loaded on a trap column (Acclaim C18 PepMap100 75  $\mu$ m ID x 2 cm) and washed for 10 min with 0.1 % FA (10  $\mu$ L/min flow rate), then transferred to an analytical column (Acclaim C18 PepMap RSLC, 75  $\mu$ m ID x 15 cm) and separated using a 125 min gradient from 3 % to 40 % (120 min from 3 % to 25 % and 5 min to 40 %) MeCN in 0.1 % FA and 5 % DMSO at a flow rate of 200 nL/min. Peptides were ionized using a nanospray source at 1.9 kV and a capillary temperature of 275 °C. Orbitrap Fusion was operated in a top speed data dependent mode with a cycle time of 3 s. Full scan acquisition (scan range of 300 – 1700 *m/z*) was performed in the orbitrap at a resolution of 120000 (at *m/z* 200) and with an automatic gain control ion target value of 4e5. Monoisotopic precursor selection as well as dynamic exclusion of 60 s were enabled. Internal calibration was performed using the ion signal of fluoranthene cations (EASY-ETD/IC source). Most intense precursors with charge states of 2 – 7 and intensities greater than 5e3 were selected for fragmentation. Isolation was performed in the quadrupole using a window of 1.6 *m/z*. Ions were collected to a target of 1e2 for a maximum injection time of 250 ms with “inject ions for all available parallelizable time” enabled (“Universal” method, Eliuk *et al*, Thermo Scientific Poster Note PN40914). Fragments were generated using higher-energy collisional dissociation (HCD) and detected in the ion trap at a rapid scan rate.

Identification was carried out using MaxQuant software (version 1.5.1.2) as described in the previous section for gel-based target identification. Quantification of SILAC pairs was carried out based on unique peptides only using “Arg6” and “Lys4” as “medium” and “Arg10” and “Lys8” as “heavy” isotope identifiers requiring a minimum ratio count of 2.

Statistical analysis was performed with Perseus 1.5.1.6. Three biological replicates with SILAC label switch were used for statistics. The MaxQuant result table *proteingroups.txt* was used for further analysis. Putative contaminants, reverse hits and proteins, that were identified by site only, were removed. SILAC ratios were  $\log_2(x)$ -transformed, filtered to have three valid values per row (from three replicates in total), and *z-score*-normalized. The average values of technical replicates were calculated and  $-\log_{10}(p\text{-values})$  were obtained by a two-sided one sample *t*-test over three biological replicates.

#### 5.2.2.5 Binding peptide identification

To determine the binding mode of falcarinol (**2.1**) to ALDH2 and to identify respective binding sites, proteins were incubated with a 30-fold excess of inhibitors for 4 h at rt. Samples were subjected to intact-protein mass-spectrometry analysis with an LTQ-FTICR. For binding site localization, labeled and DMSO treated control proteins were digested o/n with chymotrypsin (*Promega Corp.*), which was added at a ratio of 1:100 (w/w) to the protein amount. Acidifying the sample with trifluoroacetic acid to a final concentration of 0.5 % stopped the digest. Peptides were subjected to LC-MS/MS analysis on an Orbitrap Fusion.

#### 5.2.2.6 Binding site identification

LC-MS analysis of intact proteins was performed on an LTQ-FT Ultra (Thermo Electron, Bremen, Germany) mass spectrometer coupled online to a Dionex Ultimate 3000 HPLC system (Thermo Fisher Scientific). Desalting was carried out with Massprep online desalting cartridges (Waters Corp.). Briefly, proteins were loaded in 1 % FA and eluted in a 5 min gradient from 6 to 95 % acetonitrile, 1 % FA. Proteins were ionized via electrospray and spectra were acquired in the fourier transform ion cyclotron resonance analyzer at a resolution of 200.000 (at *m/z* 400) in a mass range of 600 – 2000. Raw data was deconvoluted with the software ProMass (Thermo Fisher Scientific) using basic deconvolution default settings for a mass range from 54-58 kDa for ALDH2.

LC-MS/MS analysis of digested samples was performed using an Ultimate 3000 Nano HPLC system coupled to an Orbitrap Fusion, as previously described (see **5.2.2.4**), but accepting charge states from 1+ to 7+ for fragmentation.

Identification of falcarinol-modified peptides and localization of the site was performed using ProteomeDiscoverer 2.0 (Thermo Fisher Scientific Inc.) and SEQUEST as search engine. Oxidation of methionine and binding of falcarinol to cysteines (+244.1872 Da) were added as variable modifications. Chymotrypsin was specified as the proteolytic enzyme with one missed cleavage allowed. Mass tolerances of the precursor and fragment ions were set to 3 ppm and 0.5 Da, respectively. Peptide FDR was set to 1 %.

### 5.2.2.7 Recombinant expression of target protein

The major hit of MS analysis was recombinantly expressed in *E. coli* BL21. The gene encoding a truncated version of hALDH2 (the first 17 aa were left out) was cloned in the vector pET 300 by using the Invitrogen™ Gateway® Technology (Life Technologies Corp.). The target gene was amplified from the corresponding cDNA (GeneCopoeia, GC-0231-10) by PCR with a Phusion® HF DNA Polymerase. *attB1* forward primer and *attB2* reverse primer were designed to yield *attB*-PCR Products needed for Gateway® Technology.

Expression construct for hALDH2 (PDB-ID: P05091):

N-Start-His-~~attB1~~-Start-ALDH2-stop-~~attB2~~-C

Primers for recombinant expression:

Forward: 5'-ggggacaagttgtacaaaaaagcaggctttcagccgccgccacca-3'

Reverse: 5'-ggggaccactttgtacaagaaagctgggtgtatgagttcttctgaggcactttgac-3'

### 5.2.2.8 PCR

PCR was conducted using a CFX96™ Real-Time PCR System (Bio-Rad) with following solutions according to Phusion manufacturer's protocol: 10 µL 5 x Phusion GC/HF Buffer, 1 µL 10 mM dNTPs, 1.25 µL forward primer (10 pmol/µL), 1.25 reverse primer (10 pmol/µL), 1 ng plasmide (1 ng/µL), 1.5 µL DMSO, 0.5 µL Phusion DNA polymerase (NEB) and 33.5 µL ddH<sub>2</sub>O and following temperature protocol:

98 °C	0:30 min	} 35 x
98 °C	0:10 min	
T <sub>m</sub>	0:30	
72 °C	0:30 min per kb	
72 °C	5:00 min	
4 °C	hold	

### 5.2.2.9 Gateway cloning

PCR products were identified on agarose gels (1-%, SERVA) and gel bands were isolated and extracted with an E.Z.N.A.<sup>™</sup> MicroElute<sup>™</sup> Gel Extraction Kit (Omega Bio-Tek Inc.). Concentrations of DNA were measured using an Infinite<sup>®</sup> M200 Pro multiplate reader (Tecan Group Ltd.). 100 fmol of purified *attB*-PCR product and 50 fmol of *attP*-containing donor vector pDONR<sup>™</sup> 207 in TE buffer (10 mM Tris Base, 1 mM EDTA, pH 8.0) were used for *in vitro* BP recombination reaction with BP Clonase<sup>™</sup> II enzyme mix to yield the appropriate *attL*-containing entry clone. After transformation in chemically competent One Shot<sup>®</sup> TOP10 *E. coli* (Life Technologies Corp.), cells were plated on LB agar plates containing 7.5 µg/mL gentamycin. Clones of transformed cells were selected and grown in gentamycin (15 µg/mL) LB medium. Cells were harvested and plasmids were isolated using an E.Z.N.A.<sup>™</sup> Plasmid Mini Kit (Omega Bio-Tek Inc.). The corresponding *attB*-containing expression clone was generated by *in vitro* LR recombination reaction of approx. 50 fmol of the *attL*-containing entry clone and 50 fmol of the *attR*-containing destination vector pET300 using LR Clonase<sup>™</sup> II enzyme mix in TE buffer. The expression clone was transformed in chemically competent BL21 *E. coli* cells (Novagen<sup>®</sup>, Merck KGaA) and selected on LB agar plates containing 100 µg/mL ampicillin. Validity of the clones was confirmed by plasmid sequence analysis. Recombinant cells were grown in ampicillin LB medium and target gene expression was induced with IPTG (0.2 µg/mL, 1:2000). Overexpression was conducted at 22 °C for 16 - 20 h and the cells harvested (6000 x g, 20 min, 4 °C). The bacterial cell pellets were washed with PBS, resuspended in binding buffer (50 mM NaH<sub>2</sub>PO<sub>4</sub>, 300 mM NaCl, 1 mM DTT, pH 8.0), and lysed by a Constant Cell Disruption system. Protein purification was achieved on an Äkta Purifier 10 system (GE Healthcare). The affinity chromatography was carried out with a His Trap HP 5 mL column (GE Healthcare). The column was equilibrated in His-wash buffer (50 mM NaH<sub>2</sub>PO<sub>4</sub>, 300 mM NaCl, 1 mM DTT), the lysate was loaded and was washed with 10 column volumes (CV) His-wash buffer (+ 40 mM imidazole). Elution was carried out with a steep gradient into His-elution buffer (His-wash buffer + 250 mM imidazole). hALDH2 containing elution fractions were pooled, concentrated and purified with a HiLoad 16/60 Superdex 200 pg gelfiltration column (GE Healthcare) in storage buffer (20 mM Tris-HCl, 1 mM EDTA, 1 mM DTT, 10% (v/v) glycerol, pH 7.5).

### 5.2.2.10 ALDH2 *in vitro*-labeling

To validate a covalent binding of probe **2.2** to ALDH2, 2.15 µL truncated recombinant ALDH2 (1 µg/mL, Abnova) in 40.9 µL PBS or human proteome (1.16 mg/mL) was incubated with 1 µL DMSO stock of **2.2** at various concentrations for 1 h at rt. 5 µL ABPP Mix (1 µL 5-

TAMRA-N<sub>3</sub> (baseclick, BCFA-008-10; 5 mM in DMSO), 1  $\mu$ L fresh TCEP (50 mM in ddH<sub>2</sub>O), 3  $\mu$ L TBTA ligand (1.667 mM in 80 % tBuOH and 20 % DMSO) were added. Samples were gently vortexed and the cycloaddition was initiated by the addition of 1  $\mu$ L CuSO<sub>4</sub> (50 mM in ddH<sub>2</sub>O). The reaction was incubated for 1 h at rt. SDS-PAGE, subsequent fluorescent scans and staining was conducted as described before.

#### 5.2.2.11 ALDH2 activity assay

To quantify the binding of **2.1** to ALDH2, the kinetic parameters  $K_i$  and  $k_{inact}$  were determined by the method of Kitz and Wilson.<sup>122</sup> 2.60  $\mu$ L ALDH2 (23  $\mu$ M), 145.9  $\mu$ L 50 mM TRIS-HCl, pH = 8 and 1.50  $\mu$ L **FL1**-DMSO stock of different concentrations were incubated at 15 °C (**2.1**) and 25 °C (**2.5**) for time periods of 30 min to 5 h (final enzyme concentration: 400 nM). Subsequent, 50  $\mu$ L substrate mixture containing 50 mM Tris-HCl, 100 mM KCl, 5 mM  $\beta$ -mercaptoethanol, 1 mM  $\beta$ -NAD<sup>+</sup> and 10 mM propanal were added to initiate the enzymatic reaction. The product formation of NADH was monitored by measuring the absorption increase at  $\lambda = 340$  nm at 37 °C in 96-well-plates with an Infinite 200 PRO NanoQuant microplate reader. All measurements were carried out in technical triplicates and independent duplicates. To determine the kinetic parameters, the natural log of the remaining enzyme activity after a certain pre-incubation time was plotted against the pre-incubation time for several inhibitor concentrations [I]. The observed rate of inactivation  $k_{obs}$  was derived from the negative slopes of the linear fit. A further double reciprocal plot of  $k_{obs}$  against [I] lead to  $K_i$  and  $k_{inact}$  whereas the values were derived from the slope and the intercept of the linear fit.

### 5.2.3 Biochemical procedures for Chapter 3: A whole proteome inventory of background photocrosslinker binding

#### 5.2.3.1 Analytical in situ AfBPP labelling

For analytical labelling, cells were seeded in 6-well plates and grown to 90 % confluence. After suction of the medium and washing with PBS, 10  $\mu$ M of the respective compound in 1 mL PBS and a final DMSO concentration of 0.1 % were added. After incubation for 1 h at 37 °C and 5 % CO<sub>2</sub>, the cells were irradiated with the appropriate UV lamps with ice cooling for 30 min. Cells were detached with a cell scraper, washed with PBS and lysed in 100  $\mu$ L lysis buffer (1 % (v/v) NP40 and 1 % (w/v) sodium deoxycholate in PBS; 15 min, 0 °C). Following centrifugation (2  $\cdot$ 10<sup>4</sup> x g, 15 min, 4 °C) the soluble fraction (supernatant) and insoluble fraction (pellet) were separated and the pellet resuspended in 88  $\mu$ L PBS followed by homogenization by sonication. Both fractions were supplemented with 0.20 mM

rhodamine-azide (10 mM stock in DMSO; base click; Rh-N<sub>3</sub>), 1.0 mM TCEP (52 mM stock in ddH<sub>2</sub>O) and 0.10 mM TBTA ligand (1.667 mM stock). Samples were gently vortexed and the cycloaddition was initiated by the addition of 1.0 mM CuSO<sub>4</sub> (50 mM stock in ddH<sub>2</sub>O). After incubation at rt for 1 h, 100 µL 2 x SDS loading buffer were added and the samples heated for 10 min at 95 °C. For gel electrophoresis, 50 µL were applied per gel-lane on a SDS-PAGE gel (10 % acrylamide). Fluorescence was recorded using a Fujifilm LAS 4000 luminescent image analyser with a Fujinon VRF43LMD3 lens and a 575DF20 filter.

### 5.2.3.2 Preparative *in situ* labelling and quantification via SILAC

“Heavy” and “light” A549 and HeLa cells were plated on 15 cm dishes and grown to 90 % confluence. The cells were washed with PBS, and either “heavy” or “light” cells were treated with 3 µM compound and the other isotopic label with the corresponding amount of DMSO in 10 mL PBS for 1 h at 37 °C and 5 % CO<sub>2</sub>. Following irradiation with the appropriate UV lamps (Philips TL-D BLB UV lamps were used for irradiation of diazirine and benzophenone containing probes and Luzchem LZC-UVB lamps were used for irradiation of arylazide containing probe) with ice cooling for 30 min, cells were detached with a cell scraper, washed with PBS and lysed in 1 mL lysis buffer (1 % (v/v) NP40 and 1 % (w/v) sodium deoxycholate in PBS; 15 min, 4 °C). Protein concentrations of the lysed cells were measured using a BCA assay (Roti Quant, Roth) and equal protein amounts resulting from “heavy” or “light” cells incubated with the probe and the corresponding DMSO control of the opposite label were pooled and adjusted to a final volume of 1880 µL with PBS. The lysates, containing cytosolic and membrane proteins, were supplemented with 0.20 mM azide-PEG<sub>3</sub>-biotin conjugate (10 mM stock in DMSO; Jena Bioscience), 0.52 mM TCEP (52 mM stock in ddH<sub>2</sub>O) and 0.050 mM TBTA ligand (1.67 mM stock). Samples were gently vortexed and the cycloaddition was initiated by the addition of 0.50 mM CuSO<sub>4</sub> (50 mM stock in ddH<sub>2</sub>O). The reaction mixtures were incubated at rt for 1 h. Proteins were precipitated by the addition of a 4-fold volume excess of acetone (8 mL) and incubated o/n at – 20 °C. The samples were centrifuged at  $16 \cdot 10^3 \times g$  for 15 min. The supernatant was discarded and the pellet washed two times with 500 µL of pre-chilled methanol. Subsequently, the pellet was dissolved in 1 mL of PBS with 0.4 % SDS by sonication and incubated with 50 µL of avidin-agarose beads (Sigma-Aldrich) under gentle mixing at rt for 1 h. The beads were washed three times with 1 mL of PBS with 0.4 % SDS, twice with 1 mL of 6 M urea, and three times with 1 mL of PBS. The proteins were reduced, alkylated and tryptically digested on the beads: The beads were resuspended in 200 µL X-buffer (7 M urea, 2 M thiourea in 20 mM Hepes buffer pH 7.5), 1 mM DTT (1 M stock in ddH<sub>2</sub>O) was added, and incubated under gentle mixing at 25 °C for 45 min. For alkylation, 5.5 mM

iodoacetamide (550 mM stock in ddH<sub>2</sub>O) were added and incubated under gentle mixing at rt for 30 min. The alkylation was stopped by the addition of 4 mM DTT (1 M stock in ddH<sub>2</sub>O) and incubated under gentle mixing at rt for 30 min. For digestion, 0.0025 mg/mL LysC (0.5 mg/mL stock in ddH<sub>2</sub>O, Promega) was added and the mixture was incubated under gentle mixing at rt for 2 h. 600 µL of 50 mM TEAB buffer and 1.5 µL of trypsin (0.5 mg/mL, Promega) were added. The reaction was incubated o/n at 37 °C and stopped by the addition of FA (0.1 % final concentration). The resulting peptides were desalted and concentrated using Sep-Pak C18 1 cc Vac cartridges (Waters Corp.): The C18 material was pre-treated with 1 mL MeCN, 1 mL ddH<sub>2</sub>O/0.5 % TFA, 1 mL 80 % MeCN/0.5 % FA and 2 mL ddH<sub>2</sub>O/0.1 % TFA prior to sample loading. The beads were pelleted and the peptide solution loaded to the cartridges. Peptides bound to the cartridges were washed with 3 mL ddH<sub>2</sub>O/0.1 % TFA and 1 mL ddH<sub>2</sub>O/0.5 % FA and eluted with 750 µL 80 % MeCN/0.5 % FA. The peptides were dried and stored at -80 °C.

### 5.2.3.3 Mass spectrometry

Prior to LC-MS/MS measurements, all peptide samples were reconstituted in 30 µL ddH<sub>2</sub>O/1 % FA and filtered using centrifugal filters (modified Nylon, 0.45 µm, low protein binding, VWR International, LLC).

Nanoflow LC-MS/MS analysis was performed with an UltiMate 3000 Nano HPLC system (Thermo Scientific) coupled to an Orbitrap Fusion (Thermo Scientific). Peptides were loaded on a trap column (Acclaim C18 PepMap100 75 µm ID x 2 cm) and washed for 10 min with 0.1 % FA, then transferred to an analytical column (Acclaim C18 PepMap RSLC, 75 µm ID x 15 cm) and separated using a 125 min gradient from 3 % to 40 % (120 min from 3 % to 25 % and 5 min to 40 %) MeCN in 0.1 % FA and 5 % DMSO at a flow rate of 200 nL/min. Peptides were ionised using a nanospray source at 1.9 kV and a capillary temperature of 275 °C. Orbitrap Fusion was operated in a top speed data dependent mode with a cycle time of 3 s. Full scan acquisition (scan range of 300 – 1700 m/z) was performed in the orbitrap at a resolution of 120000 (at m/z 200) and with an automatic gain control ion target value of 4e5. Monoisotopic precursor selection as well as dynamic exclusion of 60 s were enabled. Internal calibration was performed using the ion signal of fluoranthene cations (EASY-ETD/IC source). Most intense precursors with charge states of 2 - 7 and intensities greater than 5e3 were selected for fragmentation. Isolation was performed in the quadrupole using a window of 1.6 m/z. Ions were collected to a target of 1e2 for a maximum injection time of 250 ms with “inject ions for all available parallelizable time” enabled (“Universal” method, Eliuk et al., Thermo Scientific Poster Note PN40914). Fragments were



generated using higher-energy collisional dissociation (HCD) and detected in the ion trap at a rapid scan rate.

#### 5.2.3.4 Bioinformatics

Raw files were analysed using MaxQuant software (version 1.5.1.2) with the Andromeda search engine. The search included carbamidomethylation of cysteines as a fixed modification and oxidation of methionines and acetylation of protein N-termini as variable modifications. Trypsin was specified as the proteolytic enzyme with N-terminal cleavage to proline and two missed cleavages allowed. Precursor mass tolerance was set to 4.5 ppm (main search) and fragment mass tolerance to 0.5 Da. Searches were performed against the Uniprot database for *Homo sapiens* (taxon identifier: 9606, 24<sup>th</sup> November 2014, including isoforms). The second peptide identification option was enabled. False discovery rate determination was carried out using a reversed decoy database and thresholds were set to 1 % FDR both at peptide-spectrum match and at protein levels. “I = L”, “requantification” and “match between runs” (0.7 min match and 20 min alignment time windows) options were enabled. Quantification of SILAC pairs was carried out based on unique peptides only using “Arg6” and “Lys4” as “light” and “Arg10” and “Lys8” as “heavy” isotope identifiers requiring a minimum ratio count of 2. For raw files resulting from label switched experiments, the isotope identifiers were defined in reverse order resulting in ratios probe vs. DMSO. The mass spectrometry proteomics data were deposited to the ProteomeXchange Consortium via the PRIDE partner repository with the dataset identifier PXD004009.<sup>243</sup>

Statistical analysis was performed with Perseus 1.5.1.6. Two biological replicates (forward SILAC + SILAC label switch) with three technical replicates each were used for statistics. The MaxQuant result table *proteinGroups.txt* was used for further analysis. Putative contaminants, reverse hits and only identified by site hits were removed. SILAC ratios were  $\log_2$ -transformed, hits with less than 3 valid values removed, the remaining ratios z-score normalised and  $-\log_{10}(p\text{-values})$  were obtained by a two-sided one sample Student's *t*-test over six replicates.

Diazirine overlays were generated from post-MaxQuant file merges. Protein groups with identical gene names within one file were excluded from analyses. The *proteinGroups.txt* files were then compared by majority protein ID. In detail, to target the protein inference problem, an overlap of at least one majority protein ID was sufficient to account for a merge of respective protein groups. The program codes for redundancy checking and the merge can be found at [www.oc2.ch.tum.de](http://www.oc2.ch.tum.de). Thus, for each combined protein group, a maximum of 24 quantification values (six replicates x four probes) could be obtained. Putative

contaminants, reverse sequences, only identified by site hits, and protein groups with two or less valid values, were filtered out. After  $\log_2$  transformation and z-score normalisation, the mean over all logarithmized ratios  $a$  with the respective sample size  $n$  were determined according to the principle of the geometric mean  $g$  (equation 1).

$$\log_2(g) = \log_2 \left( \sqrt[n]{\prod_{i=1}^n a_i} \right) = \frac{1}{n} \sum_{i=1}^n \log_2(a_i) \quad (1)$$

With this concept, photocrosslinker-specific targets were summed up over all samples, whereas scaffold-specific protein groups resided in the noise (cf. similar algorithms in image processing procedures). Additionally,  $p$ -values were gathered for each protein group from one-sample Student's  $t$ -tests against 0. The initial significance level of  $p = 0.05$  was adjusted by the multiple testing correction method of Benjamini and Hochberg (FDR = 0.05). Finally, the  $-\log_{10}$  of  $p$ -values were plotted against the  $\log_2$  of geometric mean  $g$ .

## 5.2.4 Biochemical procedures for Chapter 4: Target identification of neocarzilin A-C in human cancer cells

### 5.2.4.1 Click reaction and preparative gel-free analysis

SILAC-ABPP was conducted with 500 nM of probe **4.4**. For full procedure, see chapters **5.2.1.4**, **5.2.2.1**, **5.2.2.4**.

### 5.2.4.2 Preparative gel free analysis using label free quantification

Cells were incubated in dishes (TC dish 150 standard) for 1 h (100  $\mu$ M stock solution in DMSO, 0.1 % end concentration of DMSO, 100 nM end concentration of **4.4**) in a cell incubator at 37 °C, 5 % CO<sub>2</sub>. 6 dishes were treated with 10  $\mu$ L DMSO for 1 h and subsequently with 10  $\mu$ L probe **4.4** in PBS (100  $\mu$ M stock solution, 100 nM end concentration), 6 dishes with 10  $\mu$ L DMSO in PBS for 1 h and 10  $\mu$ L DMSO in PBS for one further 1 h, 6 dishes with 500 nM neocarzilin A (**4.1**, 500  $\mu$ M stock solution in DMSO) in PBS and subsequently with 100 nM probe **4.4** for 1 h. The cells were scraped off and pelletized for 3 min at 600 g. The pellets were washed with PBS once and then resuspended in lysis buffer (1 % (v/v) NP40 and 1 % (w/v) sodium deoxycholate, 1 mL) and incubated at 0 °C for 15 min. Soluble and insoluble fractions were separated by centrifugation (30 min, 4 °C, 21·10<sup>3</sup> x g). The soluble fraction was used for further processing. To determine the protein concentration in lysed samples, a BCA assay (Roti®-Quant Universal Reagent 1+2 (15:1)) was conducted. All samples were set to the same protein concentration. 60  $\mu$ L gel-free ABPP Mix (20  $\mu$ L Biotin-PEG<sub>3</sub>-N<sub>3</sub> (Jena Bioscience, CLK-AZ104P4-100; 10 mM in DMSO), 10  $\mu$ L fresh TCEP (50 mM in ddH<sub>2</sub>O), 30  $\mu$ L TBTA ligand (1.667 mM in 80 % tBuOH and 20 % DMSO)) were added. The lysates were mixed by vortexing and 20  $\mu$ L CuSO<sub>4</sub> solution (50 mM in ddH<sub>2</sub>O) were added. The lysates were mixed by vortexing again and incubated for 1h at rt in the dark. After the click-reaction, the lysates were transferred to 15 mL falcon tubes and 8 mL of cold acetone (-80°C, MS grade) were added. Proteins were precipitated ON at -21°C. Then the proteins were pelletized (15 min, 4 °C, 21·10<sup>3</sup> x g) and the supernatant was discarded. The proteins were washed with pre-chilled methanol (2 x 400 mL, -80 °C, resuspension by sonication: 5-10 sec, 10 % max. intensity; 15 min, 4 °C, 21·10<sup>3</sup> x g). Subsequently, the pellet was dissolved in 1 mL 0.2 % SDS in PBS by sonication and incubated under gentle mixing with 50  $\mu$ L of pre-washed (3 x 1 mL 0.2 % SDS) avidin-agarose beads (avidin-agarose from egg white, 1.1 mg/mL in aqueous glycerol suspension, Sigma-Aldrich Co. LLC) for 1 h at rt. The beads were washed with 0.2 % SDS in PBS (4 x 1 mL), 6 M urea (4 x 1 mL) and PBS (3 x 1 mL). The beads were suspended in 20 mM

HEPES buffer (pH = 7.5) containing 7 M urea and 2 M thiourea. The proteins were reduced by addition of 1 mM DTT (45 min, rt) and then alkylated by 5.5 mM iodoacetamide (30 min, rt, in the dark). The reaction was quenched by addition of 4 mM DTT (30 min, rt). The proteins were first digested with Lys-C (0.5  $\mu\text{g}/\mu\text{L}$  in 50 mM HEPES in ddH<sub>2</sub>O, pH = 8, 1  $\mu\text{L}$ , 4 h in the dark, rt). The digest was then diluted with TEAB (50 mM in ddH<sub>2</sub>O, 600  $\mu\text{L}$ ) and trypsin (0.5  $\mu\text{g}/\mu\text{L}$  in 50 mM acetic acid in ddH<sub>2</sub>O, 1.5  $\mu\text{L}$ ) was added. After incubation for 16 h at 37 °C, the reaction was stopped by addition of formic acid (4  $\mu\text{L}$ ). The beads were pelletized (1 min,  $0.1 \cdot 10^3 \times g$ ) and the supernatant was transferred into LoBind tube (Eppendorf AG). The beads were washed once with 0.1 % FA (100  $\mu\text{L}$ , 1 min,  $21 \cdot 10^3 \times g$ ) and the supernatant was transferred into the LoBind tube. The samples were desalted using Sep-Pak C18 1 cc Vac Cartridges (Waters Corp.). The cartridges were first equilibrated with MeCN (1 x 1 mL), elution buffer (MeCN/H<sub>2</sub>O/FA = 80:19.5:0.5 v/v/v, 1 x 1 mL) and 0.1 % TFA (in ddH<sub>2</sub>O, 1 x 1 mL). Then the sample was applied and the proteins were washed with 0.1 % TFA (in ddH<sub>2</sub>O, 1 x 1 mL) and 0.5 % FA (in ddH<sub>2</sub>O, 1 x 0.5 mL). The proteins were eluted into a LoBind tube (MeCN/H<sub>2</sub>O/FA = 80:19.5:0.5 v/v/v, 2 x 250  $\mu\text{L}$ ) and concentrated *in vacuo* in a vacuum centrifuge (4 h, 1 mbar, RT). The remaining peptides were stored at -80°C.

#### 5.2.4.3 Mass spectrometry

Prior to MS measurement, the samples were dissolved in 30  $\mu\text{L}$  1 % FA by pipetting up and down, vortexing and sonication for 15 min (brief centrifugation after each step). 0.45  $\mu\text{m}$  centrifugal filter units (VWR) were equilibrated with two times 500  $\mu\text{L}$  water, 500  $\mu\text{L}$  0.05 N NaOH and two times 500  $\mu\text{L}$  1 % FA (centrifugation:  $16.2 \cdot 10^3 \times g$ , 1 min, RT). Reconstituted and mixed peptide samples were filtered through the equilibrated filters (centrifugation:  $16.2 \cdot 10^3 \times g$ , 2 min, RT). Samples were analyzed via HPLC-MS/MS using an UltiMate 3000 nano HPLC system (Dionex, Sunnyvale, California, USA) equipped with Acclaim C18 PepMap100 75  $\mu\text{m}$  ID x 2 cm trap and Acclaim C18 PepMap RSLC, 75  $\mu\text{m}$  ID x 15 cm separation columns coupled to an Orbitrap Fusion mass spectrometer (Thermo Fisher Scientific Inc., Waltham, Massachusetts, USA). Samples were loaded on the trap and washed for 10 min with 0.1 % formic acid, then transferred to the analytical column and separated using a 120 min gradient from 3 % to 25 % acetonitrile in 0.1 % FA and 5 % DMSO (at 200  $\text{nL}/\text{min}$  flow rate). Orbitrap Fusion was operated in a 3 second top speed data dependent mode. Full scan acquisition was performed in the orbitrap at a resolution of 120000 (at  $m/z$  200) and an ion target of  $4e5$  in a scan range of 300 – 1700  $m/z$ . Monoisotopic precursor selection as well as dynamic exclusion for 60 s were enabled. Precursors with charge states of 2 – 7 and intensities greater than  $5e3$  were selected for

fragmentation. Isolation was performed in the quadrupole using a window of 1.6 m/z. Precursors were collected to a target of 1e2 for a maximum injection time of 250 with “inject ions for all available parallelizable time” enabled. Fragments were generated using higher-energy collisional dissociation (HCD) and detected in the ion trap at a rapid scan rate. Internal calibration was performed using the ion signal of fluoranthene cations (EASY-ETD/IC source).

Peptide and protein identifications were performed using MaxQuant 1.5.3.8 software with Andromeda as search engine using following parameters: Carbamidomethylation of cysteines as fixed and oxidation of methionine as well as acetylation of N-termini as dynamic modifications. Trypsin was specified as the proteolytic enzyme with N-terminal cleavage to proline and two missed cleavages allowed, 4.5 ppm for precursor mass tolerance (main search ppm) and 0.5 Da for fragment mass tolerance (ITMS MS/MS tolerance). Searches were done against the *Homo sapiens* Uniprot database (taxon identifier: 9606, downloaded on 19.12.2014). Quantification was performed using LFQ (Label free quantification). Variable modifications were included for quantification. The requantify option was used as well as a minimum ratio count of 1 and “Match between runs” was enabled with default values. Identification was done with at least two unique peptides and quantification only with unique peptides.

Statistical analysis was performed with Perseus 1.5.1.6. A total of three biological replicates (groups), each consisting of six technical replicates, were used for protein identification. The MaxQuant result table *proteinGroups.txt* was used for further analysis. LFQ intensities were selected as main columns. Putative contaminants, reverse hits and only identified by site hits were removed. Main columns were *log2*-transformed, and missing values imputation (initial width of 0.3, down-shift of 1.8) was conducted for the total matrix. The average values of technical replicates were calculated and *p*-values were obtained using a two-sided two-sample *t*-test over two biological replicates. The valid value filter was disabled and “false discovery rate” control enabled using “Benjamin-Hochberg FDR” as multiple testing correction (FDR: 1 %).

#### **5.2.4.4 Recombinant expression of target protein**

The major hit of MS analysis was recombinantly expressed in Lemo21 (DE3) competent *E. coli* (New England Biolabs). The gene encoding hVAT-1 was cloned in the vector pET 300 by using the Invitrogen™ Gateway® Technology (Life Technologies Corp.). The target gene was amplified from the corresponding cDNA (GeneCopoeia, GC-T3028) by PCR with a Phusion® HF DNA Polymerase. *attB1* forward primer and *attB2* reverse primer were

designed to yield *attB*-PCR products needed for Gateway® Technology.

Expression construct for hVAT1 (PDB-ID: Q99536):

N-Start-His-attB1-TEV-~~Start~~-VAT1-Stop-attB2-C

Primers for recombinant expression:

for\_attB1\_VAT1:

5'-ggggacaagttgtacaaaaagcaggcttgagaatctttatcttcagggtccgacgagagagagtagc-3'

rev\_attB1\_VAT1:

5'-ggggaccactttgtacaagaaagctgggtgctagttctccttctctgcccc-3'

#### 5.2.4.5 PCR

The PCR was conducted using a CFX96™ Real-Time PCR System (Bio-Rad) with following solutions according to Phusion manufacturer's protocol: 10 µL 5 x Phusion GC/ HF Buffer, 1 µL 10 mM dNTPs, 1.25 µL forward primer (10 pmol/µL), 1.25 reverse primer (10 pmol/µL), 5 ng plasmide (1 ng/µL), 1.5 µL DMSO, 0.5 µL Phusion DNA polymerase (NEB) and 29.5 µL ddH<sub>2</sub>O and following temperature protocol:

98 °C	0:30 min	}	35 x
98 °C	0:10 min		
T <sub>m</sub>	0:30		
72 °C	0:30 min per kb		
72 °C	5:00 min		
4 °C	hold		

#### 5.2.4.6 Gateway cloning

PCR products were identified on agarose gels and gel bands were isolated and extracted with an E.Z.N.A.™ MicroElute™ Gel Extraction Kit (Omega Bio-Tek Inc.). Concentrations of DNA were measured using an Infinite® M200 Pro multiplate reader (Tecan Group Ltd.). 100 fmol of purified *attB*-PCR product and 50 fmol of *attP*-containing donor vector

pDONR™ 207 in TE buffer (10 mM Tris Base, 1 mM EDTA, pH 8.0) were used for *in vitro* BP recombination reaction with BP Clonase™ II enzyme mix to yield the appropriate *attL*-containing entry clone. After transformation in chemically competent One Shot® TOP10 *E. coli* (Life Technologies Corp.), cells were plated on LB agar plates containing 7.5 µg/mL gentamycin. Clones of transformed cells were selected and grown in gentamycin (15 µg/mL) LB medium. Cells were harvested and plasmids were isolated using an E.Z.N.A.™ Plasmid Mini Kit (Omega Bio-Tek Inc.). The corresponding *attB*-containing expression clone was generated by *in vitro* LR recombination reaction of approx. 50 fmol of the *attL*-containing entry clone and 50 fmol of the *attR*-containing destination vector pET300 using LR Clonase™ II enzyme mix in TE buffer. The expression clone was transformed in chemically competent *E. coli* Lemo21 (DE3) (New England Biolabs) and selected on LB agar plates containing 100 µg/mL ampicillin. Validity of the clones was confirmed by plasmid sequence analysis by GATC Biotech AG.

#### **5.2.4.7 Recombinant expression and analytical labeling in *E. coli***

Recombinant cells were grown in ampicillin (100 µg/mL) LB medium and target gene expression was induced with IPTG (0.06 µg/mL, 1:6000). Overexpression was conducted at 22 °C for 3 h and cells were harvested ( $6 \cdot 10^3 \times g$ , 20 min, 4 °C). The cells were resuspended in PBS to a theoretical OD<sub>600</sub> of 40. 2 µL probe **4.4** (500 µM in DMSO) were added to 200 µL of cell suspension. The cells were incubated for 1 h at rt. A DMSO control containing no probe and a control with no induction of VAT-1 overexpression was additionally added to each experiment. After centrifugation (10 min, 4 °C,  $6 \cdot 10^3$  rpm), the bacterial cells were washed with 800 µL PBS and lysed by sonication (3 x 20 sec, 85% max. intensity, on ice). Membrane and cytosol fraction were separated by centrifugation (30 min,  $13 \cdot 10^3$  rpm, 4 °C) and the membrane fraction was additionally washed with 800 µL PBS. Membrane fraction was resuspended in 100 µL PBS. The click reaction was carried out with 44 µL of proteome, so that after addition of all reagents a total volume of 50 µl was reached. Therefore, 5 µL ABPP Mix (1 µL 5-TAMRA-N<sub>3</sub> (baseclick, BCFA-008-10; 5 mM in DMSO), 1 µL fresh TCEP (50 mM in ddH<sub>2</sub>O), 3 µL TBTA ligand (1.667 mM in 80 % tBuOH and 20 % DMSO)) were added to the cells. After gently vortexing the samples, the cycloaddition reaction was initiated by adding 1 µL CuSO<sub>4</sub> (50 mM in ddH<sub>2</sub>O). The reaction was incubated in the dark for 1 h at room temperature and stopped by adding 50 µL 2 x SDS loading buffer. After vortexing the samples, 50 µL were applied on an analytical SDS gel, which was developed for 4-5 h (300 V). Fluorescence scans of SDS gels were performed with a Fujifilm Las-4000 luminescent image analyser with a Fujinon VRF43LMD3 lens and a 575DF20 filter. For determination of relative protein amount gels were stained with Coomassie stain solution

(0.25 % (w/v) Coomassie Brilliant Blue R250, 9.20 % (v/v) AcOH, 45.4 % (v/v) EtOH in ddH<sub>2</sub>O).

#### 5.2.4.8 Co-Immunoprecipitation<sup>217</sup>

HepG2 were grown in dishes (TC dish 150 standard) to 80-90 % confluence, the medium was removed and the cells were washed twice with cold PBS. 1 mL lysis buffer (50 mM Tris/HCl, 150 mM NaCl, 1 % NP-40, 5 % glycerol, 1 mM MgCl<sub>2</sub>, pH = 7.4) was added and cells were scraped off the dish. Cell lysis was done for 30 minutes at 4°C while rotating. Afterwards, cell debris was pelleted at  $16.1 \cdot 10^3 \times g$  for 20 min.

Meanwhile, 30  $\mu$ L beads (Pierce® Protein-A/G coupled agarose, Thermo Scientific) were equilibrated in wash buffer (50 mM Tris/HCl, 150 mM NaCl, 0.05 % NP-40, 5% glycerol, pH = 7.4): 1 mL buffer was added to 30  $\mu$ L bead slurry, vortexed, spun down on table-top mini-centrifuge, and the supernatant was discarded. 500  $\mu$ L cell lysate were added to the beads and 5  $\mu$ L antibody (antiVAt1, antikörperonline.de) or the respective isotype control (Rabbit (DA1E) mAB (IgGXP isotype control, 2.5 <sup>mg/mL</sup>), Cell Signaling). The mixture was incubated at 4°C for 3 h while rotating. Afterwards, the samples were spun down and supernatant was discarded. 1 mL wash buffer (50 mM Tris/HCl, 150 mM NaCl, 5% glycerol, 0.05% NP-40, pH = 7.4) was added, samples were centrifuged at 500 x g for 30 s and the supernatant was discarded. The pellet was resuspended in 1 mL wash buffer, mixed, and transferred to a fresh tube. Washing was repeated twice using basic buffer (50 mM Tris/HCl, 150 mM NaCl, 5% glycerol, pH = 7.4) to dispose of the detergent. Beads with precipitate were kept in 30  $\mu$ L PBS at -80°C for analysis by MS. 25  $\mu$ L elution buffer I (5 ng/ $\mu$ L trypsin, 2 M urea, 50 mM Tris-HCl pH 7.5, 1 mM DTT) were added and the mixture incubated at rt for 30 min. Then, 100  $\mu$ L elution buffer II (2 M urea, 50 mM Tris-HCl pH 7.5, 5 mM IAA) were added and the beads incubated o/n at rt with shaking. The digest was terminated by acidification of the peptide solution with 20  $\mu$ L 0.5% TFA. The beads were collected by centrifugation ( $18 \cdot 10^3 \times g$ , 3 min). Double C18 StageTips were washed with 70 mL MeOH and 3 x 70  $\mu$ L 0.5 % freshly prepared FA (centrifugation at  $1 \cdot 10^3 \times g$ ). 200  $\mu$ L of supernatant were loaded on the StageTips, the flow-through collected and the peptides desalted with 3 x 70  $\mu$ L 0.5 % FA. The peptides were eluted with 2 x 30  $\mu$ L 80 % MeCN + 0.5 % FA. The solvent was evaporated in a speedvac and the peptides stored at -80 °C. For MS analysis, they were reconstituted in 40  $\mu$ L 1 % FA by vortexing and ultrasonication for 15 min. Centrifugal filters (VWR Centrifugal Filter, Modified PES 3K, 500  $\mu$ L) were equilibrated with 2 x 500  $\mu$ L H<sub>2</sub>O, 2 x 500  $\mu$ L 50 mM NaOH, 2 x 500  $\mu$ L 1 % FA and 1 x 300  $\mu$ L 1 % FA ( $18 \cdot 10^3 \times g$ , 1 min). The peptide solutions were loaded on the filters and spun down into new LoBind tubes. The



filtrate was transferred to MS vials (PP screw top vial, Thermo Scientific) and 5  $\mu\text{L}$  were injected for MS analysis.

## 6 Bibliography

1. Li, N., Overkleeft, H. S. & Florea, B. I. Activity-based protein profiling: An enabling technology in chemical biology research. *Curr. Opin. Chem. Biol.* **16**, 227–233 (2012).
2. Cravatt, B. F., Wright, A. T. & Kozarich, J. W. Activity-based protein profiling: from enzyme chemistry to proteomic chemistry. *Annu. Rev. Biochem.* **77**, 383–414 (2008).
3. Sieber, S. A. & Cravatt, B. F. Analytical platforms for activity-based protein profiling—exploiting the versatility of chemistry for functional proteomics. *Chem. Commun. (Camb)*. 2311–2319 (2006).
4. Kam, C. M., Abuelyaman, A. S., Li, Z., Hudig, D. & Powers, J. C. Biotinylated isocoumarins, new inhibitors and reagents for detection, localization, and isolation of serine proteases. *Bioconjug. Chem.* **4**, 560–567 (1993).
5. Abuelyaman, a S., Hudig, D., Woodard, S. L. & Powers, J. C. Fluorescent derivatives of diphenyl [1-(N-peptidylamino)alkyl]phosphonate esters: synthesis and use in the inhibition and cellular localization of serine proteases. *Bioconjug. Chem.* **5**, 400–405 (1994).
6. Liu, Y., Patricelli, M. P. & Cravatt, B. F. Activity-based protein profiling: the serine hydrolases. *Proc. Natl. Acad. Sci. U. S. A.* **96**, 14694–14699 (1999).
7. Speers, A. E. & Cravatt, B. F. Profiling enzyme activities in vivo using click chemistry methods. *Chem. Biol.* **11**, 535–546 (2004).
8. Speers, A. E., Adam, G. C. & Cravatt, B. F. Activity-based protein profiling in vivo using a copper(I)-catalyzed azide-alkyne [3 + 2] cycloaddition. *J. Am. Chem. Soc.* **125**, 4686–4687 (2003).
9. Speers, A. E. & Cravatt, B. F. Chemical Strategies for Activity-Based Proteomics. *ChemBioChem* **5**, 41–47 (2004).
10. Sadaghiani, A. M., Verhelst, S. H. & Bogoy, M. Tagging and detection strategies for activity-based proteomics. *Curr. Opin. Chem. Biol.* **11**, 20–28 (2007).
11. Greenbaum, D., Medzihradszky, K. F., Burlingame, A. & Bogoy, M. Epoxide electrophiles as activity-dependent cysteine protease profiling and discovery tools. *Chem. Biol.* **7**, 569–581 (2000).

12. Wirth, T., Schmuck, K., Tietze, L. F. & Sieber, S. A. Duocarmycin analogues target aldehyde dehydrogenase 1 in lung cancer cells. *Angew. Chemie - Int. Ed.* **51**, 2874–2877 (2012).
13. Kolb, H. C. & Sharpless, K. B. The growing impact of click chemistry on drug discovery. *Drug Discov. Today* **8**, 1128–1137 (2003).
14. Meldal, M. & Tornøe, C. W. Cu-Catalyzed Azide–Alkyne Cycloaddition. *Chem. Rev.* **108**, 2952–3015 (2008).
15. Rostovtsev, V. V., Green, L. G., Fokin, V. V. & Sharpless, K. B. A stepwise Huisgen cycloaddition process: Copper(I)-catalyzed regioselective ‘ligation’ of azides and terminal alkynes. *Angew. Chemie - Int. Ed.* **41**, 2596–2599 (2002).
16. Evans, M. J. & Cravatt, B. F. Mechanism-based profiling of enzyme families. *Chem. Rev.* **106**, 3279–3301 (2006).
17. Böttcher, T. & Sieber, S. A.  $\beta$ -lactones as privileged structures for the active-site labeling of versatile bacterial enzyme classes. *Angew. Chemie - Int. Ed.* **47**, 4600–4603 (2008).
18. Weerapana, E. *et al.* Quantitative reactivity profiling predicts functional cysteines in proteomes. *Nature* **468**, 790–795 (2010).
19. Ong, S. E. *et al.* Stable isotope labeling by amino acids in cell culture, SILAC, as a simple and accurate approach to expression proteomics. *Mol. Cell. Proteomics* **1**, 376–386 (2002).
20. Chua, S. L. *et al.* Selective labelling and eradication of antibiotic-tolerant bacterial populations in *Pseudomonas aeruginosa* biofilms. *Nat. Commun.* **7**, 10750 (2016).
21. Wong, J. W. H. & Cagney, G. An overview of label-free quantitation methods in proteomics by mass spectrometry. *Methods Mol. Biol.* **604**, 273–283 (2010).
22. Cox, J. *et al.* Accurate proteome-wide label-free quantification by delayed normalization and maximal peptide ratio extraction, termed MaxLFQ. *Mol. Cell. Proteomics* **13**, 2513–2526 (2014).
23. Asara, J. M., Christofk, H. R., Freemark, L. M. & Cantley, L. C. A label-free quantification method by MS/MS TIC compared to SILAC and spectral counting in a proteomics screen. *Proteomics* **8**, 994–999 (2008).
24. Griffin, N. M. *et al.* Label-free, normalized quantification of complex mass

- spectrometry data for proteomic analysis. *Nat. Biotechnol.* **28**, 83–89 (2010).
25. Gersch, M., Kreuzer, J. & Sieber, S. A. Electrophilic natural products and their biological targets. *Nat. Prod. Rep.* **29**, 659–682 (2012).
  26. Groll, M., McArthur, K. A., Macherla, V. R., Manam, R. R. & Potts, B. C. Snapshots of the fluorosalinosporamide/20S complex offer mechanistic insights for fine tuning proteasome inhibition. *J. Med. Chem.* **52**, 5420–5428 (2009).
  27. Zeiler, E. *et al.* Vibralactone as a tool to study the activity and structure of the ClpP1P2 complex from *listeria monocytogenes*. *Angew. Chemie - Int. Ed.* **50**, 11001–11004 (2011).
  28. Bottcher, T. & Sieber, S. A. Beta-Lactams and beta-lactones as activity-based probes in chemical biology. *Medchemcomm* **3**, 408–417 (2012).
  29. Fernandes, R., Amador, P. & Prudêncio, C.  $\beta$ -Lactams: chemical structure, mode of action and mechanisms of resistance. *Rev. Med. Microbiol.* **24**, 7–17 (2012).
  30. Staub, I. & Sieber, S. A.  $\beta$ -Lactam probes as selective chemical-proteomic tools for the identification and functional characterization of resistance associated enzymes in MRSA. *J. Am. Chem. Soc.* **131**, 6271–6276 (2009).
  31. Staub, I. & Sieber, S. A. Beta-lactams as selective chemical probes for the in vivo labeling of bacterial enzymes involved in cell wall biosynthesis, antibiotic resistance, and virulence. *J. Am. Chem. Soc.* **130**, 13400–13409 (2008).
  32. Zuhl, A. M. *et al.* Competitive activity-based protein profiling identifies Aza- $\beta$ -lactams as a versatile chemotype for serine hydrolase inhibition. *J. Am. Chem. Soc.* **134**, 5068–5071 (2012).
  33. Drahl, C., Cravatt, B. F. & Sorensen, E. J. Protein-reactive natural products. *Angew. Chemie - Int. Ed.* **44**, 5788–5809 (2005).
  34. D'Souza, V. M., Brown, R. S., Bennett, B. & Holz, R. C. Characterization of the active site and insight into the binding mode of the anti-angiogenesis agent fumagillin to the manganese(II)-loaded methionyl aminopeptidase from *Escherichia coli*. *J. Biol. Inorg. Chem.* **10**, 41–50 (2005).
  35. He, Q. L. *et al.* Covalent modification of a cysteine residue in the XPB subunit of the general transcription factor TFIIH through single epoxide cleavage of the transcription inhibitor triptolide. *Angew. Chemie - Int. Ed.* **54**, 1859–1863 (2015).

36. Marquardt, J. L. *et al.* Kinetics, stoichiometry, and identification of the reactive thiolate in the inactivation of UDP-GlcNAc enolpyruvyl transferase by the antibiotic fosfomicin. *Biochemistry* **33**, 10646–10651 (1994).
37. McCallum, C. *et al.* Triptolide binds covalently to a 90 kDa nuclear protein. Role of epoxides in binding and activity. *Immunobiology* **212**, 549–556 (2007).
38. Meng, L. *et al.* Epoxomicin, a potent and selective proteasome inhibitor, exhibits in vivo antiinflammatory activity. *Proc. Natl. Acad. Sci. U. S. A.* **96**, 10403–10408 (1999).
39. Pitscheider, M., Mäusbacher, N. & Sieber, S. A. Antibiotic activity and target discovery of three-membered natural product-derived heterocycles in pathogenic bacteria. *Chem. Sci.* **3**, 2035–2041 (2012).
40. Sin, N. *et al.* The anti-angiogenic agent fumagillin covalently binds and inhibits the methionine aminopeptidase, MetAP-2. *Proc. Natl. Acad. Sci. U. S. A.* **94**, 6099–6103 (1997).
41. Czyzewska, M. M. *et al.* Dietary acetylenic oxylipin falcarinol differentially modulates GABAA receptors. *J. Nat. Prod.* **77**, 2671–2677 (2014).
42. Nodwell, M. B., Menz, H., Kirsch, S. F. & Sieber, S. A. Rugulactone and its Analogues Exert Antibacterial Effects through Multiple Mechanisms Including Inhibition of Thiamine Biosynthesis. *ChemBioChem* **13**, 1439–1446 (2012).
43. Battenberg, O. a, Yang, Y., Verhelst, S. H. L. & Sieber, S. a. Target profiling of 4-hydroxyderricin in *S. aureus* reveals seryl-tRNA synthetase binding and inhibition by covalent modification. *Mol. Biosyst.* **9**, 343–351 (2013).
44. Buey, R. M. *et al.* Cyclostreptin binds covalently to microtubule pores and luminal taxoid binding sites. *Nat. Chem. Biol.* **3**, 117–125 (2007).
45. Astelbauer, F. *et al.* High antitrypanosomal activity of plant-derived sulphur-containing amides. *Int. J. Antimicrob. Agents* **36**, 570–572 (2010).
46. Böttcher, T. & Sieber, S. A. Showdomycin as a versatile chemical tool for the detection of pathogenesis-associated enzymes in bacteria. *J. Am. Chem. Soc.* **132**, 6964–6972 (2010).
47. Wulff, J. E., Siegrist, R. & Myers, A. G. The natural product avrainvillamide binds to the oncoprotein nucleophosmin. *J. Am. Chem. Soc.* **129**, 14444–14451 (2007).

- 
48. Krahn, D., Ottmann, C. & Kaiser, M. The chemistry and biology of syringolins, glidobactins and cepafungins (syrbactins). *Nat. Prod. Rep.* **28**, 1854 (2011).
  49. Pitscheider, M. & Sieber, S. a. Cinnamic aldehyde derived probes for the active site labelling of pathogenesis associated enzymes. *Chem. Commun. (Camb)*. 3741–3743 (2009).
  50. Gallwitz, H. *et al.* Ajoene is an inhibitor and subversive substrate of human glutathione reductase and Trypanosoma cruzi trypanothione reductase: Crystallographic, kinetic, and spectroscopic studies. *J. Med. Chem.* **42**, 364–372 (1999).
  51. Ferri, N. *et al.* Ajoene, a garlic compound, inhibits protein prenylation and arterial smooth muscle cell proliferation. *Brit. J. Pharmacol.* **138**, 811–818 (2003).
  52. Kreuzer, J., Bach, N. C., Forler, D. & Sieber, S. A. Target discovery of acivicin in cancer cells elucidates its mechanism of growth inhibition. *Chem. Sci.* **6**, 237–245 (2014).
  53. Williams, K., Cullati, S., Sand, A., Biterova, E. I. & Barycki, J. J. Crystal structure of acivicin-inhibited  $\gamma$ -glutamyltranspeptidase reveals critical roles for its C-Terminus in autoprocesing and catalysis. *Biochemistry* **48**, 2459–2467 (2009).
  54. Bartolucci, C., Perola, E., Cellai, L., Brufani, M. & Lamba, D. ‘Back door’ opening implied by the crystal structure of a carbamoylated acetylcholinesterase. *Biochemistry* **38**, 5714–5719 (1999).
  55. O’Neill, P. M., Barton, V. E. & Ward, S. A. The Molecular Mechanism of Action of Artemisinin—The Debate Continues. *Molecules* **15**, 1705–1721 (2010).
  56. Wang, J. *et al.* Haem-activated promiscuous targeting of artemisinin in Plasmodium falciparum. *Nat. Commun.* **6**, 10111 (2015).
  57. Zhou, W. *et al.* Novel mutant-selective EGFR kinase inhibitors against EGFR T790M. *Nature* **462**, 1070–1074 (2009).
  58. Cohen, M. S., Zhang, C., Shokat, K. M. & Taunton, J. Structural bioinformatics-based design of selective, irreversible kinase inhibitors. *Science* **308**, 1318–1321 (2005).
  59. Singh, J. *et al.* Structure-based design of a potent, selective, and irreversible inhibitor of the catalytic domain of the erbB receptor subfamily of protein tyrosine

- kinases. *J. Med. Chem.* **40**, 1130–1135 (1997).
60. Lanning, B. R. *et al.* A road map to evaluate the proteome-wide selectivity of covalent kinase inhibitors. *Nat. Chem. Biol.* **10**, 1–10 (2014).
61. Singh, J., Petter, R. C. & Kluge, A. F. Targeted covalent drugs of the kinase family. *Curr. Opin. Chem. Biol.* **14**, 475–480 (2010).
62. Liu, Q. *et al.* Developing irreversible inhibitors of the protein kinase cysteinome. *Chem. Biol.* **20**, 146–159 (2013).
63. Noe, M. C. & Gilbert, A. M. Targeted Covalent Enzyme Inhibitors. *Annu. Rep. Med. Chem.* **47**, 413–439 (2012).
64. Smith, A. J. T., Zhang, X., Leach, A. G. & Houk, K. N. Beyond picomolar affinities: quantitative aspects of noncovalent and covalent binding of drugs to proteins. *J. Med. Chem.* **52**, 225–233 (2009).
65. Liebler, D. C. & Guengerich, F. P. Elucidating mechanisms of drug-induced toxicity. *Nat. Rev. Drug Discov.* **4**, 410–420 (2005).
66. Singh, J., Petter, R. C., Baillie, T. a & Whitty, A. The resurgence of covalent drugs. *Nat. Rev. Drug Discov.* **10**, 307–317 (2011).
67. Ikeda, T. Idiosyncratic drug hepatotoxicity: strategy for prevention and proposed mechanism. *Curr. Med. Chem.* **22**, 528–537 (2015).
68. Nakayama, S. *et al.* A zone classification system for risk assessment of idiosyncratic drug toxicity using daily dose and covalent binding. *Drug Metab. Dispos.* **37**, 1970–1977 (2009).
69. Ng, W. *et al.* Animal Models of Idiosyncratic Drug Reactions. *Adv. Pharmacol.* **63**, 81–135 (2012).
70. Kaplowitz, N. Idiosyncratic drug hepatotoxicity. *Nat. Rev. Drug Discov.* **4**, 489–499 (2005).
71. Uetrecht, J. Idiosyncratic drug reactions: current understanding. *Annu. Rev. Pharmacol. Toxicol.* **47**, 513–539 (2007).
72. Bauer, R. A. Covalent inhibitors in drug discovery: From accidental discoveries to avoided liabilities and designed therapies. *Drug Discov. Today* **20**, 1061–1073 (2015).

- 
73. Mah, R., Thomas, J. R. & Shafer, C. M. Drug discovery considerations in the development of covalent inhibitors. *Bioorg. Med. Chem. Lett.* **24**, 33–39 (2014).
74. Kobaisy, M. *et al.* Antimycobacterial polyynes of Devil's club (*Oplopanax horridus*), a north american native medicinal plant. *J. Nat. Prod.* **60**, 1210–1213 (1997).
75. Liu, X. *et al.* Polyynes hybrid compounds from *notopterygium incisum* with peroxisome proliferator-activated receptor gamma agonistic effects. *J. Nat. Prod.* **77**, 2513–2521 (2014).
76. Gehrt, A., Erkel, G., Anke, T. & Sterner, O. Nitidon, a new bioactive metabolite from the basidiomycete *Junghuhnia nitida* (Pers.: Fr.) Ryv. *Zeitschrift fur Naturforsch. - Sect. C J. Biosci.* **53**, 89–92 (1998).
77. Ko, J., Morinaka, B. I. & Molinski, T. F. Faulknerynes A-C from a Bahamian Sponge *Diplastrella* sp.: Stereoassignment by Critical Application of Two Exciton Coupled CD Methods. *J. Org. Chem.* **76**, 894–901 (2011).
78. Faulkner, D. J. Marine natural products. *Nat Prod Rep* **19**, 1–48 (2002).
79. Faulkner, D. J. Marine natural products. *Nat. Prod. Rep.* **19**, 1–49 (2002).
80. Blunt, J. W., Copp, B. R., Munro, M. H. G., Northcote, P. T. & Prinsep, M. R. Marine natural products. *Nat. Prod. Rep.* **20**, 1–48 (2003).
81. Tsuge, N. *et al.* Cinnatriacetins A and B, New Antibacterial Triacetylene Derivatives from the Fruiting Bodies of *Fistulina hepatica*. *J. Antibiot. (Tokyo)*. **52**, 578–581 (1999).
82. Bellina, F., Carpita, A., Mannocci, L. & Rossi, R. First Total Synthesis of Naturally Occurring (-)-Nitidon and Its Enantiomer. *European J. Org. Chem.* **2004**, 2610–2619 (2004).
83. Block, E., Guo, C., Thiruvazhi, M. & Toscano, P. J. Total Synthesis of Thiarubrine B [3-(3-Buten-1-ynyl)-6-(1,3-pentadiynyl)-1,2-dithiin], the Antibiotic Principle of Giant Ragweed (*Ambrosia trifida*). *J. Am. Chem. Soc.* **116**, 9403–9404 (1994).
84. Hansen, S. L., Purup, S. & Christensen, L. P. Bioactivity of falcarinol and the influence of processing and storage on its content in carrots (*Daucus carota* L.). *J. Sci. Food Agric.* **83**, 1010–1017 (2003).
85. Young, J. F., Christensen, L. P., Theil, P. K. & Oksbjerg, N. The polyacetylenes falcarinol and falcarindiol affect stress responses in myotube cultures in a biphasic



- manner. *Dose. Response.* **6**, 239–251 (2008).
86. Metzger, B. T., Barnes, D. M. & Reed, J. D. Purple carrot (*Daucus carota* L.) polyacetylenes decrease lipopolysaccharide-induced expression of inflammatory proteins in macrophage and endothelial cells. *J. Agric. Food Chem.* **56**, 3554–3560 (2008).
87. Hausen, B. M. *et al.* Allergic and irritant contact dermatitis from falcarinol and didehydrofalcarinol in common ivy (*Hedera helix* L.). *Contact Dermatitis* **17**, 1–9 (1987).
88. Hansen, L., Hammershøy, O. & Boll, P. M. Allergic contact dermatitis from falcarinol isolated from *Schefflera arboricola*. *Contact Dermatitis* **14**, 91–93 (1986).
89. Leonti, M. *et al.* Falcarinol is a covalent cannabinoid CB1 receptor antagonist and induces pro-allergic effects in skin. *Biochem. Pharmacol.* **79**, 1815–1826 (2010).
90. Bentley, R. K., Bhattacharjee, D., Jones, E. R. H. & Thaller, V. Natural acetylenes. Part XXVIII. C17-polyacetylenic alcohols from the Umbellifer *Daucus carota* L. (carrot) : alkylation of benzene by acetylenyl(vinyl)carbinols in the presence of toluene-p-sulphonic acid. *J. Chem. Soc. C Org.* 685–688 (1969).
91. Ohnuma, T. *et al.* Activation of the Nrf2/ARE pathway via S-alkylation of cysteine 151 in the chemopreventive agent-sensor Keap1 protein by falcarindiol, a conjugated diacetylene compound. *Toxicol. Appl. Pharmacol.* **244**, 27–36 (2010).
92. Hartley, D. P., Ruth, J. A. & Petersen, D. R. The hepatocellular metabolism of 4-hydroxynonenal by alcohol dehydrogenase, aldehyde dehydrogenase, and glutathione S-transferase. *Arch. Biochem. Biophys.* **316**, 197–205 (1995).
93. Yoval-Sánchez, B. & Rodríguez-Zavala, J. S. Differences in susceptibility to inactivation of human aldehyde dehydrogenases by lipid peroxidation byproducts. *Chem. Res. Toxicol.* **25**, 722–729 (2012).
94. Chen, C. H., Sun, L. & Mochly-Rosen, D. Mitochondrial aldehyde dehydrogenase and cardiac diseases. *Cardiovasc. Res.* **88**, 51–57 (2010).
95. Chen, C.-H., Ferreira, J. C. B., Gross, E. R. & Mochly-Rosen, D. Targeting aldehyde dehydrogenase 2: new therapeutic opportunities. *Physiol. Rev.* **94**, 1–34 (2014).
96. Takao, A., Shimoda, T., Kohno, S., Asai, S. & Harda, S. Correlation between

- alcohol-induced asthma and acetaldehyde dehydrogenase-2 genotype. *J. Allergy Clin. Immunol.* **101**, 576–580 (1998).
97. Koppaka, V. *et al.* Aldehyde dehydrogenase inhibitors: a comprehensive review of the pharmacology, mechanism of action, substrate specificity, and clinical application. *Pharmacol. Rev.* **64**, 520–539 (2012).
98. Brooks, P. J., Enoch, M. A., Goldman, D., Li, T. K. & Yokoyama, A. The alcohol flushing response: An unrecognized risk factor for esophageal cancer from alcohol consumption. *PLoS Med.* **6**, 0258–0263 (2009).
99. Amanuma, Y. *et al.* Protective role of ALDH2 against acetaldehyde-derived DNA damage in oesophageal squamous epithelium. *Sci. Rep.* **5**, 14142 (2015).
100. Li, Y. *et al.* Mitochondrial aldehyde dehydrogenase-2 (ALDH2) Glu504Lys polymorphism contributes to the variation in efficacy of sublingual nitroglycerin. *J. Clin. Invest.* **116**, 506–511 (2006).
101. Jo, S. A. *et al.* A Glu487Lys polymorphism in the gene for mitochondrial aldehyde dehydrogenase 2 is associated with myocardial infarction in elderly Korean men. *Clin. Chim. Acta.* **382**, 43–47 (2007).
102. Marchitti, S. A., Deitrich, R. A. & Vasiliou, V. Neurotoxicity and Metabolism of the Catecholamine- Derived 3 , 4-Dihydroxyphenylacetaldehyde and The Role of Aldehyde Dehydrogenase. *Pharmacol. Rev.* **59**, 125–150 (2007).
103. Perez-Miller, S. *et al.* Alda-1 is an agonist and chemical chaperone for the common human aldehyde dehydrogenase 2 variant. *Nat. Struct. Mol. Biol.* **17**, 159–164 (2010).
104. Wang, M. F., Han, C. L. & Yin, S. J. Substrate specificity of human and yeast aldehyde dehydrogenases. *Chem. Biol. Interact.* **178**, 36–39 (2009).
105. Takahashi, K., Weiner, H. & Filmer, D. L. Effects of pH on horse liver aldehyde dehydrogenase: alterations in metal ion activation, number of functioning active sites, and hydrolysis of the acyl intermediate. *Biochemistry* **20**, 6225–6230 (1981).
106. Nickel, S. *et al.* Chemoproteomic Evaluation of the Polyacetylene Callyspongynic Acid. *Chemistry* **21**, 10721–10728 (2015).
107. Li, Z. *et al.* Design and synthesis of minimalist terminal alkyne-containing diazirine photo-crosslinkers and their incorporation into kinase inhibitors for cell- and tissue-

- based proteome profiling. *Angew. Chemie - Int. Ed.* **52**, 8551–8556 (2013).
108. McLaughlin, N. P. *et al.* A short synthesis of (+) and (-)-falcarinol. *Tetrahedron* **66**, 9681–9687 (2010).
109. Jeffery, T. Copper(I) and phase transfer catalysed allylic substitution by terminal alkynes. *Tetrahedron Lett.* **30**, 2225–2228 (1989).
110. Liang, C. *et al.* Polyacetylenes from panax stipuleanatus and their cytotoxic effects on human cancer cells. *Bull. Korean Chem. Soc.* **32**, 3513–3516 (2011).
111. Fiandanese, V., Bottalico, D., Marchese, G. & Punzi, A. Synthesis of naturally occurring polyacetylenes via a bis-silylated diyne. *Tetrahedron* **62**, 5126–5132 (2006).
112. Turlington, M. *et al.* From highly enantioselective catalytic reaction of 1,3-dienes with aldehydes to facile asymmetric synthesis of polycyclic compounds. *J. Am. Chem. Soc.* **133**, 11780–11794 (2011).
113. Mann, T. J., Speed, A. W. H., Schrock, R. R. & Hoveyda, A. H. Catalytic Z-selective cross-metathesis with secondary silyl- and benzyl-protected allylic ethers: Mechanistic aspects and applications to natural product synthesis. *Angew. Chemie - Int. Ed.* **52**, 8395–8400 (2013).
114. Zidorn, C. *et al.* Polyacetylenes from the apiaceae vegetables carrot, celery, fennel, parsley, and parsnip and their cytotoxic activities. *J. Agric. Food Chem.* **53**, 2518–2523 (2005).
115. Brandt, K. *et al.* Health promoting compounds in vegetables and fruits. *Trends Food Sci. Technol.* **15**, 384–393 (2004).
116. Purup, S. *et al.* Differential effects of falcarinol and related aliphatic c-17-polyacetylenes on intestinal cell proliferation. *J. Agric. Food Chem.* **57**, 8290–8296 (2009).
117. Chou, S. C., Everngam, M. C., Sturtz, G. & Beck, J. J. Antibacterial activity of components from *Lomatium californicum*. *Phyther. Res.* **20**, 153–156 (2006).
118. Lechner, D., Stavri, M., Oluwatuyi, M., Pereda-Miranda, R. & Gibbons, S. The anti-staphylococcal activity of *Angelica dahurica* (Bai Zhi). *Phytochemistry* **65**, 331–335 (2004).
119. Hueisgen, R. Centenary lecture. 1,3-Dipolar cycloadditions. *Proc. Chem. Soc.*,

- London* 357–369 (1961).
120. Tornøe, C. W., Christensen, C. & Meldal, M. Peptidotriazoles on solid phase: [1,2,3]-Triazoles by regiospecific copper(I)-catalyzed 1,3-dipolar cycloadditions of terminal alkynes to azides. *J. Org. Chem.* **67**, 3057–3064 (2002).
  121. Eirich, J. *et al.* Pretubulysin derived probes as novel tools for monitoring the microtubule network via activity-based protein profiling and fluorescence microscopy. *Mol. Biosyst.* **8**, 2067–2075 (2012).
  122. Lam, J. P., Mays, D. C. & Lipsky, J. J. Inhibition of recombinant human mitochondrial and cytosolic aldehyde dehydrogenases by two candidates for the active metabolites of disulfiram. *Biochemistry* **36**, 13748–13754 (1997).
  123. Moreb, J. S. *et al.* Retinoic acid down-regulates aldehyde dehydrogenase and increases cytotoxicity of 4-hydroperoxycyclophosphamide and acetaldehyde. *J. Pharmacol. Exp. Ther.* **312**, 339–345 (2005).
  124. Koch, M. F. *et al.* Structural, Biochemical, and Computational Studies Reveal the Mechanism of Selective Aldehyde Dehydrogenase 1A1 Inhibition by Cytotoxic Duocarmycin Analogues. *Angew. Chemie - Int. Ed.* **54**, 13550–13554 (2015).
  125. Chen, C.-H. *et al.* Activation of aldehyde dehydrogenase-2 reduces ischemic damage to the heart. *Science* **321**, 1493–1495 (2008).
  126. Ebert, A. D. *et al.* Characterization of the molecular mechanisms underlying increased ischemic damage in the aldehyde dehydrogenase 2 genetic polymorphism using a human induced pluripotent stem cell model system. *Sci. Transl. Med.* **6**, 255ra130 (2014).
  127. Guo, J.-M. *et al.* ALDH2 protects against stroke by clearing 4-HNE. *Cell Res.* **23**, 915–930 (2013).
  128. Moon, K. H., Kim, B. J. & Song, B. J. Inhibition of mitochondrial aldehyde dehydrogenase by nitric oxide-mediated S-nitrosylation. *FEBS Lett.* **579**, 6115–6120 (2005).
  129. Yu, H.-S. *et al.* Characteristics of aldehyde dehydrogenase 2 (Aldh2) knockout mice. *Toxicol. Mech. Methods* **19**, 535–540 (2009).
  130. Brunner, J. New photolabeling and crosslinking methods. *Annu. Rev. Biochem.* **62**, 483–514 (1993).

131. Preston, G. W., Radford, S. E., Ashcroft, A. E. & Wilson, A. J. Analysis of amyloid nanostructures using photo-cross-linking: in situ comparison of three widely used photo-cross-linkers. *ACS Chem. Biol.* **9**, 761–768 (2014).
132. Gubbens, J. *et al.* Photocrosslinking and click chemistry enable the specific detection of proteins interacting with phospholipids at the membrane interface. *Chem. Biol.* **16**, 3–14 (2009).
133. Knowles, J. R. Photogenerated reagents for biological receptor-site labeling. *Acc. Chem. Res.* **5**, 155–160 (1972).
134. Sadakane, Y. & Hatanaka, Y. Photochemical Fishing Approaches for Identifying Target Proteins and Elucidating the Structure of a Ligand-binding Region Using Carbene-generating Photoreactive Probes. *Anal. Sci.* **22**, 209–218 (2006).
135. Schnapp, K. A., Poe, R., Leyva, E., Soundararajan, N. & Platz, M. S. Exploratory photochemistry of fluorinated aryl azides. Implications for the design of photoaffinity labeling reagents. *Bioconjug. Chem.* **4**, 172–177
136. Dubinsky, L., Krom, B. P. & Meijler, M. M. Diazirine based photoaffinity labeling. *Bioorg. Med. Chem.* **20**, 554–570 (2012).
137. Das, J. Aliphatic diazirines as photoaffinity probes for proteins: recent developments. *Chem. Rev.* **111**, 4405–4417 (2011).
138. Mackinnon, A. L. & Taunton, J. Target Identification by Diazirine Photo-Cross-linking and Click Chemistry. *Curr. Protoc. Chem. Biol.* **1**, 55–73 (2009).
139. Ford, F., Yuzawa, T., Platz, M. S., Matzinger, S. & Fülischer, M. Rearrangement of dimethylcarbene to propene: Study by laser flash photolysis and ab initio molecular orbital theory. *J. Am. Chem. Soc.* **120**, 4430–4438 (1998).
140. Preston, G. W. & Wilson, A. J. Photo-induced covalent cross-linking for the analysis of biomolecular interactions. *Chem. Soc. Rev.* **42**, 3289–3301 (2013).
141. Brunner, J., Senn, H. & Richards, F. M. 3-Trifluoromethyl-3-phenyldiazirine. A new carbene generating group for photolabeling reagents. *J. Biol. Chem.* **255**, 3313–3318 (1980).
142. Hashimoto, M. & Hatanaka, Y. Practical conditions for photoaffinity labeling with 3-trifluoromethyl-3-phenyldiazirine photophore. *Anal. Biochem.* **348**, 154–156 (2006).
143. Bush, J. T. *et al.* The Ugi four-component reaction enables expedient synthesis and

- comparison of photoaffinity probes. *Chem. Sci.* **4**, 4115–4120 (2013).
144. Sakurai, K., Ozawa, S., Yamada, R., Yasui, T. & Mizuno, S. Comparison of the reactivity of carbohydrate photoaffinity probes with different photoreactive groups. *ChemBioChem* **15**, 1399–1403 (2014).
145. Park, J., Koh, M., Koo, J. Y., Lee, S. & Park, S. B. Investigation of Specific Binding Proteins to Photoaffinity Linkers for Efficient Deconvolution of Target Protein. *ACS Chem. Biol.* Ahead of Print (2015).
146. Tan, X. *et al.* Triblock polyphiles through click chemistry: Self-assembled thermotropic cubic phases formed by micellar and monolayer vesicular aggregates. *Chem. - A Eur. J.* **19**, 16303–16313 (2013).
147. Heydenreuter, W., Kunold, E. & Sieber, S. A. Alkynol natural products target ALDH2 in cancer cells by irreversible binding to the active site. *Chem. Commun. (Camb)*. **51**, 15784–15787 (2015).
148. Finn, R. D. *et al.* The Pfam protein families database: towards a more sustainable future. *Nucleic Acids Res.* **44**, D279–D285 (2015).
149. Sigrist, C. J. A. *et al.* New and continuing developments at PROSITE. *Nucleic Acids Res.* **41**, D344–D347 (2013).
150. Blachly-Dyson, E. *et al.* Cloning and functional expression in yeast of two human isoforms of the outer mitochondrial membrane channel, the voltage-dependent anion channel. *J. Biol. Chem.* **268**, 1835–1841 (1993).
151. Smits, A. H., Jansen, P. W. T. C., Poser, I., Hyman, A. A. & Vermeulen, M. Stoichiometry of chromatin-associated protein complexes revealed by label-free quantitative mass spectrometry-based proteomics. *Nucleic Acids Res.* **41**, e28 (2013).
152. Schwanhäusser, B. *et al.* Global quantification of mammalian gene expression control. *Nature* **473**, 337–342 (2011).
153. Ishihama, Y. *et al.* Exponentially Modified Protein Abundance Index (emPAI) for Estimation of Absolute Protein Amount in Proteomics by the Number of Sequenced Peptides per Protein. *Mol. Cell. Proteomics* **4**, 1265–1272 (2005).
154. Wilhelm, M. *et al.* Mass-spectrometry-based draft of the human proteome. *Nature* **509**, 582–587 (2014).

155. Cho, I. J., Woo, N. R., Shin, I. C. & Kim, S. G. H89, an inhibitor of PKA and MSK, inhibits cyclic-AMP response element binding protein-mediated MAPK phosphatase-1 induction by lipopolysaccharide. *Inflamm. Res.* **58**, 863–872 (2009).
156. Hidaka, H., Inagaki, M., Kawamoto, S. & Sasaki, Y. Isoquinolinesulfonamides, novel and potent inhibitors of cyclic nucleotide dependent protein kinase and protein kinase C. *Biochemistry* **23**, 5036–5041 (1984).
157. Inagaki, M. *et al.* Naphthalenesulfonamides as calmodulin antagonists and protein kinase inhibitors. *Mol. Pharmacol.* **29**, 577–581 (1986).
158. Leemhuis, J., Boutillier, S., Schmidt, G. & Meyer, D. K. The protein kinase A inhibitor H89 acts on cell morphology by inhibiting Rho kinase. *J. Pharmacol. Exp. Ther.* **300**, 1000–1007 (2002).
159. Lochner, A. & Moolman, J. A. The many faces of H89: A review. *Cardiovasc. Drug Rev.* **24**, 261–274 (2006).
160. Engh, R. A, Girod, A., Kinzel, V., Huber, R. & Bossemeyer, D. Crystal structures of catalytic subunit of cAMP-dependent protein kinase in complex with isoquinolinesulfonyl protein kinase inhibitors H7, H8, and H89. Structural implications for selectivity. *J. Biol. Chem.* **271**, 26157–26164 (1996).
161. Shannon, P. *et al.* Cytoscape: A software Environment for integrated models of biomolecular interaction networks. *Genome Res.* **13**, 2498–2504 (2003).
162. DeSantis, C. E. *et al.* Cancer treatment and survivorship statistics, 2014. *CA Cancer. J. Clin.* **64**, 252–271 (2014).
163. Biemar, F. & Foti, M. Global progress against cancer-challenges and opportunities. *Cancer Biol. Med.* **10**, 183–186 (2013).
164. Gravitz, L. Liver cancer. *Nature* **516**, S1 (2014).
165. Herbst, R. S., Heymach, J. V & Lippman, S. M. Lung cancer. *N. Engl. J. Med.* **359**, 1367–1380 (2008).
166. Vincent, A., Herman, J., Schulick, R., Hruban, R. H. & Goggins, M. Pancreatic cancer. in *The Lancet* **378**, 607–620 (2011).
167. Fletcher, O. & Houlston, R. S. Architecture of inherited susceptibility to common cancer. *Nat. Rev. Cancer* **10**, 353–361 (2010).
168. De Palma, M. & Hanahan, D. The biology of personalized cancer medicine: Facing

- individual complexities underlying hallmark capabilities. *Molecular Oncology* **6**, 111–127 (2012).
169. Hayden, E. C. Personalized cancer therapy gets closer. *Nature* **458**, 131–132 (2009).
170. Meric-Bernstam, F. & Mills, G. B. Overcoming implementation challenges of personalized cancer therapy. *Nat. Rev. Clin. Oncol.* **9**, 542–548 (2012).
171. Pérez-Losada, J., Castellanos-Martín, A. & Mao, J.-H. Cancer evolution and individual susceptibility. *Integr. Biol. (Camb)*. **3**, 316–328 (2011).
172. Tyner, J. W. Functional genomics for personalized cancer therapy. *Sci. Transl. Med.* **6**, 243fs26 (2014).
173. Blakely, A. M. & Miner, T. J. Surgical Considerations in the Treatment of Gastric Cancer. *Gastroenterol. Clin. North Am.* **42**, 337–357 (2013).
174. Thomas, R. J. S. in *Textbook of Surgery: Third Edition*. 67–74 (2008).
175. Baskar, R., Ann-Lee, K., Yeo, R. & Yeoh, K.-W. Cancer and Radiation Therapy: Current Advances and Future Directions. *Int. J. Med. Sci.* **9**, 193–199 (2012).
176. Chabner, B. a & Roberts, T. G. Timeline: Chemotherapy and the war on cancer. *Nat. Rev. Cancer* **5**, 65–72 (2005).
177. Fernando, J. & Jones, R. The principles of cancer treatment by chemotherapy. *Surg. (United Kingdom)* **33**, 131–135 (2015).
178. Morrison, W. B. Cancer Chemotherapy: An Annotated History. *J. Vet. Intern. Med.* **24**, 1249–1262 (2010).
179. Vanneman, M. & Dranoff, G. Combining immunotherapy and targeted therapies in cancer treatment. *Nat. Rev. Cancer* **12**, 237–251 (2012).
180. Kawakami, Y. *et al.* Improvement of cancer immunotherapy by combining molecular targeted therapy. *Front. Oncol.* **3**, 136 (2013).
181. Hanahan, D. The Hallmarks of Cancer. *Cell* **100**, 57–70 (2000).
182. Hanahan, D. & Weinberg, R. A. Hallmarks of cancer: The next generation. *Cell* **144**, 646–674 (2011).
183. Mertsch, S., Becker, M., Lichota, A., Paulus, W. & Senner, V. Vesicle amine transport protein-1 (VAT-1) is upregulated in glioblastomas and promotes migration.



- Neuropathol. Appl. Neurobiol.* **35**, 342–352 (2009).
184. Hughes, M. J. & Harrison, E. M. Malignant liver tumours. *Surg. (United Kingdom)* **32**, 655–660 (2014).
185. Ahmed, I. & Lobo, D. N. Malignant tumours of the liver. *Surgery* **27**, 30–37 (2009).
186. Wistuba, I. I. & Gazdar, A. F. Lung cancer preneoplasia. *Annu. Rev. Pathol.* **1**, 331–348 (2006).
187. Gardel, M. L., Schneider, I. C., Aratyn-Schaus, Y. & Waterman, C. M. Mechanical integration of actin and adhesion dynamics in cell migration. *Annu. Rev. Cell Dev. Biol.* **26**, 315–333 (2010).
188. Vignjevic, D. & Montagnac, G. Reorganisation of the dendritic actin network during cancer cell migration and invasion. *Sem. Cancer Biol.* **18**, 12–22 (2008).
189. Etienne-Manneville, S. & Hall, A. Rho GTPases in cell biology. *Nature* **420**, 629–635 (2002).
190. Fukata, M., Nakagawa, M. & Kaibuchi, K. Roles of Rho-family GTPases in cell polarisation and directional migration. *Curr. Opin. Cell. Biol.* **15**, 590–597 (2003).
191. Machacek, M. *et al.* Coordination of Rho GTPase activities during cell protrusion. *Nature* **461**, 99–103 (2009).
192. Raftopoulou, M. & Hall, A. Cell migration: Rho GTPases lead the way. *Dev. Biol.* **265**, 23–32 (2004).
193. Ridley, A. J. Rho GTPase signalling in cell migration. *Curr. Opin. Cell. Biol.* **36**, 103–112 (2015).
194. Chen, J. & Gallo, K. A. MLK3 regulates paxillin phosphorylation in chemokine-mediated breast cancer cell migration and invasion to drive metastasis. *Cancer Res.* **72**, 4130–4140 (2012).
195. Engelman, J. A. Targeting PI3K signalling in cancer: opportunities, challenges and limitations. *Nat. Rev. Cancer* **9**, 550–562 (2009).
196. Kulbe, H., Levinson, N. R., Balkwill, F. & Wilson, J. L. The chemokine network in cancer--much more than directing cell movement. *Int. J. Dev. Biol.* **48**, 489–496 (2004).
197. Müller, a *et al.* Involvement of chemokine receptors in breast cancer metastasis.

- Nature* **410**, 50–56 (2001).
198. Bozzuto, G., Ruggieri, P. & Molinari, A. Molecular aspects of tumor cell migration and invasion. *Ann. dell'Istituto Super. di sanità* **46**, 66–80 (2010).
  199. Friedl, P. & Wolf, K. Tumour-cell invasion and migration: diversity and escape mechanisms. *Nat. Rev. Cancer* **3**, 362–374 (2003).
  200. Petrie, R. J., Doyle, A. D. & Yamada, K. M. Random versus directionally persistent cell migration. *Nat. Rev. Mol. Cell Biol.* **10**, 538–549 (2009).
  201. Hood, J. D. & Cheresch, D. A. Role of integrins in cell invasion and migration. *Nat. Rev. Cancer* **2**, 91–100 (2002).
  202. Varner, J. A. & Cheresch, D. A. Integrins and cancer. *Curr. Opin. Cell. Biol.* **8**, 724–730 (1996).
  203. Huttenlocher, A. & Horwitz, A. R. Integrins in cell migration. *Cold Spring Harb. Perspect. Biol.* **3**, 1–16 (2011).
  204. Gialeli, C., Theocharis, A. D. & Karamanos, N. K. Roles of matrix metalloproteinases in cancer progression and their pharmacological targeting. *FEBS Journal* **278**, 16–27 (2011).
  205. Egeblad, M. & Werb, Z. New functions for the matrix metalloproteinases in cancer progression. *Nat. Rev. Cancer* **2**, 161–174 (2002).
  206. Fridman, R. Metalloproteinases and cancer. *Cancer Metastasis Rev.* **25**, 7–8 (2006).
  207. Kessenbrock, K., Plaks, V. & Werb, Z. Matrix Metalloproteinases: Regulators of the Tumor Microenvironment. *Cell* **141**, 52–67 (2010).
  208. Millard, M., Odde, S. & Neamati, N. Integrin targeted therapeutics. *Theranostics* **1**, 154–188 (2011).
  209. Ley, K., Rivera-Nieves, J., Sandborn, W. J. & Shattil, S. Integrin-based therapeutics: biological basis, clinical use and new drugs. *Nat. Rev. Drug Discov.* **15**, 173–183 (2016).
  210. Barthel, S. R., Gavino, J. D., Descheny, L. & Dimitroff, C. J. Targeting selectins and selectin ligands in inflammation and cancer. *Expert Opin. Ther. Targets* **11**, 1473–1491 (2007).

211. Nozoe, S., Ishii, N., Kusano, G., Kikuchi, K. & Ohta, T. Neocarzilins A and B, Novel Polyenones from *Streptomyces Carzinostaticus*. *Tetrahedron Lett.* **33**, 7547–7550 (1992).
212. Otsuka, M., Ichinose, K., Fujii, I. & Ebizuka, Y. Cloning, sequencing, and functional analysis of an iterative type I polyketide synthase gene cluster for biosynthesis of the antitumor chlorinated polyenone neocarzilin in ‘*Streptomyces carzinostaticus*’. *Antimicrob. Agents Chemother.* **48**, 3468–3476 (2004).
213. Nozoe, S., Kikuchi, K., Ishii, N. & Ohta, T. Synthesis of neocarzilin A: An absolute stereochemistry. *Tetrahedron Lett.* **33**, 7551–7552 (1992).
214. Flick, K. & Kaiser, P. Protein degradation and the stress response. *Semin. Cell Dev. Biol.* **23**, 515–522 (2012).
215. Beguinot, L., Lyall, R. M., Willingham, M. C. & Pastan, I. Down-regulation of the epidermal growth factor receptor in KB cells is due to receptor internalization and subsequent degradation in lysosomes. *Proc. Natl. Acad. Sci. U. S. A.* **81**, 2384–2388 (1984).
216. Cox, J., Hein, M. Y., Lubner, C. a & Paron, I. Accurate proteome-wide label-free quantification by delayed normalization and maximal peptide ratio extraction, termed MaxLFQ. *Mol. Cell. Proteomics* **13**, 2513–2526 (2014).
217. Keilhauer, E. C., Hein, M. Y. & Mann, M. Accurate protein complex retrieval by affinity enrichment mass spectrometry (AE-MS) rather than affinity purification mass spectrometry (AP-MS). *Mol. Cell. Proteomics* **14**, 120–135 (2015).
218. Schlegel, S. *et al.* Optimizing membrane protein overexpression in the *Escherichia coli* strain Lemo21(DE3). *J. Mol. Biol.* **423**, 648–659 (2012).
219. Linial, M., Miller, K. & Scheller, R. H. VAT 1: An abundant membrane protein from torpedo cholinergic synaptic vesicles. *Neuron* **2**, 1265–1273 (1989).
220. Hayess, K. *et al.* Mammalian protein homologous to VAT-1 of torpedo californica: Isolation- from Ehrlich ascites tumor cells, biochemical characterization, and organization of its gene. *J. Cell. Biochem.* **69**, 304–315 (1998).
221. Koch, J. *et al.* Human VAT-1: A calcium-regulated activation marker of human epithelial cells. *Arch. Dermatol. Res.* **295**, 203–210 (2003).
222. Eura, Y., Ishihara, N., Oka, T. & Mihara, K. Identification of a novel protein that

- regulates mitochondrial fusion by modulating mitofusin (Mfn) protein function. *J. Cell Sci.* **119**, 4913–4925 (2006).
223. Boyden, S. The chemotactic effect of mixtures of antibody and antigen on polymorphonuclear leucocytes. *J. Exp. Med.* **115**, 453–466 (1962).
224. Nicoletti, I., Migliorati, G., Pagliacci, M. C., Grignani, F. & Riccardi, C. A rapid and simple method for measuring thymocyte apoptosis by propidium iodide staining and flow cytometry. *J. Immunol. Methods* **139**, 271–279 (1991).
225. Chazotte, B. Labeling mitochondria with mitotracker dyes. *Cold Spring Harb. Protoc.* **6**, 990–992 (2011).
226. Mignotte, B. & Vayssiere, J. L. Mitochondria and apoptosis. *Euro. J. Biochem.* **252**, 1–15 (1998).
227. Zorov, D. B., Juhaszova, M. & Sollott, S. J. Mitochondrial Reactive Oxygen Species (ROS) and ROS-Induced ROS Release. *Physiol. Rev.* **94**, 909–950 (2014).
228. Zorov, D. B., Juhaszova, M. & Sollott, S. J. Mitochondrial ROS-induced ROS release: An update and review. *Biochim. Biophys. Acta - Bioenergetics* **1757**, 509–517 (2006).
229. Hemmings, B. A. & Restuccia, D. F. PI3K-PKB/Akt pathway. *Cold Spring Harb. Perspect. Biol.* **4** (2012).
230. Vara, J. Á. F. *et al.* PI3K/Akt signalling pathway and cancer. *Cancer Treat. Rev.* **30**, 193–204 (2004).
231. Onishi, K., Higuchi, M., Asakura, T., Masuyama, N. & Gotoh, Y. The PI3K-Akt pathway promotes microtubule stabilization in migrating fibroblasts. *Genes Cells* **12**, 535–546 (2007).
232. Walczak, C. E. & Heald, R. Mechanisms of Mitotic Spindle Assembly and Function. *Int. Rev. Cytol.* **265**, 111–158 (2008).
233. Vale, R. D. The molecular motor toolbox for intracellular transport. *Cell* **112**, 467–480 (2003).
234. Watanabe, T., Noritake, J. & Kaibuchi, K. Regulation of microtubules in cell migration. *Trends Cell Biol.* **15**, 76–83 (2005).
235. Wells, C. D. *et al.* A Rich1/Amot Complex Regulates the Cdc42 GTPase and Apical-Polarity Proteins in Epithelial Cells. *Cell* **125**, 535–548 (2006).

236. Stock, A. M., Troost, G., Niggemann, B., Zanker, K. S. & Entschladen, F. Targets for anti-metastatic drug development. *Curr. Pharm. Des.* **19**, 5127–5134 (2013).
237. Li, Z. Y. *et al.* Highly enantioselective addition of trimethylsilylacetylene to aldehydes catalyzed by a zinc-amino-alcohol complex. *Chem. - A Eur. J.* **17**, 5782–5786 (2011).
238. Gansäuer, A., Fan, C. A., Keller, F. & Keil, J. Titanocene-catalyzed regiodivergent epoxide openings. *J. Am. Chem. Soc.* **129**, 3484–3485 (2007).
239. Kamijo, S. & Dudley, G. B. Tandem nucleophilic addition/fragmentation reactions and synthetic versatility of vinylogous acyl triflates. *J. Am. Chem. Soc.* **128**, 6499–6507 (2006).
240. Bennacer, B., Trubuil, D., Rivalle, C. & Grierson, D. S. The synthesis of two furan-based analogs of the  $\alpha'$ , $\beta'$ -epoxy ketone proteasome inhibitor eponemycin. *Eur. J. Org. Chem.* 4561–4568 (2003).
241. Cox, J. & Mann, M. MaxQuant enables high peptide identification rates, individualized p.p.b.-range mass accuracies and proteome-wide protein quantification. *Nat. Biotechnol.* **26**, 1367–1372 (2008).
242. Cox, J. & Mann, M. 1D and 2D annotation enrichment: a statistical method integrating quantitative proteomics with complementary high-throughput data. *BMC Bioinformatics* **13**, S12 (2012).
243. Vizcaíno, J. A. *et al.* 2016 update of the PRIDE database and its related tools. *Nucleic Acids Res.* **44**, D447–D456 (2016).

## 7 List of abbreviations, acronyms and symbols

ABPP	Activity Based Protein Profiling
Ac	Acetyl-
AfBPP	Affinity based Protein Profiling
APCI	Atmospheric-pressure chemical ionization
Brine	Saturated aqueous sodium chloride
<i>n</i> BuLi	<i>n</i> -Butyllithium
<i>tert</i> BuLi	<i>tert</i> -Butyllithium
CID	Collision-induced dissociation
CH <sub>2</sub> Cl <sub>2</sub>	Dichlormethane
Co-IP	Co-Immunoprecipitation
ddH <sub>2</sub> O	Purified water (resistivity ≥ 18.2 MΩ cm)
Da	Dalton
DIC	<i>N,N</i> -Diisopropylcarbodiimide
DIPEA	<i>N,N</i> -Diisopropylethylamine
DMF	Dimethylformamide
DMSO	Dimethylsulfoxid
DTT	Dithiothreitol
EDC	1-Ethyl-3-(3-dimethylaminopropyl)carbodiimide
eq	Equivalent(s)
ESI	Electrospray-Ionisation
HCD	Higher-energy collisional dissociation
EDTA	Sodium ethylenediaminetetraacetat
Eq	Equivalents
ESI	Electrospray-Ionisation
Et <sub>2</sub> O	Diethyl ether
EtOAc	Ethyl acetate
EtOH	Ethanol
FA	Formic acid
HOBt	1-Hydroxybenzotriazol
HPLC	High performance liquid chromatography

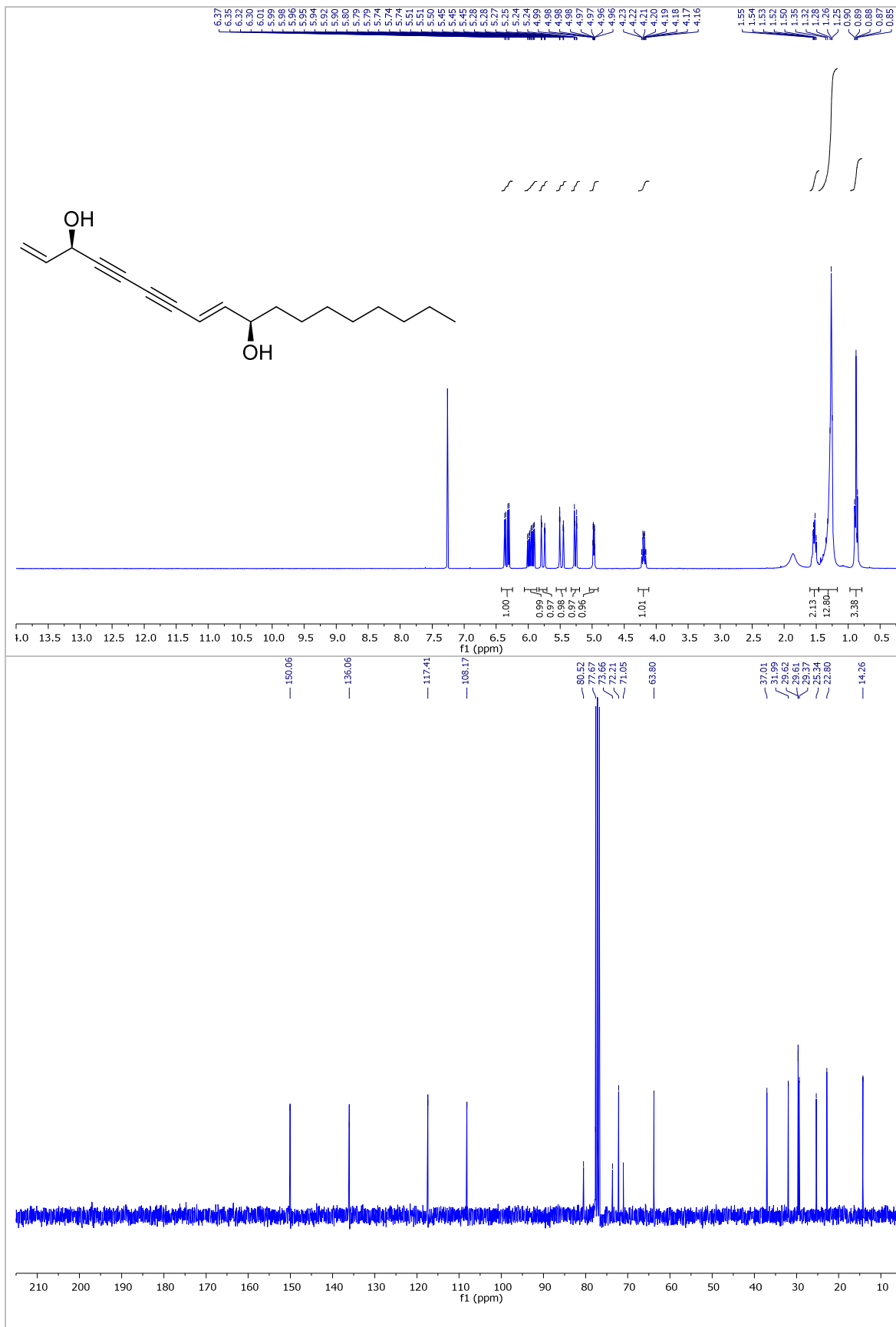
HRMS	High resolution mass spectrometry
Hz	Hertz
IC50	Half maximal inhibitory concentration
K	Kelvin
LC	Liquid chromatography
LysC	Endoproteinase Lys-C
MeCN	Acetonitrile
MeOH	Methanol
MS	Mass spectrometry
MS/MS	Tandem mass spectrometry
NMR	Nuclear magnetic resonance
o/n	overnight
PAGE	Polyacrylamide gel electrophoresis
PBS	Phosphate buffered saline
ppm	Parts per million
$R_f$	Reference value
RP-HPLC	Reversed phase high performance liquid chromatography
rpm	Rounds per minute
rt	Room temperature
SDS	Sodium dodecylsulfate
SILAC	Stable isotope labelling with amino acids in cell culture
TAMRA	Tetramethylrhodamine
TBS	<i>tert</i> Butyl-dimethylsilane
TBAF	tetra-n-Butylammonium fluoride
TBS	<i>tert</i> -Butyl-dimethylsilyl
TBTA	Tris[(1-benzyl-1H-1,2,3-triazol-4-yl)methyl]amin)
TCEP	Tris(2-carboxyethyl)phosphine
TEAB	Tetraethylammonium bicarbonat
TFA	Trifluoroacetic acid
TFL	Trifunctional linker
THF	Tetrahydrofurane
TLC	Thin layer chromatography

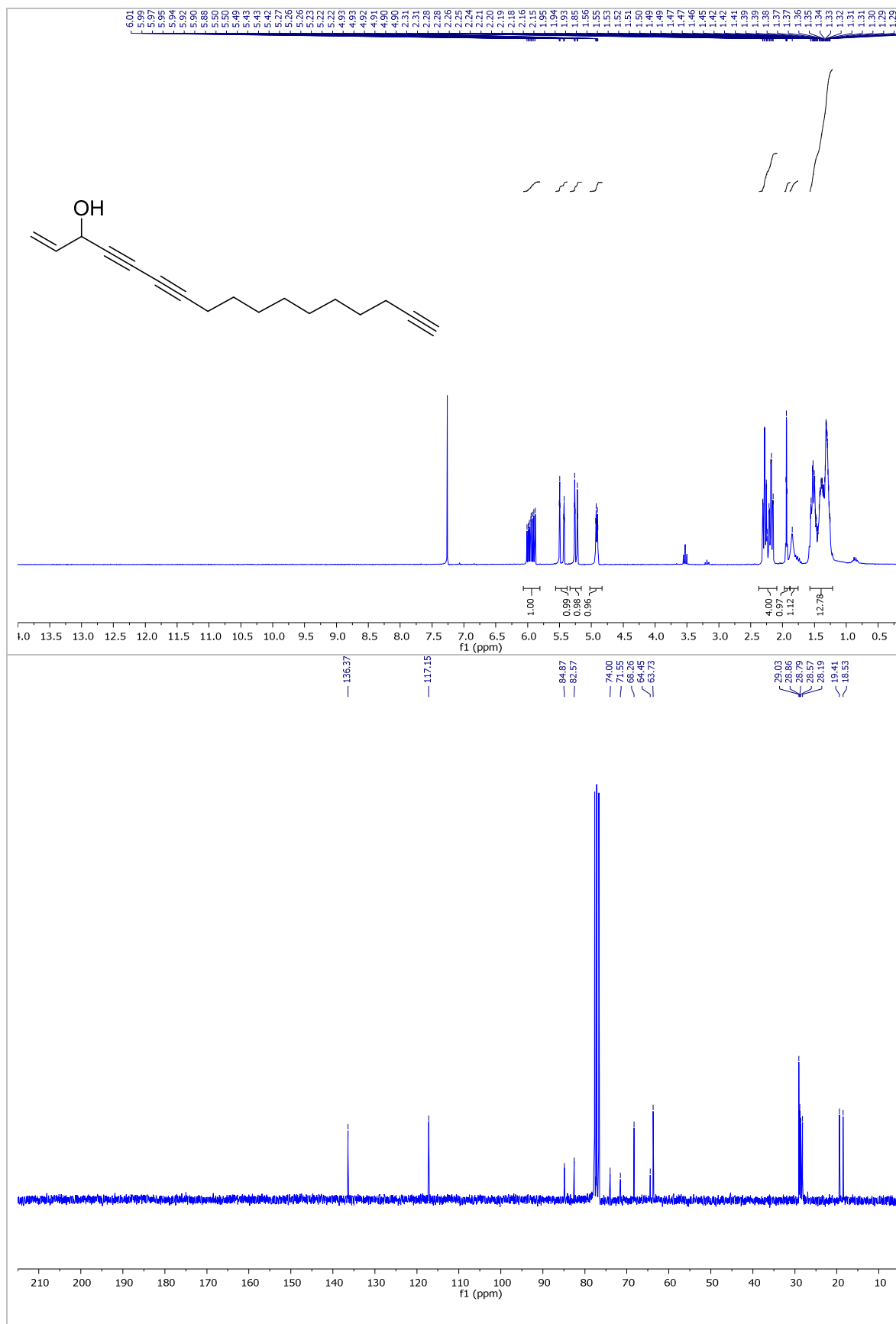
TRIS	tris(Hydroxymethyl)aminomethane
TMS	Trimethylsilyl
$t_R$	Retention time
UV	Ultraviolet

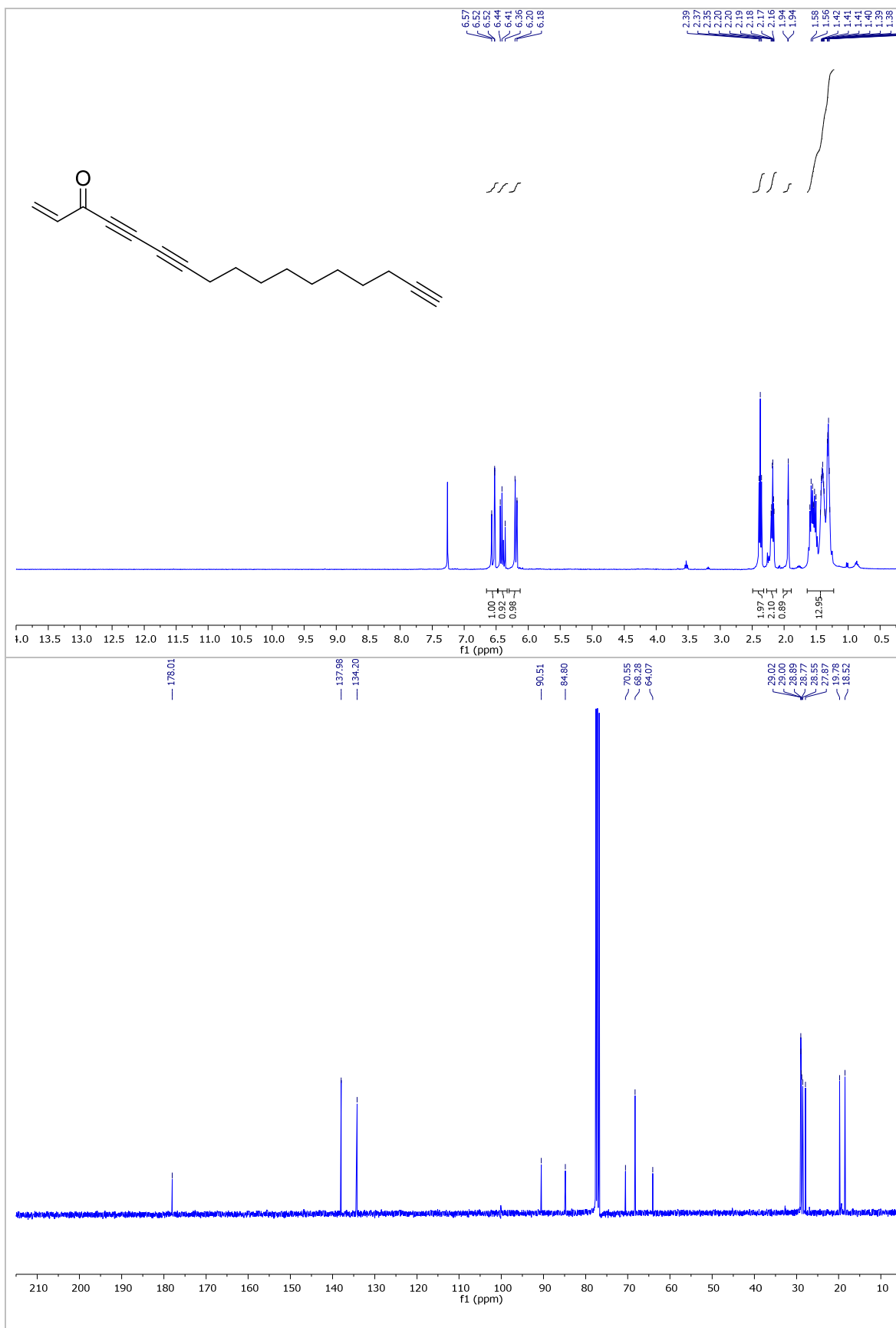


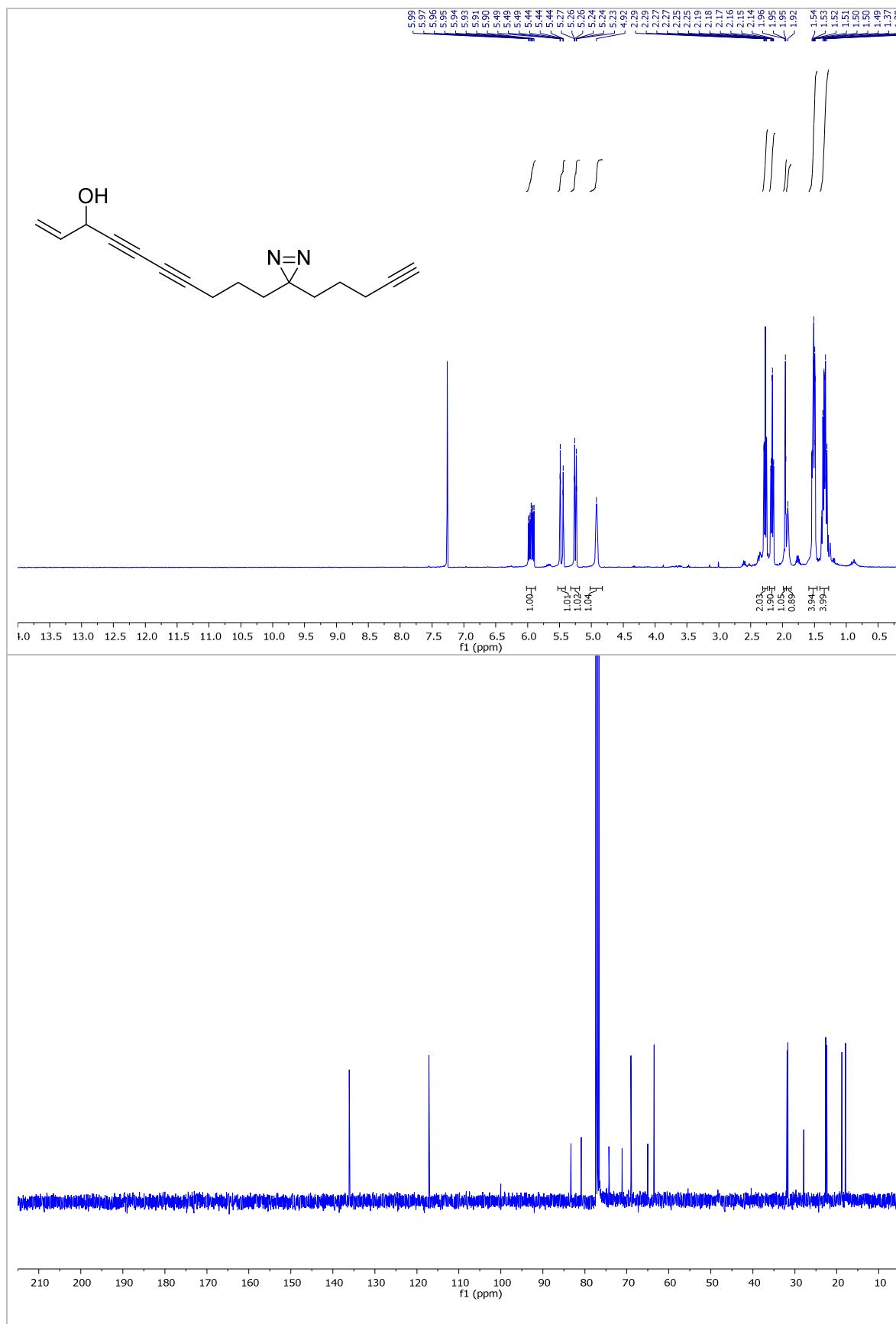
## **8 Appendices**

### **8.1 Selected $^1\text{H}$ and $^{13}\text{C}$ NMR Spectra for Chapter 2**

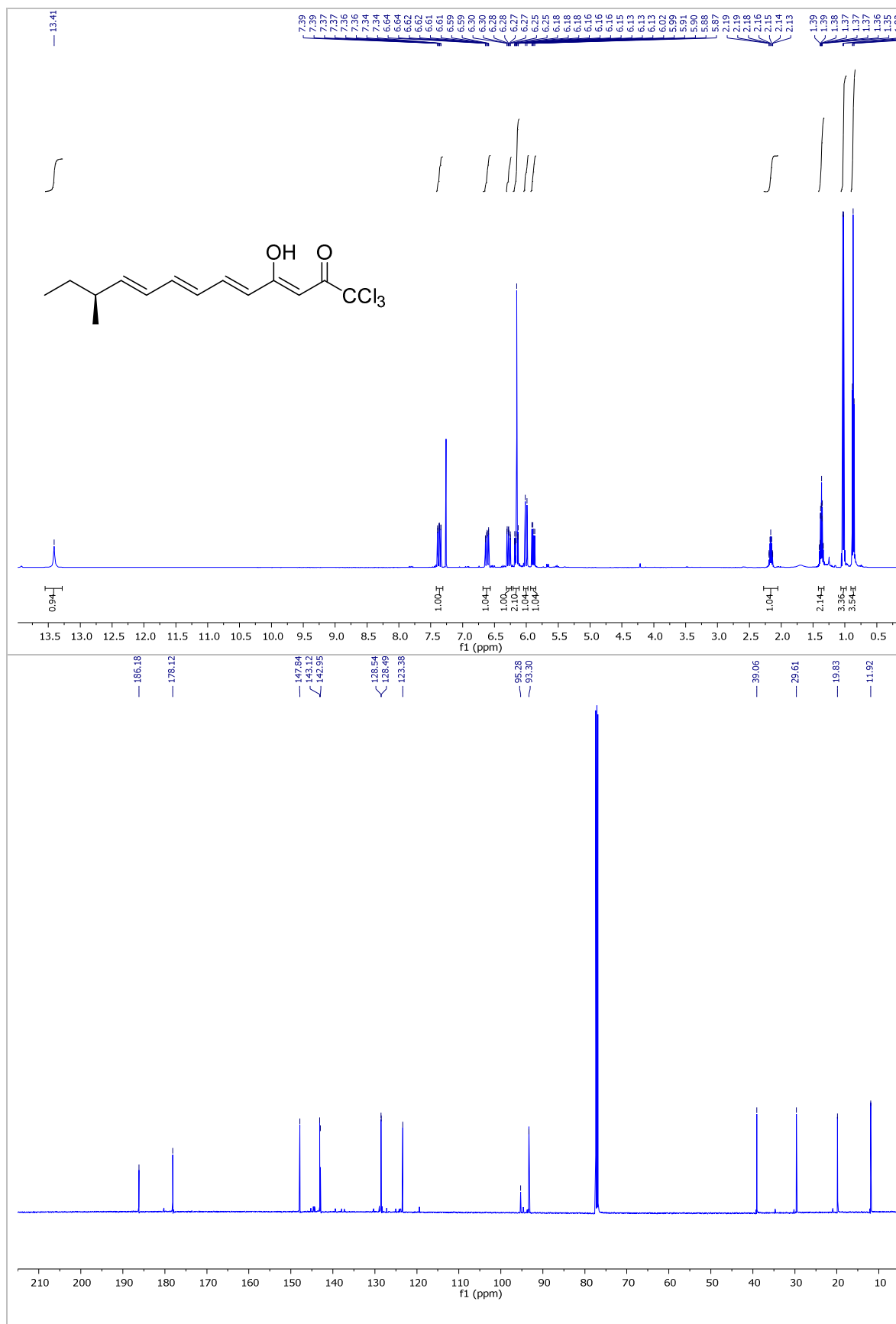


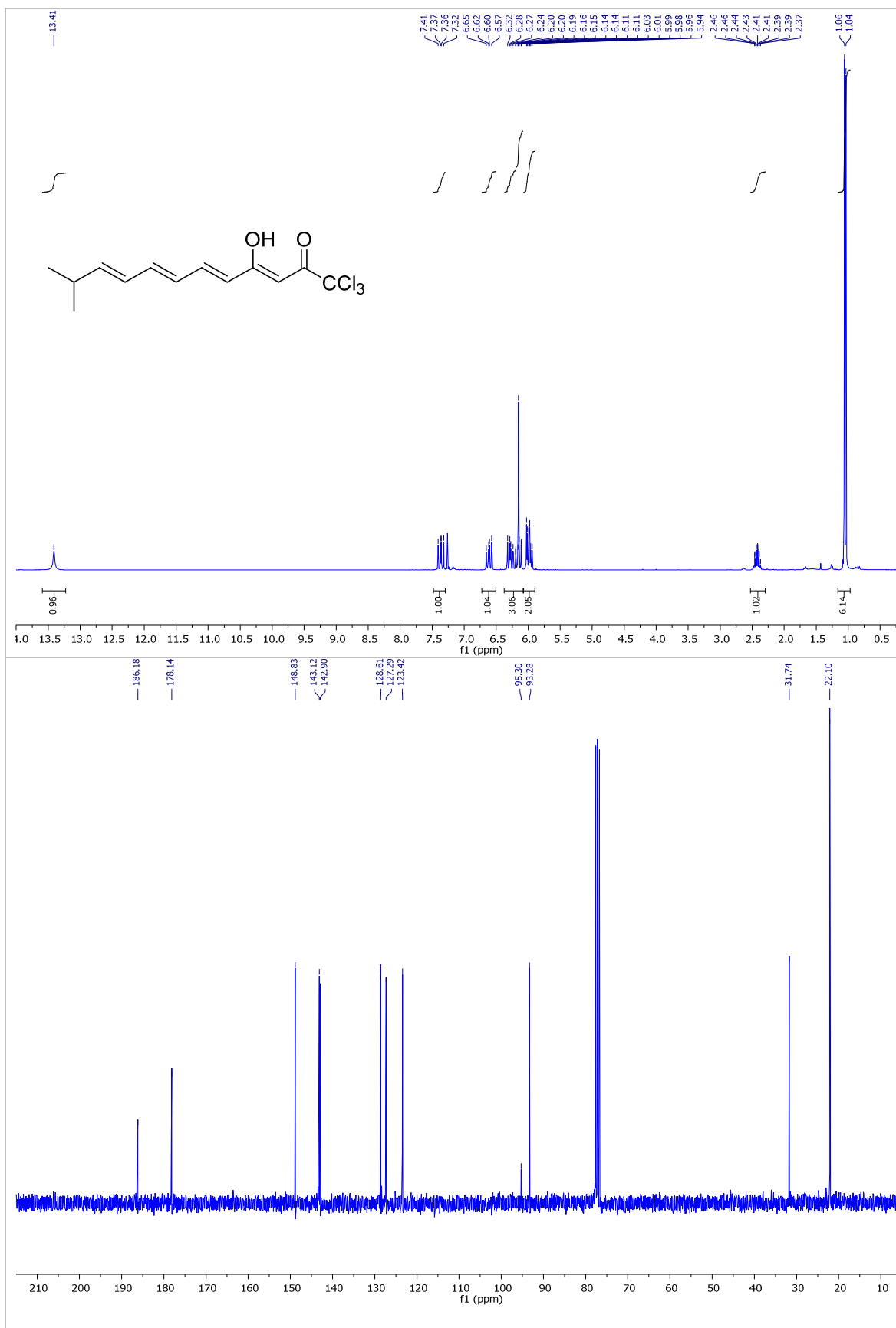




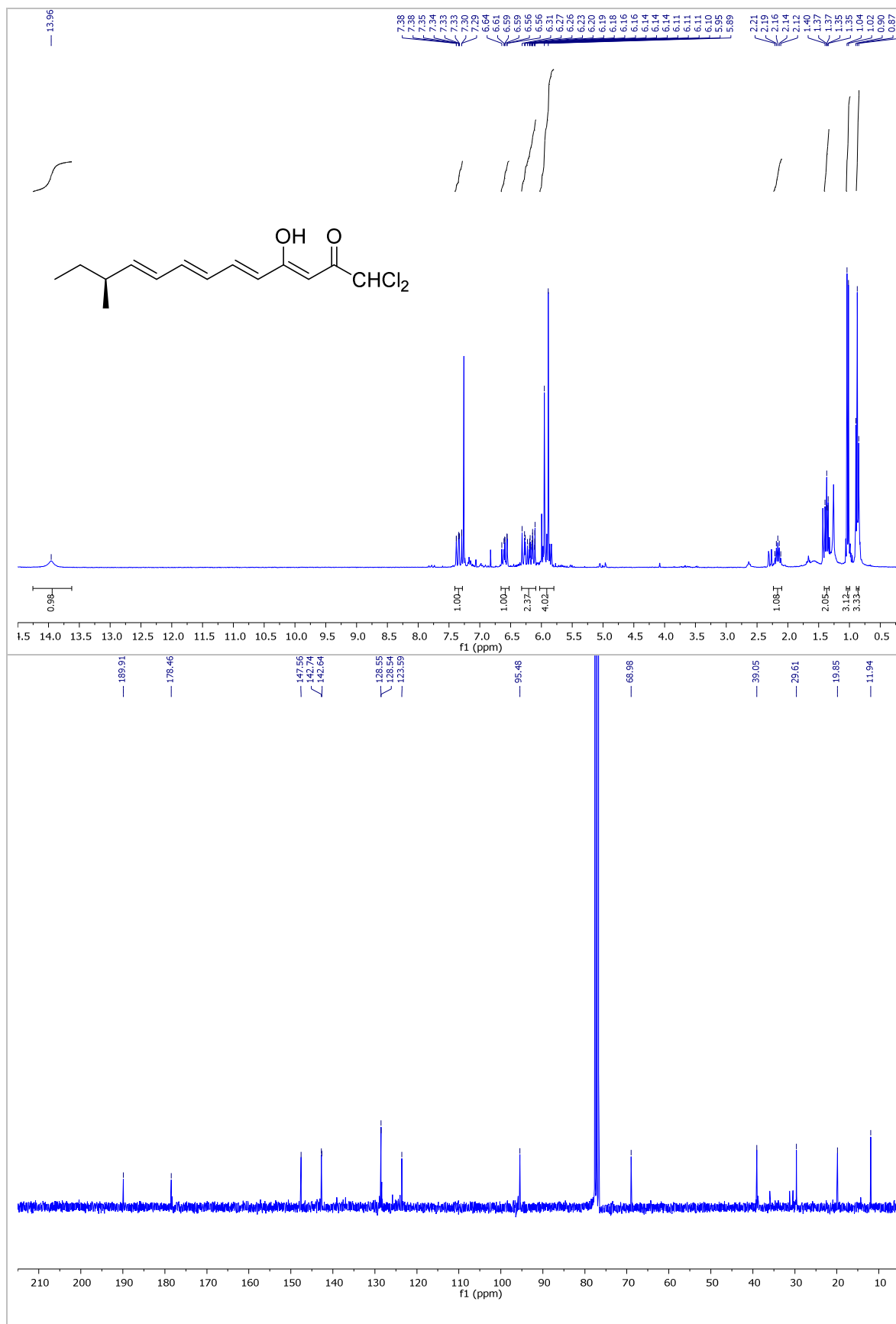


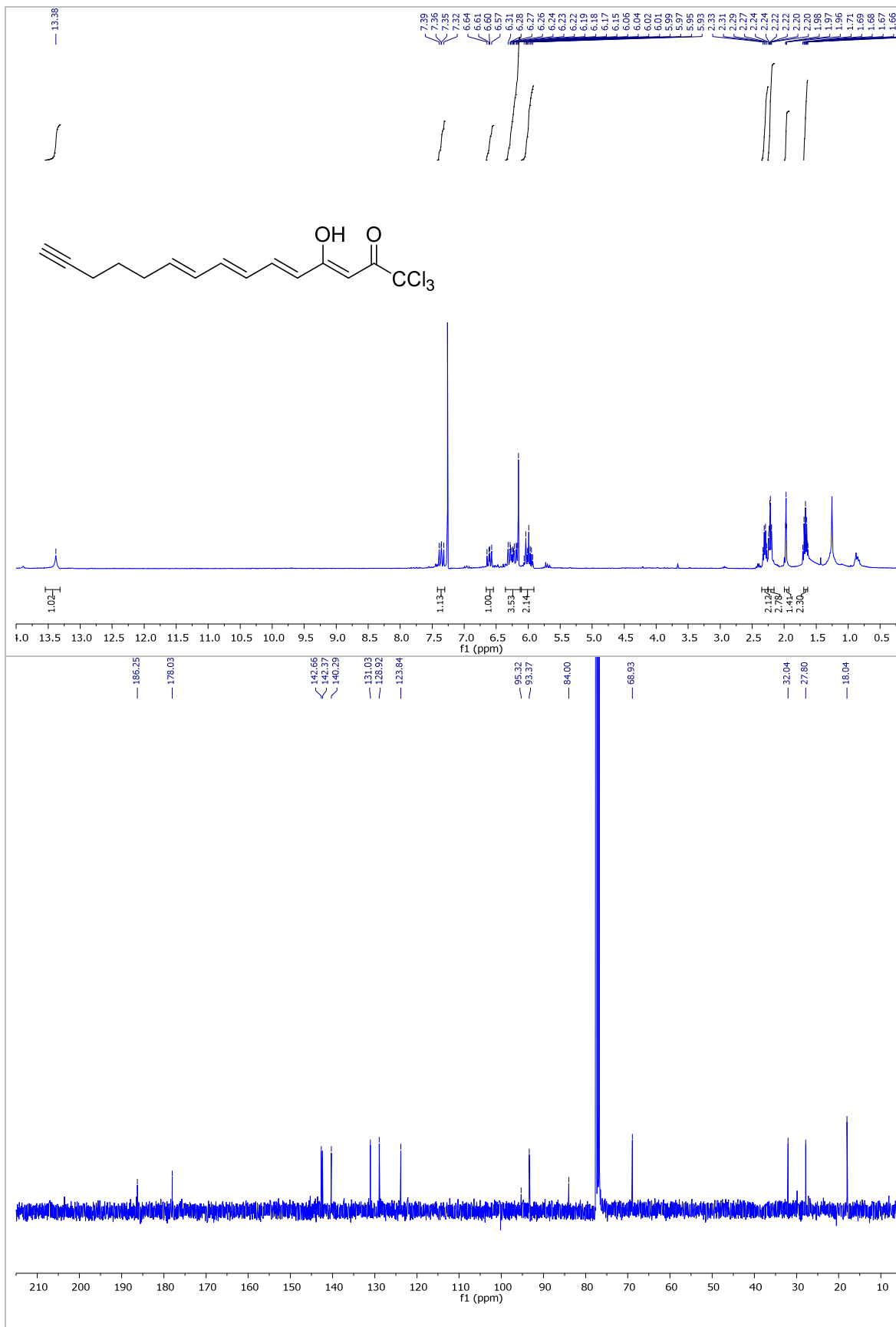
## 8.2 Selected $^1\text{H}$ and $^{13}\text{C}$ NMR Spectra for Chapter 4











## 9 Curriculum Vitae

**Wolfgang Heydenreuter**, born 29<sup>th</sup> march 1985 in Kempten, Germany

### Academic Education

- 02.2012 – 08.2016      **Doctoral Studies** under Prof. Dr. Stephan A. Sieber, Chair of Organic Chemistry 2, TU München:  
*“Target identification of natural products by activity based protein profiling and a whole proteome inventory of background photocrosslinker binding”*
- 01.2011 – 07.2011      **Visiting Researcher** with Prof. Dr. Barry Trost, Stanford University, USA: *“Efforts to expand the scope of Dual Catalysis: Combining Vanadium-catalyzed Meyer-Schuster-rearrangement with Palladium-catalyzed allylic alkylation”*
- 04.2010 – 11.2010      **Master Thesis:** Supervisor Prof. Dr. Stefan Kirsch, TU München: *“Synthesis of new IBX derivatives”*
- 10.2008 – 04.2010      **Master of Science** in Organic Chemistry, TU München
- 10.2005 – 10.2008      **Bachelor of Science** in Chemistry, TU München

### Civil Service

- 07.2004 - 04.2005      Civil service at the Bavarian Red Cross in Marktobendorf

### School Education

- 09.1995 – 06.2004      Higher education entrance qualification (“Abitur”),  
Gymnasium Marktobendorf